2017

Evaluating the Potential of a Geospatial/Geostatistical Methodology for Locating Rain-Derived Infiltration and Inflow into Wastewater Treatment Systems in the Minneapolis/St. Paul Metropolitan Area, Minnesota, USA

Vinson Aaron Williams
Minnesota State University, Mankato

Evaluating the Potential of a Geospatial/Geostatistical Methodology for Locating Rain-Derived Infiltration and Inflow into Wastewater Treatment Systems in the Minneapolis/St. Paul Metropolitan Area, Minnesota, USA

By

Vinson A. Williams Jr.

A Thesis Submitted in Partial Fulfillment of the

Requirements for the Degree of

Masters of Science

in

Geography

Minnesota State University, Mankato

Mankato, MN

Nov 2017

November 10, 2017

Evaluating the Potential of a Geospatial/Geostatistical Methodology for Locating Rain-Derived Infiltration and Inflow into Wastewater Treatment Systems in the Minneapolis/St. Paul Metropolitan Area, Minnesota, USA

Vinson A. Williams Jr.

This thesis has been examined and approved by the following members of the student's committee.

_____
Dr. Phillip Larson

_____
Dr. Rama Mohapatra

_____
Dr. Cynthia Miller

_____
Mr. John Berrigan Jr.

Abstract

A significant issue facing municipal wastewater treatment infrastructure (WWTI) is how to manage infiltration and inflow (I/I). I/I of rain and ground water permeate into WWTI after precipitation events, periods of groundwater table rise, and percolation from surrounding surface waters. This can create discharges above the infrastructure's flow capacity, increase costs for processing the wastewater and add undesired stress to aging wastewater networks. In an attempt to assess this problem cost and time inefficient approaches have commonly been applied. This study utilizes a new and more radical methodology to try and make WWTI management more efficient. This study applies ArcGIS and Geostatistical Analysis to seven counties within the Metropolitan Council Environmental Services (MCES) network in the Minneapolis/St. Paul metro area. Data is collected from rain gauges and flow meters an average ten-year flow record is created from this data. The data is then analyzed in ArcGIS through Kriging to interpolate and predict where significant rates of I/I, due to high magnitude precipitation events, are located throughout the study area. I/I rates for high magnitude precipitation events are estimated through the comparison of the max flow rate data and the ten-year average flow rate. A percentage of increase flow is then calculated. Results reveal spatial patterns indicating variable I/I susceptibility across the MCES WWTI. By collaborating with MCES it is possible to determine how accurately this methodology can locate areas of high-risk I/I potential within the existing WWTI.

Acknowledgements

I would like to thank my advisor, Dr. Phillip Larson for encouraging me to pursue a master's degree in Geography and for pushing me to do the best work I could possibly do. As he said, "what reason is there to do something if you are not going to do your best work?" I would also like to thank my other committee members, Dr. Rama Mohapatra, Dr. Cynthia Miller, and Mr. John Berrigan Jr. for their support. Their expertise in their various fields was an integral part of making this thesis a well-rounded and holistic project. I want to thank the faculty and staff of the geography department and my fellow graduate students for the friendly and supportive atmosphere they have fostered. I would also like to thank Dr. Ron Schirmer and the anthropology department for allowing me to receive funding for my thesis by working on the MNDOT project.

Thank you to the Metropolitan Council Environmental Services (MCES) for providing me an internship and the data and support necessary to make this project a reality. I specifically would like to say thank you to Lori Sands, GIS Specialist III, for being my mentor and supporting me to pursue this project in my free time. I would also like to thank Ryan Vial, Data Analyst, for taking the time out of his busy schedule to answer questions about their processes and also providing me with the Flow Exception Reports necessary to complete this project.

Last, but not least of all, I would like to thank all of my family and friends for their encouragement and support, even when I did not think I could complete such a hefty task. They have always been my biggest fans and supporters throughout all my experiences, from going to school for my undergraduate degree, deploying to Kuwait, to coming back to MSU for my graduate degree. They are the reason I fight so hard to be successful and I appreciate all that they do for me.

Table of Contents

List of Tables

List of Figures

Abbreviations

CCTV – Closed Circuit Television
CK – Co-Kriging
CS – Combined Sewer System
CSO – Combined Sewer Overflow
DEM – Digital Elevation Model
DK – Disjunctive Kriging
EPA – Environmental Protection Agency
FS – Foul Sewage
GIS – Geographic Information System
GPM – Gallons Per Minute
GWI – Groundwater Infiltration
I/I – Infiltration and Inflow
IK – Indicator Kriging
MCES – Metropolitan Council Environmental Services
MGD – Million Gallons per Day
OK – Ordinary Kriging
PK – Probability Kriging
RDI – Rain-Derived Inflow
RDII – Rain-Derived Infiltration and Inflow
RII – Rain-Induced Infiltration
RK – Regression Kriging
SK – Simple Kriging
SSO – Sanitary Sewer Overflows
WWTF – Wastewater Treatment Facilities
WWTI – Wastewater Treatment Infrastructure
UK – Universal Kriging

Introduction

The collection and treatment of wastewater is a crucial part of the infrastructure necessary for modern metropolitan areas. The methods used to treat wastewater have dramatically changed over the past 200 years to accommodate the steady increase in population around the world (Water Environment Federation 2010a; Metropolitan Council of the Twin Cities 2011). Without the treatment of wastewater, groundwater and surface water contamination will occur (Metropolitan Council of the Twin Cities 2007; Obeidat et al. 2007; Water Environment Federation 2010b; Rojas Fabro et al. 2015). Metropolitan areas worldwide have established protocols with the intention of reducing human disease, eliminating environmental pollutants, and, most importantly, attain a level of water quality that is acceptable for reuse (Water Environment Federation 2008, 2010a).

In the United States of America, the quality of treated wastewater is regulated by the U.S. Environmental Protection Agency (EPA) in accordance with the Clean Water Act (1977), Water Quality Act (1987), and the Clean Air Act (1990) (US EPA 2016a). However, each state has the ability to impose additional water and air quality standards upon delegation of the EPA's authority (Water Environment Federation 2010a; US EPA 2016a). Table 1 briefly describes the various wastewater treatment processes used in metropolitan areas primarily in the developed world.

Table 1. List of wastewater treatment processes.

Type	Description	References
Preliminary	Removal, reduction, or modification of wastewater components that may cause operational and equipment problems later in the wastewater treatment process.	(Water Environment Federation 2010b)
Secondary ("Primary")	This is the primary method of wastewater treatment necessary to meet the minimum requirements expected of all treatment facilities according to the U.S. EPA and other regulations. Except for a few countries that discern nutrient-removal for ecological reasons, this treatment is currently the norm in most developed countries around the world.	(Water Environment Federation 2008, 2010a, 2010b; US EPA 2016a)
Advanced	This treatment type is used to attain a more stringent level of treatment necessary to produce a significant reduction in toxic pollutants. This form of treatment is used when there is an increased need for reuse of wastewater. For example in dry or drought stricken regions, like the southwestern United States and areas of Australia (Andersen, Lewis, and Sargent 2004).	(Water Environment Federation 2008, 2010a)
Natural Systems	Wastewater treatment through natural sources such as wetlands (natural and constructed), soil absorption, ponds, land treatment, biomass feedstock, and floating aquatic plants. These can be one of the most cost effective options, but they are typically suited for small areas and rural regions because of the need for land and smaller output of wastewater.	(Huddleston and Rodgers 2008; Nelson and Gladden 2008; Peterson and Lanning 2009; Water Environment Federation 2010b; Kosse, Lübken, and Wichern 2015)

Treating waste and stormwater is an expensive process. The annual total cost of waste and stormwater collection/treatment in the United States of America was approximately $271 billion as of January 1, 2012 (Figure 1). This includes capital needs for publicly owned wastewater pipes and treatment facilities (~$197.8 billion), combined sewer overflow (CSO) correction (~$48.0 billion), stormwater management (~$19.2 billion), and recycled water treatment and distribution (~$6.1 billion) (US EPA 2016b).

One of the most crucial and costly aspects of the entire wastewater treatment system is the collection systems that transport wastewater to the facilities for processing. These collection systems account for 35.3 percent of the annual expenditures (~$95 billion) made towards collection systems according to the US EPA website (US EPA 2016c). This includes the installation of new collection systems as well as rehabilitating the defective pipes and connections. A collection system refers to a network of pipes, conduits, tunnels, equipment, and appurtenances used to collect, transport, and pump wastewater (Water Environment Federation 2008). Flow of wastewater typically occurs by means of gravity-based sewer pipes that take advantage of natural gradients in surface topography to reach the wastewater treatment plant. Lift stations are placed along the network when topographic impediments to flow prohibit gravity flow. The lift stations transport wastewater from lower to higher elevations most commonly by means of centrifugal pumps (United States Environmental Protection Agency 2000; Water Environment Federation 2008). Collection systems are also broken down into three basic types: sanitary sewers, storm sewers, and combined sewers. Sanitary sewers transport wastewater from business and residential areas to the treatment facilities, as well as groundwater and storm water that is introduced through defects in the infrastructure and/or malfunctioning sewer pipes. Storm sewers direct storm water runoff and other drainage to prevent flooding within urban and city limits. Lastly, combined sewers transport both sanitary waste and stormwater (Water Environment Federation 2008). All of these sewer types can transport pollutants to surrounding surface and groundwater if not properly maintained, but the focus of this research will be related to sanitary and combined sewer networks.

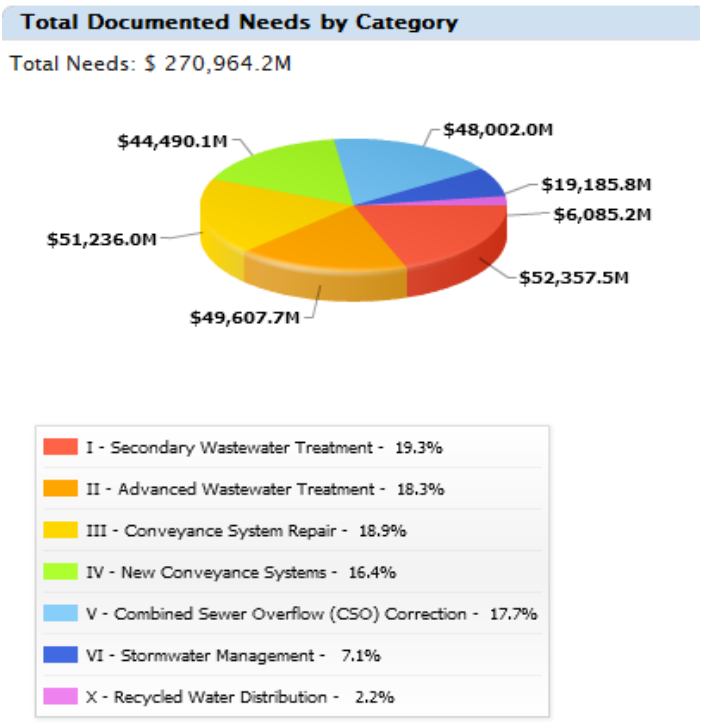

Figure 1. Annual total capital cost for wastewater treatment plants and infrastructure (US EPA 2016c).

Deteriorating and malfunctioning elements of the collection system are an inevitable complication that all waste managing organizations encounter. There are approximately 600,000 miles of sanitary sewer systems and wastewater treatment infrastructure in the United States (Shelton et al. 2011) some of which were built over 100 years ago (Fenner 2000; Wade 2000; Ellis 2001; Lai 2008; Staufer, Scheidegger, and Rieckermann 2012). ASCE's 2009 report card gave the U.S.'s wastewater and drinking-water infrastructure a D- and since then it has raised to a D+ (American Society of Civil Engineers 2011). Failure to act will lead to detrimental effects on the nation's economic performance as well as environmental effects associated with faulty systems. For more information on the issue at hand, refer to American Society of Civil Engineers report called "Failure to Act" (2011). Defective storm water and sanitary sewer systems lead to a wide variety of problems; not only for the wastewater treatment organizations, but also for the

communities they serve and the environment they work to protect by means of wastewater purification (Shelton et al. 2011; Staufer, Scheidegger, and Rieckermann 2012).

Infiltration and Inflow

One of the most common issues around the world, as exemplified in Table 2, is the introduction of undesirable water into the collection system that is transported to wastewater treatment facilities (WWTF). The phenomenon is generally referred to as Infiltration and Inflow (I/I), which is derived from precipitation and groundwater (Zhang 2005; Staufer, Scheidegger, and Rieckermann 2012). Infiltration refers to the unintentional seepage and leaking of water into sewer pipe cracks and crevices; and inflow refers to the direct addition of stormwater into foul sewage flows (Figure 2) (Water Environment Federation 2010b). I/I produces higher total flow rates while also increasing the volume of materials that need to be transported and purified through wastewater treatment infrastructure (Karpf and Krebs 2011). Table 3 describes some factors that influence the rates of infiltration and inflow (I/I) into sewer pipes through cracks, crevices, and poor connections.

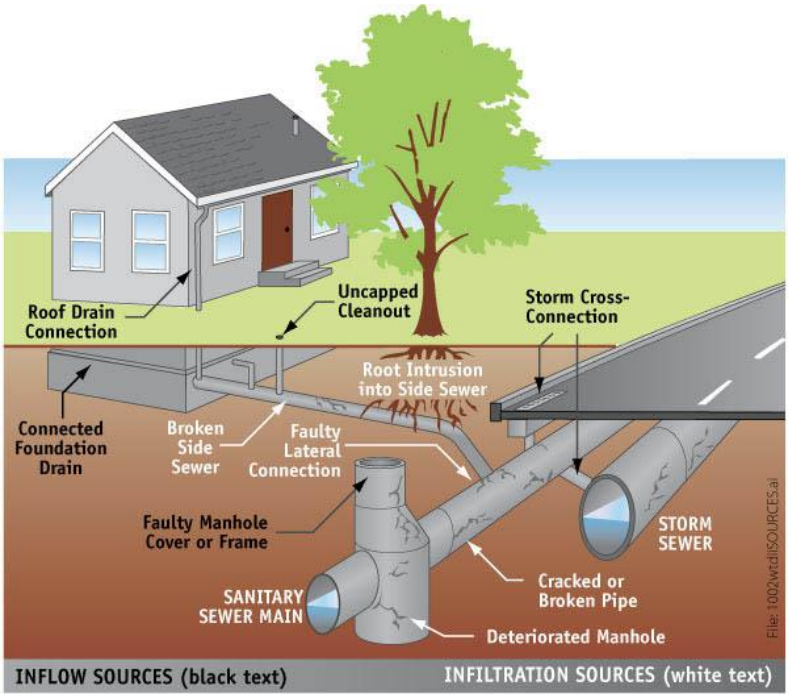

Figure 2. I/I enters the system the collection system through various means (King County 2015).

Table 2. Examples of communities around the world facing the issue known as I/I.

Case Study Area	References and Issues
France	Conducted evaluation of the impact of I/I on a subcatchment scale in Yzeron catchment and Ecully catchment Lyon, France (De Bénédittis and Bertrand-Krajewski 2005); Attempted to analyze the risk of sediment build-up (Fenner 2000).
United Kingdom (UK)	Increased pumping costs due to hydraulic overloading; approximately 23% of sewers in the UK are classified as "critical" condition (Ellis 2001). Fenner (2000) found that less than 20% of the sewer system contributed to 80% of the economic, social, and political problems associated with I/I.
Seattle, WA, USA	Modelling and physical inspection (smoke and dye testing) revealed the primary contributors of I/I in Seattle, Washington was due to backfill trenches (Ellis 2001).
Belgium	Hydroplan procedure developed to group sewers into categories to reflect social and ecological policies and priorities (Fenner 2000).
Australia	Grade sewer conditions based on CCTV inspections (Fenner 2000).
Japan	Created a complex method for awarding condition grades; calculated predictions for when the sewer pipes will need repairs based on knowledge of sewer pipe type, length, materials and other sewer characteristics (Fenner 2000).
Phoenix, AZ, USA	Large diameter unlined concrete sewers prone to hydrogen sulfide corrosion damage (Ellis 2001).
Norway	CCTV inspections grouped into sewer condition classes and 90% of all water and wastewater pipe were digitally recorded in the GIS database (Fenner 2000).

Dresden, Germany	Used model approach of least squares to assess the effectiveness of I/I rehabilitation efforts. 79% of mean I/I flow was expected in 3% of the total length of the sewer system (Karpf and Krebs 2011).
Oahu, HI, USA	Investigated flux stability of select chemical and biological sewage markers, such as caffeine, total nitrogen, total suspended solids, E. coli, and enterococci (Shelton et al. 2011).
Munich, Germany	Assessed the performance of rehabilitation efforts to determine if they made a statistical influence or not. Found that groundwater infiltration was reduced, but the stormwater inflow was not statistically significant (Staufer, Scheidegger, and Rieckermann 2012)

Table 3. Factors that potentially influence the rates of infiltration and inflow depending on the geographic setting and setup of the underground network of pipes.

Influential Factor	Reference
Human Activity (e.g. time of day)	(De Bénédittis and Bertrand-Krajewski 2005)
Rainfall (e.g. intensity, quantity, etc)	(Karpf and Krebs 2011; Staufer, Scheidegger, and Rieckermann 2012)
Groundwater Table Level (constant exchange of water through cracks and crevices in the pipe).	(Fenner 2000; Ellis 2001; De Bénédittis and Bertrand-Krajewski 2005; Karpf and Krebs 2011; Staufer, Scheidegger, and Rieckermann 2012)
Soil Characteristics (e.g. porosity)	(Wirahadikusumah et al. 1998)
Lack of or insufficient maintenance and investment into sewer pipes rehabilitation due to high costs.	(Wirahadikusumah et al. 1998; Fenner 2000; Ellis 2001; Karpf and Krebs 2011; Shelton et al. 2011)
Poor/Outdated Construction Quality (e.g. failure due to clay or concrete pipes).	(Wirahadikusumah et al. 1998; Fenner 2000; Ellis 2001)
Pipe Age, Size, and Length	(Wirahadikusumah et al. 1998; Fenner 2000; Ellis 2001; Shelton et al. 2011; Staufer, Scheidegger, and Rieckermann 2012)
Additional/Illegal connections to the sewer system create vulnerable points of contact.	(Fenner 2000; Ellis 2001)

Staufer, Scheidegger, and Rieckermann (2012) classified I/I into three different components: groundwater infiltration (GWI), rain-induced infiltration (RII), and rain-derived inflow (RDI). Table 4 provides an overview of how the various components influence sanitary sewer flow rates and the methods of I/I quantification used in various case studies like Staufer, Scheidegger, and Rieckermann's (2012) study.

Table 4. Procedures utilized to assess the different components of I/I from flow data acquired from hydrographs and various other sources. (*Original table modified from Staufer, Scheidegger, and Rieckermann (2012, p. 5187)).*

I/I Component	Associated Problem	Quantification Methods	Reference
GWI = groundwater infiltration	Contributes the largest annual volume of I/I and the potential lowering of the groundwater table.	Average of the night-time minima from all dry days for a given month.	(Ellis 2001; Weiss, Brombach, and Haller 2002; De Bénédittis and Bertrand-Krajewski 2005; Karpf and Krebs 2011; Pawlowski et al. 2014)
RDI* = rain-derived inflow	Quickest influence on peak flows and leads to frequent overloading of sanitary sewer systems.	Cumulative differences between discharge and base flow from the beginning of the rain up to 4 hours after the end of the rainfall event.	(Wright et al. 2001; Stevens 2002; Zhang 2008, 2005, 2007; Lai 2008; Muleta and Boulos 2008; D.-J. Lee et al. 2009; Gustafsson et al. 2010; Sadri and Graham 2011; Shelton et al. 2011)
RII* = rain-induced infiltration	Provides a significant increase to peak flows, but has a significant lag time due to percolation through soil.	Cumulative differences between discharge and base flow from the time after the end of the RDI until max. 24 hours after the end of the rainfall event.	Included in the case studies/journals above referring to RDI.
*Combined to determine the volume of I/I during significant precipitation events.			

Ground Water Infiltration (GWI)

GWI refers to groundwater that enters sanitary sewer systems at a constant rate through defects in the piping (Weiss, Brombach, and Haller 2002; Staufer, Scheidegger, and Rieckermann 2012). Infiltration into the collection system occurs when the soil around the infrastructure is saturated by either a high water table or surface water within a close enough proximity (deMonsabert and Thornton 1997; Staufer, Scheidegger, and Rieckermann 2012). These saturated soils are directly correlated with seasonal and meteorological variability;

therefore the groundwater table increases or decreases in height based on the average annual precipitation or seasonal variability (Ellis 2001; Karpf and Krebs 2011, 2013; Staufer, Scheidegger, and Rieckermann 2012). The groundwater table may also be impacted by anthropogenic depletion through overconsumption and, in these instances, GWI is not a factor to consider (Helland 2004; Jossi 2013; Vainu and Terasmaa 2016). Overall, GWI has the highest average infiltration rates, but does not have a noticeable impact on hydrographs, since it slowly percolates into the collection system (Bertrand-Krajewski et al. 2005; Staufer, Scheidegger, and Rieckermann 2012).

Rain-Derived Infiltration and Inflow (RDII)

Most studies of I/I focus on the periods of drastic variability in hydrographs associated with precipitation; commonly referred to as rain-derived infiltration and inflow (RDII) (e.g. Zhang 2007; Staufer, Scheidegger, and Rieckermann 2012). RDII can be further broken down into two subcategories of rain-induced infiltration (RII) and rain-derived inflow (RDI).

Rain-Induced Infiltration (RII)

RII pertains to precipitation that permeates through the vadose zone (the unsaturated soil between the surface and groundwater table) until it reaches the collection system where it is able to infiltrate cracks, holes, or collapses found along the wastewater infrastructure (Figure 2) (deMonsabert and Thornton 1997; Staufer, Scheidegger, and Rieckermann 2012). The primary factors that directly affect the rate at which storm water can infiltrate the ground is strongly correlated with the magnitude and duration of precipitation (Zhang 2005, 2007; Lai 2008), as well as the soil type, geologic characteristics and land use practice (Staufer, Scheidegger, and Rieckermann 2012). Due to these factors, RII has the second most-noticeable impact on

hydrographs during rainfall. This is due to its considerable lag time as observed in Figure 3 (Staufer, Scheidegger, and Rieckermann 2012). The lag time can vary depending on the region's geologic and soil makeup, but generally RII is more similar to GWI since they are both influenced by the permeability of the soil (Staufer, Scheidegger, and Rieckermann 2012).

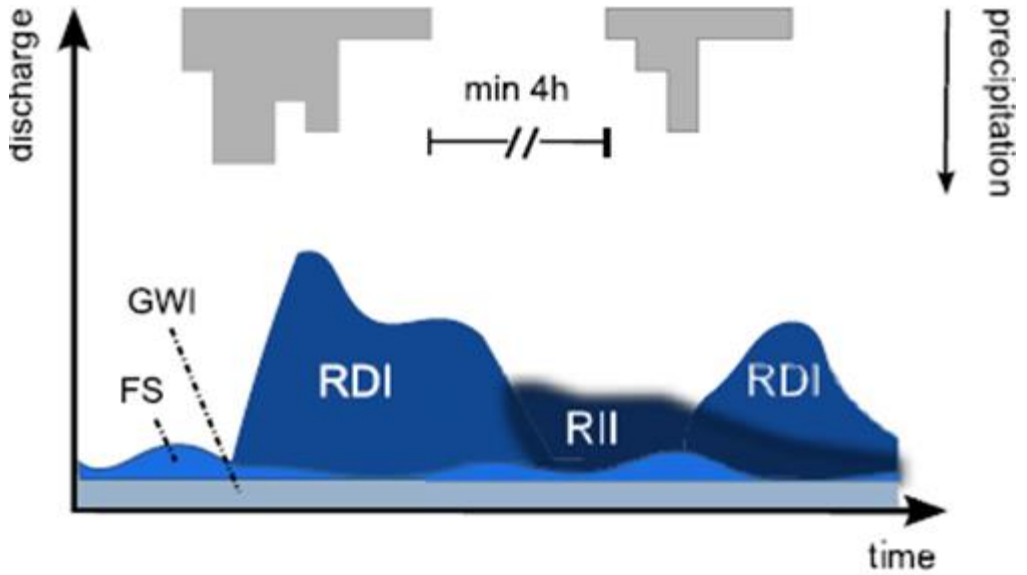

Figure 3. A visual representation of the properties of RDII, foul sewage (FS), and GWI in relations to precipitation (Staufer, Scheidegger, and Rieckermann 2012, p. 5187).

Rain-Derived Inflow (RDI)

RDI describes storm water that enters sanitary sewer systems through surface connections that were poorly secured or, in some cases, illegally connected (Figure 2) (Staufer, Scheidegger, and Rieckermann 2012). Out of all the I/I components, RDI has the shortest lag time and directly affects hydrographs and flow at an exponential rate compared to the other two components (Staufer, Scheidegger, and Rieckermann 2012). This dramatic increase is only possible due to the direct connection to the sanitary sewer network. These direct inlets to collection systems (e.g. combined and sanitary sewer systems) include open or poorly sealed manhole covers, direct connections from street drains, roof and yard drains, foundation drains,

gully pots, basement sump pumps, overflow from storm drains, and various other types of illegal connections into the subsurface wastewater network (Ellis 2001; Staufer, Scheidegger, and Rieckermann 2012).

Influence of I/I on Wastewater Treatment Facilities Performance

The introduction of I/I decrease wastewater treatment facilities' performance because of the increased volume of sewage that needs to be processed. Excess flow produces a greater strain on the equipment which reduces the hydraulic efficiency of a WWTF. Decreased hydraulic efficiency tends to produce more frequent sanitary sewer overflows (SSO) (De Bénédittis and Bertrand-Krajewski 2005; Zhang 2007; Lai 2008; Shelton et al. 2011; Staufer, Scheidegger, and Rieckermann 2012) and can also reduce effectiveness of the foul sewage treatment (Ellis 2001; Karpf and Krebs 2011). Furthermore, the increased discharge and infiltration of water will lead to increased deterioration rates of sanitary sewer systems (De Bénédittis and Bertrand-Krajewski 2005); 75% of sanitary sewer systems are performing at 50% of their optimal capacity according to Shelton et al. (2011).

Environmental Impact due to I/I

The infiltration of rain water into the sewer system also means that the exfiltration of raw sewage can occur under the right conditions (Ellis 2001; Bertrand-Krajewski et al. 2005; De Bénédittis and Bertrand-Krajewski 2005; Rutsch, Rieckermann, and Krebs 2006; Rutsch et al. 2008; Nikpay, Lazik, and Krebs 2015). Generally speaking, exfiltration will occur during intervals of reduced external pressure when the soil encompassing the sanitary sewer systems is no longer saturated via a high groundwater table. Pollution of soils and groundwater ensues when foul sewage has escaped the sewer pipes and can ultimately lead to contaminated drinking water supply (Ellis 2001; De Bénédittis and Bertrand-Krajewski 2005). Apart from pollution,

other detrimental impacts include a reduction of the groundwater table due to GWI into the sewer defects and SSO. The reduction can reach the point to where it can impact surface waters and soil moisture (Gustafsson 2000; Karpf and Krebs 2011).

I/I is a strong contributor to both environmental and community concerns that stem from SSO (Zhang 2005; McLellan et al. 2007; Lai 2008) and back flooding into buildings, public and private property, neighborhood lawns, basements, driveways, streets and even surface waters (Zhang 2005; Karpf and Krebs 2011; Staufer, Scheidegger, and Rieckermann 2012). One common contaminant found in wastewater is Escherichia coli and McLellan et al. (2007) examined the distribution caused by SSO and combined sewer overflows (CSO). These events occur during heavy rainfall when the wastewater treatment plants become hydraulically encumbered and back up or when rain water directly intermingles with foul sewage which leads to overflows. This is the primary cause of human fecal pollution of surface waters (Zhang 2005; McLellan et al. 2007; Lai 2008). Through the use of sampling around the city shore of Lake, Michigan McLellan et al. (2007) found that E. Coli samples drastically increased after rainfall events, but the dilution rates tend to reduce the spread of E. Coli contamination as it moves farther from the harbor and shore (McLellan et al. 2007). The aforementioned environmental problems associated with I/I are financially demanding for both the community and wastewater treatment organizations.

Economic Influence of I/I

In order to process and purify an increased volume of wastewater, more energy must be consumed. High energy consumption increases expenditures for the wastewater treatment facilities and the communities they service (deMonsabert and Thornton 1997; Zhang 2007; American Society of Civil Engineers 2011; Karpf and Krebs 2011; Staufer, Scheidegger, and

Rieckermann 2012). Not only does the cost to purify the wastewater increase, but the reduction of I/I through various rehabilitation methods is very expensive as well (Ellis 2001; Staufer, Scheidegger, and Rieckermann 2012). During the time of Ellis' (2001) study, it was estimated that I/I mitigation cost wastewater treatment organization a capital sum of £100 - £150 million for the mitigation of I/I in highly populated areas. According to Lai (2008), it is estimated to cost approximately $1-2 trillion to replace the entire sanitary sewer systems of the United States of America. This includes the entire I/I rehabilitation process, from surveying for defects to the completion of repairs on the sewer piping. Just the surveying itself can be expensive, time consuming and labor intensive (Lee 2005; Roper and Blanco 2016). The various methods used to assess I/I range from physical inspections to more modern GIS based approaches.

A Review of Methods Which Assess I/I

In order to proactively prevent sanitary sewer deterioration, organizations must take a variety of measures necessary to find the problem before they reach a critical level of severity. All methods used to investigate conditions of I/I are used to assess the structural condition of the sewer network, to predict the financial investment necessary to maintain efficiency, and to see if the rehabilitation efforts have a significant effect in reducing I/I (Staufer et. al., 2012). To do so engineers' tend to use a variety of monitoring methods to investigate and pinpoint I/I locations along the sewer network. A majority of engineer's research tend to be geared towards optimizing methods of I/I measurement through various means like statistics (De Bénédittis and Bertrand-Krajewski 2005; Zhang 2005, 2007). However, traditional methods are still used in municipalities all over the world due to a lack of knowledge of the various methods at their disposal, limited awareness of international sewer rehabilitation efforts, or just a lack of

capabilities to complete some of the more complex I/I assessments (De Bénédittis and Bertrand-Krajewski 2005). A wide variety of monitoring methods are used to assess the condition of wastewater treatment infrastructure, to estimate potential investments necessary to maintain services, and to determine the effectiveness of rehabilitation projects throughout the network (Bennett 1999; Bertrand-Krajewski et al. 2005; Staufer, Scheidegger, and Rieckermann 2012).

Sewer Assessment Methodology

Traditionally used methods include visual inspections, such as smoke tests, dye tests, and closed circuit television (CCTV) (Wirahadikusumah et al. 1998; Zhang 2007; Metropolitan Council of the Twin Cities 2009). Technological advances have allowed flow measurements to be monitored and utilized to calculate I/I more effectively (Wirahadikusumah et al. 1998; Zhang 2007; J. H. Lee et al. 2009; Staufer, Scheidegger, and Rieckermann 2012). The Metropolitan Council of the Twin Cities is an example of a wastewater treatment organization that uses a variety of methods to monitor the conditions of their sanitary sewer systems, which include: floatable cameras also known as CCTVs, and the use of dye and smoke tests that allow the engineers to assess and rate each section of piping based on its severity (Wirahadikusumah et al. 1998; Lee 2005; Zhang 2007; Metropolitan Council of the Twin Cities 2009, 2011). These physical methods are commonly practiced throughout the world, but remain costly, time intensive, and/or inefficient in appropriately assessing spatial zones of vulnerability within a wastewater treatment network (Shelton et al. 2011). Upon completion of surveys with methods like CCTV, the sewer systems are ranked based on their severity which is used to prioritize rehabilitation efforts (Karpf and Krebs 2011; Shelton et al. 2011). Also by knowing the year sewer sections were installed and the height of the water table in the region, it is possible to estimate areas more susceptible to I/I (Karpf and Krebs 2011).

Modern monitoring of RDII is estimated through the use of monitoring methods based on volume of flow, but as mentioned by Zhang (2007) most of these methods are "ad hoc" in practice and do not calculate the statistical relevance of the measured flows. Monitoring of inflow is most commonly accomplished through the comparison of sewer discharge data collected from the exit of a catchment or sub-basin against concurrent rainfall measurements (Bennett 1999; Zhang 2007, 2008; Staufer, Scheidegger, and Rieckermann 2012).

Only a limited number of countries have ever completed a comparative study of the I/I assessment methods used around the world (De Bénédittis and Bertrand-Krajewski 2005). A few studies have been conducted to compare multiple types of monitoring methods used to assess the severity of RDII including Fenner (2000), Ellis (2001), and De Bénédittis and Bertrand-Krajewski (2005). It has been observed that at this time there are not any methods that encompass all of the components of I/I (De Bénédittis and Bertrand-Krajewski 2005).

There are two categories of modern I/I monitoring methods: (i) flow rate methods that are based off hydrographs produced through spectrometers and other various monitoring systems, and (ii) chemical based methods that measure the dilution of the wastewater from clean water (De Bénédittis and Bertrand-Krajewski 2005; Shelton et al. 2011). In order to monitor large sewer systems it is necessary to have properly established assessment tools in various locations along the network, but this can be extremely expensive to implement (Shelton et al. 2011).

RDII can typically be measured by industries through the collection and analysis of rainfall and flow data at various locations along the wastewater network (Zhang 2005). This data provides the information necessary to calculate the ratio of total rainfall that enters the system at various locations; this ratio is commonly referred to as the "I/I ratio" (Zhang, 2005, 1). The I/I

ratio has be used to make several key management decisions when it comes to evaluating the severity of sewer deterioration which is discussed more in depth by Zhang (2005, 1). Obtaining accurate flow measurements of RDII from direct flow rates comes with inherent error in the data due to various conditions including SSO (Shelton et al. 2011) and high velocity flows that are not accurately measured due to the limitations of the spectrometer used (Zhang 2005).

Night-time minimum flows are a simpler method used for monitoring I/I because it provides the least amount of fluctuations in the data from day to day. Generally, night-time minimum flows only measures one day of dry weather instead of a statistically significant amount of cases to provide an acceptable margin of uncertainties for day time datasets (De Bénédittis and Bertrand-Krajewski 2005; Staufer, Scheidegger, and Rieckermann 2012). Hydrological fluctuations during the day can change by the hour due to significant times of day such as breakfast, lunch, dinner, weekdays, weekends, etc. Each of these periods will provide a different amount of flow based on the local populace's routine.

There are a variety of studies that attempt to integrate stochastic approaches to overcome the major flaws of conventional methods that lack statistical significance of flow rate, RDII, and I/I reduction measurements (De Bénédittis and Bertrand-Krajewski 2005; Zhang 2005, 2007, 2008; Karpf and Krebs 2011; Shelton et al. 2011; Staufer, Scheidegger, and Rieckermann 2012). They are briefly discussed below:

De Bénédittis and Bertrand-Krajewski (2005) compared fourteen methods of infiltration measurement at two study sites in Lyon, France: (i) the first study was at the Yzeron catchment as a temporary monitoring station set up for the sake of a diagnostic; (ii) whereas the study at the Ecully catchment used the permanent monitoring station at that location. Due to the setup and

calibration errors, temporary monitoring stations are not as reliable due to insignificant use to conclude that the device is accurately recording consistent data. On the other hand, permanent stations are usually properly equipped to estimate the uncertainty in the wastewater discharge rates and have a long enough record to show any discrepancies in the measurements (De Bénédittis and Bertrand-Krajewski 2005).

De Bénédittis and Bertrand-Krajewski (2005, 2) described the various data and calculation techniques used in order to predict theoretic strict wastewater flows as:

> "(i) a mean daily strict wastewater flow based on the annual drinking water consumption on the studied catchment, (ii) the number of inhabitants on the studied catchment and references values of sewage discharge per capita, (iii) the number of inhabitants on the studied catchment or wastewater flow measurements in low water period for the estimation of a residual night flow and (iv) the continuous or daily measurements of pollutants concentration (COD, BOD, ammonia, etc.) at the outlet of the studied catchment and reference values of pollutant discharges per capita."

The introduction of flow data and a better understanding of chemical and biological attributes of wastewater have led to more sophisticated methods of monitoring I/I. For example dynamic pollutographs and stable environmental isotopes (Karpf and Krebs 2011; Staufer, Scheidegger, and Rieckermann 2012). The examination of multiple isotopes at specific controlled locations to measure the amount of I/I being induced in certain areas (Houhou et al. 2010) and biological sewage markers (Shelton et al. 2011; Staufer, Scheidegger, and Rieckermann 2012) provide an innovative method for measuring I/I.

Ultraviolet (UV) sensors are placed on pontoons or within bypass flumes and allow spectrometer sensors to measure various aspects of the water quality, ranging from 'ultra-pure waters' to 'highly concentrated wastewaters' by assessing chemical oxygen demand, total suspended solids, and nitrate levels in the flow (Gruber et al. 2005; Shelton et al. 2011). Chemical and biological analyses of wastewater dilution is a more cost effective method and can be automated to assess an entire system with ease compared to direct flow measurements (Shelton et al. 2011). Markers used for analyses of I/I by Shelton et. al. (2011, p.8684) included, "fecal bacteria such as Escherichia coli and enterococci, caffeine, total nitrogen, and total suspended solids (TSS)." Shelton et. al. (2011) found that concentrations of total nitrogen (TN) were the most optimal indicators due to their outstanding stability throughout the day; caffeine and TSS concentrations provided practical patterns, but were still secondary to TN when it came to regularity. In conclusion it was found that the biological markers are a lot less stable than the physiochemical markers due to larger fluctuations in the concentrations over time (Shelton et al. 2011).

Drawbacks

I/I is fundamentally difficult to accurately estimate due to the vast amount of variability found across an entire region, and even at the same location. This occurs from inaccurate and incomplete data for rainfall and runoff, as well as climatic influences such as groundwater tables height, which all contribute to the increased discharge of foul sewage (Zhang 2005; Staufer, Scheidegger, and Rieckermann 2012).

Three major shortcomings that make current I/I assessment unreliable include the stability of the reference base, variation in the precipitation events duration, and limitation of the data processing capabilities (Zhang 2005). More specifically when referring to reference base

stability, Zhang (2005) is referring to the typical comparison of average dry weather flow rates to precipitation event baseline and max flows. Wastewater flow rates can drastically fluctuate from day to day (De Bénédittis and Bertrand-Krajewski 2005) or even a weekday compared to a weekend day (Zhang 2005; Shelton et al. 2011); these fluctuations are strongly governed by the daily routines of residents in each sewershed. Therefore a single days values are not significant enough to provide a compelling conclusion; in order to attain optimal estimations conclusions should be based on several successive dry weather days (De Bénédittis and Bertrand-Krajewski 2005).

The I/I ratio previously discussed have been used to estimate various rain events with a large range of flows based on the duration and intensity of each event which inevitably creates an impractical comparison of the data leaving no real stochastic structure (Zhang 2005, 2007). Lastly, as mentioned before the limitations of the devices used are not able to accurately detect flow rates once discharge velocity reaches the photometric device's detection limits; as a result the data produces, "missing values, measurement errors, serial correlation, and heteroscedasticity," according to Zhang (2005), but if the flow data is properly modeled these complications can be overcome as discussed in detail by Zhang (2005, 2007, 2008).

According to Staufer, Scheidegger, and Rieckermann (2012), a lot of money is spent rehabilitating sewer systems, but very little effort goes in to the assessment of how effective the projects are at reducing I/I. This is important since most engineers generally use fairly ad-hoc comparisons of average I/I before and after the completion of their rehabilitation projects, but this quantitative assessment can lead to an inaccurate portrayal of I/I reduction by not having an equal amount of measured events before and after (Zhang 2005; Staufer, Scheidegger, and Rieckermann 2012).

Most traditional methods do not take into consideration the margin of error that comes from underlying assumptions and general principles used for monitoring I/I (De Bénédittis and Bertrand-Krajewski 2005). Proper understanding of uncertainty is a vital practice that needs to be implemented when dealing with expensive sewer rehabilitation projects. According to Zhang (2005), engineers tend to throw percentages in their reports after rehabilitation projects are complete, but they forget to include a margin of error that is inherently found in any measurements. Without this proper use of statistics, a high percentage decrease in I/I therefore has no statistical validity to the estimates provided.

For example, in Muetzenich, Germany, the city attempted to reduce I/I by sealing air holes on manhole covers, disconnecting surface drainage pipes that were directly connected to the sewers, constructed hillside drainage, roadside ditches which in turn redirected rainfall runoff on roads into drainage ditches (Staufer, Scheidegger, and Rieckermann 2012). From Staufer et. al.'s (2012) regression analysis these methods did not make a statistically significant impact on the reduction of I/I. However, the efforts to mitigate GWI were been found to be "successful" with a reduction of groundwater infiltration by 23.9% , but the reduction of I/I from precipitation was found to not be statistically significant even though estimates of 35.7% decrease in flow after the projects were complete (Staufer, Scheidegger, and Rieckermann 2012). By understanding the statistical significance of the rehabilitation efforts they put in place, managers can potentially improve the methods used to reduce otherwise inefficient measures.

I/I into combined and sanitary sewers is a phenomenon that occurs all throughout the world. It can be detrimental to municipalities' infrastructure, the surrounding environment and the economic status of wastewater organizations and the communities they serve. Inherently populations have developed methods to mitigate this problem, but in order to repair defects in the

sewer system they first need to locate these areas vulnerable to I/I. Traditionally this was completed through labor intensive, time consuming, and expensive means (Lee 2005; Roper and Blanco 2016), but with the advancement of technology they have produced more efficient methods of monitoring I/I. With the introduction of flow rate data and even the use of biological/chemical markers, they have greatly improved rehabilitation efforts, but it has been revealed that inadequate understanding of statistical validity can lead to unreliable results. In order to improve rehabilitation efforts, analyses of I/I must be properly modeled or else the level of uncertainty will leave the output statistically irrelevant and therefore misleading to the actual effectiveness of I/I reduction.

Overall trends are following a pattern of assessing I/I through the use of flow rates and other data, but none of the previously discussed methods utilize a geospatial approach to assess I/I issues in a particular location.

It is clear that understanding wastewater infrastructure vulnerability is becoming an increasingly pressing issue in many cities and the methods applied vary a great deal. Many methods remain costly, time intensive and/or inefficient in appropriately assessing spatial zones of vulnerability within a wastewater treatment network. The first step in addressing the I/I issues in any municipality is locating the piping that has the highest I/I risk and treating those first. But, this is a significant hurdle when there are hundreds of miles of piping to be considered. It can take years to visually inspect an entire system using the normal methods outlined earlier. In this work an new method is proposed focusing on geospatial and geostatistical analysis by utilizing ArcGIS and kriging methodologies to assess vulnerability within a wastewater treatment network.

Geospatial Approach

The Concept of Interpolation

Real world problems often span large areas of interest at varying scales. It often is not possible to identify variations in different phenomenon across a large study area within the finite time and resource limitations of a particular study (Knotters, Brus, and Oude Voshaar 1995; Einax and Soldt 1999; Bao et al. 2014; Omuto and Vargas 2014; Kang, Jin, and Li 2015). Sometimes it is necessary to estimate unknown values of phenomenon that vary across broad spatial extents. In order to analyze these variables across these large study reaches, it is possible to take a limited number of sample points and create a continuous surface by interpolating the values in between them (Figure 4). Through the use of sample points in an area of interest, you can statistically interpolate the values at locations not measured throughout the landscape. This is a valuable resource in predicting locations of interest with greater accuracy than ever before (Oliver and Webster 1990; Johnston et al. 2001; Milillo and Gardella 2008; Hengl 2009; Meng, Liu, and Borders 2013; Curtarelli et al. 2015). We can interpolate data across space through the use of various spatial analysis methods that have become available through the use of Geographic Information Systems (GIS). This is an exceptionally useful tool for a variety of fields and originally was used to predict the locations of ore for mining purposes (Einax and Soldt 1999).

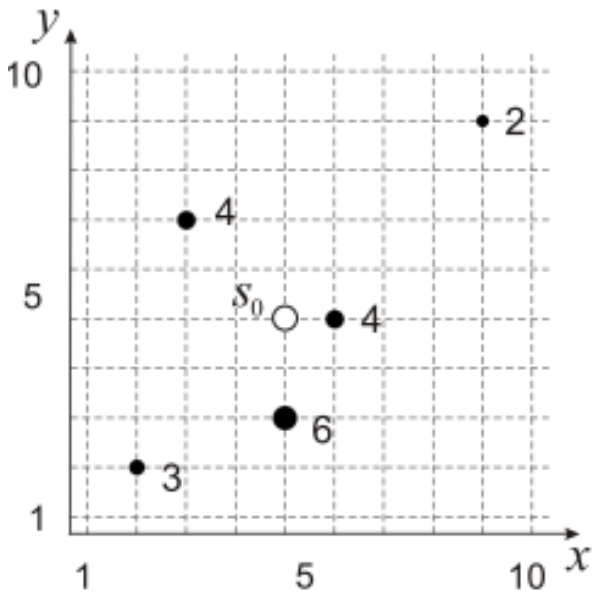

Figure 4. This is a simplified version of the interpolation process. Each point is given a weight, which is the number next to each black dot. The hollow dot is the unknown location that is determined based off the known values surrounding it. Overall, the black point with a 6 will have the greatest influence on that unknown points value, but in geostatistical methods like kriging, they would use cross validation to measure the accuracy of the model. This would be completed by taking awawy the 6 and attempting to estimate the value at that known location until it is as close as possible without distorting the entire model (Hengl, Heuvelink, and Rossiter 2007).

Interpolation Methods

There are two types of interpolation methods: deterministic and stochastic (geostatistical). They both take scattered point data or aerial imagery and use them to create a continuous surface that fills in values for the all unknown locations through mathematical means. Deterministic methods mathematically compute values across a continuous surface. Stochastic methods take into consideration both statistical and mathematical functions in order to interpolate a surface with values for unknown locations and then compute a margin of error that is generated from the smoothing process (Johnston et al. 2001). The most commonly used deterministic product is an elevation surface created from a variety of sample points that have z values, also known as a digital elevation model (DEM) (Johnston et al. 2001). These interpolation methods are based around the fundamental principle of Geography that describes

variables that are closer together tend to be more alike than variables that are farther apart (Tobler 1970; Johnston et al. 2001; Hengl 2009).

When using deterministic methods, a continuous surface is created by mathematically calculating the weight of predicted points based on their distance from measured points. In theory, the closer the sample points are to one another the higher the accuracy of the predicted values (Johnston et al. 2001). Even with sample points neatly clustered together, there can still be a margin of error when it comes to calculating the unknown values because phenomena in the real world can be random. So geostatistical methods are available in an attempt to counteract this problem with the lowest residual error possible (Johnston et al. 2001). They are able to estimate the statistical relationship between measured points, referred to as spatial autocorrelation, as well as the mathematical functions of a typical deterministic method in order to produce a measure of uncertainty (Mitas and Mitasova 1999; Johnston et al. 2001).

Geostatistical Workflow and Kriging

The most commonly used geostatistical interpolation method in GIS is kriging, a process that uses random functions to assume that the surface or values created follow a pattern of spatial covariance. Random variables that vary in the same direction produce a positive correlation between two random values, or they may follow opposite directions which will produce a negative correlation between sample points (Mitas and Mitasova 1999). The overall process behind kriging was derived from the Regionalized Variable theory which takes into consideration stochastic variables such as trends, correlated variations, and uncorrelated variations (Oliver and Webster 1990). Two major tasks make up the kriging process: First analyzing and determining spatial patterns of the data and second inputting those to create a prediction product.

The first aspect of the statistical analysis is to explore the spatial data to see if there are any noticeable patterns, such as spatial variability, global trends, or how dependent each sample point is on one another after acquiring measured sample points (Johnston et al. 2001). Once the sample data has been analyzed for statistical patterns through the use of various spatial data exploration tools and statistical programs geostatistical analysis can be conducted (Hengl, Heuvelink, and Rossiter 2007). This consists of modeling the semivariogram or covariance to measure the surface qualities and begin the kriging process.

A semivariogram is a visual representation of the relationship between the various input attributes to determine spatial correlation (Einax and Soldt 1999). They should follow a generally normal distribution as seen in Einax and Soldt's (1999) semivariogram (Figure 5). As the line moves toward the upper right corner of the graph, the distance and the difference in values should become greater compared to the lower left corner where the values should be clustered and have similar values.

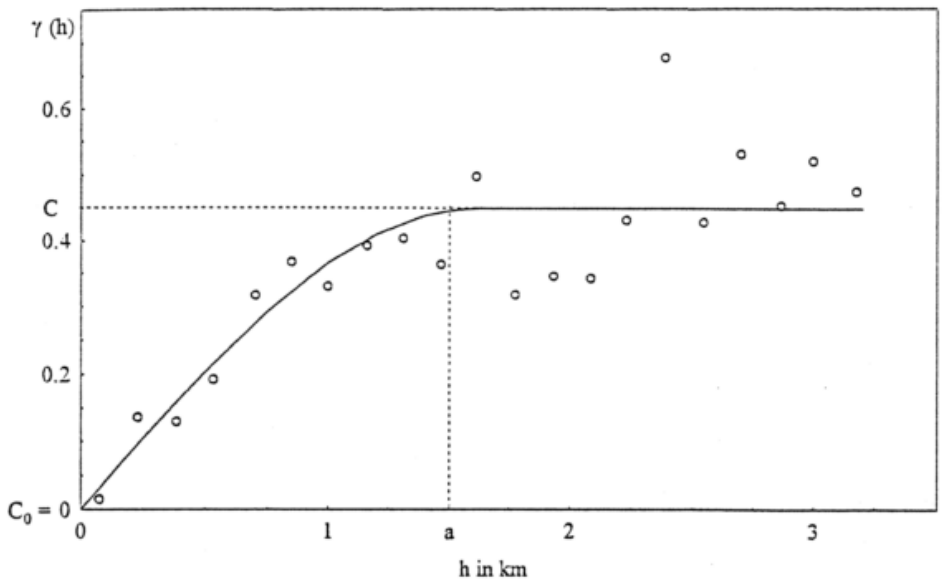

Figure 5. Semivariograms are used to determine a datasets trend so the geostatistical processes can more accurately predict unknown values during interpolation. It is optimal for the curve to follow the trend of the sample points. (Einax and Soldt 1999)

A strong modelling of the spatial covariance through the use of semivariogram models can either make or break the validity of the output prediction (Oliver and Webster 2014). The semivariogram is a vital part to set up the rest of the geostatistical process and accurately model the dataset. This is a recurring topic discussed in a variety of studies on how important it is to properly model the semivariogram to match the trends of the sample region (Clark 1977; White and Ayyub 1990; Zimmerman and Zimmerman 1991; Yamamoto 2005; Zhang and Zimmerman 2007; Goovaerts 2008; Chiles and Delfiner 2009; Pardo-Igúzquiza et al. 2009; Sakata, Ashida, and Tanaka 2010). This can be the difference between accurate and reliable output prediction maps versus products that produce large margins of error. It is important to understand the similarities and differences among several semivariogram estimators since they determine the accuracy of the output prediction map (Zimmerman and Zimmerman 1991). Next, users must understand the different types of methods so that they can pick the appropriate method for their analysis.

Various methods of Kriging

The kriging process itself has a variety of different methods including Ordinary Kriging (OK), Simple Kriging (SK), Universal Kriging (UK), Co-Kriging (CK), Probability Kriging (PK), Indicator Kriging (IK) and Disjunctive Kriging (DK). These are a few of the mainstream methods mentioned by Johnston et al. (2001), but more studies have brought to light a variety of more specialized methods used to solve specific problems.

All of the geostatistical methods previously mentioned are able to provide a measurement of error through the use of cross-validation (Johnston et al. 2001; Lado, Hengl, and Reuter 2008; Hengl 2009). The cross-validation process assesses the accuracy of the created continuous surface by temporarily removing one measured sample point at a time and uses the remaining

sample points within the specified proximity area to the predict the value at the removed sample points location. Depending on the accuracy of the predicted value to the actual measurement, it can statistically calculate the amount of error found in that location and adjust the interpolated surface accordingly and it continues this process for every point throughout the map to assess the level of uncertainty (Mitas and Mitasova 1999; Johnston et al. 2001). Upon completion it provides the user with a root mean square (RMS) of error. By assessing the error provided with the end product, analysts can better adjust and validate their results to create highly accurate prediction products.

One of the simplest forms of kriging is "OK", which uses an unknown constant mean as the deterministic trend for the prediction process. This is a flexible process to use when there are no scientific reasons to reject a constant mean as a possibility (Johnston et al. 2001). It is strongly recommended that the sample points follow a strong autocorrelated pattern continuous throughout space. Simple Kriging uses a known constant mean, which is generally unrealistic in most cases, but in a scenario where the estimated error of the sample points is known it is possible to predict the constant mean trend (Johnston et al. 2001; Hengl 2009).

Universal Kriging follows a more deterministic trend that attempts to determine error based on a polynomial regression instead of the constant mean used in OK and SK (Johnston et al. 2001). In terms of the semivariogram, UK curves the mean to the trend instead of taking the average as the base line across the graph. Ordinary Kriging interpolates based off of the mean value, while universal kriging is adjustable to fit varying spatial trends (Wang and Zhu 2015). One drawback to the complexity of this process is the need for a highly adequate understanding of the data provided. This is necessary for proper adjustment of the semivariogram model to fit the trends of the sample data.

Indicator Kriging uses an unknown constant and a binary variable to separate points into two groups (Johnston et al. 2001). Values that fall above the threshold are marked as 1 and those that fall below are marked as 0. This method is more often used in determining probability of a value falling into the group classifications (Johnston et al. 2001). Probability Kriging attempts to do the same thing as indicator kriging, but by using two error values it can do a better job through autocorrelation and cross validation of those two error values. Disjunctive Kriging can be used to predict the indicator or the value that will create the threshold between points (Johnston et al. 2001).

Cokriging takes into consideration multiple variables to create a more accurate prediction model. The main variable is both autocorrelated and then cross-correlated with the other variables to potentially provide better predictions (Johnston et al. 2001). On the other hand, more variables can lead to greater variability and not necessarily better results. According to Meng, Liu, and Border (2013), CK depends on how well the variables correlate, which can vary case by case on whether it is significantly effective or not compared to the other stochastic and even deterministic methods. It was also discussed that cokriging has an inherent risk of outliers depending on the weights of the auxiliary variables which most of the time are small enough to where the variables do not impact the interpolation process very much (Meng, Liu, and Borders 2013).

Lastly, one method that is not as commonly mentioned in tutorial guides is Regression Kriging (RK) which combines multivariate regression and kriging in order to produce a more accurate prediction model. Similar to cokriging in its ability to apply multiple variables to the variable of interest, but different due to the strong correlation between an auxiliary variable and the variable of interest, and the unbiased spatial estimation with minimized variance (Meng, Liu,

and Borders 2013). Unlike CK, regression kriging needs a sound correlation between the main variable and the auxiliary variable prior to interpolation.

Focus

In general, geostatistics is described by Johnston et al. (2001) as producing maps with kriging predicted values, standard error of those predicted values, probability (whether or not critical thresholds were exceeded), and quantiles for a predetermined level of probability. Kriging has a vast amount of applications, but how well does it equate to other methods when it comes to solving problems and analyzing phenomena? Does it have a specific specialty? Could it produce results for a wide variety of dilemmas? Does it have any flaws or limitations that need to be considered? These are all questions that need to be answered**.**

For a more in depth understanding of the behind the scenes processes of each methodology refer to these sources (Burrough 2001; Johnston et al. 2001; Esri 2006; Hengl 2009; Morari, Castrignanò, and Pagliarin 2009; Oliver and Webster 2014; Environmental Systems Research Institute 2016). Instead the focus will be on the different types of interpolation methods utilized, any limitations the geostatistical processes pose, and a summary of case studies pertinent to constructing a holistic picture of the optimal kriging strategy.

Geostatistical Applicability

When spatially interpolating scattered sample point data it can be hard to find a process that is absolutely sound. Careful consideration of the various kriging types need to be speculated before completing the process or else it could lead to false representation of the data. Kriging's strengths lie in the fact that it leads to statistically unbiased prediction and is capable of predicting the level of error and uncertainty found throughout the sample region. Kriging is often

used in the mining and petroleum industries, geochemistry, geology, soil science and ecology, where its statistical properties are of great value (Mitas and Mitasova 1999). In other situations it is not as capable of working out local geometric variations across the surface on a localized scale and is not the most competent methodology out there for maximizing smoothness of the surface (Mitas and Mitasova 1999) which is referring to the generalization of unknown point values based off of measured sample points.

Hengl (2009) described the results of his research which showed the top ten fields that use geostatistical methods as geosciences, water resources, environmental sciences, agriculture and soil sciences, mathematics and statistics, ecology, civil engineering, petroleum engineering, and limnology. These results will obviously vary location to location depending where you are in the world since different countries pursue different interests based on their needs. Table 5 depicts some common environmental variables that are analyzed using Geostatistics and provides the reader with a great idea of how they are analyzed. The table displays how the various aspects of interest are analyzed, whether they focus on variability vertically, temporally, locally, density among the sample sites, or how detectable variations are with remote sensing imagery. Most of the variables reviewed in other articles tend to fit into one of the categories found in Table 5 (Hengl 2009).

Table 5. Some common environmental variables of interest to decision making and their properties: SRV – short-range variability; TV – temporal variability; VV – vertical variability; SSD – standard sampling density; RSD – remote-sensing detectability; ★ - high, ⋆ - medium, - - low or non-existent. Approximated by Hengl (2009).

Environmental features/topics	Common variables of interest to decision making	SRV	TV	VV	SSD	RSD
Mineral exploration: oil, gas, mineral resources	mineral occurrence and concentrations of minerals; reserves of oil and natural gas; magnetic anomalies;	⋆	–	★	⋆	⋆
Freshwater resources and water quality	O_2, ammonium and phosphorus concentrations in water; concentration of herbicides; trends in concentrations of pollutants; temperature change;	⋆	⋆	⋆	⋆	–
Socio-economic parameters	population density; population growth; GDP per km^2; life expectancy rates; human development index; noise intensity;	⋆	⋆	–	★	★
Land degradation: erosion, landslides, surface runoff	soil loss; erosion risk; quantities of runoff; dissolution rates of various chemicals; landslide susceptibility;	⋆	⋆	–	–	★
Natural hazards: fires, floods, earthquakes, oil spills	burnt areas; fire frequency; water level; earthquake hazard; financial losses; human casualties; wildlife casualties;	★	★	–	⋆	★
Human-induced radioactive contamination	gama doze rates; concentrations of isotopes; PCB levels found in human blood; cancer rates;	⋆	★	–	⋆	★
Soil fertility and productivity	organic matter, nitrogen, phosphorus and potassium in soil; biomass production; (grain) yields; number of cattle per ha; leaf area index;	★	⋆	⋆	⋆	⋆
Soil pollution	concentrations of heavy metals especially: arsenic, cadmium, chromium, copper, mercury, nickel, lead and hexachlorobenzene; soil acidity;	★	⋆	–	★	–
Distribution of animal species (wildlife)	occurrence of species; biomass; animal species density; biodiversity indices; habitat conditions;	★	★	–	⋆	–
Distribution of natural vegetation	land cover type; vegetation communities; occurrence of species; biomass; density measures; vegetation indices; species richness; habitat conditions;	⋆	⋆	–	★	★
Meteorological conditions	temperature; rainfall; albedo; cloud fraction; snow cover; radiation fluxes; net radiation; evapotranspiration;	⋆	★	⋆	⋆	★
Climatic conditions and changes	mean, minimum and maximum temperature; monthly rainfall; wind speed and direction; number of clear days; total incoming radiation; trends of changes of climatic variables;	–	★	⋆	⋆	⋆
Global atmospheric conditions	aerosol size; cirrus reflectance; carbon monoxide; total ozone; UV exposure;	⋆	★	★	–	★
Air quality in urban areas	NO_x, SO_2 concentrations; emission of greenhouse gasses; emission of primary and secondary particles; ozone concentrations; Air Quality Index;	★	★	★	★	–
Global and local sea conditions	chlorophyll concentrations; biomass; sea surface temperature; emissions to sea;	⋆	★	⋆	⋆	⋆

Trends

So far kriging has been used for a variety of scenarios and disciplines, but in many different ways, depending on the questions trying to be answered and the variables being analyzed. A consistent trend is that most applications of geostatistics apply multiple interpolation methods, both deterministic and stochastic, to each case study to compare their strengths and limitations (Table 6) (Lam 1983; Zimmerman and Zimmerman 1991; Hengl, Heuvelink, and Stein 2003).

Table 6. Based off Hengl (2009) environmental features and topics table. The various ways geostatistical methods are used for a wide variety of topics and interests. Along with supporting case studies for each type.

Study Focus/Topic	Methods Used	Reference
Freshwater resources and water quality	Ordinary Kriging, Universal Kriging, Indicator Kriging, Factorial Kriging	(Gundogdu and Guney 2007; Adhikary et al. 2011; Hassan and Atkins 2011; Arslan 2012; Blanco et al. 2013; Narany et al. 2013; Machiwal and Jha 2015)
Soil fertility, productivity, and management	Regression Kriging, Ordinary Kriging, Indicator Kriging, Disjunctive Kriging, Block Kriging, Ordinary Kriging integrated with land-use type (OK_LU or CoKriging), soil land inference model (SoLIM)	(Knotters, Brus, and Oude Voshaar 1995; Zhang and McGrath 2004; Hengl 2006; Morari, Castrignanò, and Pagliarin 2009; Dafonte et al. 2010; Bao et al. 2014; Wen et al. 2014; Chen et al. 2015)
Soil Pollution (e.g. heavy metals, magnetic susceptibility, acid mine drainage)	Regression Kriging, Factorial Kriging, Indicator Kriging, CoKriging, Universal Kriging, External Drift Kriging, Lognormal Kriging, Directional Variogram, Penalized Regression Splines and Tensor Product Smooths	(Einax and Soldt 1999; Oldak, Jackson, and Pachepsky 2002; Lin et al. 2002; Mueller et al. 2004; Zhang and McGrath 2004; Diodato and Ceccarelli 2004; Hengl, Heuvelink, and Stein 2004; Liu, Wu, and Xu 2006; Pebesma 2006; Minasny and McBratney 2007; Tavares, Sousa, and Abreu 2008; Lado, Hengl, and Reuter 2008; Dafonte et al. 2010; Amirinejad et al. 2011; Sun et al. 2013; Zhang et al. 2013; Dindaroğlu 2014; Zawadzki et al. 2015; Ihl et al. 2015; Lee and Toscas 2015)
Climatic conditions and changes		(Ahrens 2005; Ashiq et al. 2010; Chen et al. 2010; Chappell et al. 2013; Sajid, Rudra, and Systematic 2013; Ahmed, Shahid, and Harun 2014; Pereira, Oliva, and Misiune 2015; Seo, Kim, and Singh 2015)
Air quality in urban areas	Ordinary Kriging, Inverse Distance Weighted, Lidar,	(Matějíček, Engst, and Jaňour 2006; Wang, Li, and Christakos 2009; Shiode and Shiode 2011) (Liao et al. 2006; Matějíček, Engst, and Jaňour 2006; Guo, Guo, and Thiart 2007; Pearce et al. 2009; Shad et al. 2009; Mercer et al. 2011; Shiode and Shiode 2011; Liu et al. 2014)
Health and Disease Mapping	Ordinary Kriging, Universal Kriging	(Berke 2004)

Case Studies

A comparison of kriging methods for spatial estimation and spatial regression revealed kriging was superior to traditional methods when it comes to modeling spatial data (Calderón 2009). Fernández-Avilés Calderón (2009) focused on crime analysis of Columbus, Ohio as a subject to compare model-driven and data-driven spatial analysis approaches and concluded that spatial interpolation methods produced a smaller margin of error.

As previously mentioned, many case studies use different interpolations not only to test strengths and flaws, but also to compare different methods as a way of examining which method is the best fit for their specific study. From the research of Meng, Liu, and Borders (2013), three case studies were used to test seven different interpolation methods. They discovered that little evidence supported the theory that OK, UK, and CK were any better at outputting predictions versus the simple deterministic methods. The only noticeable advantage to the geostatistical methods is that they took into consideration a standard deviation of error, but depending on the purpose of the analysis the deterministic interpolation methods are relatively easy to use and understand compared to the kriging methods. As previously discussed, cokriging can provide noticeable results depending on the scenario, which was the result of the third case study. Overall, the strongest evidence pointed to RK as a superior method to the other six interpolation processes.

Regression kriging has been used to analyze a variety of other scenarios, but this one was a prime example of its advantages. Through the use of both quantitative and qualitative results, Meng, Liu, and Borders (2013) were able to produce strong evidence that RK is by far the most accurate interpolation method if used with an auxiliary variable that strongly correlates with the main variable of interest. Through proper analysis using three case studies, it was possible to

show that RK and UK are very different for more reasons than the amount of variables input into the process. Also it is strongly recommended that one use RK over CK if they wish to use multivariate interpolation methods. The three case studies showed a strong, medium, and weak correlation, respectively, between the variable of interest and the auxiliary variable. Strong correlation used 4 meter resolution Ikonos imagery and attempted to interpolate a continuous surface using band 2 and 3 image pixels and resulted in an almost identical accuracy with RK, whereas as the other six interpolation methods were distorted. The second case study compared temperatures with elevation data as the auxiliary variable to provide an example of a medium correlation. In this scenario, RK provided the prediction model with the lowest standard deviation of error. Lastly, they created an example of a weak correlation by using Landsat TM band 1 and 6 with band 6 being the main variable of interest. Once again RK produced the least amount of error, but this time CK was more accurate according to the Bayes Factor. In support of these results, Hengl (2009) has come to the same conclusion about RK: It is by far the Best Linear Unbiased Predictor (BLUP) of spatial data.

Both the strengths and limitations of regression kriging are discussed by Hengl, Heuvelink, and Rossiter (2007). Three case studies are used to illustrate these aspects of RK and included the mapping of soil organic matter, the presence and absence of yew, and land surface temperatures. RK's strength lies in the fact that it allows for a broader spectrum of regression techniques to be used with the method and also allows the separation of two interpolated components for better interpolation. A limitation found with RK is that the analyst must construct the prediction map through the use of a variety of different software environments, GIS and stochastic (Hengl, Heuvelink, and Rossiter 2007).

Goovaerts (1999) used multiple kriging methods to map soil's erosive values based on monthly and annual rainfall data with three kriging methods: "simple kriging with varying local means (SKlm), kriging with an external drift (KED), and collocated cokriging (CK)" (Goovaerts 1999, 227). All of the different geostatistical algorithms used in this study had their pros and cons, but with the introduction of elevation data into the interpolation process the cokriging method was found to provide the best results. Through the proper use of the semivariogram model within CK, the elevation data can be directly integrated into the continuous surface instead of computing them separately (Goovaerts 1999).

In order to account for the limitations brought up by previously discussed journals, Wang and Zhu (2015) used various kriging methods and a multi-fractal analysis to compensate for kriging's inability to analyze local trend variations due to average smoothing effects. So with the use of spatial autocorrelation, cross-validation, and multi-fractal analysis they were able to depict local anomalies with greater accuracy (Wang and Zhu 2015). For the sake of this experiment, boreholes of soil were used as the sample sites for the analysis. A variety of kriging methods were used, but the multi-fractal kriging had an advantage at more accurately evaluating the local abnormalities. Among the traditional methods of kriging, cokriging was found to produce greater results due to the high-inter-correlation.

Another adapted kriging method is presented by Skøien, Merz, and Blöschl (2005) as a method that can be used to interpolate streamflow-related variables called Top-kriging, also known as topological kriging. This method is tested on the 100-year flood scenario for two Austrian regions and allows them to conclude the practicality of this method on stream-flow related variables such as flow temperature, mean annual discharge, flood characteristics, low flow characteristics, concentrations, and turbidity.

From the various case studies discussed it is apparent that alone, kriging has limitations such as smoothing, which leads to local variation discrepancies. However, studies have revealed possible ways of compensating for limitations by combining GIS methods with traditional statistical models and external programs, such as SPSS and R (Knotters, Brus, and Oude Voshaar 1995; Goovaerts 1999; Hengl, Heuvelink, and Stein 2003, 2004; Skøien, Merz, and Blöschl 2005; Hengl, Heuvelink, and Rossiter 2007; Liu, Kyriakidis, and Goodchild 2008; Calderón 2009; Wang, Li, and Christakos 2009; Hengl et al. 2009; Zhang et al. 2013; Meng, Liu, and Borders 2013; Seo, Kim, and Singh 2015).

One particular form of this combined endeavor is known as regression kriging and has been used throughout a variety of case studies and articles to more accurately produce interpolated surfaces (Knotters, Brus, and Oude Voshaar 1995; Hengl, Heuvelink, and Stein 2003, 2004; Hengl, Heuvelink, and Rossiter 2007; Liu, Kyriakidis, and Goodchild 2008; Calderón 2009; Hengl et al. 2009; Meng, Liu, and Borders 2013; Zhang et al. 2013; Seo, Kim, and Singh 2015). Without the multivariate regression applied to the kriging process it was assessed that deterministic interpolation methods provide a much easier to use and interpret output compared to the more complex stochastic interpolation methods such as OK, UK, and CK (Meng, Liu, and Borders 2013).

Testing a New Geospatial Kriging Methodology to Detect I/I

This thesis proposes a new method utilizing geospatial and geostatistical analysis through kriging to identify potential locations of vulnerability within a wastewater treatment network/collection system. This study will focus on the Minneapolis-St. Paul metropolitan area in Minnesota to test the proposed method (Figure 6). For 75 years the Metropolitan Council

Environmental Services (MCES) has been treating wastewater in Minneapolis and St. Paul. The MCES consists of seven Wastewater Treatment Facilities (WWTF) and over 600 miles of sewer pipes, they referred to as interceptors, that intersect 107 communities sewer networks around the metro area. These plants and sewer systems transport 251 million gallons of wastewater per day and treat approximately 75% of the metro areas wastewater (Metropolitan Council of the Twin Cities 2011). The vast area and age of the sewers has often led to problematic issues related to I/I, which are now in need of a more effective way to focus rehabilitation efforts of the sanitary sewers. Over the course of the next 20 years, wastewater infrastructure repair could cost upwards of 4.1 billion dollars in Minneapolis-St.Paul Metropolitan area (Metropolitan Council of the Twin Cities 2011).

On a positive note, infiltration and inflow derived from precipitation can be an indicator of sewer deterioration or can provide insight into the severity of sewer system defects (Zhang 2007, 2008; Shelton et al. 2011). By properly understanding and utilizing RDII, it is possible to be proactive with rehabilitation efforts to increase sewer system functionality, prevent sanitary sewer overflows (SSO), and reduce substantial expenditures (Zhang 2005, 2007, 2008; Karpf and Krebs 2011; Shelton et al. 2011).

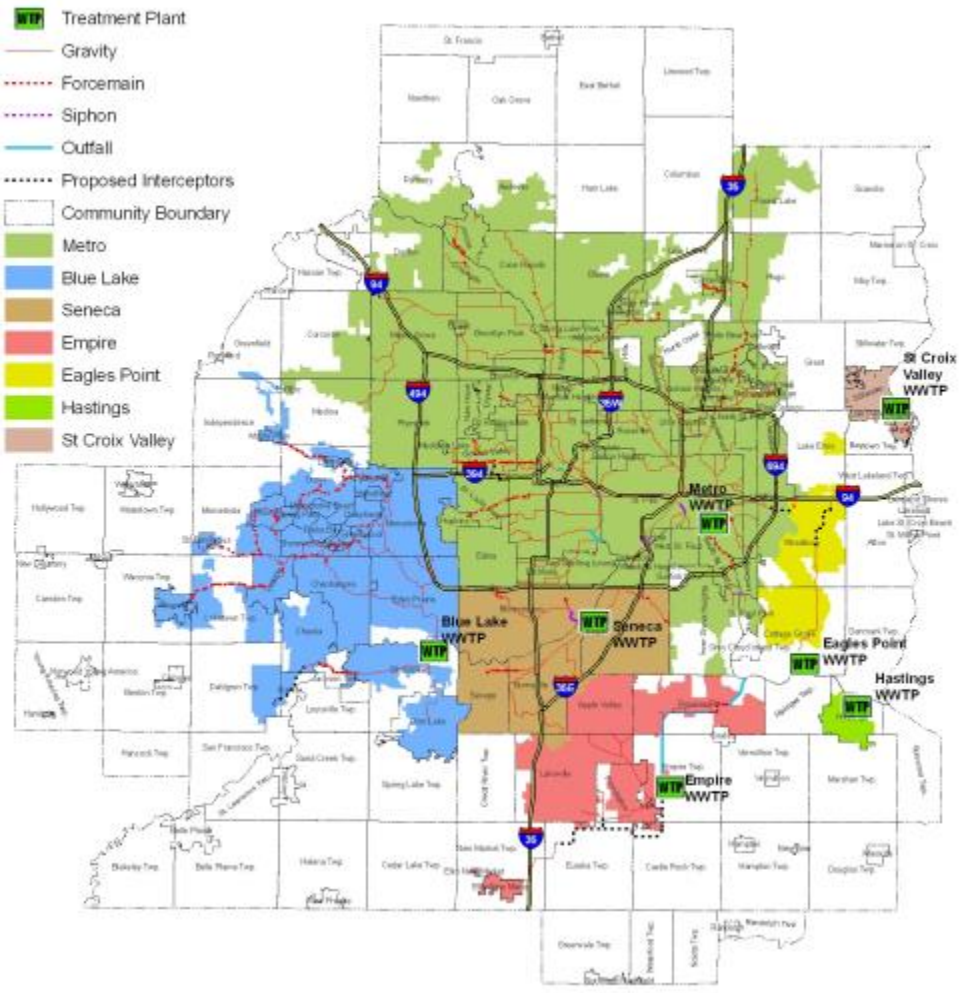

Figure 6. The Metropolitan Council Environmental Service is accountable for the seven county metro area of the Twin Cities, MN (Metropolitan Council of the Twin Cities 2011).

The MCES has used CCTV for most of their interceptor system and has done inch-by-inch inspection for I/I. In addition, engineers assess and score every section of pipe by conducting dye and smoke testing, as well as monitoring flow conditions by comparing rainfall data versus average and max discharge measurements. However, MCES does not have detailed information on the cities collection systems that connect to their interceptors and this can be a major contributor to I/I. The use of ArcGIS and geostatistics can potentially assist in identifying areas of high I/I risk, as there is a need to prioritize high-risk areas before they become extremely damaging and the price of repair increases (Shelton et. al., 2011). If successful, the method tested in this thesis provides a geospatial/geostatistical means for identifying I/I prone areas of the

collection systems that are not monitored, determining where I/I is occurring, and determining the magnitude of I/I is in those areas.

A variety of interpolation methods can be used to create these continuous surfaces and one in particular, kriging, stands out among the rest (Johnston et al. 2001; Hengl 2009; Oliver and Webster 2014). Kriging is not like most interpolation methods as it produces a surface based off of mathematical and stochastic functions that deterministic methods overlook (Johnston et al. 2001; Hengl, Heuvelink, and Rossiter 2007; Hengl 2009). From this stochastic approach, kriging is able to assess uncertainty in the values produced from the analytical process (Mitas and Mitasova 1999; Johnston et al. 2001; Hengl 2009; Oliver and Webster 2014). Kriging provides a large potential for analysis and has a wide array of applications, but the true limitations of its capabilities are still up for debate. We seek to assess the potential of this method by researching and answering these questions:

1) Is it practical, efficient, and effective to assess spatial patterns of infiltration and inflow of rain water by creating a continuous surface to analyze a network of subterranean linear features?
2) Can kriging be modelled to accurately assess small changes in variation across the landscape or does the interpolation mask small variability?
3) Does Kriging provide accurate insight into the I/I problem as a whole or what aspect of I/I is being displayed in the Twin Cities Metro area case study?

These questions will allow me to evaluate whether or not kriging and geospatial analysis can more efficiently identify spatial variability of I/I problems in wastewater infrastructure.

It is also necessary for a defined interval between rainfall events to accurately differentiate the various components of I/I as completed by Staufer, Scheidegger, and

Rieckermann (2012). In their case study they separated rainfall events based on the length of the dry periods, and the minimum duration necessary to be classified as a dry period was four hours.

Overall various stochastic methods, including linear regression (Zhang 2005; Staufer, Scheidegger, and Rieckermann 2012), least squares (Karpf and Krebs 2011), and other equations (De Bénédittis and Bertrand-Krajewski 2005; Zhang 2007, 2008) have been used to identify I/I and estimate its quantity. Zhang (2005) mentions that for an optimal analysis of I/I one must consider the data size being used, the time/season in which the data was collected, wetness index of the soil, groundwater level, and a few other stochastic variables that can all greatly alter the results of how much I/I enters the system. In order to further develop improved monitoring methods for locating areas of I/I susceptibility, proper use of these variables and innovative ways to implement them into various other disciplines is the next step. This is a never ending problem with the inevitable deterioration of wastewater water treatment infrastructure, but these methods help to locate and reduce to the negative effects I/I can have on the surrounding infrastructure, environment, and economies.

Methods

To begin the analysis the Meter shapefile and the July 13, 2013 I/I Flow Exception Report were acquired from the Metropolitan Council Environmental Services (MCES). Included in these datasets were readings from every flow meter in the seven county metropolitan areas. The data included Community Name, Average Flow, Max Flow Time, Max Flow (MGD: million gallons per day), Allowable Peak, Pct (Percent) Cap Used, and Rainfall. MCES changed max flow (MGD) to max flow (GPM: gallons per minute) in the 2016 I/I Flow Exception Reports. Each meter's average annual flow is based off of ten year average flow rates and each meter

provides peak flows that occur at different times during the rainfall period. It is also important to note percent cap used is the percentage of each municipalities allotted "I/I goal" used, which is calculated using past flow data (10 year average), is adjusted for growth, and allows for standard peaking factor. The major precipitation event from July 11-13, 2013 was used to optimize the workflow and kriging process in ArcMap 10.3 to determine the ideal method properties, semivariogram modeling, searching neighborhood, and scale (Figure 7).

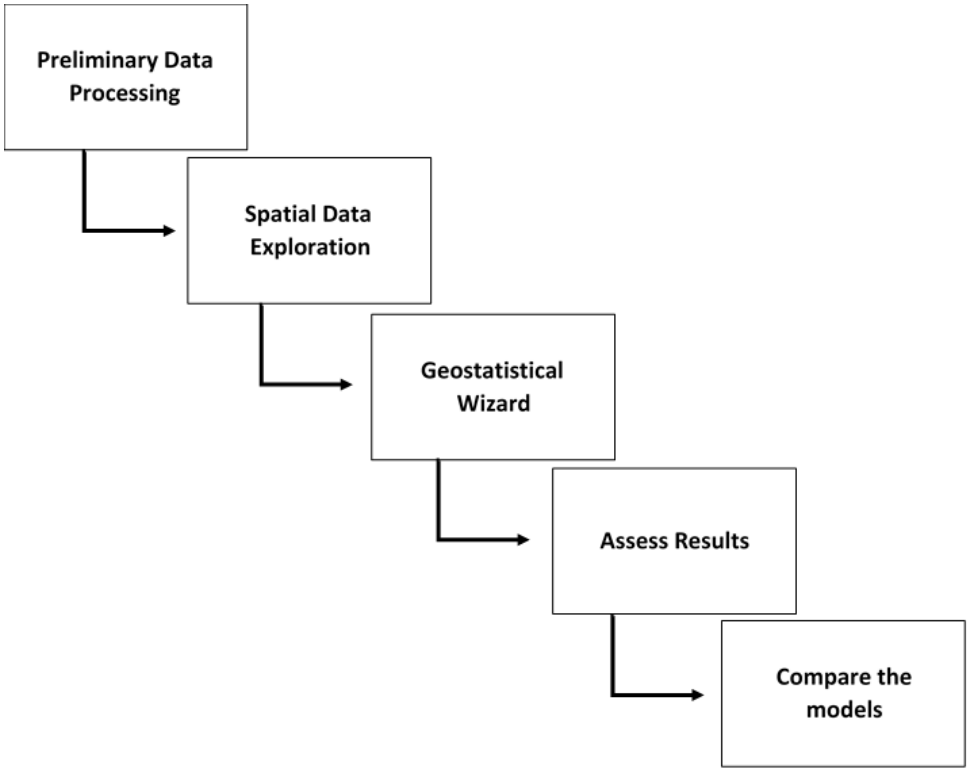

Figure 7. The Geostatistical Analysis workflow for this case study.

Preliminary Data Processing

Max Flow (MGD) and Average Flow were the primary values used to calculate the effects of I/I using an Excel spreadsheet. There were originally 202 meters in the meter shapefile, but after joining with the flow data for each rainfall event in ArcMap that number decrease. Five

meters and three effluent meters were permanently excluded from the original sample because they were on small isolated Wastewater Treatment Facilities (WWTF) networks that are over eight miles from any other meter. These meters were removed to prevent the lack of data in these regions from skewing the surface result predictions.

Flow data from a large precipitation event was recorded on July 11-13, 2013 and was utilized as a case study for this analysis. It must be noted that out of the 202 meters in the meter shapefile, only 136 meters were utilized when processing the July 13, 2013 I/I Flow Exception Report. This decrease resulted from meter discrepancies, performance meters not used in the I/I program, the occurrence of multiple meters at the same location, and manual adjustments made by the MCES's Data Analyst. Flow data discrepancies include meter malfunctioning, overflow, or calibration issues.

The MCES's Data Analyst reviewed the I/I Flow Exception Report for discrepancies and created a table that was compatible with ArcGIS. A new "Meter" label field was added to the table document in order to join the table data to the Meter shapefile via the meter shapefile's label field. Lastly, all of the I/I equations were processed in the table before joining the table and the Meter shapefile in ArcMap. Four new fields were created: Flow Increase, Percentage Flow Increase, RDII (Rain-Derived Infiltration and Inflow) Contribution, and RDII Severity.

Flow increase was calculated by dividing the Max Flow (MGD) by the Average Flow. The output signified how much the flow surged during the rainfall event compared to the ten year average flow. If the results displayed anything greater than one, then there was an increase in flow from the average ten year flow. If the results were one or less, then it signified reduced

flow from the average flow. Percentage Flow Increase is the flow increase times 100 to produce the percentage of the flow increase.

Shelton et al. (2011) compared dry day flows to wet day flows to determine the ratio, contribution, and severity of Rain-Derived Infiltration and Inflow (RDII). This equation was also utilized to determine if their flux stability equations would provide different geostatistical results. Using the data provided, it was possible to replicate their work using Max Flow (wet day flows) and the Average Flows (which consist of dry and wet days). RDII Contribution was derived from Max Flow (MGD) minus Average Flow. Then RDII Severity was derived from RDII Contribution divided by Average Flow.

Finally, the Meter shapefile was joined to the I/I Flow Exception Report excel in ArcMap and "only keep matching records" was selected to remove the zero values on the kriging process. A new Meter shapefile was created from this to have a permanent shapefile with the flow data included. The western and metro WWTF networks were queried from the new Meter shapefile and exported so analysis could be done to determine local trends in those regions. There are three key steps to the geostatistical process: exploratory spatial data analysis, structural analysis, and surface prediction and assessment of results.

Spatial Data Exploration

Before using the Geostatistical Wizard, it is crucial to understand the dataset by using the exploratory spatial data analysis tools within the Geostatistical Analyst extension in ArcMap. Exploring the data allows the analyst to observe any errors in the sample dataset, global and local outliers, distribution of the points, identification of potential trends, and spatial autocorrelation.

The following attributes from the Meter shapefile were used in the exploratory tools: Flow_Increase, Percentage Flow Increase, and RDII_Severity.

First, a histogram was created to determine whether the data was normally distributed or skewed. Important features on a histogram include the dissemination of the central values, spread, and symmetry. A bell curve (or close mean and median values) indicates the data is normally distributed and will provide the best results for most interpolation methods, especially for deterministic methods (Figure 8). However, if the data is skewed, a histogram can be used to test transformations to normalize the dataset. The three transformations found in geostatistics include Box-Cox, arcsine, and log transformations (Johnston et al. 2001). Most kriging methods can make accurate predictions using randomly distributed data due to the cross validation process. On the other hand, the dataset must be normally distributed for quantile and probability kriging. Another Meter shapefile was created for the interpolation process based on the removal of major outliers higher than the 4^{th} quantile in the histogram. This was used to reveal the influence of the 11 anomalies' excessive values on the prediction surface.

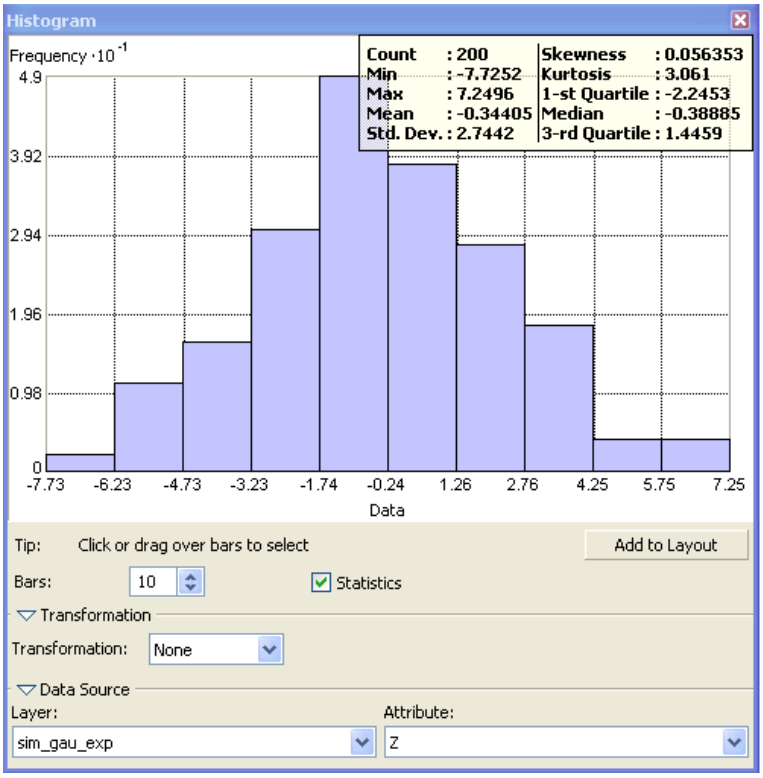

Figure 8. A histogram with normal distribution (or bell curve) (ArcGIS 10.3.1 Help).

The second method involved a Normal QQPlot that is used to determine how close the distribution of the dataset is to the standard normal distribution (Johnston et al., 2001) Points clustering around the line in a QQPlot indicate the level of distribution. So the closer the points follow the average line the better the normal distribution and the further they curve away from the average line the more randomly distributed the dataset (Figure 9). The histogram and QQPlot allow for easy identification of outliers in the dataset for further investigation. This can be accomplished by highlighting the outliers on the graphs and it will highlight them in ArcMap.

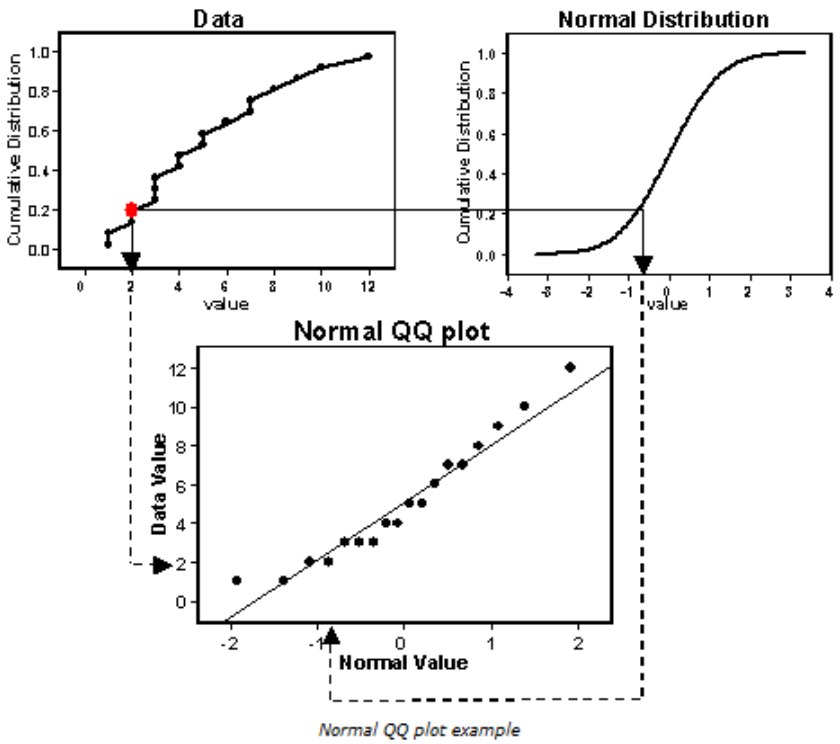

Figure 9. A Normal QQPlot with standard normal distribution (ArcGIS 10.3.1 Help).

Next, a Global Trend Analysis was performed to determine if the data follows a global (nonrandom) trend that could potentially influence the primary focus, such as the slope of a valley (Johnston et al., 2001). Removal of the global trend leaves only the residual trends to be modelled and reapplied after interpolation, further enhancing the interpolation process. This allowed for the analysis of short-range variations in the output surface without overall trend influence, which creates a more realistic prediction. The Global Trend Analysis, as seen in Figure 10, depicts a vertical stick at varying heights that are attuned to that data point's value. Along the east-west and north-south planes, lines will project any trends found in the data. Rotation of the planes is also possible to better grasp directional influences of the data also known as anisotropy.

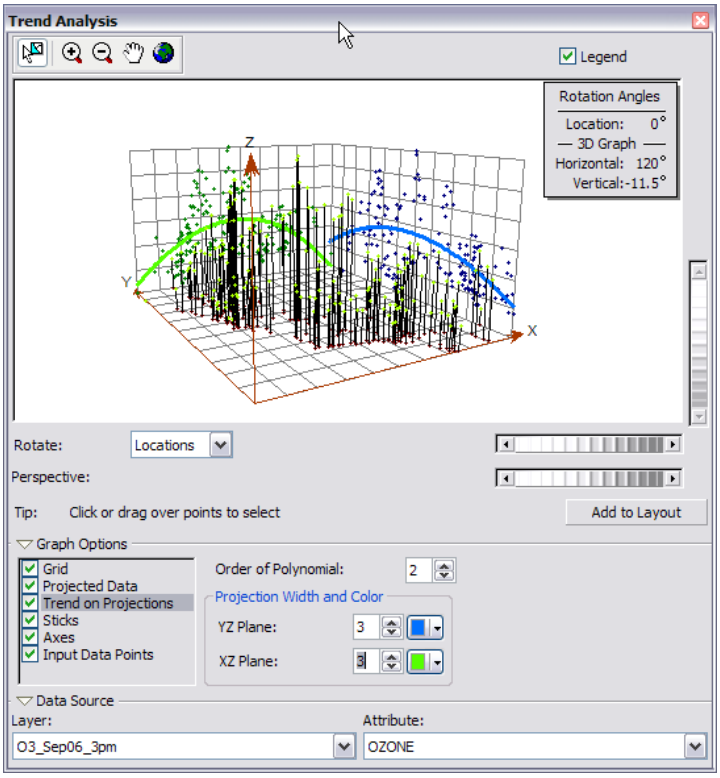

Figure 10. A Global Trend Analysis with a strong trend on both the north-south and east-west planes creating an inverted "U" shape (ArcGIS 10.3.1 Help).

Lastly, it was necessary to understand the spatial autocorrelation between each sample point in the dataset, which was possible by observing the Semivariogram/Covariance Cloud. Spatial autocorrelation assumes that points closer to one another are more alike and as the distance between sample points increases so does the difference in their values (Johnston et al., 2001). The semivariogram/covariance cloud depicts this trend by pairing every point in the analysis and measuring their distance from one another (x-axis) compared with their similarity in values (y-axis) (Figure 11). This is known as binning and depending on the lag size and number of lags it can affect the influence on each point on one another when modeling the data. The lag size has a significant impact on the semivariogram because it is the line that separates two locations. If it is too large then small autocorrelation may be overlooked; whereas if the lag size is too small then it will not correctly portray the averages of the bins. For an irregular or random

sampling scheme, the Average Nearest Neighbor tool can be used to determine a good lag size. Then the number of lags can be set to half the largest distance among all sample points. The semivariogram cloud should be clustered together towards the left side of the x-axis (the closest distance between points) and the bottom of the y-axis (greatest similarity between the points). Search direction can be selected to verify directional influences found in the Global Trend Analysis.

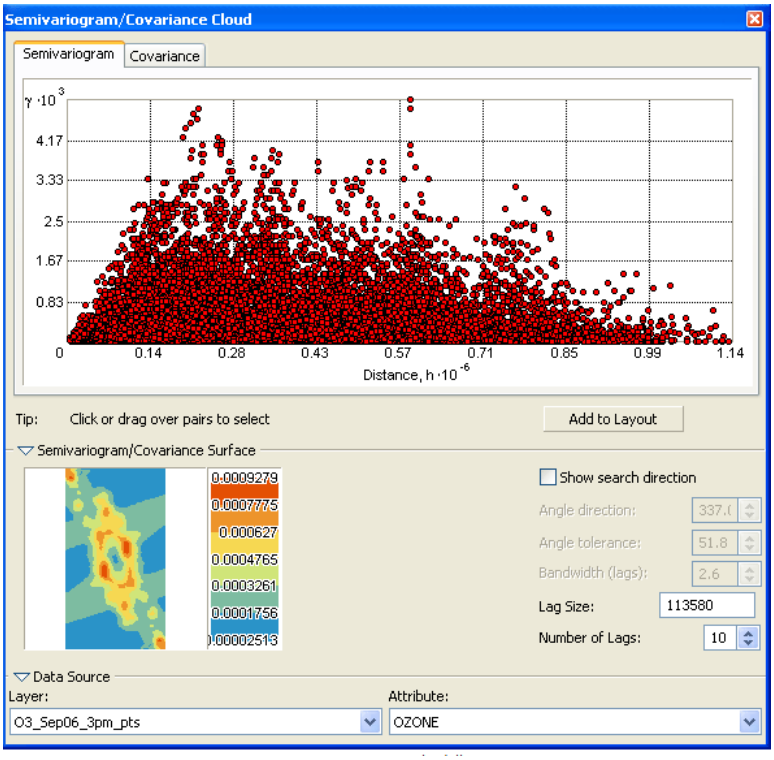

Figure 11. A Semivariogram/Covariance Cloud with a strong spatial autocorrelation towards the left x-axis and bottom of the y-axis. Every point represents the relationship between two point distance (x-axis) from one another and difference in values (y-axis) (ArcGIS 10.3.1 Help).

Geostatistical Wizard

The first step after exploring the spatial data for influential factors like global trends and normal or random distribution was to complete a structural analysis. This part pertained to creating a model that would produce minimal residual error based on the assumptions we can

make about the data. The modeling was completed in ArcMap's Geostatistical Wizard, which is a user friendly interface designed to help novice to advanced geostatistical users create accurate interpolated surfaces. By using sample points from a variety of locations in an area of interest, it is possible to examine the relationship between each point and create a continuous surface that accurately portrays real world aspects. However, unlike deterministic methods, the Geostatistical Wizard produces standard errors or uncertainty results for the interpolated surface, so it is possible to gauge the accuracy of the model.

The creation of a continuous modeled surface using default settings within the Geostatistical Wizard is a straightforward process. Initially, default prediction surface maps of the July 13, 2013 precipitation event were created by running the Geostatistical Wizard through multiple iterations utilizing the meter shapefile as the "Source Dataset" along with Flow Increase as the "Data Field" (Figure 12). Ordinary Kriging and Universal Kriging were used to create the default prediction surfaces. No adjustments were made to the model so a comparison between the generic prediction surface and modelled prediction surface could be conducted.

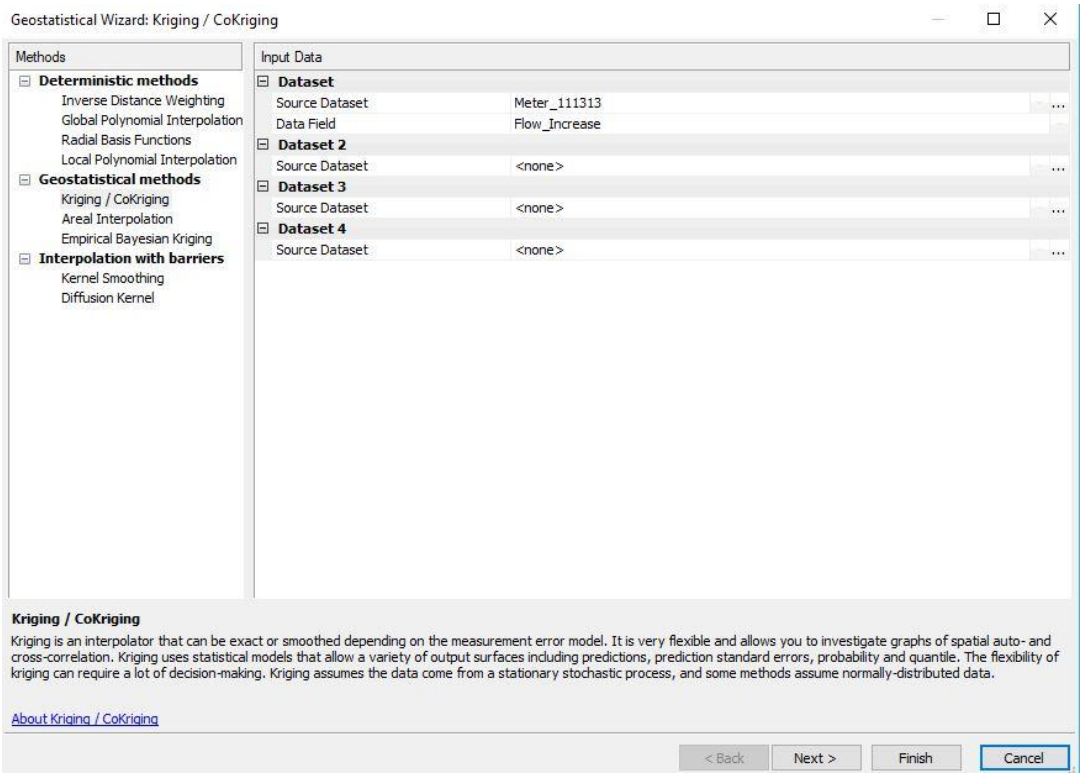

Figure 12. Step 1 of Geostatistical wizard involves selection of the interpolation method, the source dataset, and data field.

Next, the interpolation process was modelled to take into consideration any trends or directional influences found in the phenomenon. This was based off the information derived from the previous spatial data exploration. The second step after selecting the source dataset and data field was to select the kriging type, output surface type, and select any transformations or order of trend removals necessary based on the data exploration (Figure 13). Universal kriging follows a more deterministic trend that attempts to determine error based on a polynomial regression; whereas ordinary kriging follows an unknown constant mean in the data (Johnston et al., 2001). For this case study universal kriging and ordinary kriging were used in this study to compare which model would provide the best prediction.

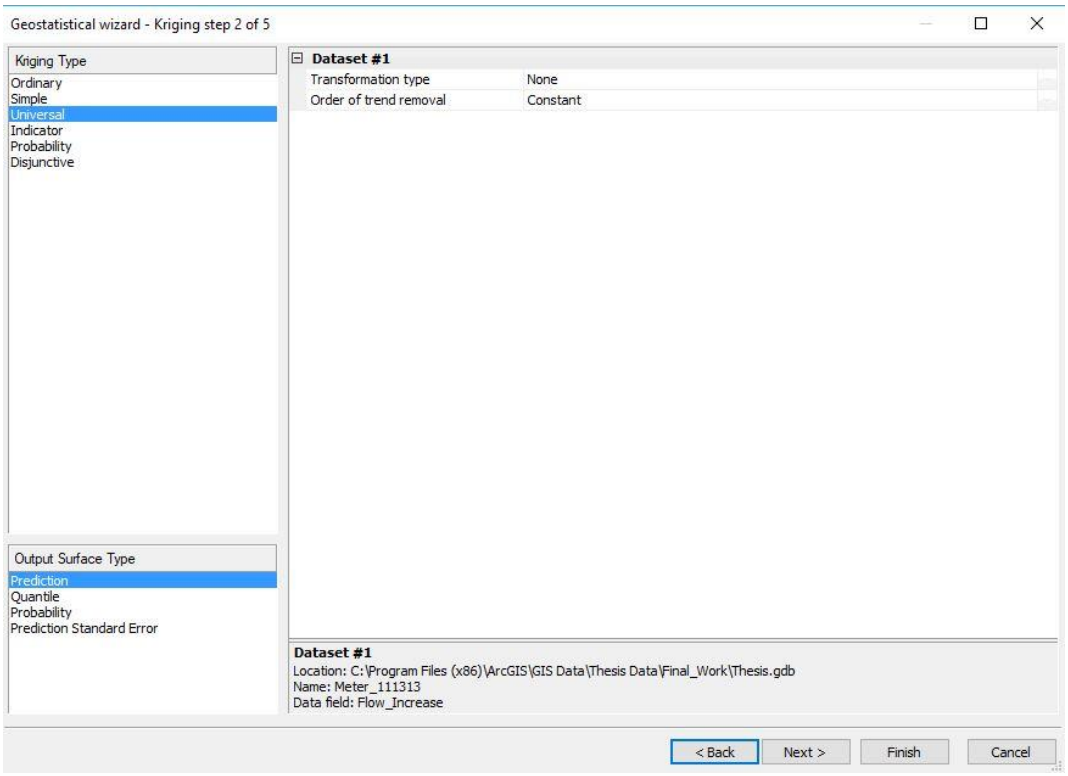

Figure 13. Step 2 of Geostatistical wizard involves the selection of the Kriging Type, Output Surface Type, and any transformations or trend removal.

The following transformations and trends were used during the various iterations to produce the best results. Flow Increase was the only attribute transformed using a lognormal transformation due to the results of the exploratory analysis whereas RDII Severity was not able to be transformed. Ordinary kriging was processed using the second order polynomial trend removal compared to no trend removal. Universal kriging separately tested the application of first order and second order polynomial trend removals, while also transforming the data with a lognormal transformation.

The next step in the kriging process was to adjust the Method Properties, which was only an option for universal kriging (Figure 14). This step was used as a way to preview the final output before completing the model. No adjustments were made during the first iteration, while

the second iteration took into account the cross validation statistics process. The optimize model tool for the method properties step determines the best Bandwidths, Spatial Condition Number, and Search Neighborhood based on cross validation statistics of the dataset.

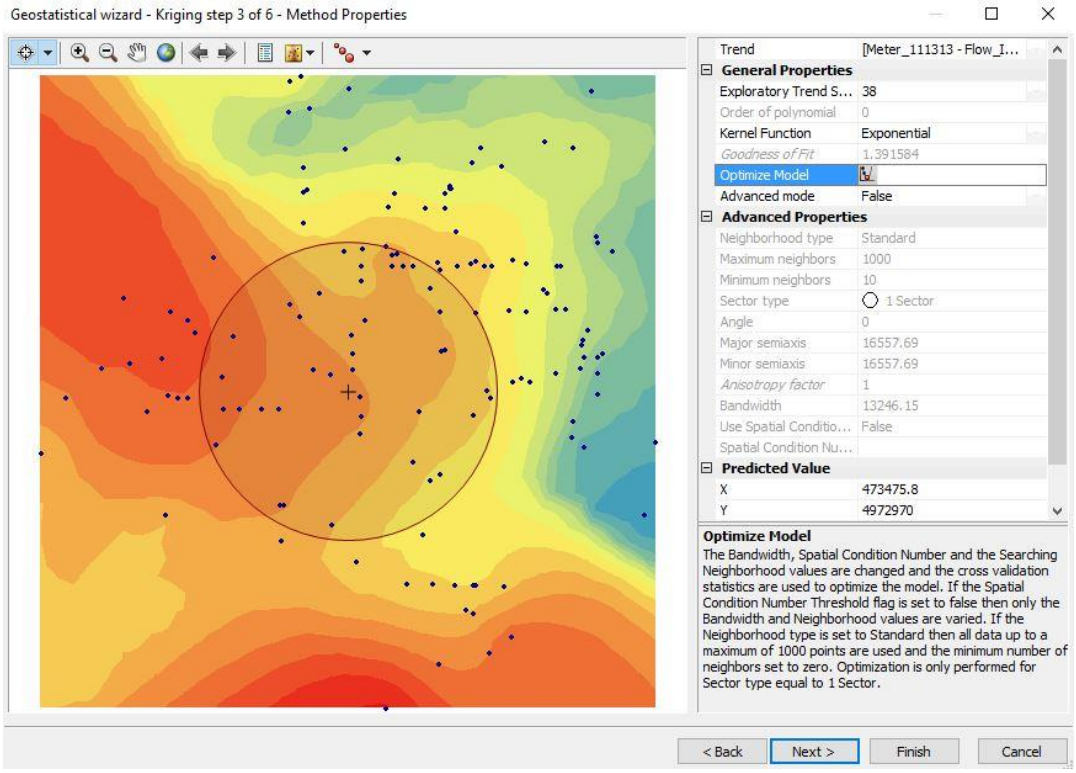

Figure 14. Step 3 of Universal Kriging in the Geostatistical wizard: Method Properties. Provides a preview screen of the output prediction surface.

Following the Method Properties step was the Semivariogram/Covariance Modeling step of the kriging process (Figure 15). This was crucial to determine the best fit of the model so that the line passes through a majority of the points in the semivariogram (Johnston et al., 2001). The Semivariogram/Covariance requires trial and error by adjusting key parameters in order to create the best model. This is necessary to accurately depict the autocorrelation of the datasets values versus the distance between them. Important parameters to understand for the semivariogram include anisotropy, range, sill, partial sill, nugget, and lag size (Johnston et al. 2001) (Figure 16 displaying these key parameters).

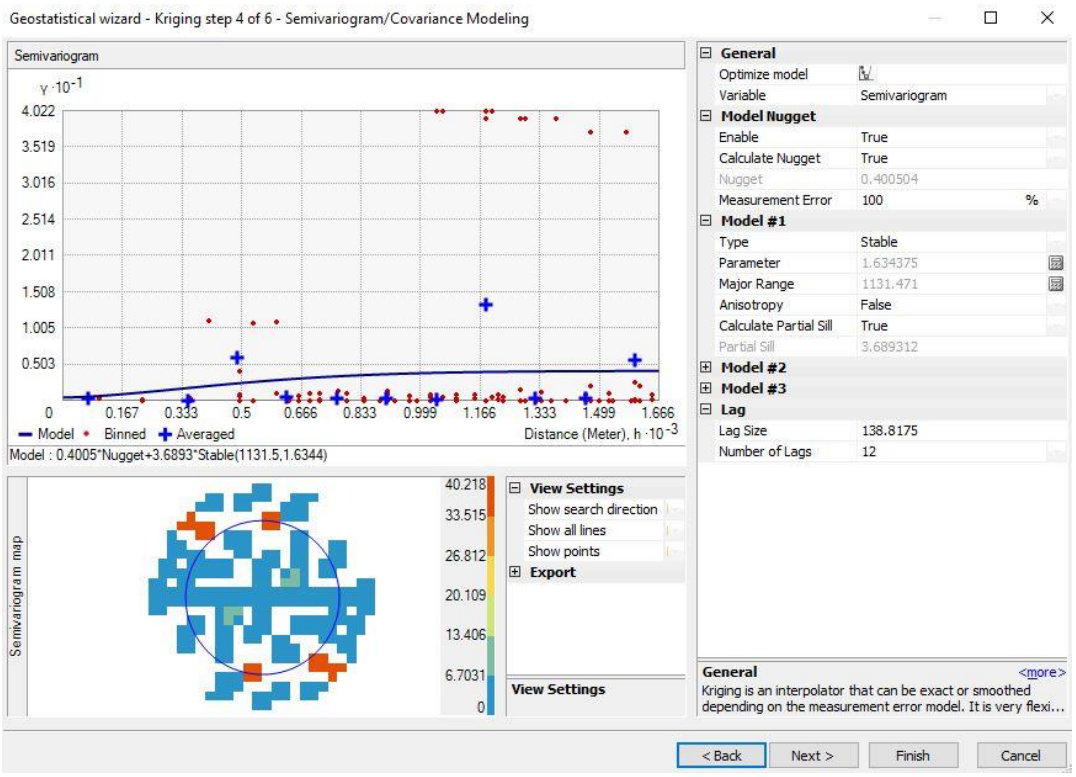

Figure 15. Step 4 of Geostatistical Wizard: Semivariogram Modelling includes key parameters, like anisotropy, range, sill, partial sill, nugget, and lag size, can be adjusted to create an optimal Semivariogram model.

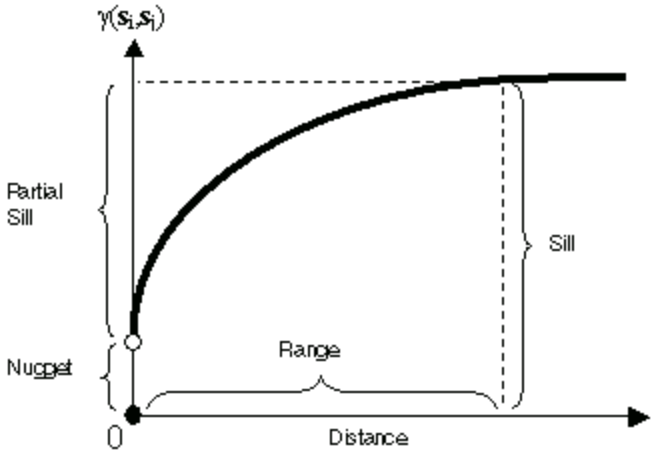

Figure 16. Key parameters of the semivariogram: anisotropy, range, sill, partial sill, nugget, and lag size. All these values directly affect the semivariogram and the output prediction surface (ArcGIS 10.3.1 Help).

Anisotropy is defined as spatial dependence (autocorrelation) of both distance and direction between locations found in data or spatial processes (Johnston et al. 2001). The range in a semivariogram/covariance model is a distance beyond which little to no autocorrelation exists between variables. Sill represents the value where the distance between points is too far apart for the model. Nugget represents details that are too fine to detect and may be smoothed out leading to independent error, measurement error, and/or microscale variations (Johnston et al. 2001). Lastly, an optimal lag size is necessary to group pairs of locations so that the number of possible combinations is reduced. This is also referred to as binning and can greatly assist in revealing spatial correlations. The first iteration was left to the default parameters, while the second iterations utilized the optimize model tool again. However, for the semivariogram/covariance modeling it optimized the key parameters via cross validation to select the best range parameter for the model. Other attempts adjusted the anisotropy, lag size, and number of lag sizes to try and create a more accurate model based off of numbers tested in exploratory analysis of the semivariogram.

The last adjustable step is the Searching Neighborhood step which allows the user to adjust the influential weight of each point on the surrounding points (Figure 17). The Cross Validation interface that follows the Searching Neighborhood step breaks down the prediction errors of the model for estimating unknown values (Figure 18). The term "prediction errors" refers to how well the model estimates omitted known values using the surrounding known values via interpolation. This cross validation process reveals how much error is found in the prediction. The Geostatistical Wizard allows for going back and forth between steps to reduce the error in the model. On the Cross Validation screen, optimal mean error should be near zero, root-mean-square (RMS) error and average standard error should be as small as possible relative

to other models, and root-mean-square standardized should be as close to one as possible. It is important to note that the negative values for mean error and various others are a script error that causes the sign to flip in the case of a loss function where low is good.

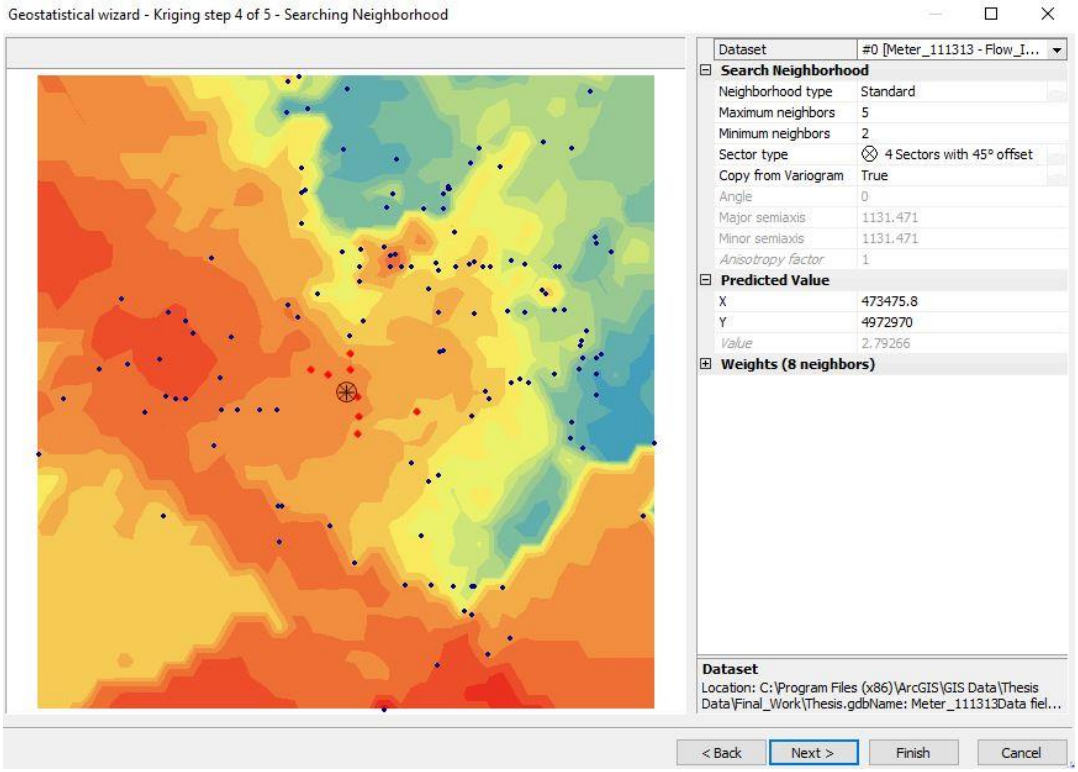

Figure 17. Step 5 of Geostatistical wizard: Search Neighborhood. This step allows the user to adjust the influential radius of each point's value on interpolation process.

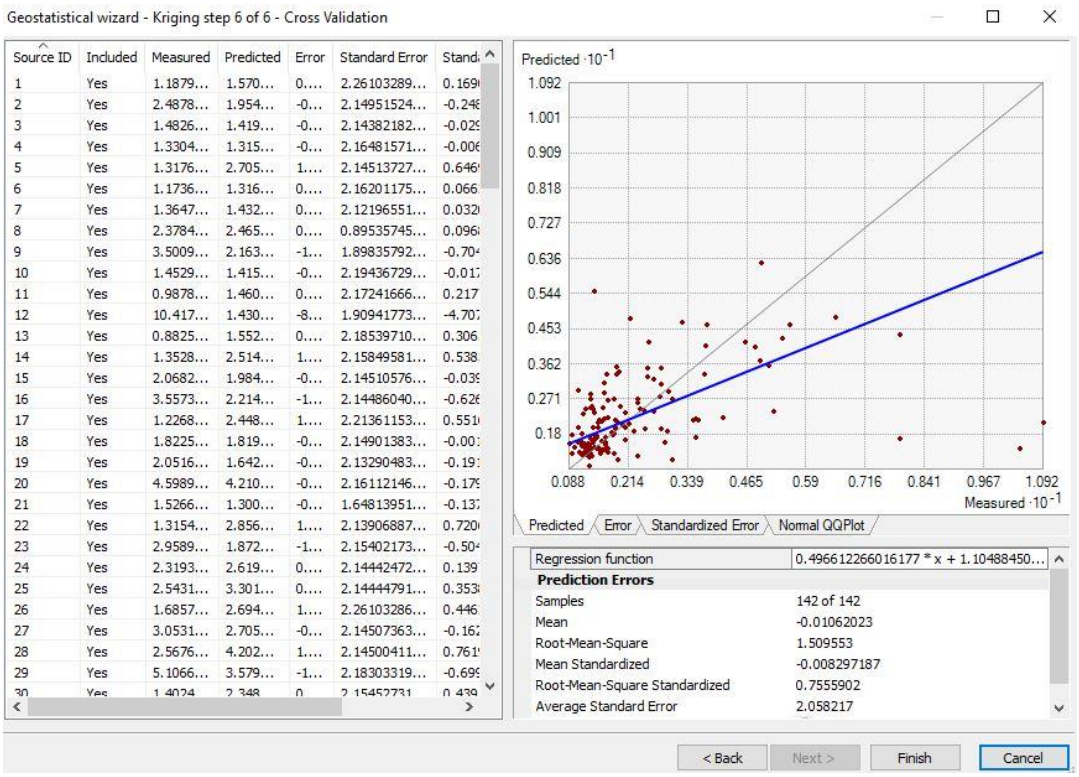

Figure 18. Step 6 of Geostatistical Wizard: Cross Validation Prediction Error Report. This step calculates prediction error due to cross validation to determine the effectiveness of the output prediction surface.

After the prediction error was deemed suitable to produce an accurate output the model was finished and then the final stage could begin: surface prediction and assessment of the results. It is possible to compare prediction errors between each prediction surface by right clicking on the kriging output you want to compare in the table of contents and selecting "Compare…". This opens a new user interface that allows easy comparison of models one at a time, side by side (Figure 19). When comparing models, it is important to have the optimal prediction error values previously discussed, except when comparing models the smaller RMS and the average standard error that is closer to RMS error is the better model (Johnston et al. 2001).

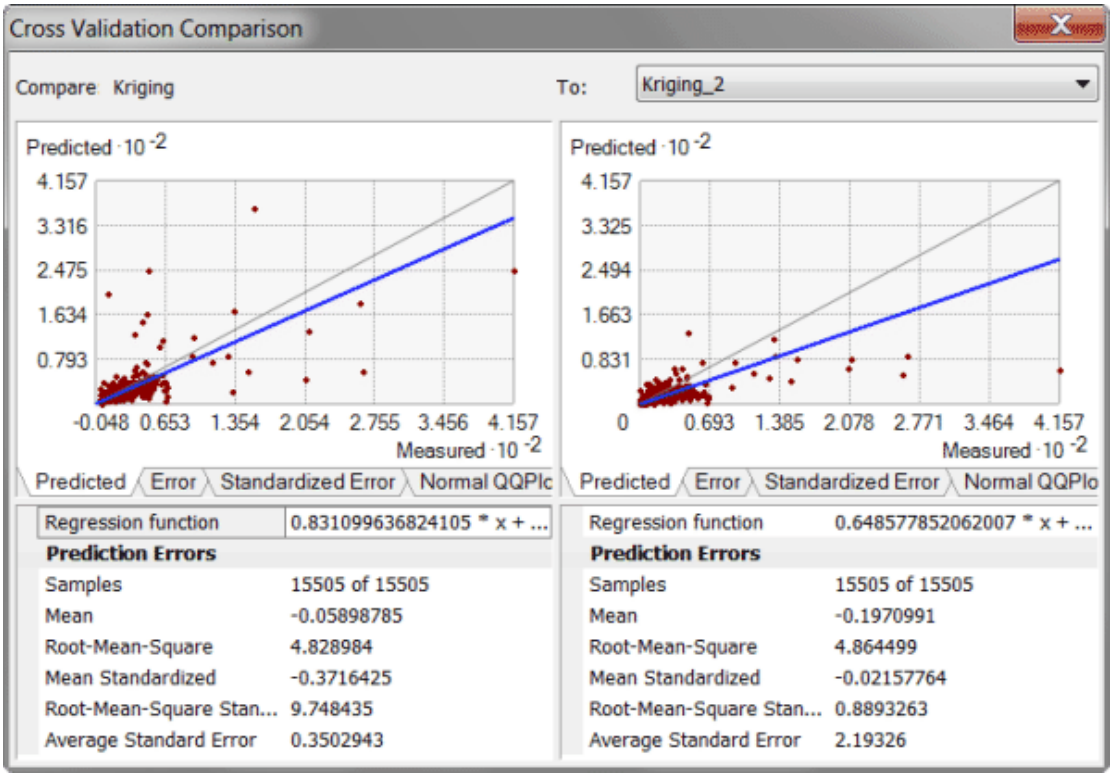

Figure 19. Cross Validation Comparison of two model's prediction errors to determine which one has the best statistical results for the interpolation process.

Alternate Analysis

The previous workflow was employed for the Rainfall attribute to create continuous prediction surfaces for a visual correlation between Flow Increase prediction surfaces and the Rainfall prediction surfaces. The overall workflow was completed for 14 precipitation events that were tracked during 2016 rainfall. Flow Increase was the primary attribute of interpolation with Rainfall maps for reference.

Cokriging and Probability (Threshold) Kriging were also considered as ways to better display the I/I dilemma. Cokriging utilized Flow Increase as the primary variable of interest and Rainfall as the secondary variable. The Probability Kriging utilized the Percent Cap Used attribute that MCES uses as a gauge based each municipality's I/I goal.

Cokriging follows the same procedure previously discussed via the Geostatistical wizard. The cokriging process is known to have more options for customization since it takes in to consideration multiple variables when modelling and creating a prediction surface. Optimal settings were selected for cokriging based on the previous exploratory analysis and universal kriging process. The first iteration utilized default setting and the second iteration consisted of trial and error to reduce prediction error.

Probability Kriging was considered since MCES already has a threshold (%) designated for each community. The meter shapefile for July 13, 2013 was selected as the input and the Percent Cap Used was selected for the Data Field. Step two consisted of selecting Universal as the Kriging Type, Output Surface Type was changed from Prediction to Probability, transformation type was set to a log transformation type to normalize the distribution, and the threshold value was set to indicate variables if they exceed 100% of their Percent Cap Used (Figure 20). Default settings were selected for the first iteration and the second iteration was optimized using the optimize model buttons for step three and four.

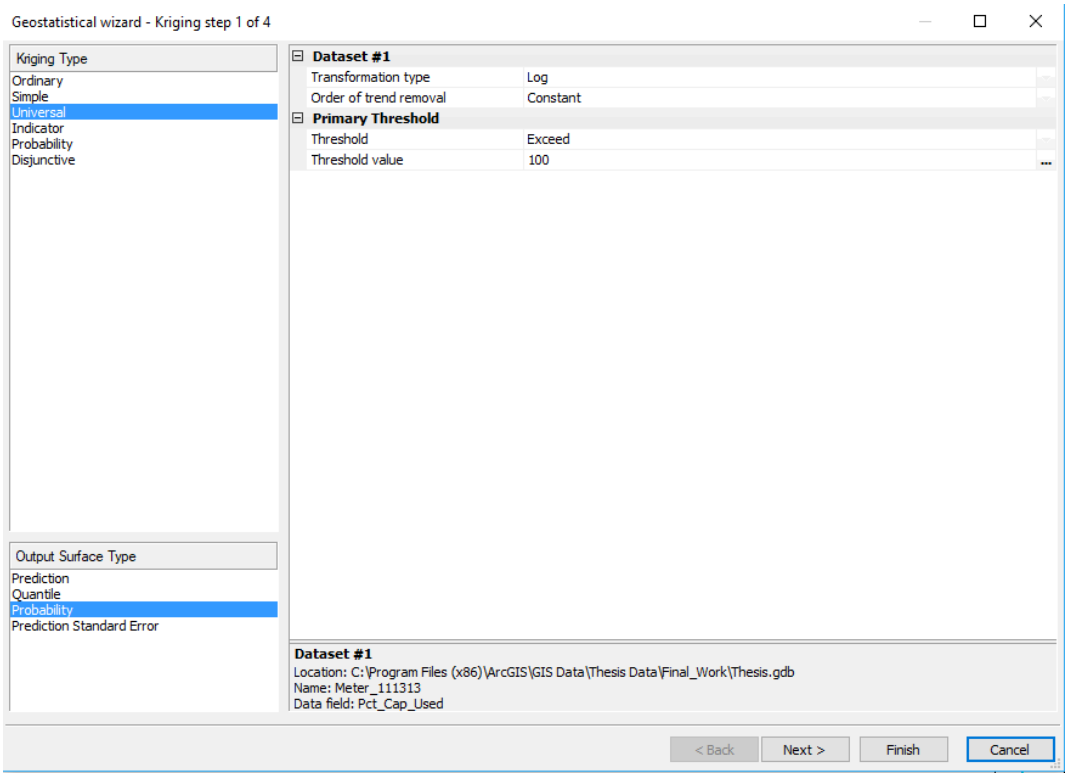

Figure 20. Probability kriging setup step is used to designate any transformations or trend removal, but more importantly designate the threshold for the binary split of the dataset.

Results

Exploratory Spatial Data Analysis

The use of the histogram revealed a random distribution of the points and data values for the July 13, 2013 flow data with a majority of the data falling in the first quantile of the dataset (Figure 21). The symmetrical distribution of the data observed in Figure 21 was positively skewed since there was a long right tail of quantiles due to the major outliers. All of the flow meters had at some amount of flow increase during the rainfall event, but this may be due to a variety of factors (Table 3). The majority of the dataset fell into the first three quantiles, while the rest were outliers in the quantiles four to ten. These major outliers are the values related to

the drastic increase in flow at their respective flow meter. They are a vital part to the analysis as they represent areas susceptible to I/I.

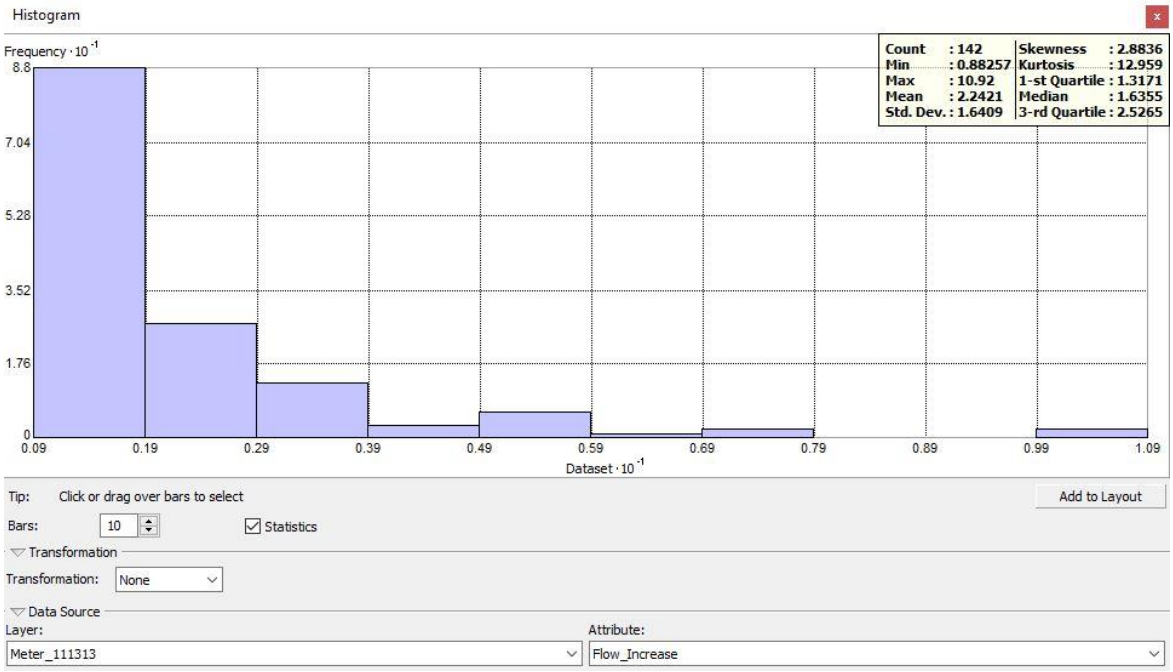

Figure 21. The histogram for the July 13, 2013 Flow Increase attribute revealed a random distribution due to positively skewed long right tail of quantiles.

Due to the heavily skewed histogram, the data could be lognormally transformed to make the variances more constant and attempt to normalize the distribution (Figure 22). Lognormal transformation produced a mean and median that was approximately the same value, the data is nearly normally distributed. However, kriging is proficient at interpolating data that is randomly distributed so the Flow Increase value along with RDII Contribution and Severity were examined as well. It was observed that all three variables without transformation follow the same right tail skew because of those outliers (Figure 21).

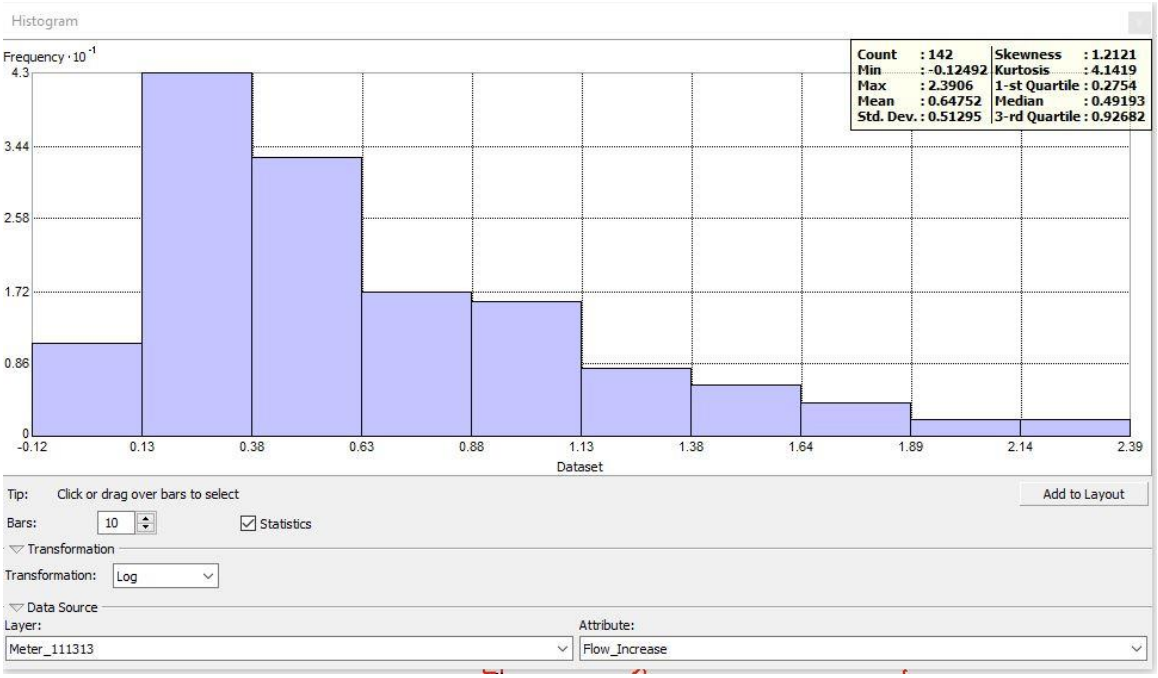

Figure 22. Lognormal transformation was used to attempt to normalize the distribution, but still depicts a strong right tail skew for the July 13, 2013 Flow Increase attribute.

In addition to the histogram, the QQPlot revealed a large fluctuation in the data along the straight line. In this case, the log transformed flow increase attribute was the closest to being a generally straight line, but the dataset distribution slopes from the lower flow values until it reaches the higher values that are almost off the chart (Figure 23).

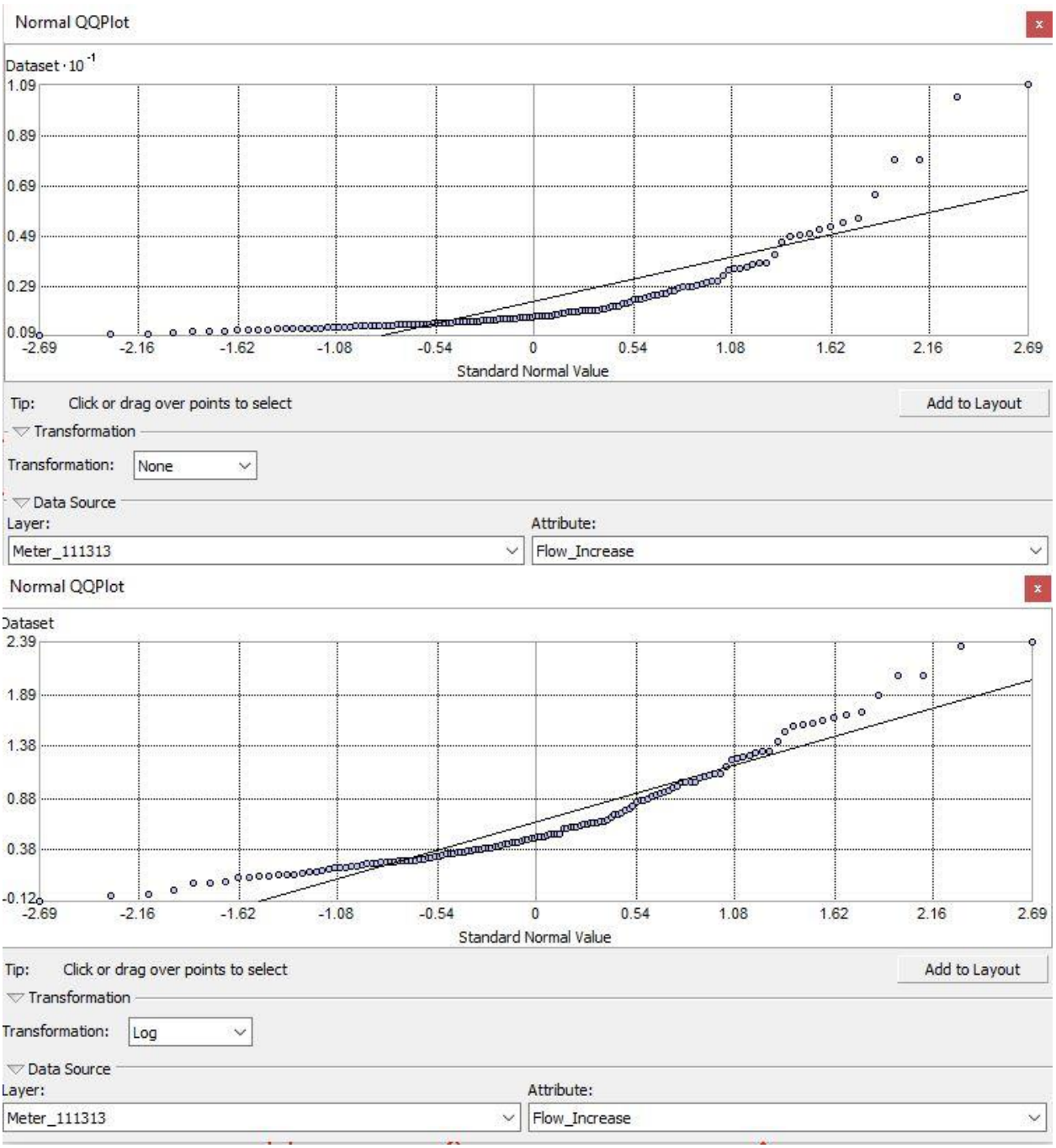

Figure 23. Normal QQPlot of July 13, 2013 Flow Increase with (bottom)/without (top) lognormal transformations. If the points follow the solid line then the dataset is normally distributed. In this case the dataset is randomly distributed.

Global Trend Analysis used the three main attributes of the July 2013 meter shapefile to reveal that there was no trend for both the east-west and north-south directions since the lines are almost straight with a minimal slope (Figure 24). When rotating the angle to 40 degrees as shown in Figure 25, it is apparent that there displayed a slight northeast-southwest trend. This trend is most likely related to the pattern of the rainfall, but is not influential enough to detrend the dataset before the geostatistical analysis. However, with the removal of the anomalies the trend was strong enough to try a first order polynomial. This was selected because it can remove a slight global trend from the analysis and provided the best prediction error for the universal kriging with no anomalies prediction map. A first order polynomial trend removal can measure the error by subtracting each measured point from its predicted values on the plane, squaring it, and adding the results together. While a second order polynomial is used to allow for one bend trend. Second order would only work for the meters shapefile that removed major outliers because it created a more distinct "U" shape trend in the global trend analysis (Figure 26).

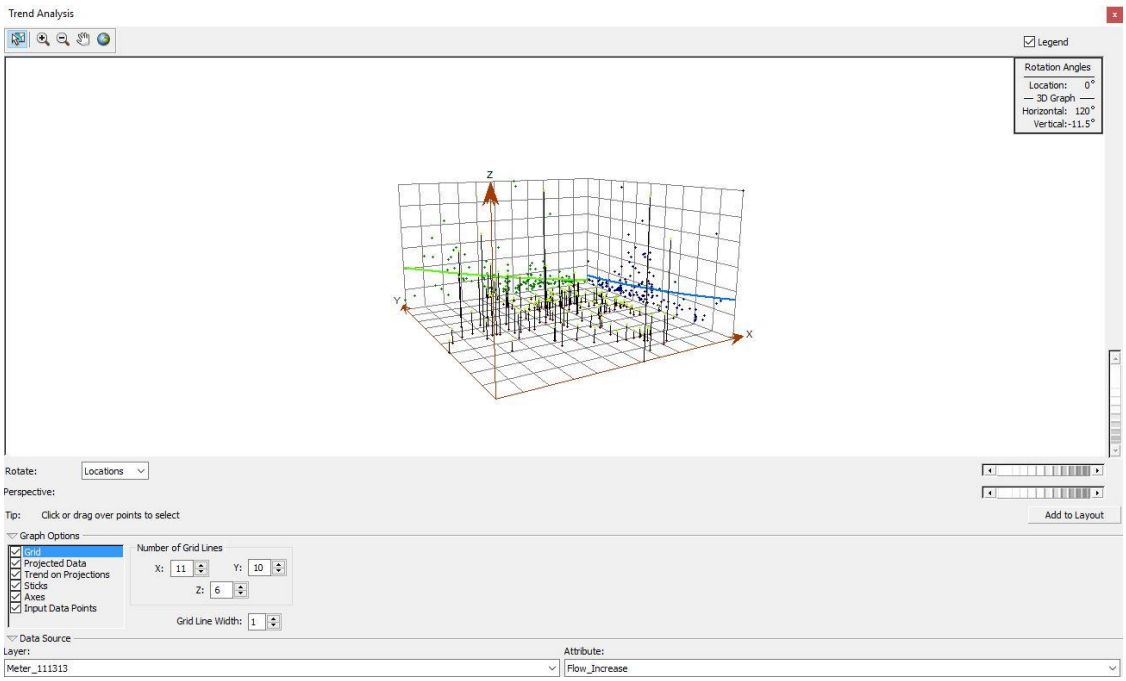

Figure 24. Global Trend Analysis of July 13, 2013 Flow Increase attribute at 0 degrees. No global trend observed from this angle.

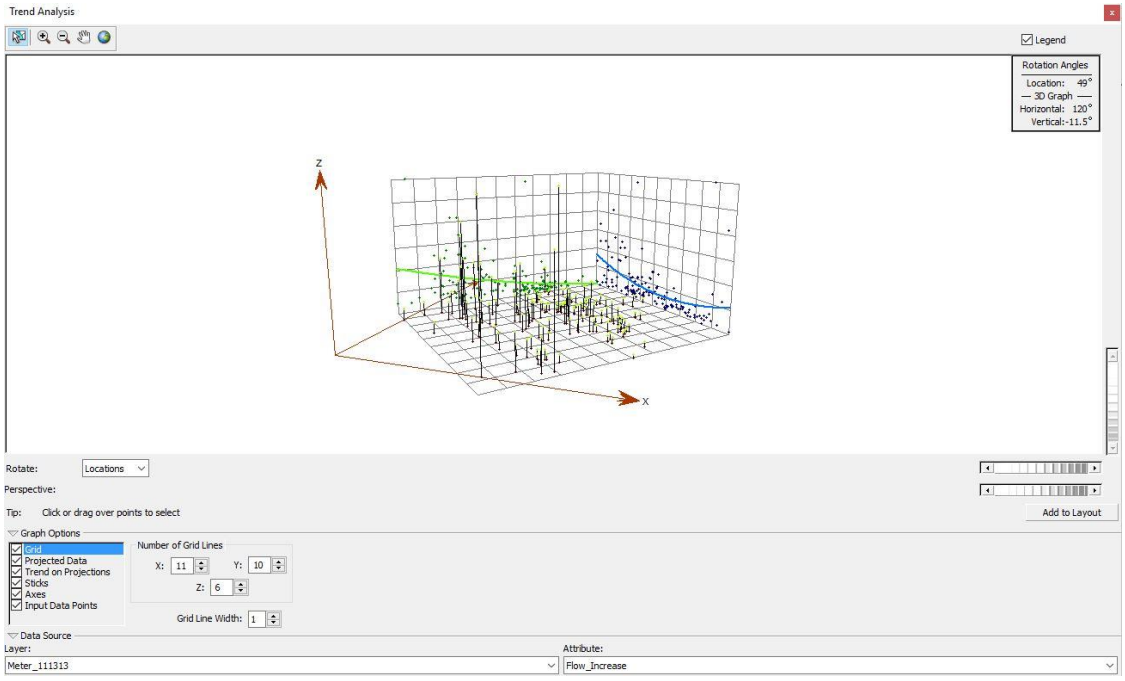

Figure 25. Global Trend Analysis of July 13, 2013 Flow Increase attribute at 40 degrees with slight northeast-southwest trend.

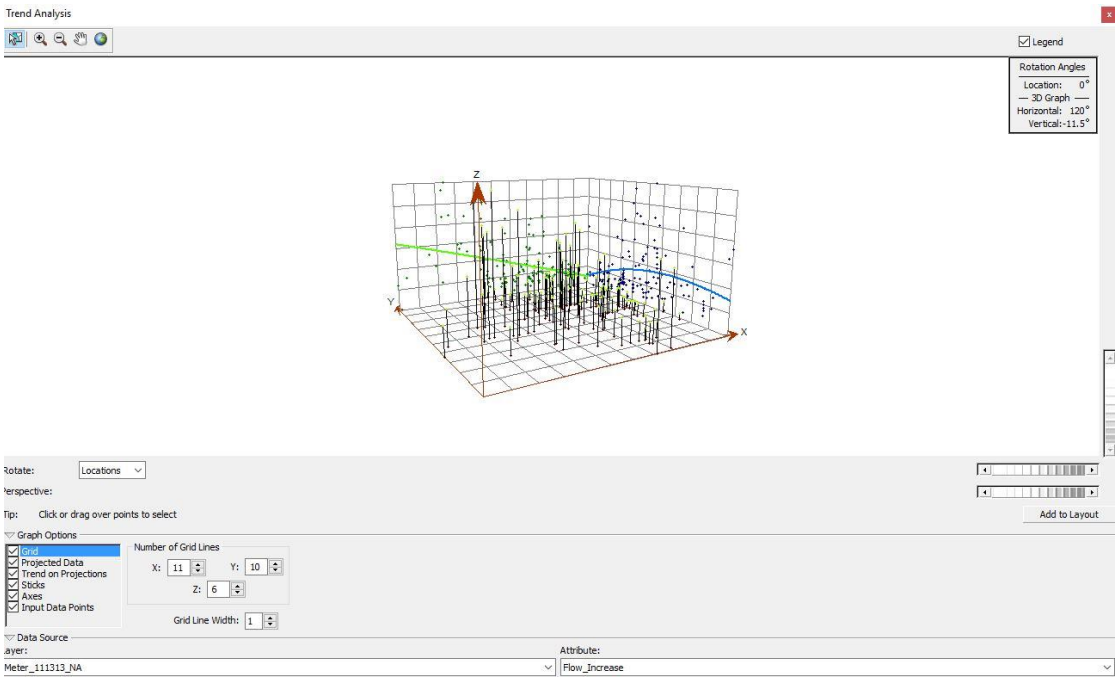

Figure 26. Global Trend Analysis with a very slight "U" shape trend due to the removal of major outliers from the analysis. There is a slight north-south trend that could influence the prediction results.

The Semivariogram/Covariance Cloud produced from the flow meter's data is randomly distributed across the chart (Figure 27). Major outliers are found on both ends of the cloud which means there are points in close proximity that have large difference in their values and points that are far apart that have similar values. For the July 13, 2013 case study, this is most likely related to the eleven major outliers found during the spatial data exploration. Flow increase, PFI, and RDII Severity all exhibited the same random pattern during exploration. Flow increase was determined to be the best option for the rest of the iterations because it is the simplest equation of the three input attributes. According to the Average Nearest Neighbor tool discussed in the methods, the best lag size for the prediction model should have been around 2100 for the July 13, 2013 event. The number of lags was adjusted from 12-20 for varying results. All of the extra data exploration figures can be found in Appendix A.

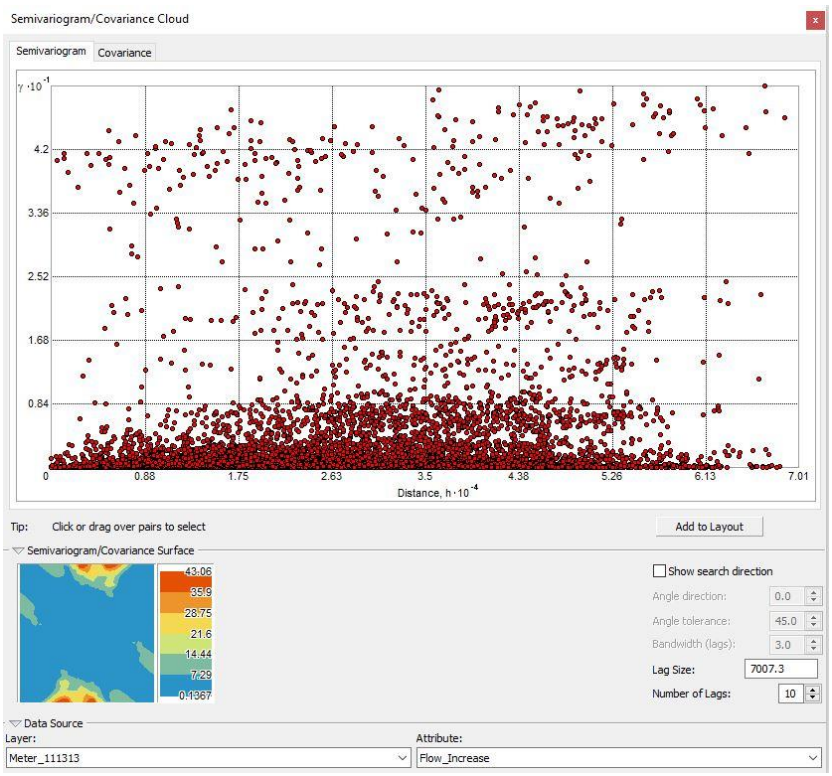

Figure 27. Semivariogram/Covariance Cloud of July 13, 2013 Flow Increase revealed a random spatial autocorrelation between the points.

Structural Analysis

Selection of the correct kriging type was an important part of creating the prediction surface and ordinary kriging was not the best option for this case study due to the nature of the dataset. This study relies on the major outliers created from a drastic increase in flow from rainfall which is used to identify locations susceptible to I/I. However, ordinary kriging assumes an unknown mean constant and in this case, the influence of the major outliers on the unknown mean constant was not an accurate form of prediction. Universal kriging follows a deterministic function and was found to be the best method since it can be modelled based off of the surrounding points influence instead of an inherent mean constant in the dataset. When compared

to iterations of ordinary kriging and cokriging, universal kriging was the most statistically sound (Figure 31 & 32).

Surface Prediction

The surface prediction results included a continuous surface for the variety of interpolation parameters selected, comparison of standard errors (uncertainty) of predictions, and probability surfaces that reveal critical thresholds that are exceeded. The first step after creating all of the kriging surfaces was to compare them using the "Compare…" option. All of the comparisons can be found in Appendix B. See Figure 28 to Figure 37 for comparison and surface prediction results. A common assumption would be that the introduction of additional variables into the interpolation process would improve the prediction surface, but it was found that universal kriging with just the flow increase attribute provided more statistically significant results compared to cokriging (Figure 32).

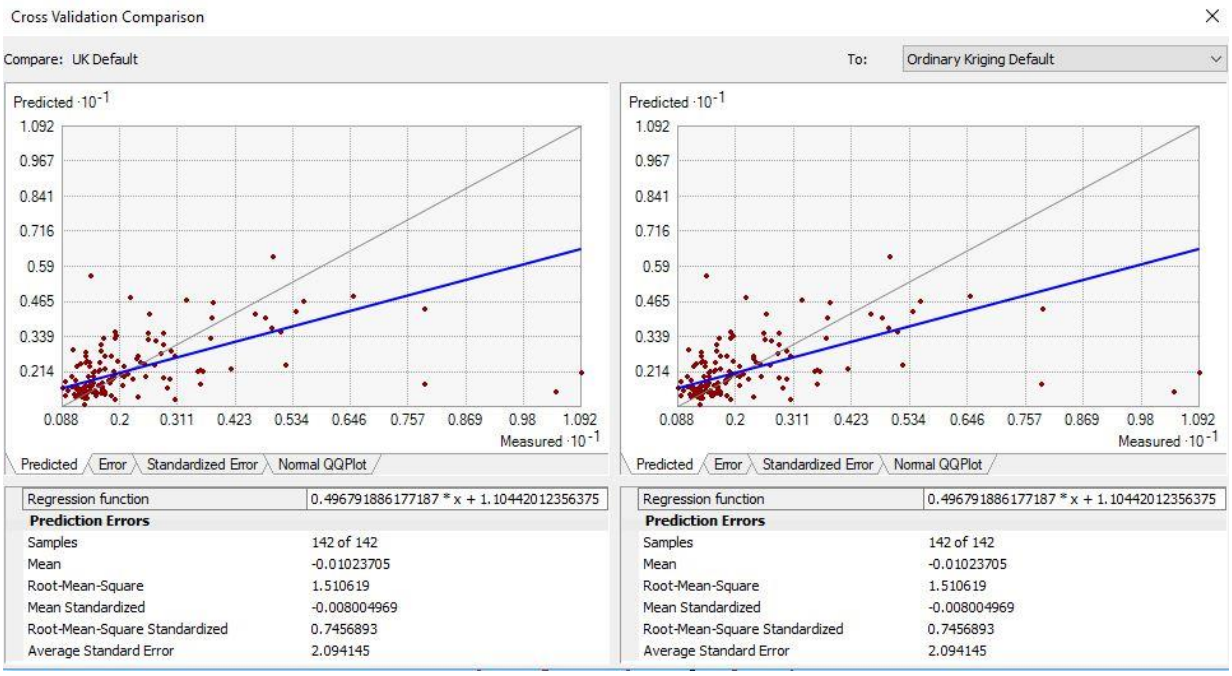

Figure 28. The comparison of prediction error reports revealed that universal kriging and ordinary kriging both using default settings resulted in the exact same prediction error values.

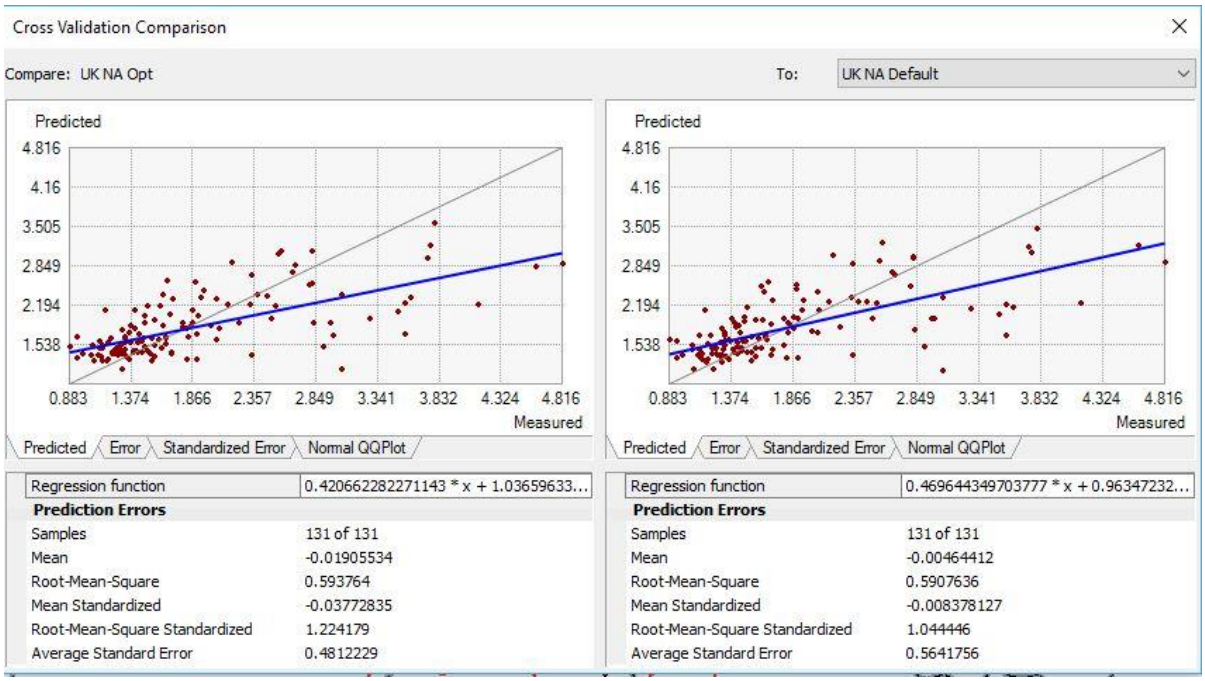

Figure 29. A comparison of all universal kriging without anomalies revealed that default settings with a first order polynomial trend removal produced the best prediction error results.

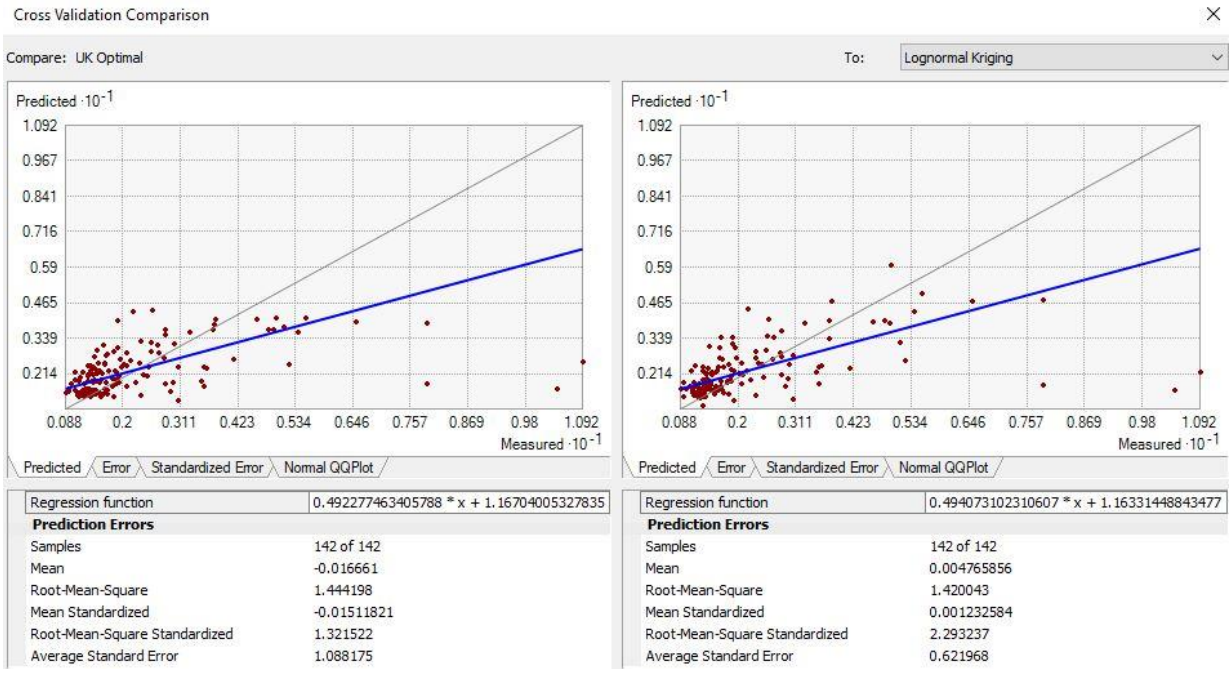

Figure 30. Lognormal kriging with default settings had the lowest mean error out of all the error reports. Overall it did not produce better results than universal kriging with optimal settings.

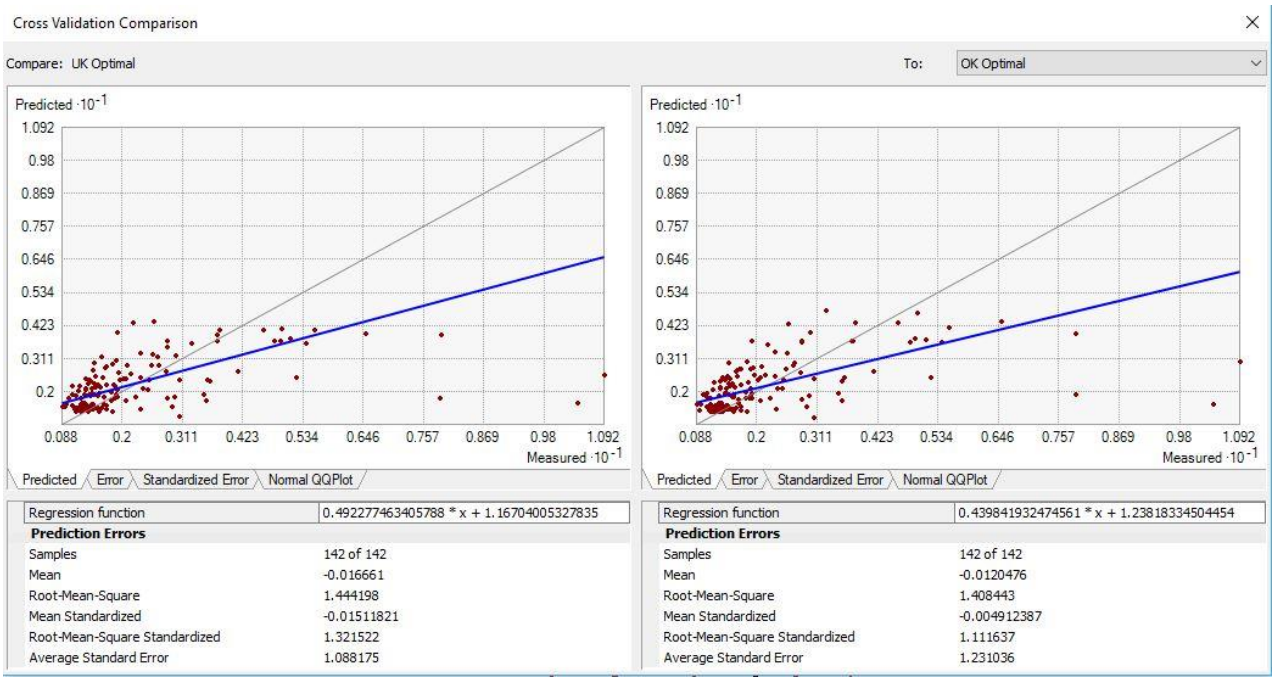

Figure 31. The most accurate prediction error compared to every other iteration attempted was universal kriging with optimal settings.

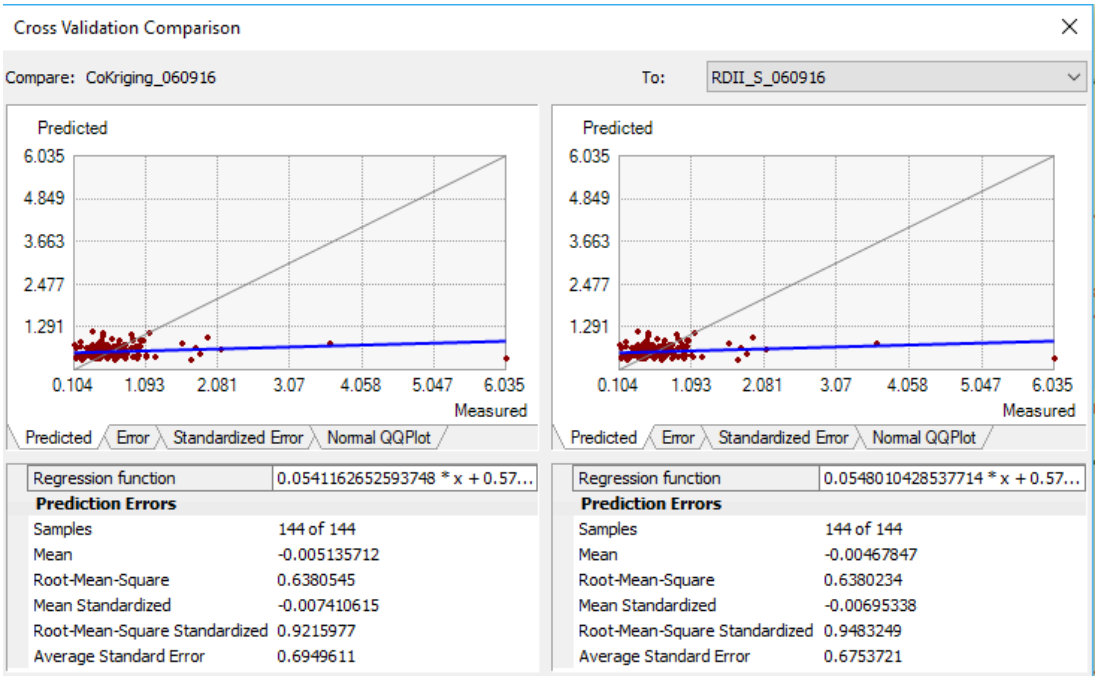

Figure 32. Universal kriging with optimal settings provided better prediction error results when compared to cokriging with optimal setting utilizing both rainfall and flow increase data.

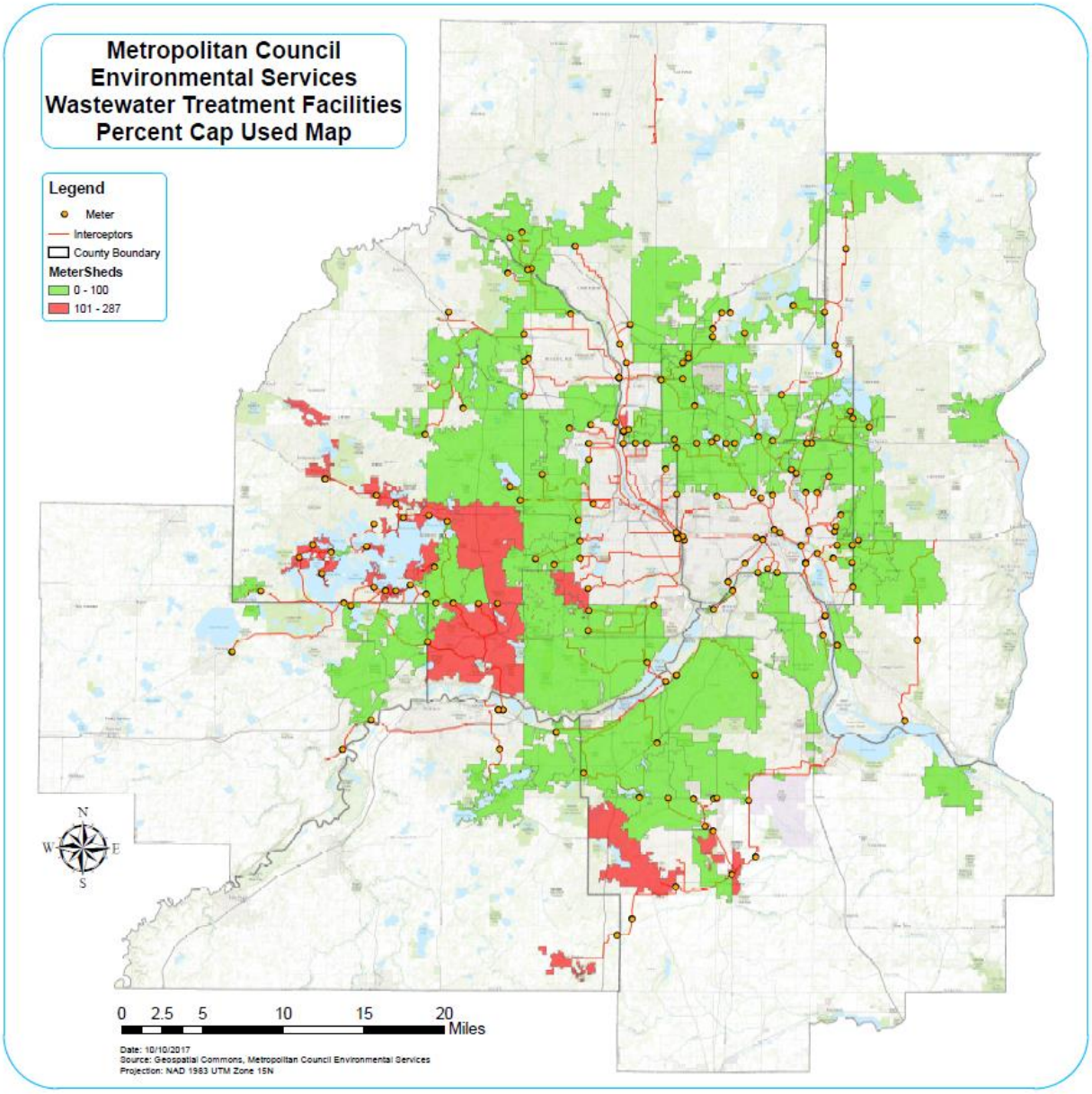

Figure 33. MCES Metershed Shapefile with PCT Cap Used as the displayed attribute. Areas that exceed their 100% I/I Goal are depicted in red. This is a simpler method of displaying each municipality's Percent Cap Used for each Metershed.

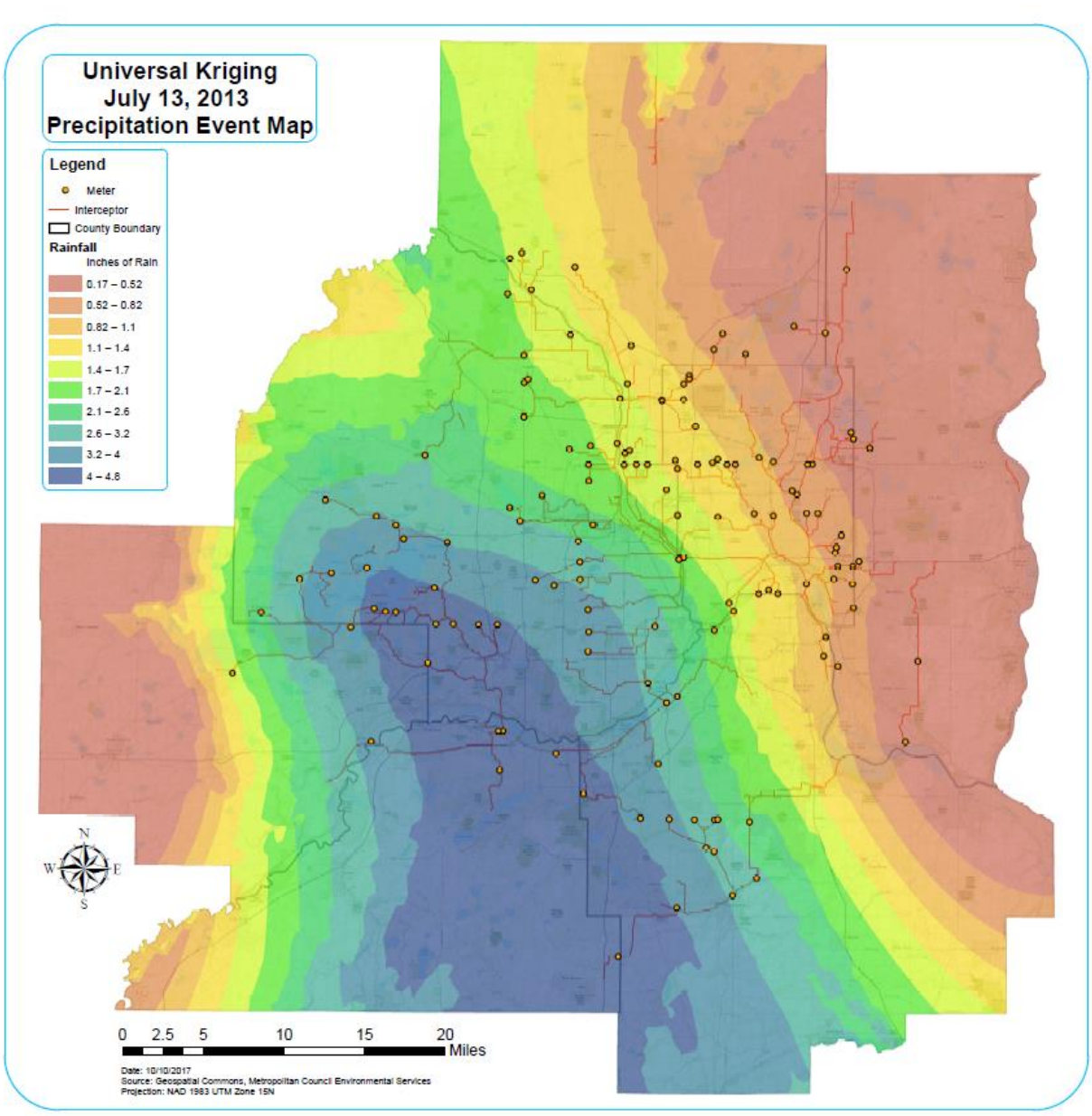

Figure 34. Rainfall kriging prediction surface for July 13, 2013 event. The kriging output for RDII Severity and Flow Increase positively correlates with the rainfall pattern.

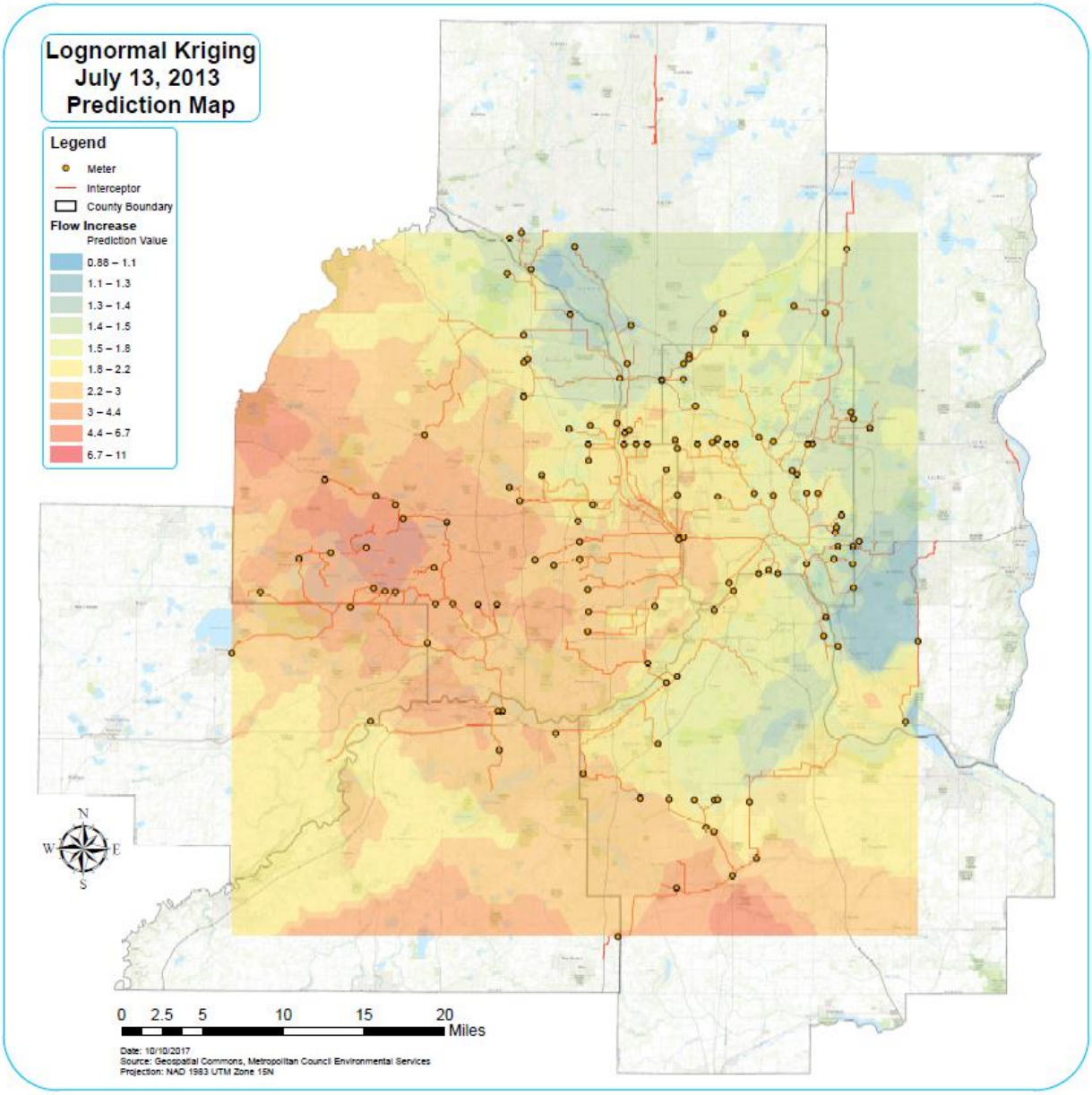

Figure 35. Lognormal kriging with optimal settings provided one of the prediction error results, but universal kriging with optimal settings was better. The output kriging surface for flow increase and RDII severity were very similar, but a lognormal transformation of flow increase modified the shape of the hotspot locations.

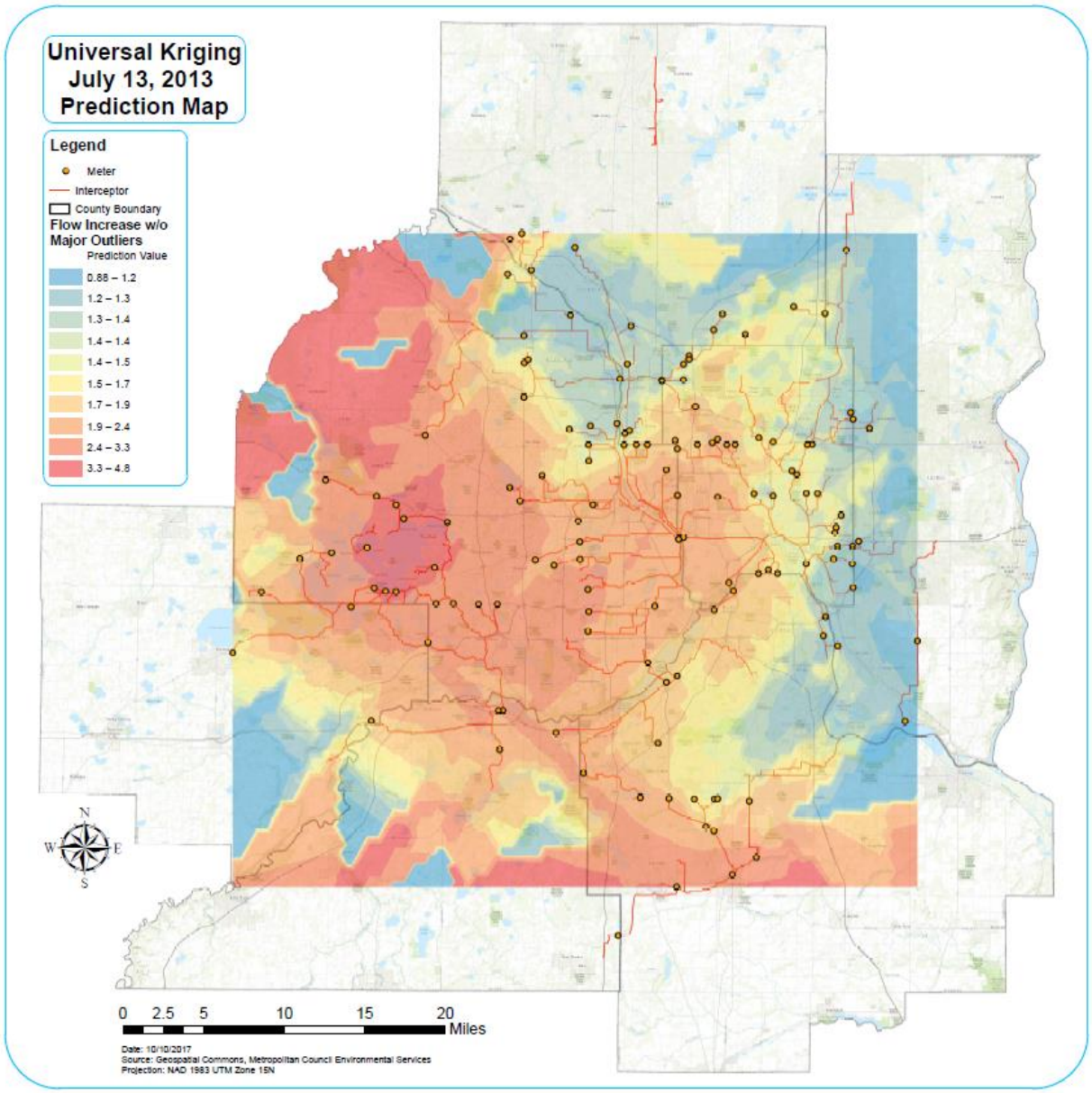

Figure 36. This prediction map was created using universal kriging without anomalies using default settings and a first order polynomials trend removal. Multiple iterations with varying parameters were attempted, but the above output had the best prediction errors for models using the no anomalies dataset. Removal of major outliers more adequately depicts the underlying flow increase trend of areas susceptible to I/I instead of being masked by the major outliers. However, all the prediction maps tend to designate a similar pattern of trouble areas compared to one another.

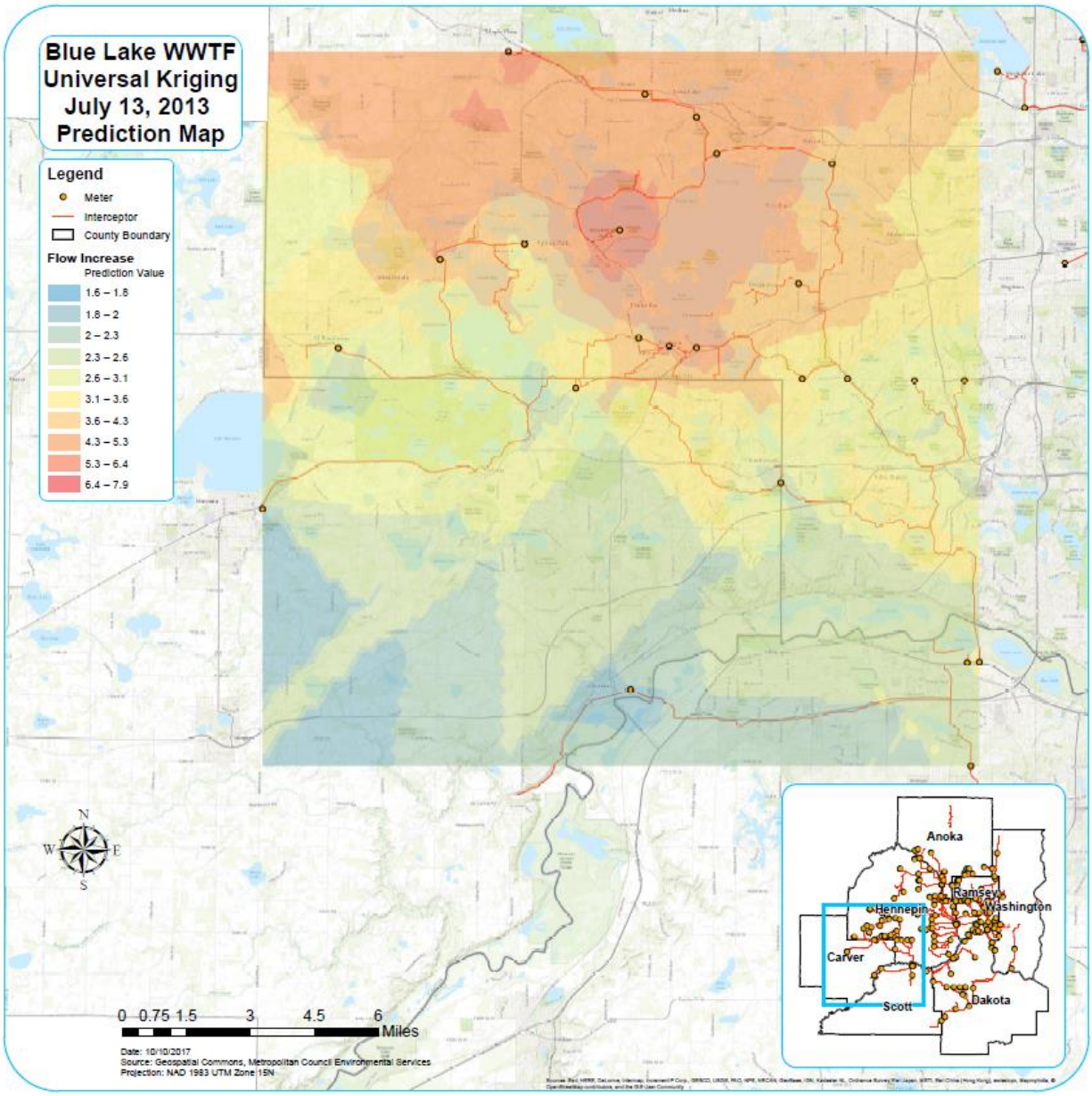

Figure 37. Western region large scale kriging map. This area displayed the highest flow increase during the July 13, 2013 rainfall event so it was used for scale variation in this study. Results reveal that anomalies mask overall trend from the rest of the points in the network area when interpolation is conducted for a larger area at a smaller scale.

The kriging outputs for RDII Severity and Flow Increase exhibited the same positive correlation to the rainfall event's prediction surface. The results revealed that areas with more rainfall generally had higher flow rates except for one outlier in the middle of the metropolitan

area for the July 13, 2013 precipitation event. This meter would require further investigation to determine if it is a faulty meter or if there is a huge influence from minimal rainfall in the area.

The lognormal transformation of Flow Increase did not adjust the data enough to make it a normally distributed bell curve (Figure 22). This is why the lognormal kriging prediction error was not better than the optimal or even default settings of universal and ordinary kriging (Figure 30). However, it is not necessary to normalize the distribution when using these kriging methods. Kriging is the best interpolation method to use for this case study due to the random distribution of the dataset values.

The following prediction surfaces (Figure 38 to Figure 43) displayed unique prediction errors and had the best prediction errors out of all the compared models for their unique attributes. The fourteen prediction products created from 2016 precipitation events can be found in Appendix C, whereas the fourteen interpolated rainfall maps from 2016 can be found in Appendix D.

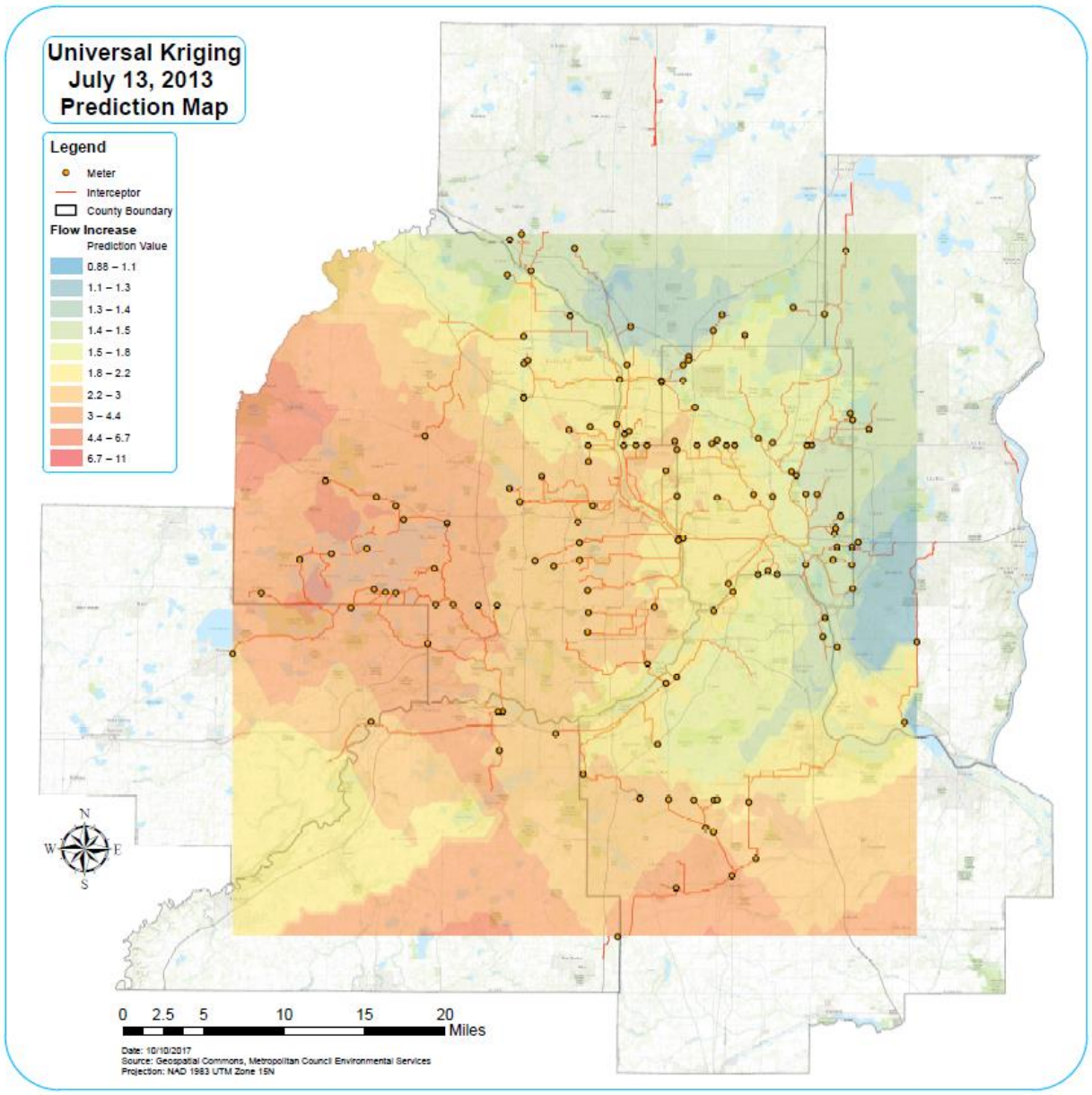

Figure 38. The prediction surface above was created using universal kriging with optimized method properties and semivariogram modelling. This model provided the best prediction error results compared to the all other iterations.

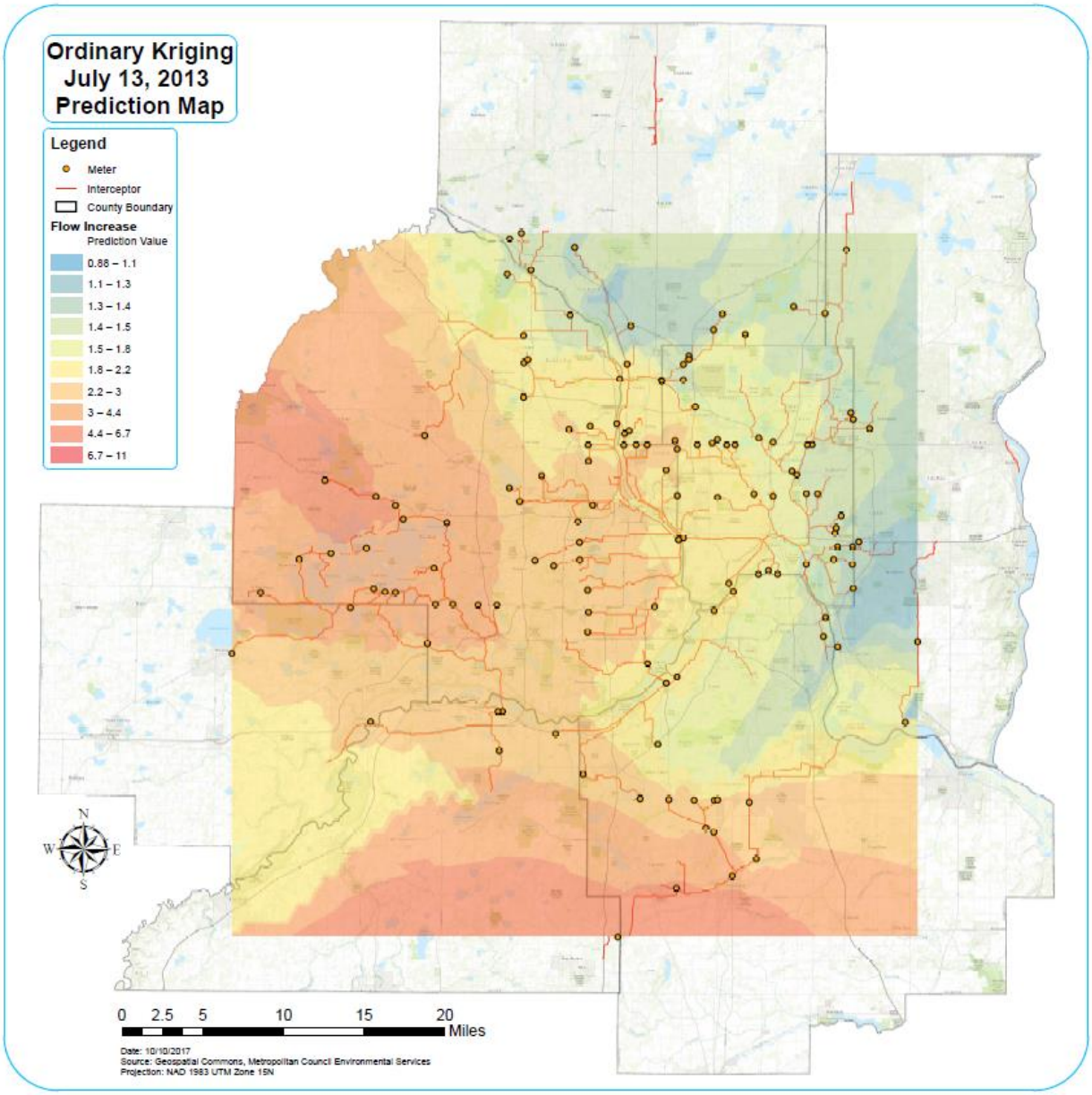

Figure 39. The prediction surface above was created using ordinary kriging with optimized settings. It provided low prediction error, but the RMS and RMS standardized are not as close as with Universal Kriging.

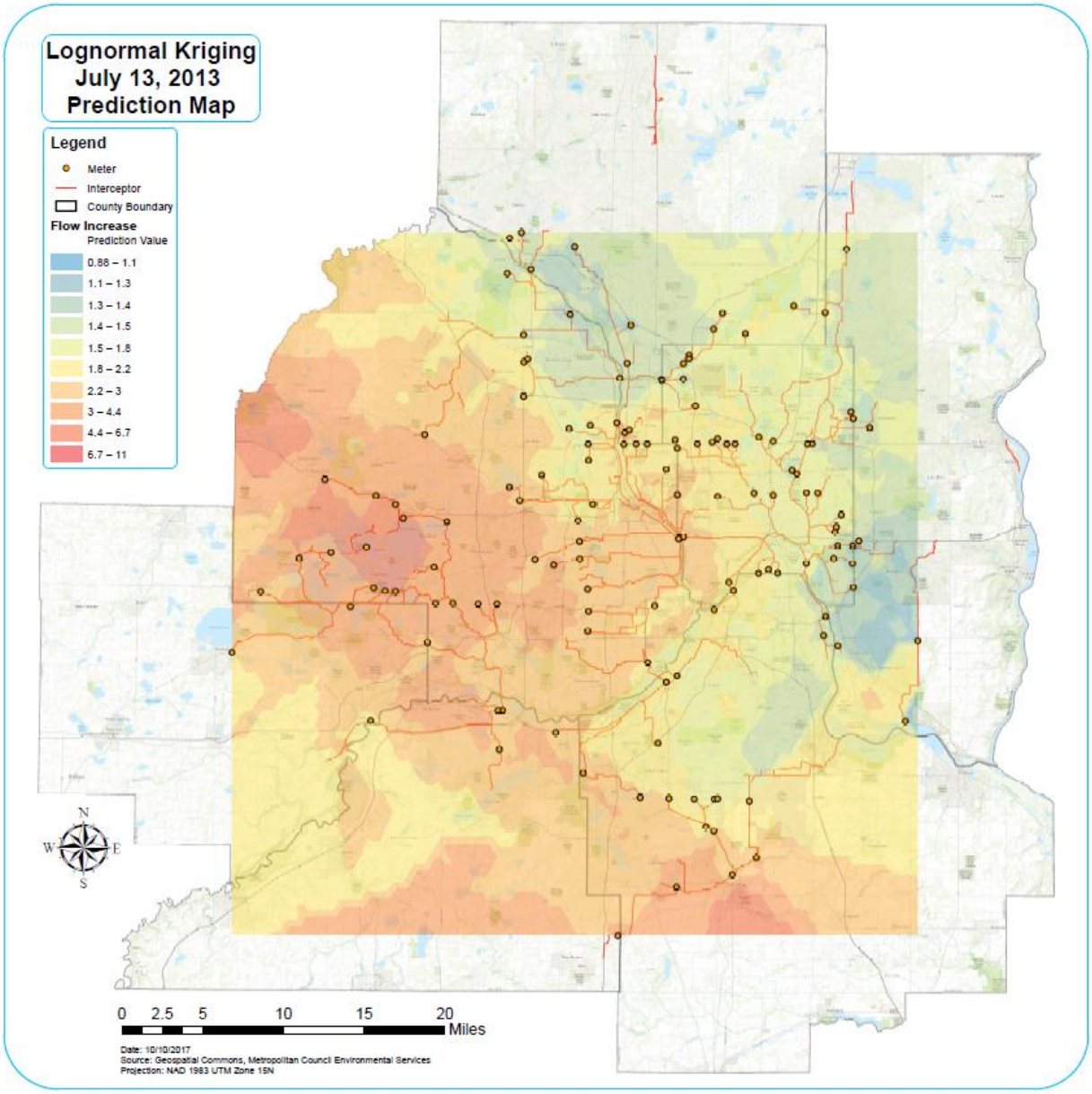

Figure 40. Lognormal kriging using default settings.

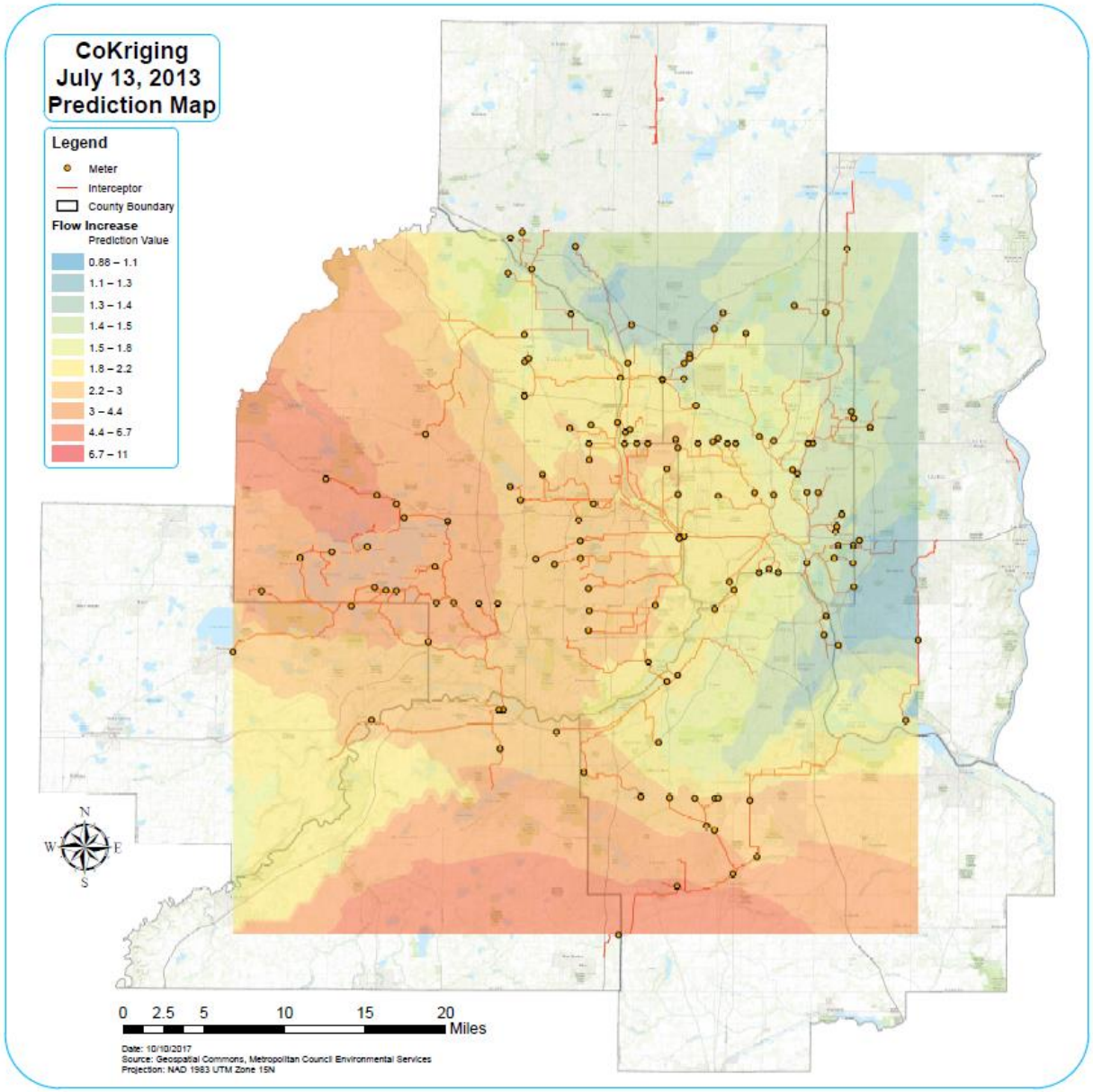

Figure 41. The prediction surface displayed above was created using CoKriging with optimal settings. Flow Increase and Rainfall were the two variables used. It did not have better prediction error than the interpolation of flow increase utilizing universal kriging with optimal settings.

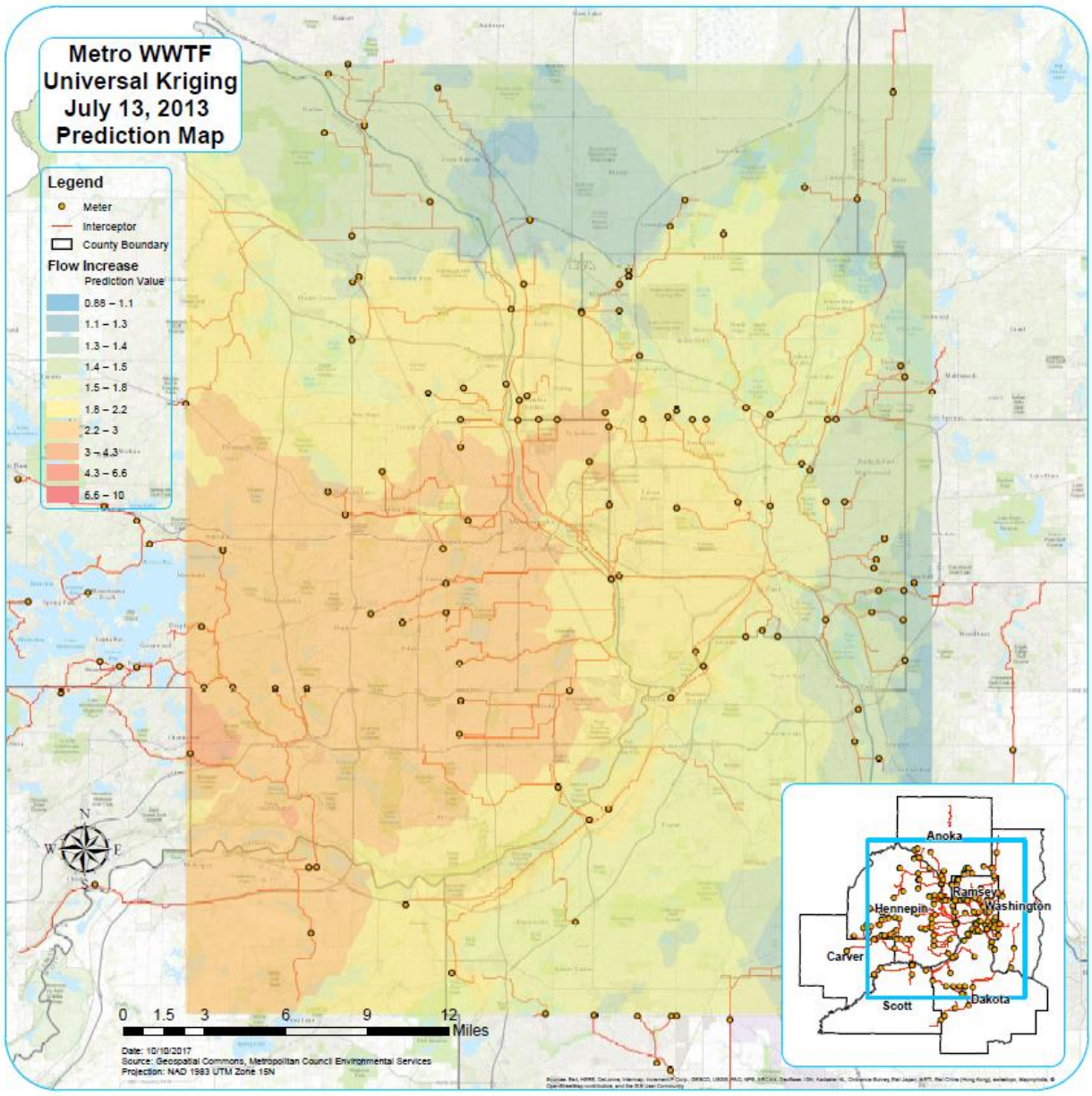

Figure 42. Metro large scale interpolation using universal kriging.

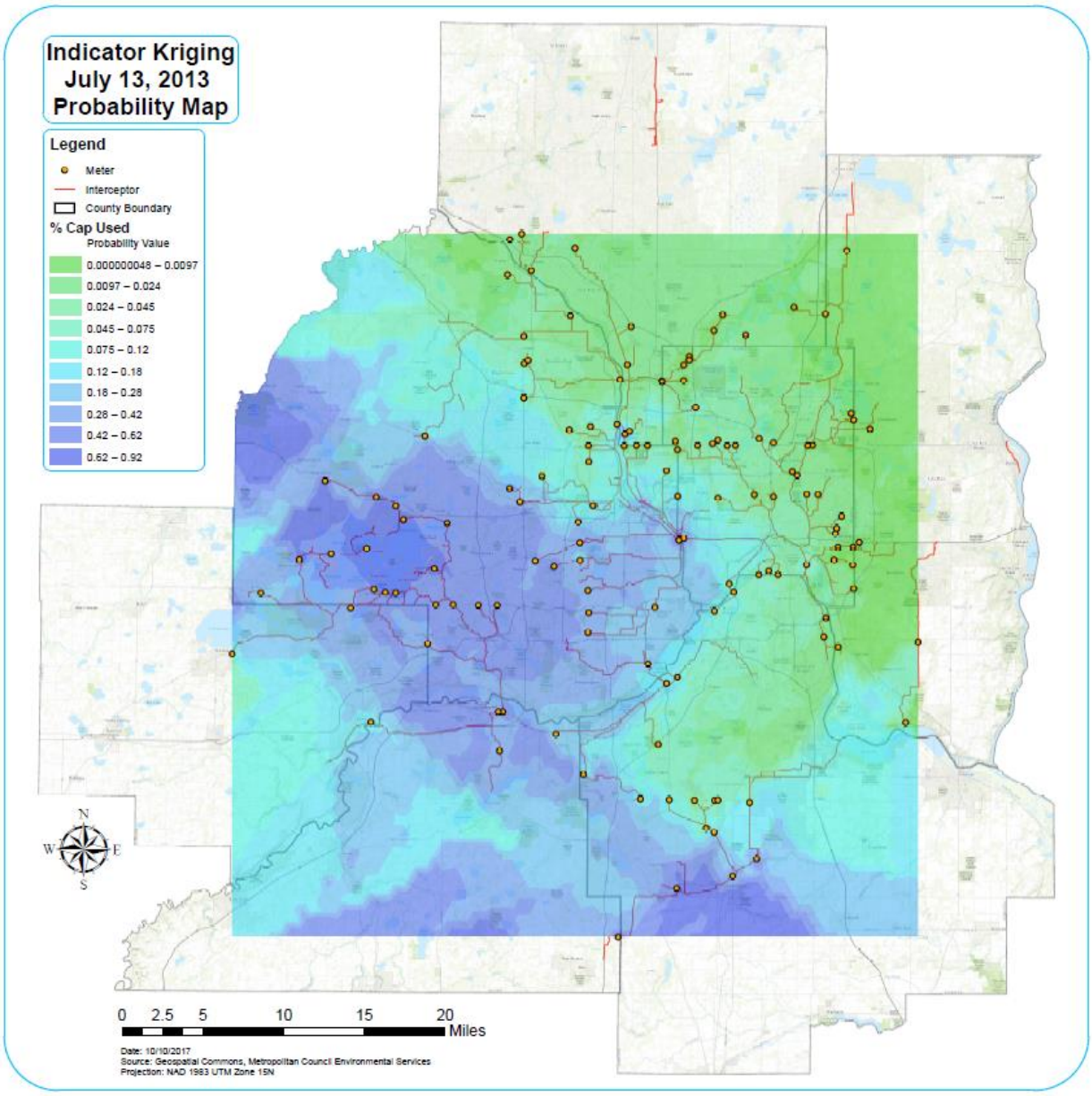

Figure 43. Probability map of PCT Cap Used attribute. The values represent the probability of that region exceeding their 100% limit for each municipalities "I/I goal".

Discussion

This research has attempted to answer three primary questions regarding testing of this novel methodology in predicting I/I vulnerable locations within wastewater infrastructure. The

remainder of this section will address each of these questions as it relates to the results produced from this methodological test and then conclude with an overall assessment of the results.

Is it practical, efficient, and effective to assess spatial patterns of infiltration and inflow of rain water by creating a continuous surface to analyze a network of subterranean linear features?

First, it must be understood that this geostatistical/geospatial analysis of I/I does not conduct a network analysis of the sewer system's susceptibility to I/I. Instead this analysis creates a continuous prediction surface that attempts to locate "hotspot" areas of increased flow rates during rainfall events (e.g. Figure 38). By cross referencing the prediction surface with the sewer network shapefile, this method has the potential to identify areas most likely to be susceptible to I/I, and in turn, help to narrow the search area for maintenance crews to locate I/I in the field. Furthermore, more comprehensive field based research into the "hotspot" areas may lead to a better understanding of what factors play a vital role in introducing I/I into certain areas. Whether these "hotspots" represent locations with faulty flow meters, poorly maintained sewer systems, variations in porosity of the soil, specific pipe characteristics (size/shape/age/type) resulting in high flow, topographic variability, land use practices, the level of the groundwater table in the region, or some other factor(s) is yet to be discerned.

The fundamental purpose of this work is to create a visual representation of the I/I problem via flow increase prediction surfaces with the hope that they can be a useful tool for decision makers. This method provides a statistical means to validate the results of the prediction surface and to quantify residual error after the creation of the prediction surface during the last step of the geostatistical wizard (Figure 18). The cross validation comparison (Figure 19) is also very important for determining which model is the best for the analysis and therefore provides us

with a way to produce the most effective prediction surface. However, until visual inspections of this method's results are conducted in future studies, the full effectiveness of this methodology is not known. What is understood is that this methodology becomes increasingly effective when comparing the high flow prediction surfaces to their respective rainfall prediction surfaces (e.g. Figure 34). In appendix C and D, most of the prediction models exhibited a positive correlation between rainfall and increased flow. However, from one prediction surface to the next, flow increase was inconsistent in the same areas most likely due to the location and intensity of the rainfall and/or the completion of maintenance to the sewer network to reduce I/I between rainfall events (Figure 44).

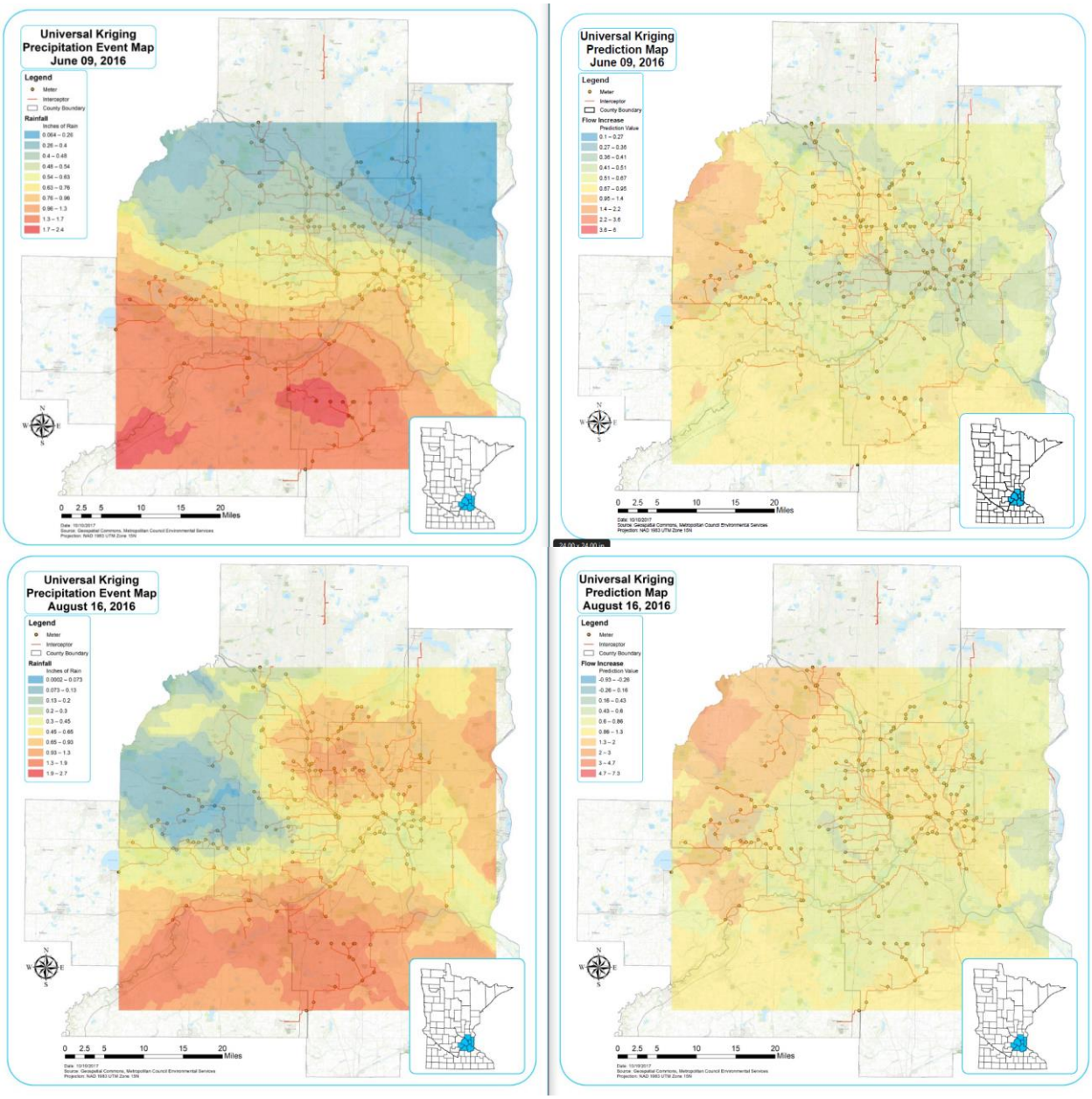

Figure 44. Two similar rainfall events from June 09, 2016 and August 16, 2016 (left column) resulted in different prediction surfaces (right column). Most likely the result of varying intensity of rainfall and/or completion of maintenance to the pipes to reduce I/I in those areas.

It is pertinent to reference each prediction surface with its corresponding rainfall event map. The 07/27/16, 08/30/16, and 09/15/16 rainfall events from appendix C and D identified locations of interest for further inspection due to high flow increase occurring at corresponding locations with low rainfall (Figure 45). The location of rainfall in the study area affects what locations will be influenced by the event. For example, if only one county is affected by rainfall,

then the prediction surface may provide a false assessment of the areas with little to no rain as seen in the southern portion of Figure 46. However, a location of high flow distant from the most intense rain, may also represent a location in need of repair. Less intense precipitation may be generating high flows in these locations due to relatively high I/I. It must also be considered that between rainfall events, MCES may be conducting maintenance to their pipes, which may lead to changes in the amount of flow increase from one rainfall event to the next (Figure 44). Therefore, in applying this method we must coordinate our work with maintenance records. This was beyond the scope of this study and was not recognized as significant in the testing of this methodology. However, this provides another opportunity for the practical application of this method to determine the effectiveness of rehabilitation to the sewer networks. If the rainfall location and intensity are not the issue then the problem most likely stems from either poor rehabilitation of pipes and/or I/I entering the sewers through another source like the local community's sewer networks.

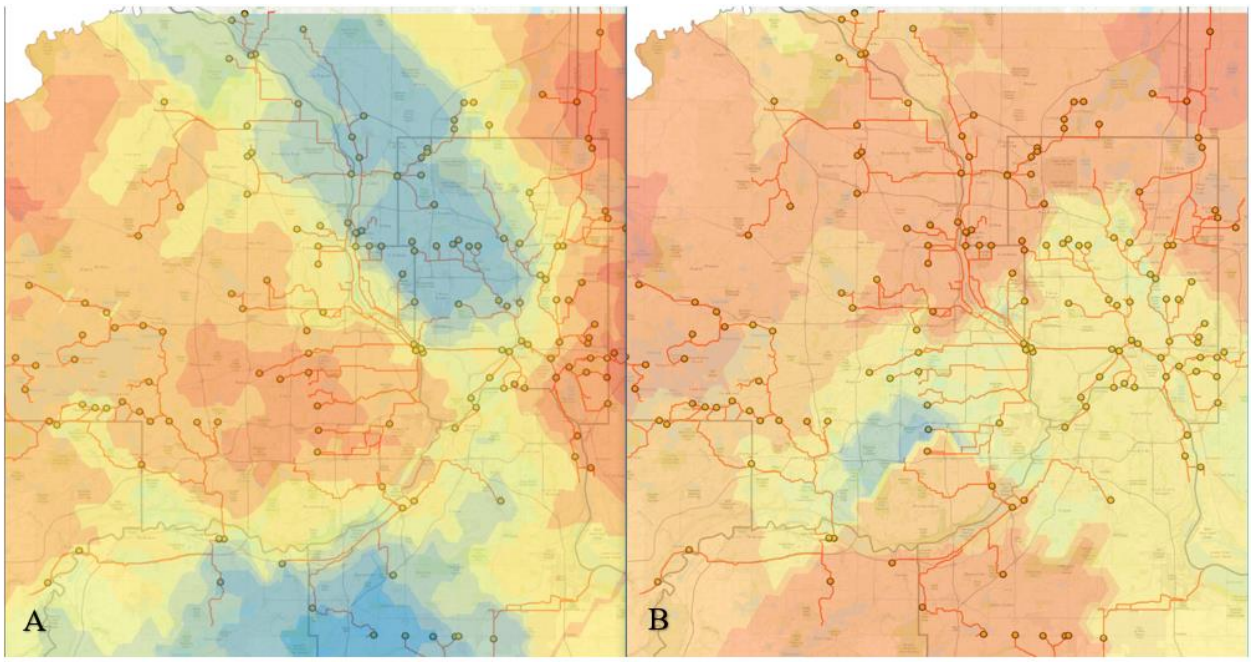

Figure 45. Comparison of areas with contradicting increase in rainfall and flow. Map A is the precipitation map and Map B is the flow increase prediction map. Each map represents their respective values from red (high values) to blue (low values). This comparison is of the rainfall event from August 30, 2016.

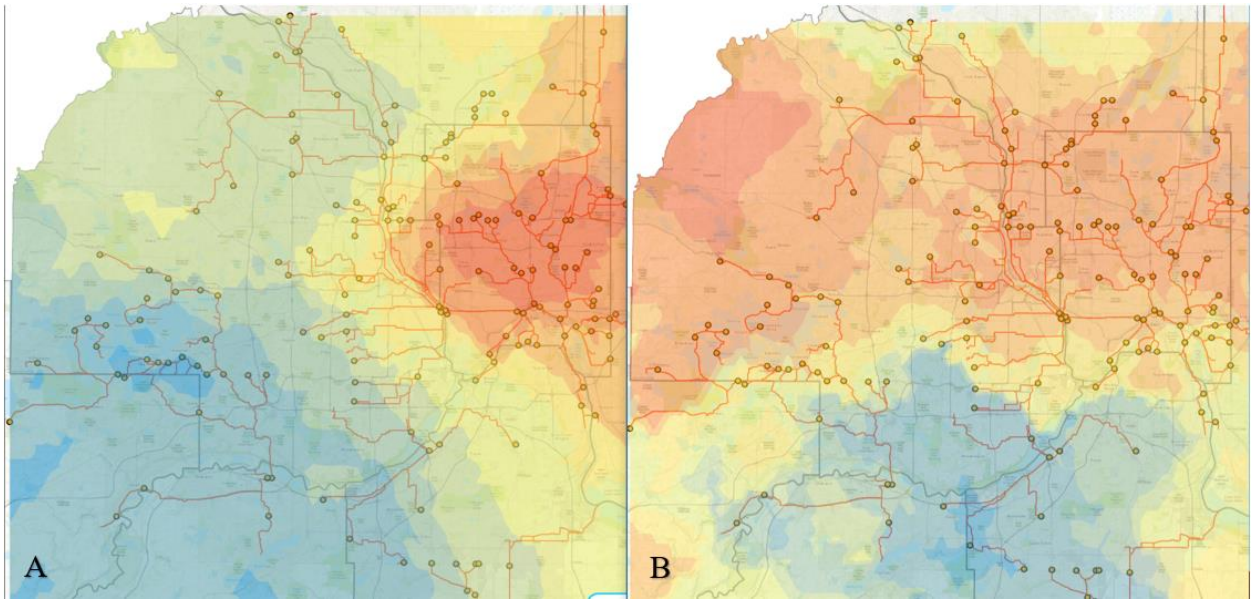

Figure 46. Heavy rainfall on one part of the map may skew the prediction surface making it appear that certain areas are in good condition even if they are not. This demonstrates the significance of looking at the rainfall prediction maps. Map A is the precipitation map and Map B is the flow increase prediction map. Each map represents their corresponding values from red (high values) to blue (low values). This comparison is of a rainfall event from July 27, 2016.

Although the overall impact and effectiveness of this method is still uncertain, it is evident that this method has potential to be more practical and efficient compared to the sewer inspection methods currently used like CCTV inspections, dye tests, and smoke tests. Those methods are time consuming, costly, and require workers to go out in the field and assess every inch of the sewer networks for faults (Metropolitan Council of the Twin Cities 2009; American Society of Civil Engineers 2011; Shelton et al. 2011). In addition, multiple studies have attempted to use GIS to locate failing or deteriorating sewer pipes before they reached the point of critical failure, but none of them have used flow meter data to attempt a prediction map on this scale (e.g. Koo and Ariaratnam 2006; Halfawy, Dridi, and Baker 2008; Younis and Knight 2010; Boersma 2012). This analysis provides a practical and efficient five step workflow (Figure 7) that only requires one GIS user to explore the spatial data and adjust the model to create the best prediction surface possible. The most important feature required for this workflow is accurate input data produced by the flow meters. From this data, the GIS user can assess which results are the most statistically sound (Figure 19) and can create the final prediction surface like in Figure 38.

Can kriging be modelled to accurately assess small changes in variation across the landscape or does the interpolation mask small variability?

Kriging can be utilized to assess changes in variation across a large study area through interpolation (Johnston et al. 2001). However, each sample point's value has the strongest influence on the interpolated prediction surface surrounding that point's location (Figure 47). Therefore, distribution of the sample points and how the semivariogram is modelled inherently lead to some form of measurement error and data variation (Krivoruchko 2004). Most measurements in spatial data contain errors both in attribute values and in locations, but this

should not limit the use of the data for decision-making. The final results are prediction surfaces and therefore it should be understood that they are not an exact representation of the subject's trends, but the most accurate estimate using the available data.

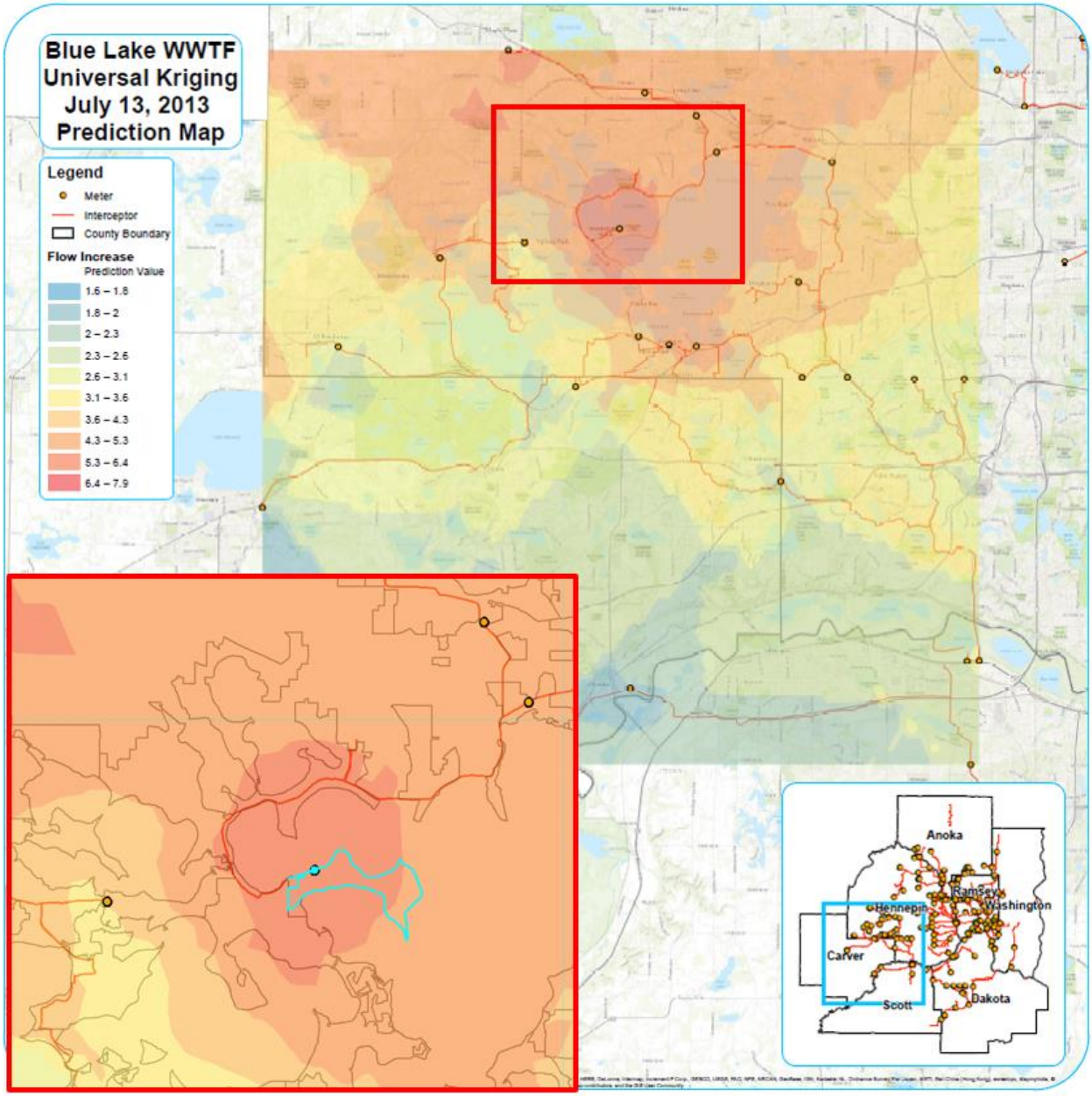

Figure 47. Close up of the hotspot around the corresponding meter and the related metershed highlighted. The effect of each sample point's value has the most noticeable influence on the surrounding interpolated surface when zoomed in to a large scale map as shown above.

Fundamentally, it should be understood that some errors and anomalies in the kriging process are due to the spatial distribution of data points throughout the study reach and as this distribution is related to the nugget and the sill. The nugget and sill are two key parameters of the semivariogram that relate to changes in distribution across the landscape (Figure 16). The sill parameter of the semivariogram is a value that represents distances that are too large between points to be significant (Johnston et al. 2001; Krivoruchko 2004; Oliver and Webster 2014). At large distances the points are no longer spatially correlated. Therefore, the sill is equal to the variance of random variables or, in the case of this work, the flow meters that have excessive flow (Figure 49). The nugget parameter of the semivariogram represents independent error, measurement error, and/or microscale variations at spatial scales that are too fine to detect (Johnston et al. 2001; Krivoruchko 2004). Therefore, the nugget is seen as the discontinuity at the starting point of the semivariogram or covariance model's slope (Figure 15 & 16).

The nugget and sill help to understand how the distances between the sample points in the interpolation process influence the final result. Interpolation provides the best results when more points are within close proximity of one another, but if some points are isolated this can lead to gaps in the dataset that the interpolation process attempts to fill based on the data that is available (Figure 50) and, therefore, a higher degree of uncertainty in that portion of the prediction surface. Scale plays a crucial role in the interpolation process as well. Figure 48 compares the same location when interpolating only the Blue Lake WWTF network and when interpolating the entire MCES interceptor network. This revealed that the major outliers in the area mask the meters in the western region that did not have drastic increases in flow during the July 13, 2013 rainfall event. Figure 36 represents the interpolation surface without major outliers

in the interpolation process and it created a more generalized prediction surface around the trouble areas due to the removal of the major outliers when compared with Figure 38.

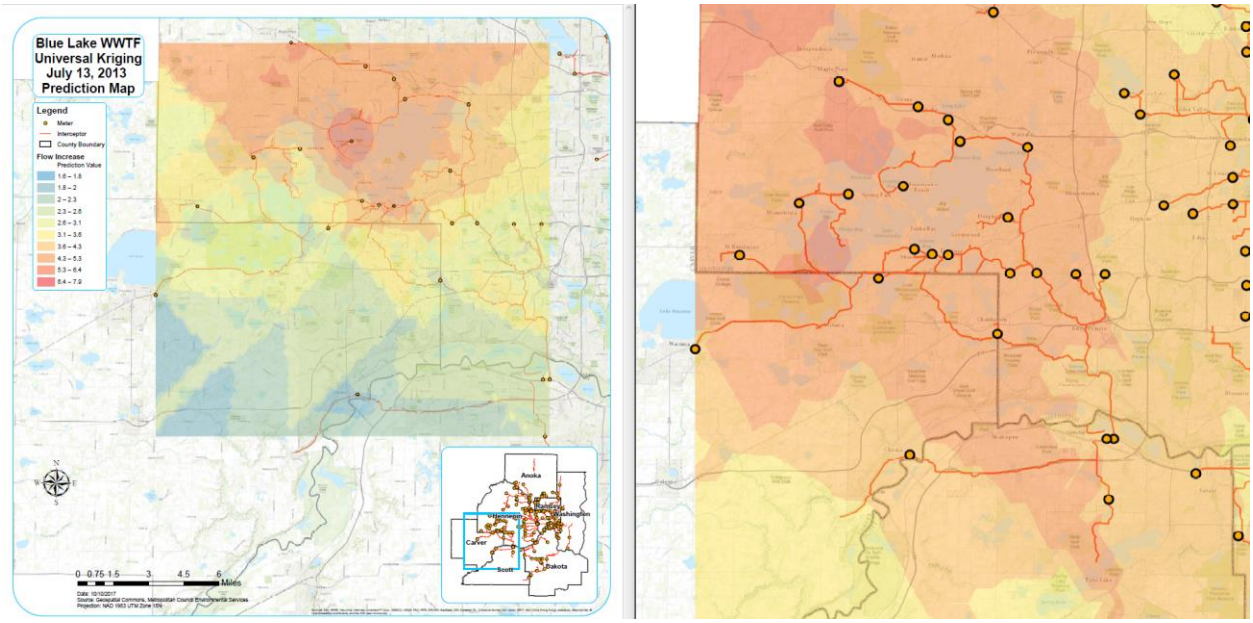

Figure 48. Comparison of the western region on the small-scale Blue Lake WWTF prediction map and the same location on the large-scale prediction map to show how variation in scale affects the interpolated surface and how each point influences the rest of the dataset.

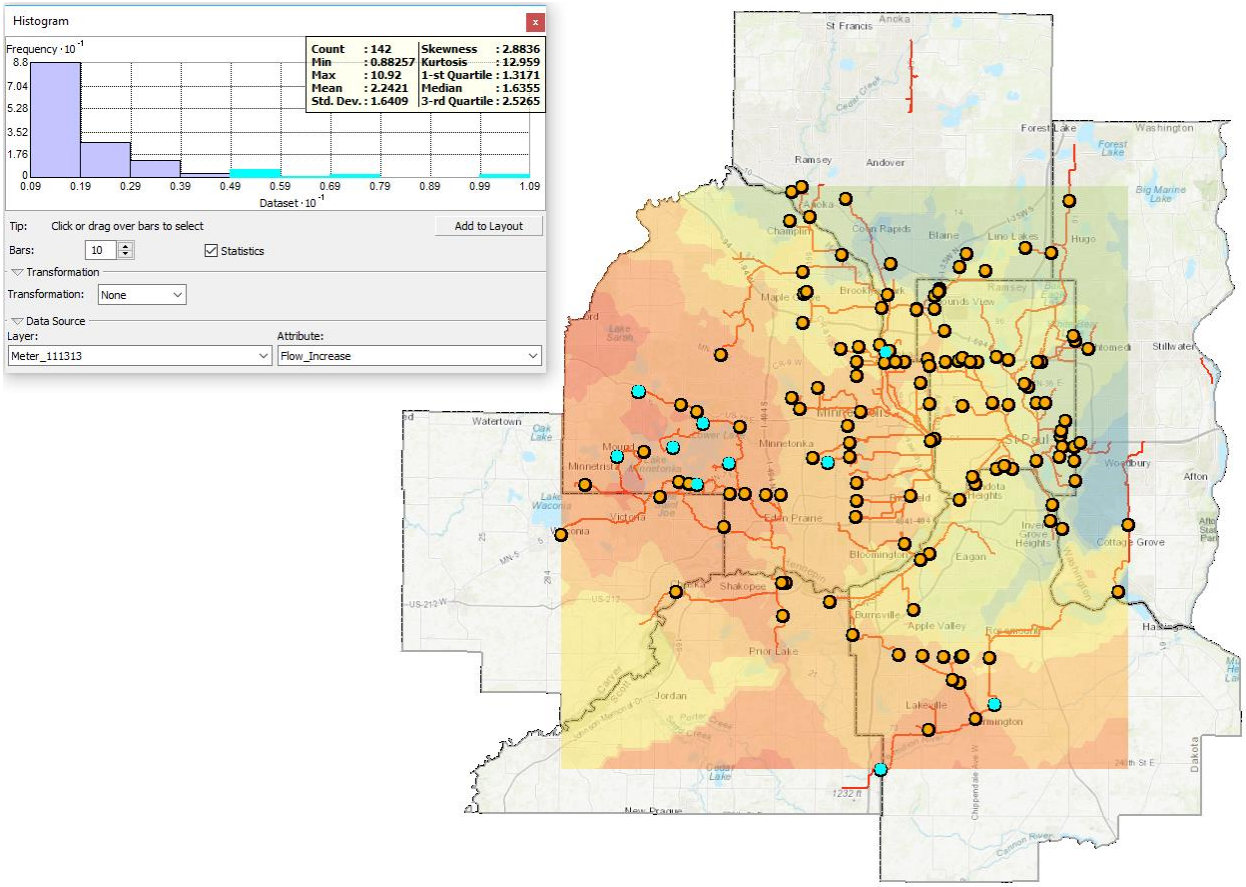

Figure 49. Major outliers from the July 13, 2013 rainfall event.

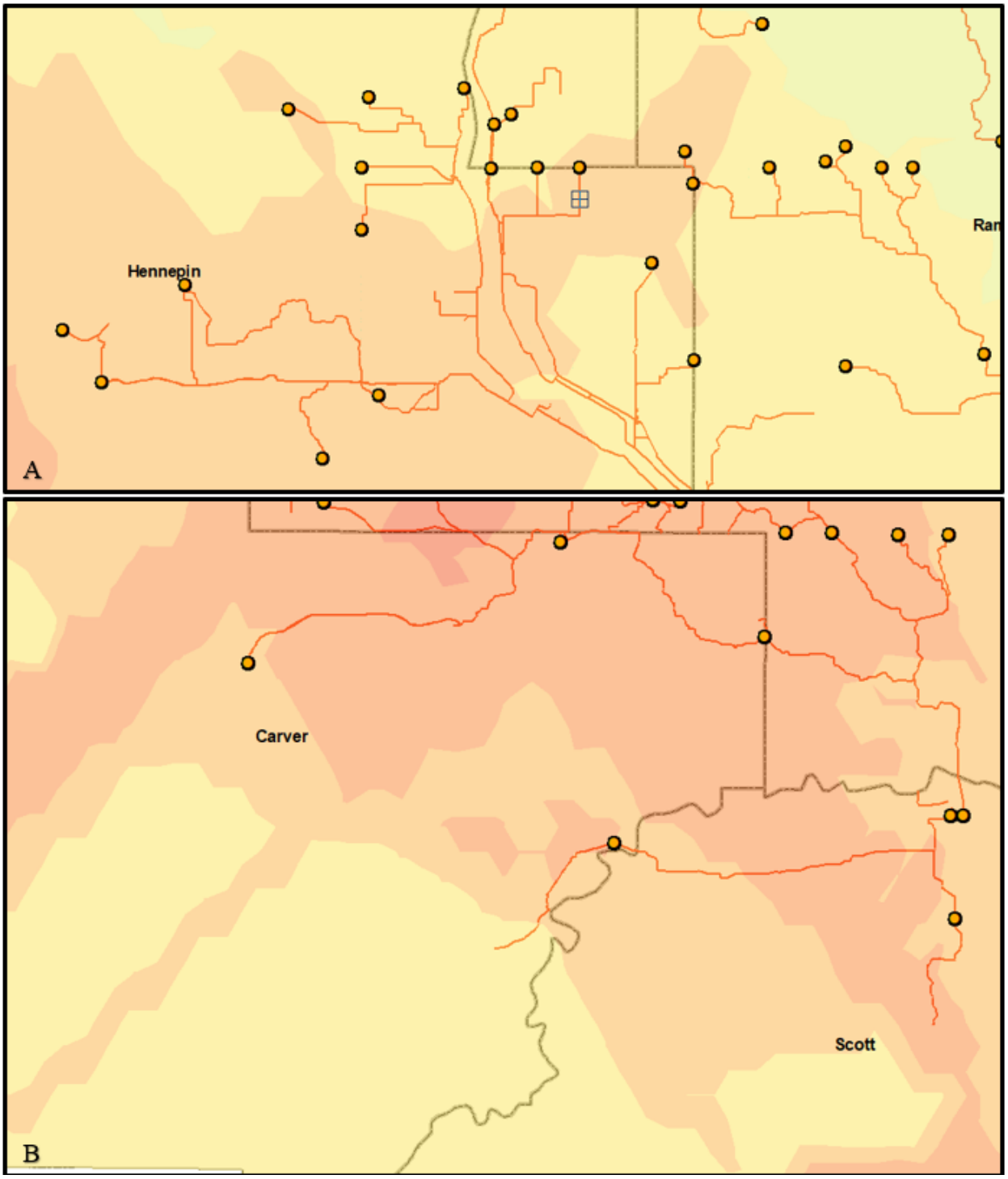

Figure 50. A comparison between an interpolated surface from clustered data points (A) and an interpolated surface from sparse data points (B). Each meter in the example B are about 10 miles apart. Most of the meters in example A are at no more than 5 miles apart which creates a better prediction in those areas. The above images are from the July 13, 2013 rainfall event.

Does Kriging provide accurate insight into the I/I problem as a whole or what aspect of I/I is being displayed in the Twin Cities Metro area case study?

The influence of I/I on flow increase in the sewer system was calculated using the max flow rate during the rainfall event and the average 10 year flow at each flow meter. This was the primary dataset used for the prediction surface to determine the impact of I/I on the study area. When cross-referenced with the sewer network shapefile in ArcMap, it provided a visual representation of which MCES interceptors capture areas of significant flow increase, which is significant when a small amount of rain occurred in that area (Figure 45). However, these "hotspots" do not represent the I/I problem as a whole, but instead represents one of the three I/I components: GWI, RII, or RDI.

This geostatistical analysis of I/I using ArcGIS does not measure the three components of I/I (GWI, RII, and RDI), but utilizes the maximum peaks on hydrographs related to RDI (Figure 2). This means that this methodology does not, specifically, detect GWI, because it does not have a noticeable impact on hydrograph peak flows due to its slow infiltration into the collection system (Staufer, Scheidegger, and Rieckermann 2012). Lastly, peak flows identified on the hydrograph represent areas that are susceptible to RDI instead of RII, because RII has a significant lag time before it registers on hydrographs and is not nearly as aggressive with entry in to the sewer system as RDI.

Assessment of the Results

Clearly, kriging is a powerful spatial interpolation method that can be used to interpolate sampled variables from a series of known data points that are distributed throughout an area of interest. This is a very useful technique to determine the value of unsampled locations throughout a study reach through the use of these known data points and interpolating values

between these points where no known data exists. The overarching benefit of kriging is that it has the potential to save time, money, and manpower necessary for intensive field-based surveys to collect data. However, kriging is not without its limitations and it has, to my knowledge, never been used in research focusing on increased flow from meters within waste water infrastructure. Therefore, in evaluating kriging's effectiveness, applicability and future potential in work such as this, a discussion of limitations in this work must be presented. Those limitations as they apply to this case study are as follows: First, the prediction surface results may not accurately represent the I/I issue of each flow meter and metershed that reside in the "hotspots." Second, the inherent error found in the interpolation process lead to discrepancies in the prediction surface. Lastly, the overall quality of this method and a positive perspective on how these limitations may produce unexpected results.

Prediction Surface Inconsistencies

The primary purpose of this analysis is to create "hotspots" on the map to identify I/I, but it is important to speculate what is actually being represented by the final prediction surface. The "hotspots" can be used for multiple reasons: to identify flow meters that need maintenance, to find flow meters that have faulty data, or to identify what areas are in need of an I/I inspection to determine if there is potentially faulty sewer pipes in that area.

Currently, this method is focusing the "hotspots" around the flow meters instead of their respective metershed (Figure 47), which are the boundaries of each city's sewer network that flows through the flow meter at the edge of their city (Figure 51). This may lead to an incorrect representation of the issue since the excess flow comes from upstream of the flow meters and not in a perfect circumference around the flow meter. Also, this case study is currently only depicting MCES's interceptor sewer pipes and not the municipality's sewer pipes that connect to

the interceptors (Figure 47). This begs the question of whether or not MCES's sewers are in pristine condition or if the communities they service are actually introducing I/I into MCES's sewer pipes resulting in spiked flow on their hydrographs. Further investigation will be required to determine which is true.

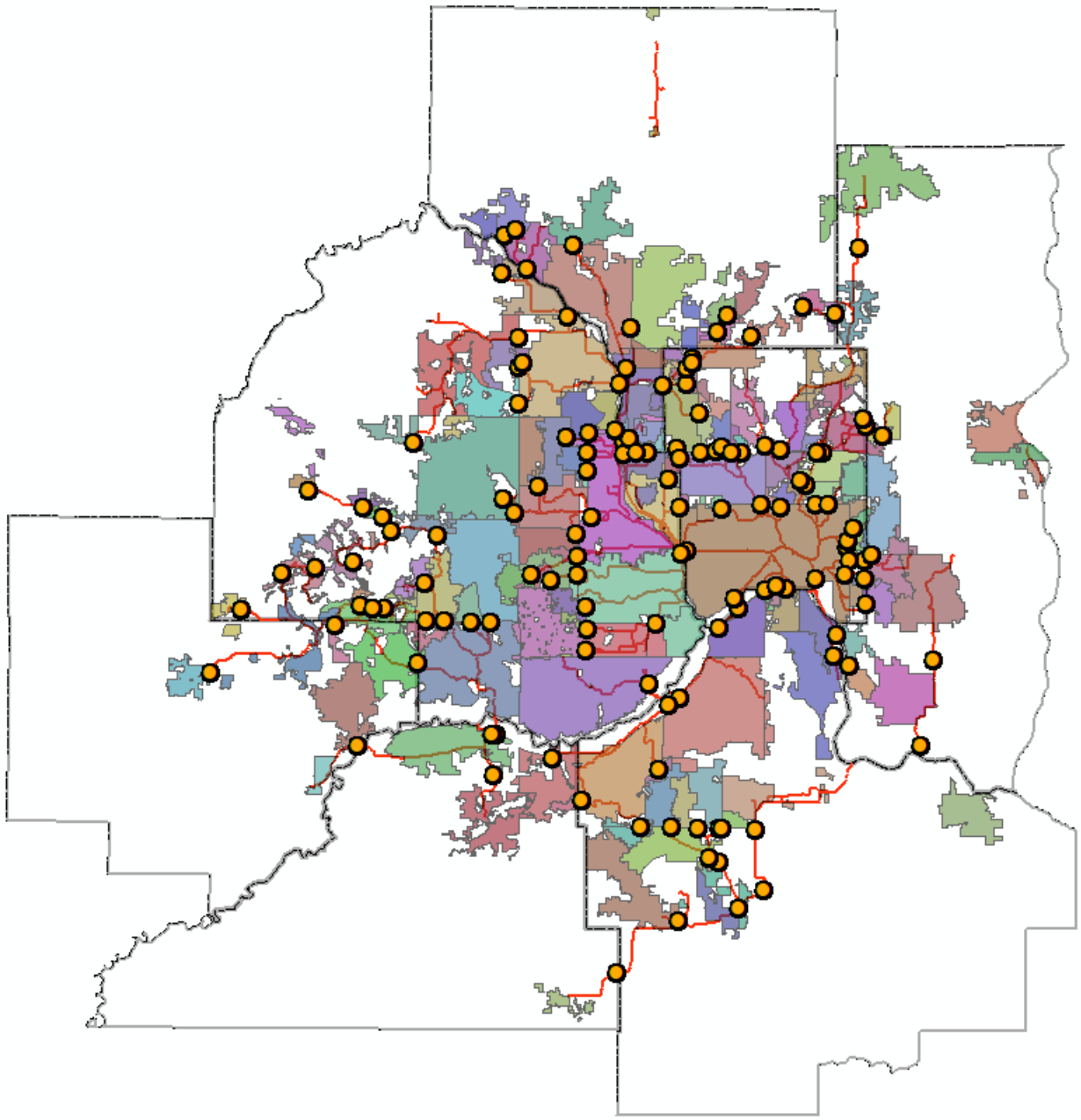

Figure 51. Close up of flow meters and their Metersheds color coordinated.

Lastly, the interpolation of increased flow around the flow meter may be misrepresenting the I/I issue since the exit point from each municipality is from one metershed (Figure 47). It would potentially be more accurate to create a centroid (center point) for each community's metershed and interpolate from that point, which would possibly give a better representation of where the flow issues really reside. This is assuming that the community's sewer networks are the reason I/I is occurring in the MCES's interceptors.

Spatial Interpolation Defects

Another issue to consider in this analysis is how the density of the dataset affects the interpolation process. Inherent biases in the dataset due to fixed locations of the flow meters does not allow for random sampling of the points. This also leads to the radical gaps between meters (Figure 50). These gaps lead to generalization and streaking of the dataset in some areas as seen in the southwest portion of the Blue Lake WWTF Prediction Map (Figure 37). During interpolation, clustering of the dataset can create a more accurate prediction surface (Figure 50) whereas sparsely placed sample points leads to a lack of data resulting in anomalies like streaking or generalization of the data (Figure 52). Streaking occurs when extrapolation of the dataset goes beyond the sampled region and there is not a strong enough trend to create a valid prediction. The July 13, 2013 rainfall prediction map was effectively extrapolated to the seven county boundaries without streaking (Figure 34), because the rainfall had a strong spatial autocorrelation unlike the flow meters that are random due to varying flow increase. Error due to sparsely distributed sample points in this study area could be remedied by adding flow meters to the landscape. The spatial distribution of the meters plays an important role that must be considered and areas with sparse data will need to be evaluated and compensated for by other means.

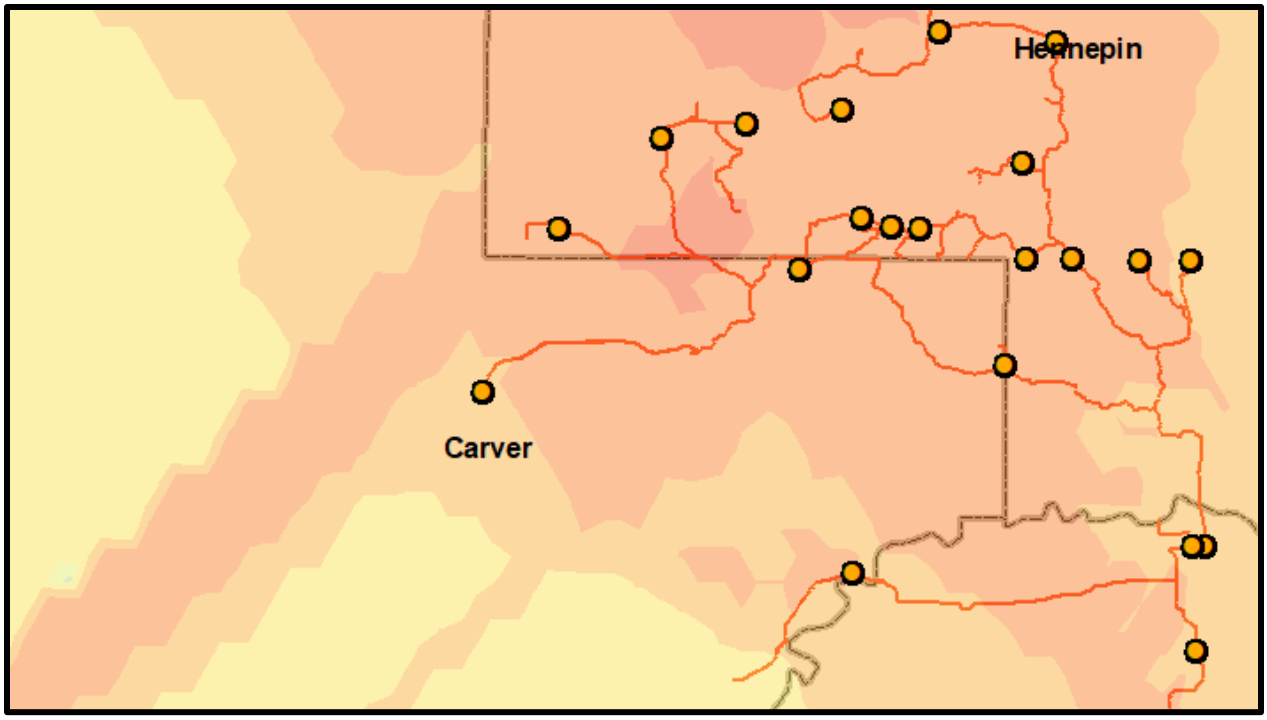

Figure 52. Close up of a streak due to lack of data in the region and the kriging processes attempt at extrapolating the dataset from the last known sample points into the abyss. Carver County and Hennepin County July 13, 2013.

This analysis provides a practical and efficient five step workflow (Figure 7) that only requires one GIS user to explore the spatial data and adjust the parameters in the geostatistical wizard to create the best prediction surface possible. The most important feature required for this workflow is accurate input data produced by the flow meters. This case study is a testament to the significance of flow monitoring and metering. The interpolation process reflects any residual error found in the data (Lam 1983; Mitas and Mitasova 1999; Johnston et al. 2001; Li and Heap 2011; Oliver and Webster 2014), so more accurate flow data will lead to better results. It is possible to refine the method for addressing metering data issues by collaborating with agencies like MCES. Metering data issues refers to the 200 flow meters owned by MCES and the limited use of only 136 of those meters for the July 13, 2013 analysis (Figure 49) due to meter discrepancies, performance meters not used in the I/I program, the occurrence of multiple meters

at the same location, and manual adjustments made by the MCES's Data Analyst. It is possible to see these gaps in the metershed when observing Figure 33.

This process appears to be a statistical and visual success for locating areas susceptible to I/I based on the basic parameters of rainfall and flow increase. It does pose the inherent flaw of generalizing the "hotspots" around each flow meter if there are not enough points within the search neighborhood (Figure 47), but this flaw can be remedied by adding more flow meters to the area of interest. Many case studies have added temporary flow meters to their study areas to improve the overall equation, but this would require research in to the cost and effectiveness of the extra flow meters (Metropolitan Council of the Twin Cities 2009; Shelton et al. 2011; Staufer, Scheidegger, and Rieckermann 2012).

Additional flow meter locations along the MCES's interceptors and along each municipality's sewer networks would provide a more accurate prediction surface. Over 200 flow meters are currently used to provide MCES with a means to monitor flow rates and flow influx, but with more data input into this method it would be possible to better locate weaknesses in all sewer networks in the metropolitan area. Access to each municipality's sewer data would also show the complete density of the network in the metropolitan area. Currently the MCES's interceptors appear to be the only problem to fix, but they are just the junction for all cities pipes to reach the WWTF.

Applicability/Best Use of this Method

Despite these limitations, this method presents a promising approach to narrow the focus of work in wastewater infrastructure maintenance. Kriging methods presented in this thesis provide both a visual and statistical representation of an interpolated dataset across the spatial extent of the wastewater infrastructure, which can be utilized by a GIS user and decision makers

to potentially identify areas at risk of I/I or identify malfunctioning meters. Assuming the organization concerned with maintaining the wastewater treatment infrastructure is similar to the MCES, they can produce this analysis using flow meter data and follow the workflow presented here with ease. To complete this analysis, this organization would need flow meters distributed throughout the area of interest and GIS users who can process the flow meter data to create the prediction surface.

That said, the broad assessment of the results of this work can best be described as demonstrating a high degree of potential for applicability. But, this method requires more field-based testing, that was beyond the scope of this thesis research, to evaluate the true applicability in a study reach or in multiple, varied study reaches (e.g. across varied municipalities. Future work should investigate I/I "hotspots" presented by this method through more intensive techniques (as discussed in the introduction) to verify how accurate/precise this method can be.

Overall, the results of the fourteen rainfall events and their respective flow increase prediction maps revealed a consistent correlation between Rainfall and Flow Increase (Appendix C and D). Therefore, the interpolation method is positively identifying areas of increase flow that correlate to the rainfall in that region. Further inspection may find other environmental and anthropogenic factors play a role in the results of the prediction surfaces. However, a few events did depict areas with low precipitation and a high flow increase (Figure 45). This potentially indicates that the methodology has effectively located areas that are susceptible to I/I, but requires ground-truthing via collaboration with agencies like MCES to validate its effectiveness.

Conclusion

This work presents the use of ArcGIS and geostatistics in assisting with the identification of areas susceptible to I/I during rainfall. There is a need to prioritize high-risk areas before they reach critical failure and the price of repairs increases (Shelton et. al., 2011). Geospatial and geostatistical analysis provides the potential for identifying I/I prone areas of the collection systems that are not monitored, determining where I/I is occurring, and determining the magnitude of I/I in those areas. This case study provides a practical and efficient five step workflow (Figure 7) that only requires one GIS user to explore the spatial data and adjust the kriging model to create the best prediction surface possible.

The vast area and age of the Metropolitan Council Environmental Services (MCES) sewers has often led to problematic issues related to I/I, which are now in need of a more effective way to focus rehabilitation efforts of the sanitary sewers. Over the course of the next 20 years, wastewater infrastructure repair are estimated to cost upwards of 4.1 billion dollars in Minneapolis-St. Paul Metropolitan area (Metropolitan Council of the Twin Cities 2011). The MCES has used CCTV for most of their interceptor system and has done inch-by-inch inspection for corrosion (Metropolitan Council of the Twin Cities 2009). In addition, engineers assess and score every section of pipe by conducting dye and smoke testing, as well as monitoring flow conditions by comparing rainfall data versus average and max discharge measurements. However, MCES does not have detailed information on the cities collection systems that connect to their interceptors and this can be a major contributor of I/I. Overall, MCES would benefit from kriging prediction maps to locate high risk areas of I/I.

By collaborating with MCES it is possible to determine how accurately this methodology can locate areas susceptible to I/I or if it is actually depicting some other characteristic of the

WWTF collection system like malfunctioning flow meters. MCES could provide more insight into this method and what is being represented by using the geostatistical analysis of I/I in their identification process. Whether the I/I problem is directly related to faulty flow meters, poorly maintained sewer systems, variations in porosity of the soil, specific pipe characteristics (size/shape/age/type) resulting in high flow, topographic variability, land use practices, the level of the groundwater table in the region, or some other factor(s) is yet to be revealed.

Metropolitan areas worldwide struggle with maintaining wastewater treatment infrastructure and preventing I/I from impacting their wastewater treatment facilities, environments, and economy. The application of kriging to identify areas of high risk to I/I may become an instrument to provide economic justice for smaller municipalities who do not have the funds to investigate the I/I problem themselves. Overall, this may be a major contribution to I/I identification process and the wastewater treatment industry around the world, but the limitations discussed should be addressed in the future to test the effectiveness of this method with helping identify the real world scenario.

References

Adhikary, P. P., C. J. Dash, R. Bej, and H. Chandrasekharan. 2011. Indicator and probability kriging methods for delineating Cu, Fe, and Mn contamination in groundwater of Najafgarh Block, Delhi, India. Environmental Monitoring and Assessment 176 (1–4):663–676.

Ahmed, K., S. Shahid, and S. Bin Harun. 2014. Spatial interpolation of climatic variables in a predominantly arid region with complex topography. Environment Systems and Decisions 34 (4):555–563.

Ahrens, B. 2005. Distance in spatial interpolation of daily rain gauge data. Hydrology and Earth System Sciences Discussions 2 (5):1893–1922.

American Society of Civil Engineers. 2011. Failure to Act: The Economic Impact of Current Investment Trends in Electricity Infrastructure.

http://www.asce.org/uploadedFiles/Infrastructure/Failure_to_Act/energy_report_FINAL2.pdf.

Amirinejad, A. A., K. Kamble, P. Aggarwal, D. Chakraborty, S. Pradhan, and R. B. Mittal. 2011. Assessment and mapping of spatial variation of soil physical health in a farm. Geoderma 160 (3–4):292–303.

Andersen, C. B., G. P. Lewis, and K. A. Sargent. 2004. Influence of wastewater-treatment effluent on concentrations and fluxes of solutes in the Bush River, South Carolina, during extreme drought conditions. Environmental Geosciences 11 (1):28–41.

Arslan, H. 2012. Spatial and temporal mapping of groundwater salinity using ordinary kriging and indicator kriging: The case of Bafra Plain, Turkey. Agricultural Water Management 113:57–63.

Ashiq, M. W., C. Zhao, J. Ni, and M. Akhtar. 2010. GIS-based high-resolution spatial interpolation of precipitation in mountain–plain areas of Upper Pakistan for regional climate change impact studies. Theoretical and Applied Climatology 99 (3–4):239–253.

Bao, Z., W. Wu, H. Liu, S. Yin, and H. Chen. 2014. Geostatistical analyses of spatial distribution and origin of soil nutrients in long-term wastewater-irrigated area in Beijing, China. Acta Agriculturae Scandinavica, Section B — Soil & Plant Science 64 (3):235–243.

De Bénédittis, J., and J. L. Bertrand-Krajewski. 2005. Infiltration in sewer systems: comparison of measurement methods. Water science and technology : a journal of the International Association on Water Pollution Research 52 (3):219–27.

Bennett, D. 1999. Using flow prediction technologies to control sanitary sewer overflows: project 97-CTS-8. Water Environment Research Foundation.

Berke, O. 2004. Exploratory disease mapping: kriging the spatial risk function from regional count data. International journal of health geographics 3 (1):18.

Bertrand-Krajewski, J. L., M. A. Cardoso, B. Ellis, T. Frehmann, M. Giulianellli, W. Gujer, P. Krebs, Z. Pliska, J. Pollert, and K. Pryl. 2005. Towards a better knowledge and management of infiltration and exfiltration in sewer systems: the APUSS project. 10th International Conference on Urban Drainage (November 2015).

Blanco, R. I., G. Melodie Naja, R. G. Rivero, and R. M. Price. 2013. Spatial and temporal changes in groundwater salinity in South Florida. Applied Geochemistry 38:48–58.

Boersma, A. 2012. Inflow and Infiltration. GIS for Water Resources (June):55101.

Burrough, P. a. 2001. GIS and geostatistics: Essential partners for spatial analysis. Environmental and Ecological Statistics 8 (4):361–377.

Calderón, G. F.-A. 2009. Spatial regression analysis vs. kriging methods for spatial estimation. International Advances in Economic Research 15 (1):44–58.

Chappell, A., L. J. Renzullo, T. H. Raupach, and M. Haylock. 2013. Evaluating geostatistical

methods of blending satellite and gauge data to estimate near real-time daily rainfall for Australia. Journal of Hydrology 493:105–114.

Chen, C., K. Hu, H. Li, A. Yun, and B. Li. 2015. Three-Dimensional Mapping of Soil Organic Carbon by Combining Kriging Method with Profile Depth Function ed. W. Liang. PLOS ONE 10 (6):1–15.

Chen, D. L., T. H. Ou, L. B. Gong, C. Y. Xu, W. J. Li, C. H. Ho, and W. H. Qian. 2010. Spatial Interpolation of Daily Precipitation in China: 1951-2005. Advances in Atmospheric Sciences 27 (6):1221–1232.

Chiles, J.-P., and P. Delfiner. 2009. Geostatistics: Modeling Spatial Uncertainty.

Clark, I. 1977. Regularization of a semivariogram. Computers & Geosciences 3 (2):341–346.

Curtarelli, M., J. Leão, I. Ogashawara, J. Lorenzzetti, and J. Stech. 2015. Assessment of Spatial Interpolation Methods to Map the Bathymetry of an Amazonian Hydroelectric Reservoir to Aid in Decision Making for Water Management. ISPRS International Journal of Geo-Information 4 (1):220–235.

Dafonte, J. D., M. U. Guitián, J. Paz-Ferreiro, G. M. Siqueira, and E. V. Vázquez. 2010. Mapping of soil micronutrients in an european atlantic agricultural landscape using ordinary kriging and indicator approach. Bragantia 69:175–186.

deMonsabert, S., and P. Thornton. 1997. A Benders Decomposition Model for Sewer Rehabilitation Planning for Infiltration and Inflow Planning. Water Environment Research 69 (2):162–167.

Dindaroğlu, T. 2014. The use of the GIS Kriging technique to determine the spatial changes of natural radionuclide concentrations in soil and forest cover. Journal of Environmental Health Science and Engineering 12 (1):130.

Diodato, N., and M. Ceccarelli. 2004. Multivariate indicator Kriging approach using a GIS to classify soil degradation for Mediterranean agricultural lands. Ecological Indicators 4 (3):177–187.

Einax, J. W., and U. Soldt. 1999. Geostatistical and multivariate statistical methods for the assessment of polluted soils—merits and limitations. Chemometrics and Intelligent Laboratory Systems 46 (1):79–91.

Ellis, J. 2001. Sewer infiltration/exfiltration and interactions with sewer flows and groundwater quality. http://apuss.insa-lyon.fr/c001_sewer_infiltration_exfiltration_and_interactions_with_sewer_flows_and_groudwater_quality.pdf.

Environmental Systems Research Institute, I. (ESRI). 2016. The geostatistical workflow—Help | ArcGIS for Desktop. https://desktop.arcgis.com/en/arcmap/10.3/guide-books/extensions/geostatistical-analyst/the-geostatistical-workflow.htm (last accessed 9 November 2016).

Esri. 2006. ArcGIS Geostatistical Analyst Tutorial. :40. http://help.arcgis.com/en/arcgisdesktop/10.0/pdf/geostatistical-analyst-tutorial.pdf.

Fenner, R. . 2000. Approaches to sewer maintenance: a review. Urban Water 2 (2000):343–356.

Goovaerts, P. 1999. Using elevation to aid the geostatistical mapping of rainfall erosivity. Catena 34 (3–4):227–242.

Goovaerts, P. 2008. Kriging and semivariogram deconvolution in the presence of irregular geographical units. Mathematical Geosciences 40 (1):101–128.

Gruber, G., J.-L. Bertrand-Krajewski, J. De Beneditis, M. Hochedlinger, and W. Lettl. 2005. Practical aspects, experiences and strategies by using UV/VIS sensors for long-term sewer monitoring. In 10th International Conference on Urban Drainage, 1–8. Copenhagen/Denmark http://www.water-security.com/medialibrary/publications/p_2005_03.pdf.

Gundogdu, K. S., and I. Guney. 2007. Spatial analyses of groundwater levels using universal kriging. Journal of earth system science 116 (1):49–55.

Guo, D., R. Guo, and C. Thiart. 2007. Predicting air pollution using fuzzy membership grade Kriging. Computers, Environment and Urban Systems 31 (1):33–51.

Gustafsson, A.-M., L.-G. Gustafsson, S. Ahlman, M. von Scherling, E. Wilmin, and L. Kjellson. 2010. Modelling rainfall dependent infiltration and inflow (RDII) in a separate sewer system in Huddinge, Stockholm. In International MIKE by DHI conference 2010, P061.

Gustafsson, L.-G. 2000. Alternative Drainage Schemes for Reduction of Inflow / Infiltration - Prediction and Follow-Up of Effects with the Aid of an Integrated Sewer / Aquifer Model. 1st International Conference on Urban Drainage via Internet :21–37.

Halfawy, M. R., L. Dridi, and S. Baker. 2008. Integrated Decision Support System for Optimal Renewal Planning of Sewer Networks. Journal of Computing in Civil Engineering 22 (6):360–372.

Hassan, M. M., and P. J. Atkins. 2011. Application of geostatistics with Indicator Kriging for analyzing spatial variability of groundwater arsenic concentrations in Southwest Bangladesh. Journal of environmental science and health. Part A, Toxic/hazardous substances & environmental engineering 46 (11):1185–1196.

Helland, J. 2004. Minnesota and Wisconsin Groundwater Withdrawal Laws.

Hengl, T. 2006. Finding the right pixel size. Computers and Geosciences 32 (9):1283–1298.

———. 2009. A Practical guide to Geostatistical Mapping. http://book.spatial-analyst.net/system/files/cover_geostat_2009.pdf.

Hengl, T., G. B. M. Heuvelink, and D. G. Rossiter. 2007. About regression-kriging: From equations to case studies. Computers and Geosciences 33 (10):1301–1315.

Hengl, T., G. B. M. Heuvelink, and A. Stein. 2004. A generic framework for spatial prediction of

soil variables based on regression-kriging. Geoderma 120 (1–2):75–93.

Hengl, T., G. Heuvelink, and A. Stein. 2003. Comparison of kriging with external drift and regression-kriging. Technical note, ITC :17. http://www.itc.nl/library/Papers_2003/misca/hengl_comparison.pdf.

Hengl, T., H. Sierdsema, A. Radovic, and D. Arta. 2009. Spatial prediction of species' distributions from occurrence-only records: combinging point pattern analysis, ENFA and regression-kriging. Ecological Modelling 220 (24):3499–3511.

Houhou, J., B. S. Lartiges, C. France-Lanord, C. Guilmette, S. Poix, and C. Mustin. 2010. Isotopic tracing of clear water sources in an urban sewer: A combined water and dissolved sulfate stable isotope approach. Water Research 44 (1):256–266.

Huddleston, G. M., and J. H. Rodgers. 2008. Design of a constructed wetland system for treatment of copper-contaminated wastewater. Environmental Geosciences 15 (1):9–19.

Ihl, T., F. Bautista, F. Rubén, C. Ruíz, C. Delgado, P. Q. Owen, and D. Aguilar. 2015. Concentration of Toxic Elements in Top Soils of the Metropolitan Area of Mexico City: A Spatial Analysis using Ordinary Kriging and Indicator Kriging. sidad Nacional Autónoma de México , Campus Morelia , Antigua Carretera a Pátzcuaro 8701 , Col . Ex-Hacien. Revista Internacional de Contaminación Ambiental 31 (1):47–62.

Jian Kang, Rui Jin, and Xin Li. 2015. Regression Kriging-Based Upscaling of Soil Moisture Measurements From a Wireless Sensor Network and Multiresource Remote Sensing Information Over Heterogeneous Cropland. IEEE Geoscience and Remote Sensing Letters 12 (1):92–96.

Johnston, K., J. M. Ver Hoef, K. Krivoruchko, and N. Lucas. 2001. Using ArcGIS geostatistical analyst. Redlands. http://direitosminerarios.com/pdf/ESRI - Using ArcGIS Geostatistical Analyst.pdf.

Jossi, F. 2013. White Bear Lake retreat in Minnesota has big price tag. Finance and Commerce.

Karpf, C., and P. Krebs. 2011. Quantification of groundwater infiltration and surface water inflows in urban sewer networks based on a multiple model approach. Water Research 45 (10):3129–3136.

———. 2013. Modelling of groundwater infiltration into sewer systems. Urban Water Journal 10 (4):221–229.

King County. 2015. Regional Infiltration and Inflow Control program - King County. http://www.kingcounty.gov/services/environment/wastewater/ii.aspx (last accessed 9 November 2016).

Knotters, M., D. J. Brus, and J. H. Oude Voshaar. 1995. A comparison of kriging, co-kriging and kriging combined with regression for spatial interpolation of horizon depth with censored observations. Geoderma 67 (3–4):227–246.

Koo, D. H., and S. T. Ariaratnam. 2006. Innovative method for assessment of underground sewer

pipe condition. Automation in Construction 15 (4):479–488.

Kosse, P., M. Lübken, and M. Wichern. 2015. Urban lignocellulosic biomass can significantly contribute to energy production in municipal wastewater treatment plants – A GIS-based approach for a metropolitan area. Biomass and Bioenergy 81:568–573.

Krivoruchko, K. 2004. Introduction to Modeling Spatial Processes Using Geostatistcal Analyst. Esri :1–27. http://www.esri.com/library/whitepapers/pdfs/intro-modeling.pdf.

Lado, L. R., T. Hengl, and H. I. Reuter. 2008. Heavy metals in European soils: A geostatistical analysis of the FOREGS Geochemical database. Geoderma 148 (2):189–199.

Lai, F. 2008. Review of Sewer Design Criteria and RDII Prediction Review of Sewer Design Criteria and RDII Prediction Methods.

Lam, N. S.-N. 1983. Spatial Interpolation Methods: A Review. Cartography and Geographic Information Science 10 (2):129–150.

Lee, D.-J., J.-H. Choi, J. Chung, Y.-W. Lee, and Y.-I. Kim. 2009. Effect of Infiltration and Inflow in Dry Weather on Reducing the Pollution Loading of Combined Sewer Overflows. Environmental Engineering Science 26 (5):897–906.

Lee, D. J., and P. Toscas. 2015. Flexible geostatistical modeling and risk assessment analysis of lead concentration levels of residential soil in the Coeur D'Alene River Basin. Environmental and Ecological Statistics 22 (3):551–570.

Lee, J. H., C. W. Baek, J. H. Kim, H. D. Jun, and D. J. Jo. 2009. Development of a Decision Making Support System for Efficient Rehabilitation of Sewer Systems. Water Resources Management 23 (9):1725–1742.

Lee, R. K. 2005. Interpreting storm flow data to determine types of infiltration and inflow. :497–509.

Li, J., and A. D. Heap. 2011. A review of comparative studies of spatial interpolation methods in environmental sciences: Performance and impact factors. Ecological Informatics 6 (3–4):228–241.

Liao, D., D. J. Peuquet, Y. Duan, E. a. Whitsel, J. Dou, R. L. Smith, H. M. Lin, J. C. Chen, and G. Heiss. 2006. GIS approaches for the estimation of residential-level ambient PM concentrations. Environmental Health Perspectives 114 (9):1374–1380.

Lin, Y. P., T. K. Chang, C. W. Shih, and C. H. Tseng. 2002. Factorial and indicator kriging methods using a geographic information system to delineate spatial variation and pollution sources of soil heavy metals. Environmental Geology 42:900–909.

Liu, X. H., P. C. Kyriakidis, and M. F. Goodchild. 2008. Population-density estimation using regression and area-to-point residual kriging. International Journal of Geographical Information Science 22 (4):431–447.

Liu, X., J. Shannon, H. Voun, M. Truijens, H.-L. Chi, and X. Wang. 2014. Spatial and Temporal

Analysis on the Distribution of Active Radio-Frequency Identification (RFID) Tracking Accuracy with the Kriging Method. Sensors 14 (11):20451–20467.

Liu, X., J. Wu, and J. Xu. 2006. Characterizing the risk assessment of heavy metals and sampling uncertainty analysis in paddy field by geostatistics and GIS. Environmental Pollution 141 (2):257–264.

Machiwal, D., and M. K. Jha. 2015. Identifying sources of groundwater contamination in a hard-rock aquifer system using multivariate statistical analyses and GIS-based geostatistical modeling techniques. Journal of Hydrology: Regional Studies :1–31.

Matějíček, L., P. Engst, and Z. Jaňour. 2006. A GIS-based approach to spatio-temporal analysis of environmental pollution in urban areas: A case study of Prague's environment extended by LIDAR data. Ecological Modelling 199 (3 SPEC. ISS.):261–277.

McLellan, S. L., E. J. Hollis, M. M. Depas, M. Van Dyke, J. Harris, and C. O. Scopel. 2007. Distribution and Fate of Escherichia coli in Lake Michigan Following Contamination with Urban Stormwater and Combined Sewer Overflows. Journal of Great Lakes Research 33 (3):566.

Meng, Q., Z. Liu, and B. E. Borders. 2013. Assessment of regression kriging for spatial interpolation – comparisons of seven GIS interpolation methods. Cartography and Geographic Information Science 40 (1):28–39.

Mercer, L. D., A. a. Szpiro, L. Sheppard, J. Lindström, S. D. Adar, R. W. Allen, E. L. Avol, A. P. Oron, T. Larson, L.-J. S. Liu, and J. D. Kaufman. 2011. Comparing universal kriging and land-use regression for predicting concentrations of gaseous oxides of nitrogen (NOx) for the Multi-Ethnic Study of Atherosclerosis and Air Pollution (MESA Air). Atmospheric Environment 45 (26):4412–4420.

Metropolitan Council of the Twin Cities. 2007. 100 + Years of Water Quality Improvements in the Twin Cities A chronology of significant events affecting water quality in the Mississippi River in the Twin Cities metropolitan area. :1–5.

———. 2009. Inflow and Infiltration Tool Box. :1–39.

———. 2011. About MCES: An overview of Metropolitan Council Environmental Services. (March).

Milillo, T. M., and J. a. Gardella. 2008. Spatial analysis of time of flight-secondary ion mass spectrometric images by ordinary kriging and inverse distance weighted interpolation techniques. Analytical Chemistry 80 (13):4896–4905.

Minasny, B., and A. B. McBratney. 2007. Spatial prediction of soil properties using EBLUP with the Matérn covariance function. Geoderma 140 (4):324–336.

Mitas, L., and H. Mitasova. 1999. Spatial interpolation. Geographical Information Systems: Principles, Techniques, Management and Applications (1):481–492. http://skagit.meas.ncsu.edu/~helena/gmslab/papers/hgint39.pdf.

Morari, F., a. Castrignanò, and C. Pagliarin. 2009. Application of multivariate geostatistics in delineating management zones within a gravelly vineyard using geo-electrical sensors. Computers and Electronics in Agriculture 68 (1):97–107.

Mueller, T. G., N. B. Pusuluri, K. K. Mathias, P. L. Cornelius, R. I. Barnhisel, and S. a. Shearer. 2004. Map Quality for Ordinary Kriging and Inverse Distance Weighted Interpolation. Soil Science Society of America Journal 68 (6):2042.

Muleta, M. K., and P. F. Boulos. 2008. Analysis and Calibration of RDII and Design of Sewer Collection Systems. World Environmental and Water Resources Congress 2008 :1–10.

Narany, T., M. Ramli, A. Aris, W. Sulaiman, and K. Fakharian. 2013. Spatial Assessment of Groundwater Quality Monitoring Wells Using Indicator Kriging and Risk Mapping, Amol-Babol Plain, Iran. Water 6 (1):68–85.

Nelson, E. A., and J. B. Gladden. 2008. Full-scale treatment wetlands for metal removal from industrial wastewater. Environmental Geosciences 15 (1 PART 1):39–48.

Nikpay, M., D. Lazik, and P. Krebs. 2015. Permeability changes by surfactant solution: an experimental study to represent wastewater loss from sewers to saturated soil. Environmental Earth Sciences 73 (12):8443–8450.

Obeidat, M. M., A. M. Massadeh, A. M. Al-Ajlouni, and F. S. Athamneh. 2007. Analysis and evaluation of nitrate levels in groundwater at Al-Hashimiya area, Jordan. Environmental Monitoring and Assessment 135 (1–3):475–486.

Oldak, A., T. J. Jackson, and Y. Pachepsky. 2002. Using GIS in passive microwave soil moisture mapping and geostatistical analysis. International Journal of Geographical Information Science 16 (7):687–698. http://www.tandfonline.com.ezproxy.mnsu.edu/doi/pdf/10.1080/13658810210149407 (last accessed 9 October 2015).

Oliver, M. A., and R. Webster. 1990. Kriging: a method of interpolation for geographical information systems. International journal of geographical information systems 4 (3):313–332.

Oliver, M. A., and R. Webster. 2014. A tutorial guide to geostatistics: Computing and modelling variograms and kriging. CATENA 113:56–69.

Omuto, C. T., and R. R. Vargas. 2014. Re-tooling of regression kriging in R for improved digital mapping of soil properties. Geosciences Journal 19 (1):157–165.

Pardo-Igúzquiza, E., M. Chica-Olmo, M. J. Garcia-Soldado, and J. a. Luque-Espinar. 2009. Using semivariogram parameter uncertainty in hydrogeological applications. Ground Water 47 (1):25–34.

Pawlowski, C. W., L. Rhea, W. D. Shuster, G. Barden, and M. Asce. 2014. Some Factors Affecting Inflow and Infiltration from Residential Sources in a Core Urban Area : Case Study in a Columbus , Ohio , Neighborhood. Journal of Hydraulic Engineering 140 (January):105–114.

Pearce, J. L., S. L. Rathbun, M. Aguilar-Villalobos, and L. P. Naeher. 2009. Characterizing the spatiotemporal variability of PM2.5 in Cusco, Peru using kriging with external drift. Atmospheric Environment 43 (12):2060–2069.

Pebesma, E. J. 2006. The role of external variables and GIS databases in geostatistical analysis. Transactions in GIS 10 (4):615–632.

Pereira, P., M. Oliva, and I. Misiune. 2015. Spatial interpolation of precipitation indexes in Sierra Nevada (Spain): comparing the performance of some interpolation methods. Theoretical and Applied Climatology.

Peterson, E. W., and A. Lanning. 2009. Effectiveness of pilot-scale wetland designs in removing estrogenic compounds from municipal wastewater plant effluent. Environmental Geosciences 16 (2):61–69.

Rojas Fabro, A. Y., J. G. Pacheco Ávila, M. V. Esteller Alberich, S. A. Cabrera Sansores, and M. A. Camargo-Valero. 2015. Spatial distribution of nitrate health risk associated with groundwater use as drinking water in Merida, Mexico. Applied Geography 65:49–57.

Roper, W. E., and A. Blanco. 2016. Color Infrared Survey for Identification of Failing Onsite Treatment Systems. Compare A Journal Of Comparative Education (August):1–12.

Rutsch, M., J. Rieckermann, J. Cullmann, J. B. Ellis, J. Vollertsen, and P. Krebs. 2008. Towards a better understanding of sewer exfiltration. Water Research 42 (10–11):2385–2394.

Rutsch, M., J. Rieckermann, and P. Krebs. 2006. Quantification of sewer leakage: A review. Water Science and Technology 54:135–144.

Sadri, S., and E. Graham. 2011. Development of an antecedent moisture condition model for prediction of Rainfall-Derived Inflow/Infiltration (RDII). American Geophysical Union.

Sajid, A. H., R. P. Rudra, and G. P. Systematic. 2013. Systematic Evaluation of Kriging and Inverse Distance Weighting Methods for Spatial Analysis of Soil Bulk Density. Canadian Biosystems Engineering 55 (1983):1–14. http://www.csbe-scgab.ca/docs/journal/55/C13141.pdf.

Sakata, S., F. Ashida, and H. Tanaka. 2010. Stabilization of parameter estimation for Kriging-based approximation with empirical semivariogram. Computer Methods in Applied Mechanics and Engineering 199 (25–28):1710–1721.

Seo, Y., S. Kim, and V. P. Singh. 2015. Estimating Spatial Precipitation Using Regression Kriging and Artificial Neural Network Residual Kriging (RKNNRK) Hybrid Approach. Water Resources Management 29 (7):2189–2204.

Shad, R., M. S. Mesgari, A. Abkar, and A. Shad. 2009. Predicting air pollution using fuzzy genetic linear membership kriging in GIS. Computers, Environment and Urban Systems 33 (6):472–481.

Shelton, J. M., L. Kim, J. Fang, C. Ray, and T. Yan. 2011. Assessing the severity of rainfall-derived infiltration and inflow and sewer deterioration based on the flux stability of

sewage markers. Environmental science and technology 45 (20):8683–90.

Shiode, N., and S. Shiode. 2011. Street-level Spatial Interpolation Using Network-based IDW and Ordinary Kriging. Transactions in GIS 15 (4):457–477.

Skøien, J. O., R. Merz, and G. Blöschl. 2005. Top-kriging – geostatistics on stream networks. Hydrology and Earth System Sciences Discussions 2 (6):2253–2286.

Staufer, P., a. Scheidegger, and J. Rieckermann. 2012. Assessing the performance of sewer rehabilitation on the reduction of infiltration and inflow. Water Research 46 (16):5185–5196.

Stevens, P. 2002. Evaluation of Gauge Adjusted Radar for Rainfall Measurement in RDII Programs. Urban Drainage 2002 112:234–234.

Sun, C., J. Liu, Y. Wang, L. Sun, and H. Yu. 2013. Multivariate and geostatistical analyses of the spatial distribution and sources of heavy metals in agricultural soil in Dehui, Northeast China. Chemosphere 92 (5):517–523.

Tavares, M. T., A. J. Sousa, and M. M. Abreu. 2008. Ordinary kriging and indicator kriging in the cartography of trace elements contamination in São Domingos mining site (Alentejo, Portugal). Journal of Geochemical Exploration 98 (1–2):43–56.

Tobler, W. R. 1970. A Computer Movie Simulating Urban Growth in the Detroit Region. Economic Geography 46 (2):234–240.

United States Environmental Protection Agency. 2000. Collection Systems Technology Fact Sheet Sewers , Lift Station. :1–8.

US EPA. 2016a. About the Clean Watersheds Needs Survey (CWNS). https://www.epa.gov/cwns/about-clean-watersheds-needs-survey-cwns (last accessed 21 October 2016).

———. 2016b. Clean Watersheds Needs Survey (CWNS) – 2012 Report and Data. https://www.epa.gov/cwns/clean-watersheds-needs-survey-cwns-2012-report-and-data#access (last accessed 21 October 2016).

———. 2016c. CWNS 2012 Data and Reports. https://ofmpub.epa.gov/apex/cwns2012/f?p=cwns2012:3: (last accessed 21 October 2016).

Vainu, M., and J. Terasmaa. 2016. The consequences of increased groundwater abstraction for groundwater dependent closed-basin lakes in glacial terrain. Environmental Earth Sciences 75 (2):1–12.

Wade, M. G. 2000. Controlling Inflow and Infiltration in Wastewater Collection Systems. In Environmental and Pipeline Engineering 2000, 201–212. Reston, VA: American Society of Civil Engineers.

Wang, C., and H. Zhu. 2015. Combination of Kriging methods and multi-fractal analysis for

estimating spatial distribution of geotechnical parameters. Bulletin of Engineering Geology and the Environment :1–11.

Wang, J.-F., L.-F. Li, and G. Christakos. 2009. Sampling and kriging spatial means: efficiency and conditions. Sensors (Basel, Switzerland) 9 (7):5224–40.

Water Environment Federation. 2008. Operation of Municipal Wastewater Treatment Plants: MoP No. 11, Sixth Edition. WEF Press : New York, Chicago, San Francisco, Lisbon, London, Madrid, Mexico City, Milan, New Delhi, San Juan, Seoul, Singapore, Sydney, Toronto. https://accessengineeringlibrary.com/browse/operation-of-municipal-wastewater-treatment-plants-mop-no-11-sixth-edition.

———. 2010a. BACKGROUND. In Design of Municipal Wastewater Treatment Plants: WEF Manual of Practice No. 8 ASCE Manuals and Reports on Engineering Practice No. 76, Fifth Edition. McGraw Hill Professional, Access Engineering.

———. 2010b. Design of Municipal Wastewater Treatment Plants: WEF Manual of Practice No. 8 ASCE Manuals and Reports on Engineering Practice No. 76, Fifth Edition. McGraw-Hill Education: New York, Chicago, San Francisco, Lisbon, London, Madrid, Mexico City, Milan, New Delhi, San Juan, Seoul, Singapore, Sydney, Toronto.

Weiss, G., H. Brombach, and B. Haller. 2002. Infiltration and inflow in combined sewer systems: long-term analysis. In Mechanical & Transporation Engineering Abstracts, 11–19.

Wen, W., Y. Wang, L. Yang, D. Liang, L. Chen, J. Liu, and A. X. Zhu. 2014. Mapping soil organic carbon using auxiliary environmental covariates in a typical watershed in the Loess Plateau of China: a comparative study based on three kriging methods and a soil land inference model (SoLIM). Environmental Earth Sciences 73 (1):239–251.

White, G. J., and B. M. Ayyub. 1990. Semivariogram and kriging analysis in developing sampling strategies (corrosion). In [1990] Proceedings. First International Symposium on Uncertainty Modeling and Analysis, 360–365. IEEE Comput. Soc. Press.

Wirahadikusumah, R., D. M. Abraham, T. Iseley, and R. K. Prasanth. 1998. Assessment technologies for sewer system rehabilitation. Automation in Construction 7 (4):259–270.

Wright, L., S. Dent, C. Mosley, P. Kadota, and Y. Djebbar. 2001. Comparing rainfall dependent inflow and infiltration simulation methods. In Models and Applications to Urban Water Systems. Monograph 9, 235–257.

Yamamoto, J. K. 2005. Correcting the Smoothing Effect of Ordinary Kriging Estimates. Mathematical Geology 37 (1):69–94.

Younis, R., and M. A. Knight. 2010. A probability model for investigating the trend of structural deterioration of wastewater pipelines. Tunnelling and Underground Space Technology 25 (6):670–680. http://dx.doi.org/10.1016/j.tust.2010.05.007.

Zawadzki, J., P. Fabijańczyk, T. Magiera, and M. Rachwał. 2015. Geostatistical Microscale Study of Magnetic Susceptibility in Soil Profile and Magnetic Indicators of Potential Soil

Pollution. Water, Air, & Soil Pollution 226 (5):142.

Zhang, C., and D. McGrath. 2004. Geostatistical and GIS analyses on soil organic carbon concentrations in grassland of southeastern Ireland from two different periods. Geoderma 119 (3–4):261–275.

Zhang, H., and D. L. Zimmerman. 2007. Hybrid estimation of semivariogram parameters. Mathematical Geology 39 (2):247–260.

Zhang, S. wen, C. yang Shen, X. yang Chen, H. chun Ye, Y. fang Huang, and S. Lai. 2013. Spatial Interpolation of Soil Texture Using Compositional Kriging and Regression Kriging with Consideration of the Characteristics of Compositional Data and Environment Variables. Journal of Integrative Agriculture 12 (9):1673–1683.

Zhang, Z. 2005. Flow Data, Inflow/Infiltration Ratio, and Autoregressive Error Models. Journal of Environmental Engineering 131 (3):343–349.

———. 2007. Estimating Rain Derived Inflow and Infiltration for Rainfalls of Varying Characteristics. Journal of Hydraulic Engineering 133 (1):98–105.

Zhang, Z. 2008. Nonlinear extrapolation of inflow and infiltration behavior under heavy storms. Journal of Hydrologic Engineering 13 (12):1125–1132.

Zimmerman, D. L., and M. B. Zimmerman. 1991. A Comparison of Spatial Semivariogram Estimators and Corresponding Ordinary Kriging Predictors. Technometrics 33 (1):77–91.

Appendix A. Spatial Data Exploration

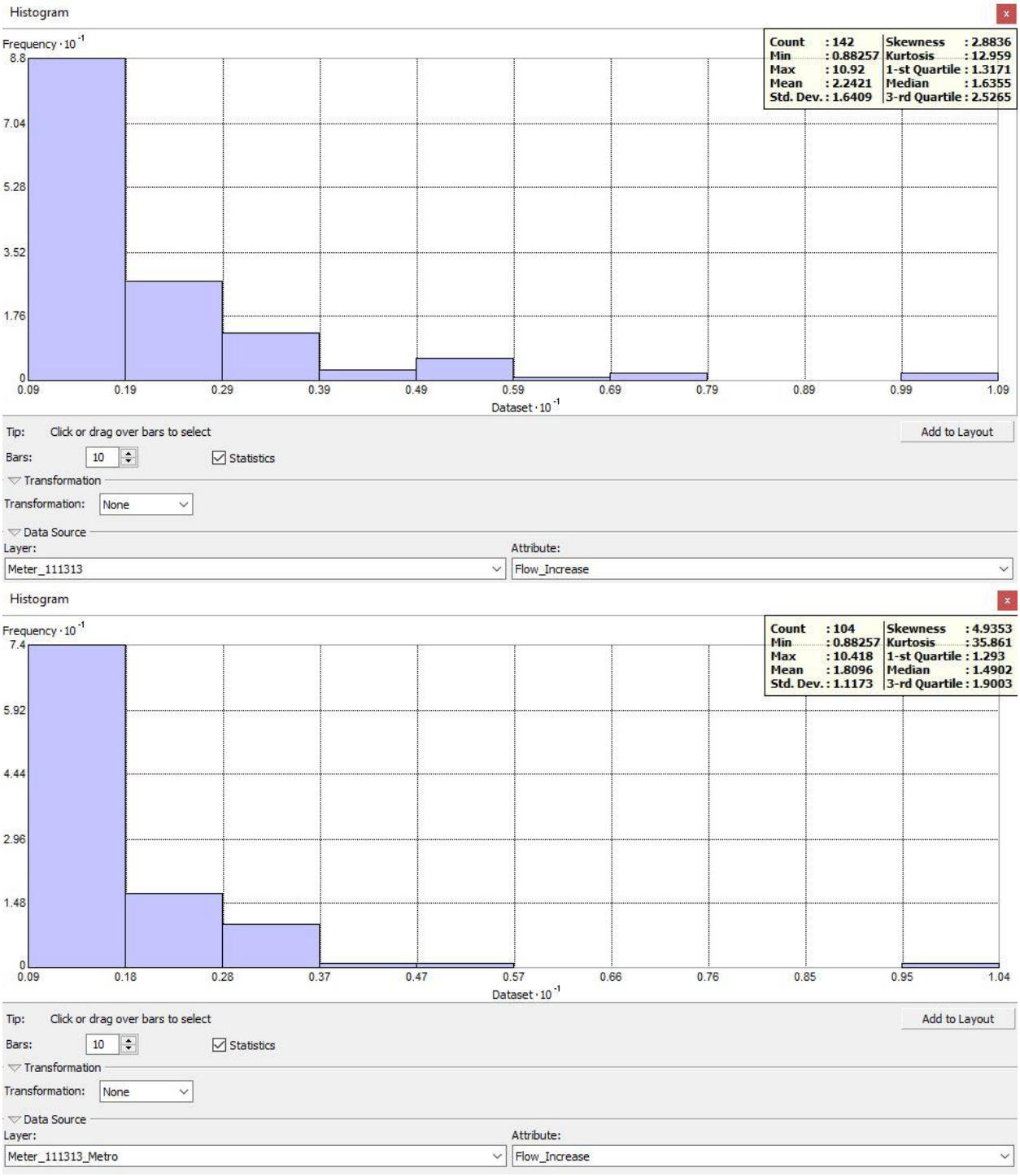

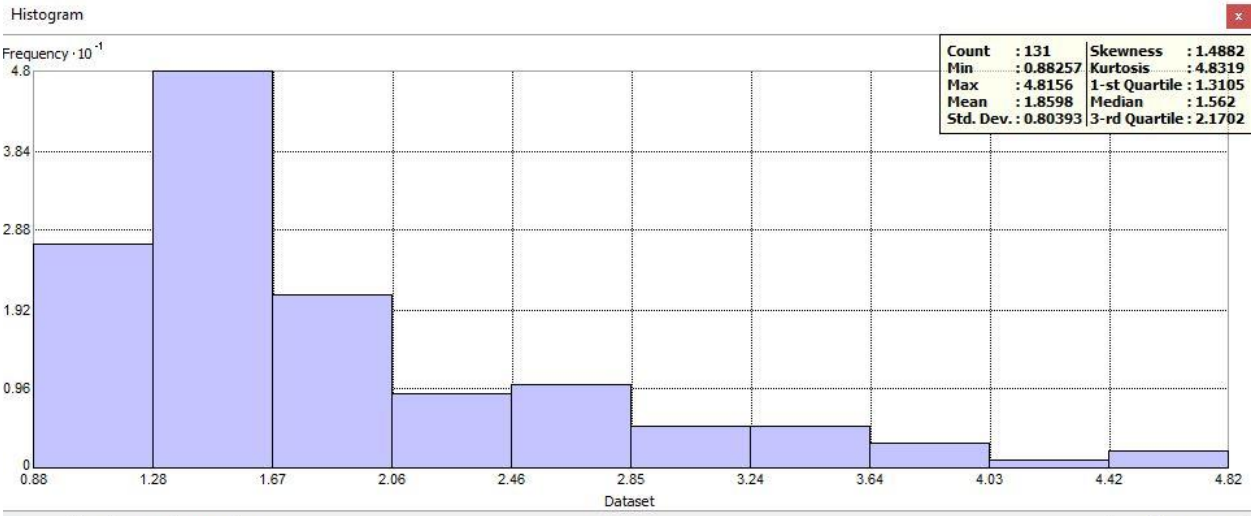
Histogram
Frequency · 10 -1
4.8
3.84
2.88
1.92
0.96
0
0.88
1.28
1.67
2.06
2.46
2.85
3.24
3.64
4.03
4.42
4.82
Dataset
Count : 131
Min : 0.88257
Max : 4.8156
Mean : 1.8598
Std. Dev. : 0.80393
Skewness : 1.4882
Kurtosis : 4.8319
1-st Quartile : 1.3105
Median : 1.562
3-rd Quartile : 2.1702
Tip: Click or drag over bars to select
Add to Layout
Bars: 10
Statistics
Transformation
Transformation: None
Data Source
Layer: Meter_111313_NA
Attribute: Flow_Increase

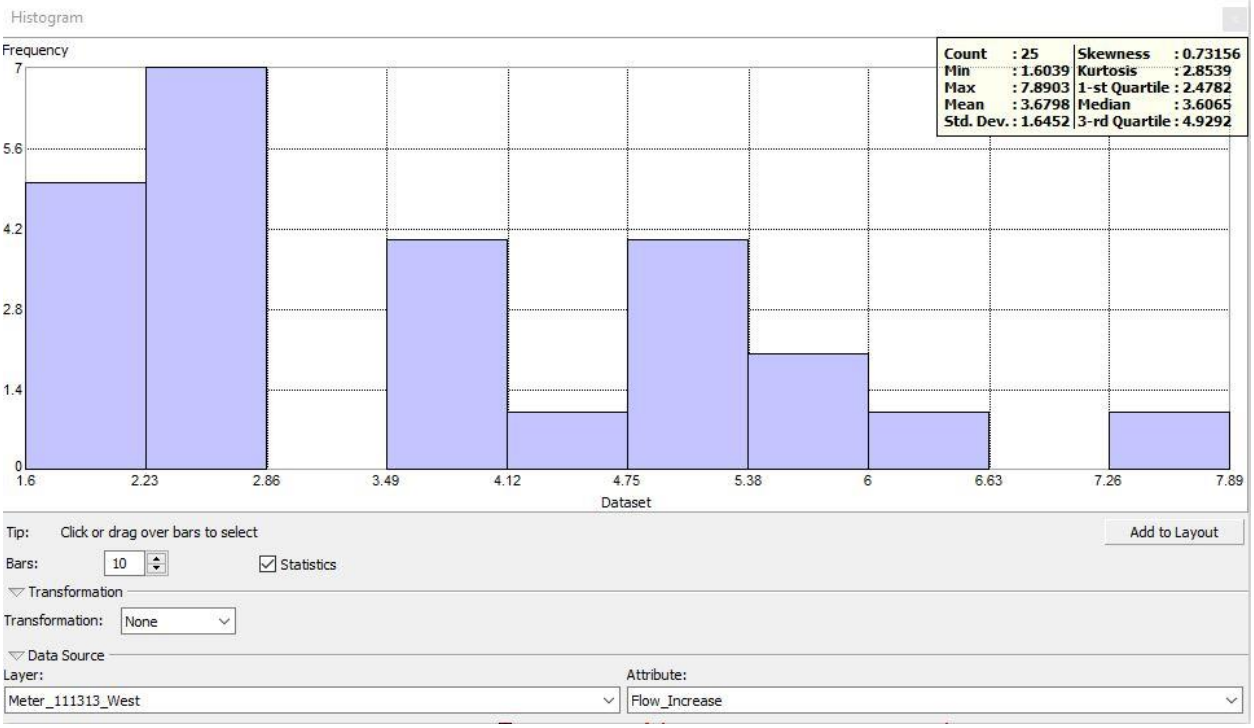
Histogram
Frequency
7
5.6
4.2
2.8
1.4
0
1.6
2.23
2.86
3.49
4.12
4.75
5.38
6
6.63
7.26
7.89
Dataset
Count : 25
Min : 1.6039
Max : 7.8903
Mean : 3.6798
Std. Dev. : 1.6452
Skewness : 0.73156
Kurtosis : 2.8539
1-st Quartile : 2.4782
Median : 3.6065
3-rd Quartile : 4.9292
Tip: Click or drag over bars to select
Add to Layout
Bars: 10
Statistics
Transformation
Transformation: None
Data Source
Layer: Meter_111313_West
Attribute: Flow_Increase

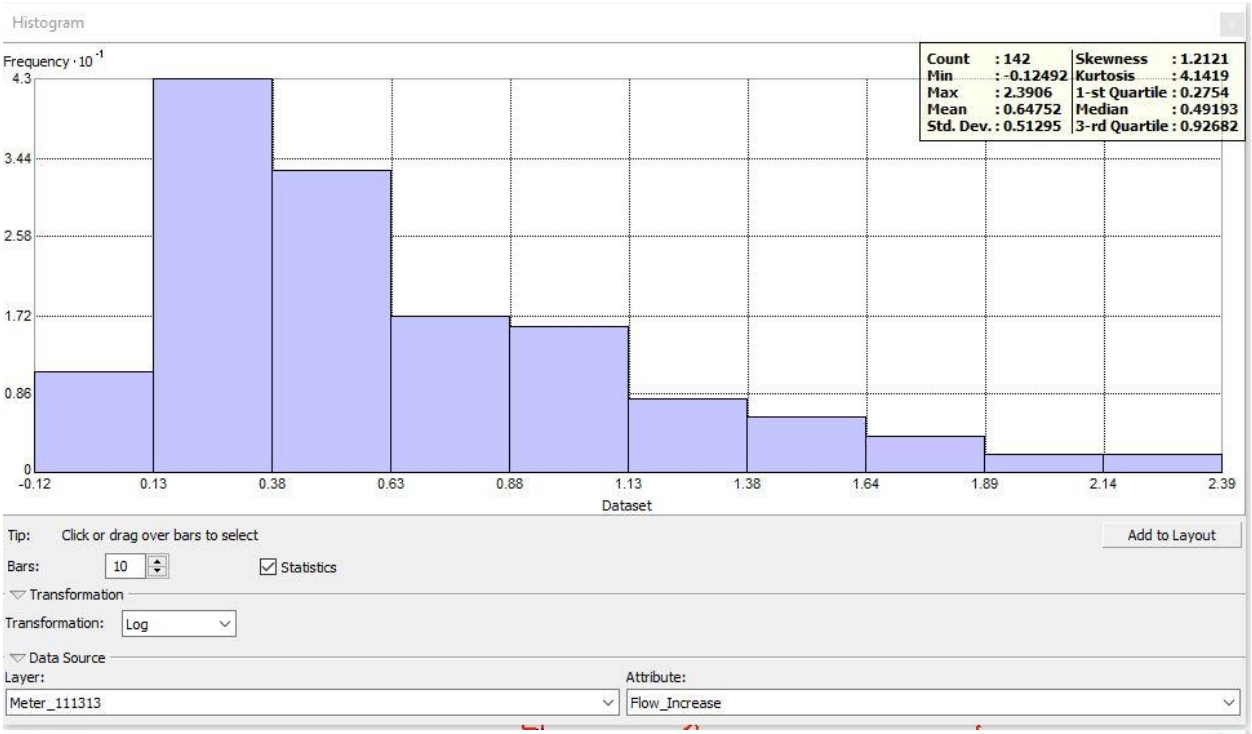
Histogram
Frequency · 10 -1
4.3
3.44
2.58
1.72
0.86
0
-0.12
0.13
0.38
0.63
0.88
1.13
1.38
1.64
1.89
2.14
2.39
Dataset
Count : 142
Min : -0.12492
Max : 2.3906
Mean : 0.64752
Std. Dev. : 0.51295
Skewness : 1.2121
Kurtosis : 4.1419
1-st Quartile : 0.2754
Median : 0.49193
3-rd Quartile : 0.92682
Tip: Click or drag over bars to select
Add to Layout
Bars: 10
Statistics
Transformation
Transformation: Log
Data Source
Layer:
Meter_111313
Attribute:
Flow_Increase

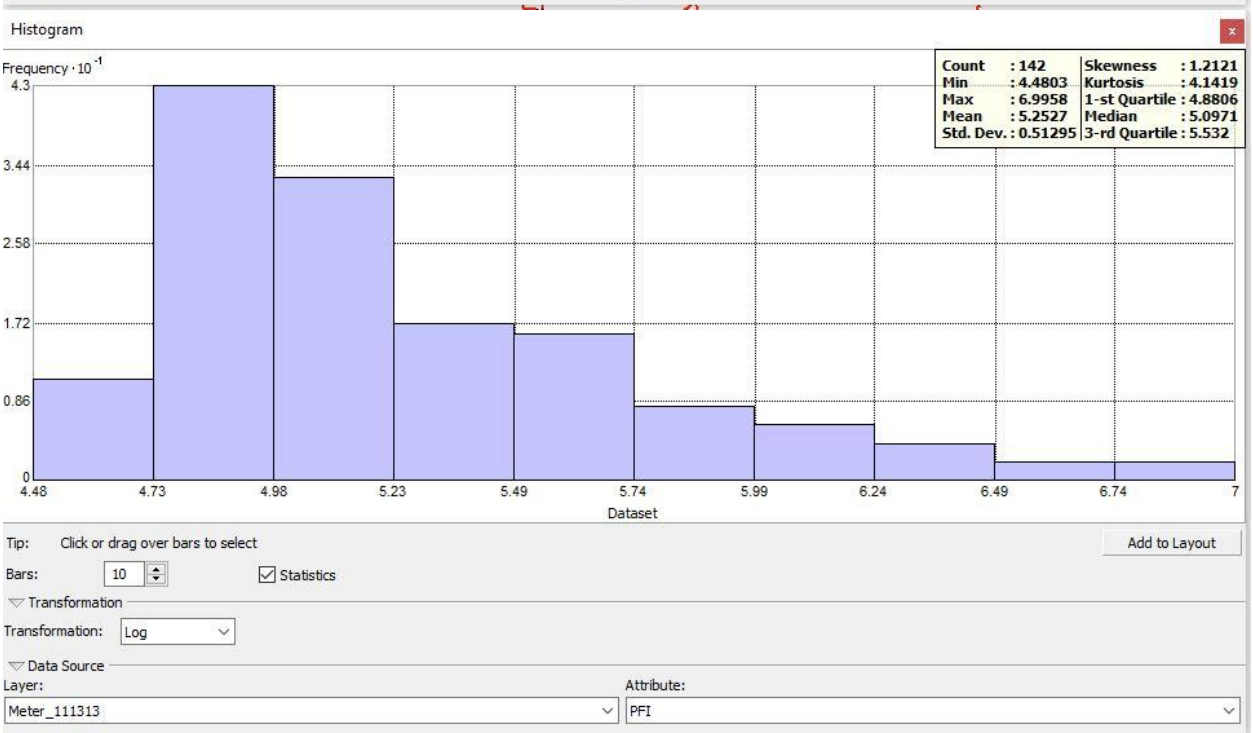
Histogram
Frequency · 10 -1
4.3
3.44
2.58
1.72
0.86
0
4.48
4.73
4.98
5.23
5.49
5.74
5.99
6.24
6.49
6.74
7
Dataset
Count : 142
Min : 4.4803
Max : 6.9958
Mean : 5.2527
Std. Dev. : 0.51295
Skewness : 1.2121
Kurtosis : 4.1419
1-st Quartile : 4.8806
Median : 5.0971
3-rd Quartile : 5.532
Tip: Click or drag over bars to select
Add to Layout
Bars: 10
Statistics
Transformation
Transformation: Log
Data Source
Layer:
Meter_111313
Attribute:
PFI

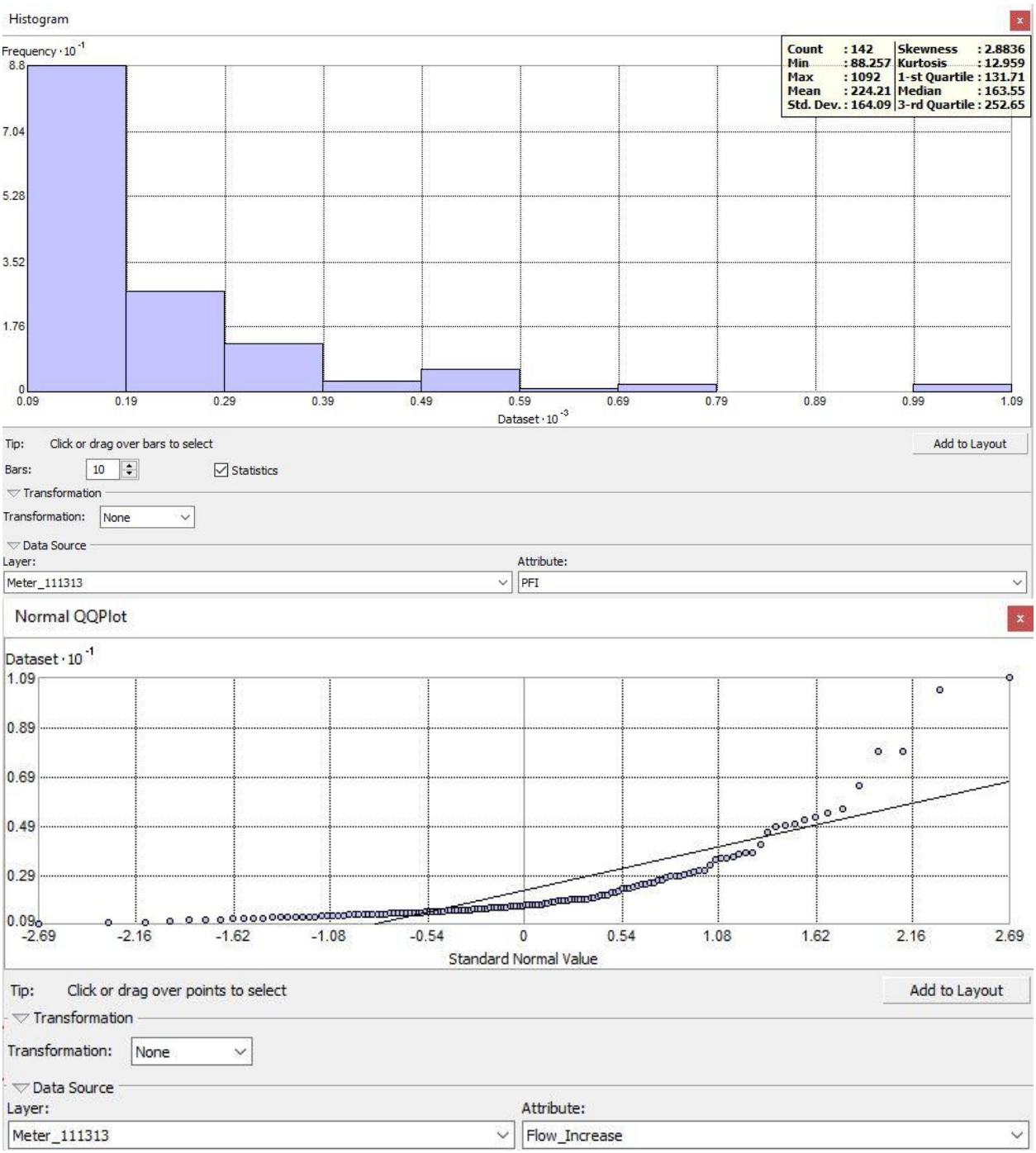
Histogram
Frequency · 10 -1
8.8
7.04
5.28
3.52
1.76
0
0.09
0.19
0.29
0.39
0.49
0.59
0.69
0.79
0.89
0.99
1.09
Dataset · 10 -3
Count : 142
Min : 88.257
Max : 1092
Mean : 224.21
Std. Dev. : 164.09
Skewness : 2.8836
Kurtosis : 12.959
1-st Quartile : 131.71
Median : 163.55
3-rd Quartile : 252.65
Tip: Click or drag over bars to select
Add to Layout
Bars: 10
Statistics
Transformation
Transformation: None
Data Source
Layer:
Meter_111313
Attribute:
PFI
Normal QQPlot
Dataset · 10 -1
1.09
0.89
0.69
0.49
0.29
0.09
-2.69
-2.16
-1.62
-1.08
-0.54
0
0.54
1.08
1.62
2.16
2.69
Standard Normal Value
Tip: Click or drag over points to select
Add to Layout
Transformation
Transformation: None
Data Source
Layer:
Meter_111313
Attribute:
Flow_Increase

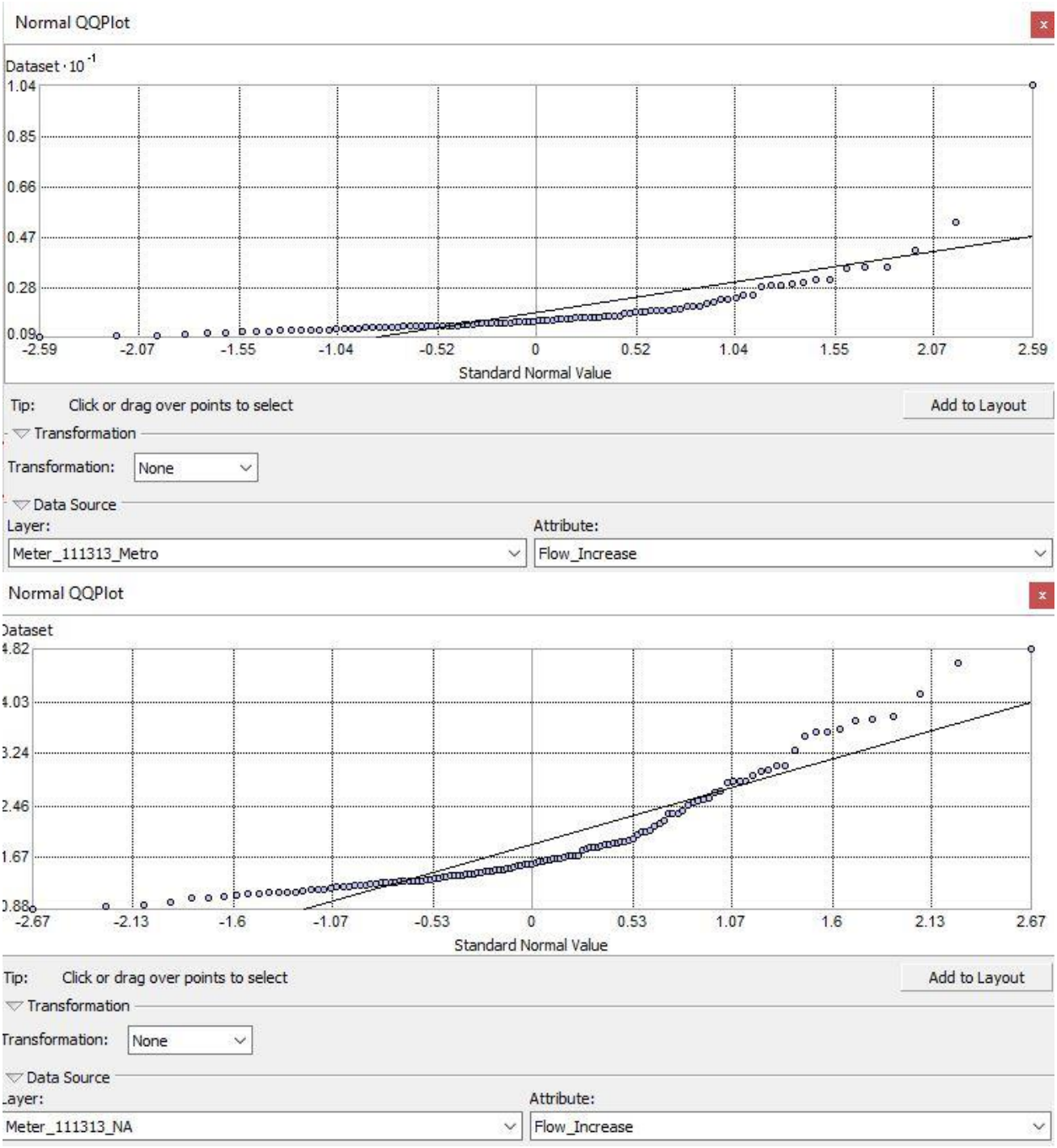
Normal QQPlot
Dataset · 10 -1
1.04
0.85
0.66
0.47
0.28
0.09
-2.59
-2.07
-1.55
-1.04
-0.52
0
0.52
1.04
1.55
2.07
2.59
Standard Normal Value
Tip: Click or drag over points to select
Add to Layout
Transformation
Transformation: None
Data Source
Layer:
Attribute:
Meter_111313_Metro
Flow_Increase
Normal QQPlot
Dataset
4.82
4.03
3.24
2.46
1.67
0.88
-2.67
-2.13
-1.6
-1.07
-0.53
0
0.53
1.07
1.6
2.13
2.67
Standard Normal Value
Tip: Click or drag over points to select
Add to Layout
Transformation
Transformation: None
Data Source
Layer:
Attribute:
Meter_111313_NA
Flow_Increase

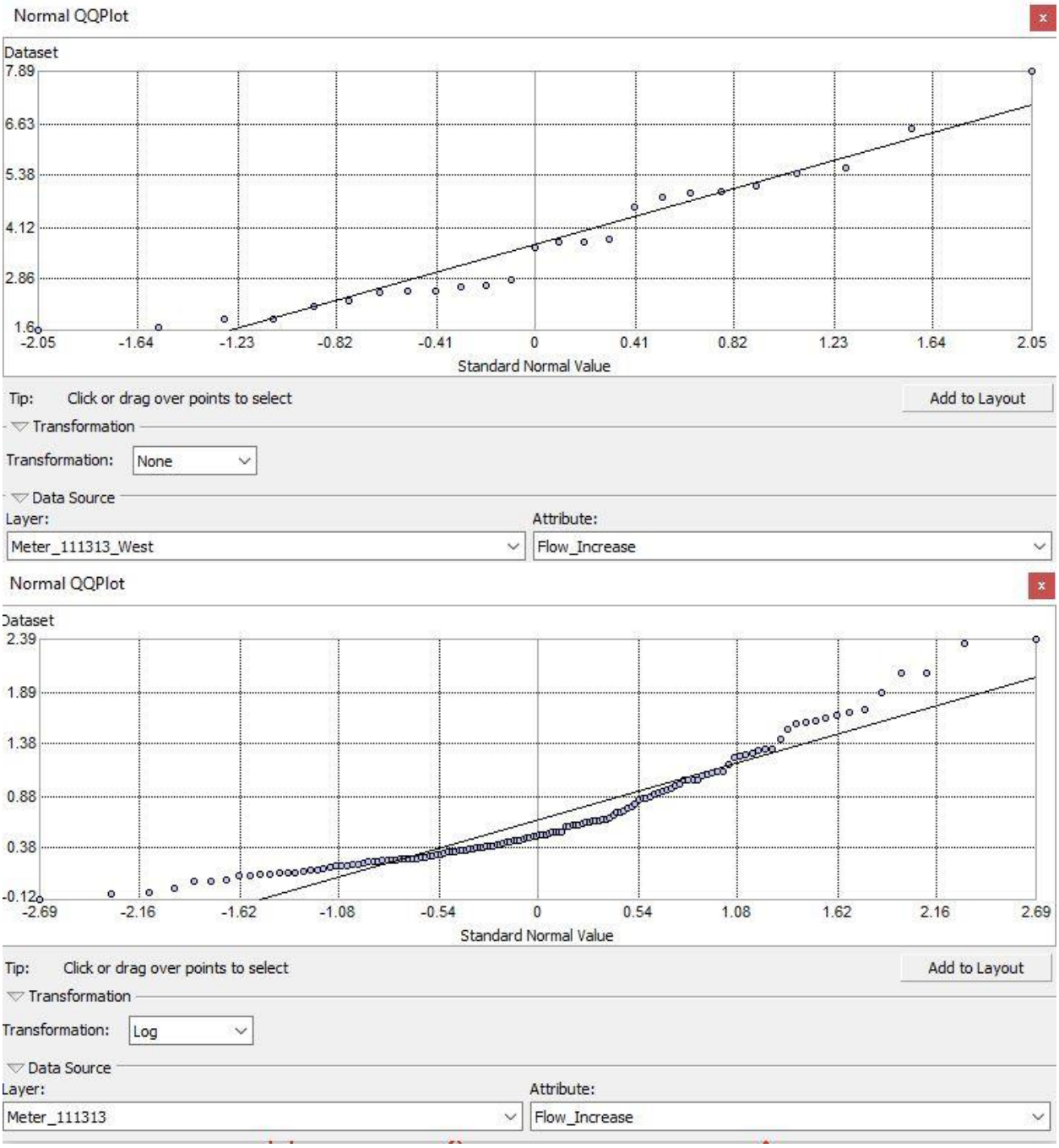
Normal QQPlot
Dataset
7.89
6.63
5.38
4.12
2.86
1.6
-2.05
-1.64
-1.23
-0.82
-0.41
0
0.41
0.82
1.23
1.64
2.05
Standard Normal Value
Tip: Click or drag over points to select
Add to Layout
Transformation
Transformation: None
Data Source
Layer:
Meter_111313_West
Attribute:
Flow_Increase
Normal QQPlot
Dataset
2.39
1.89
1.38
0.88
0.38
-0.12
-2.69
-2.16
-1.62
-1.08
-0.54
0
0.54
1.08
1.62
2.16
2.69
Standard Normal Value
Tip: Click or drag over points to select
Add to Layout
Transformation
Transformation: Log
Data Source
Layer:
Meter_111313
Attribute:
Flow_Increase

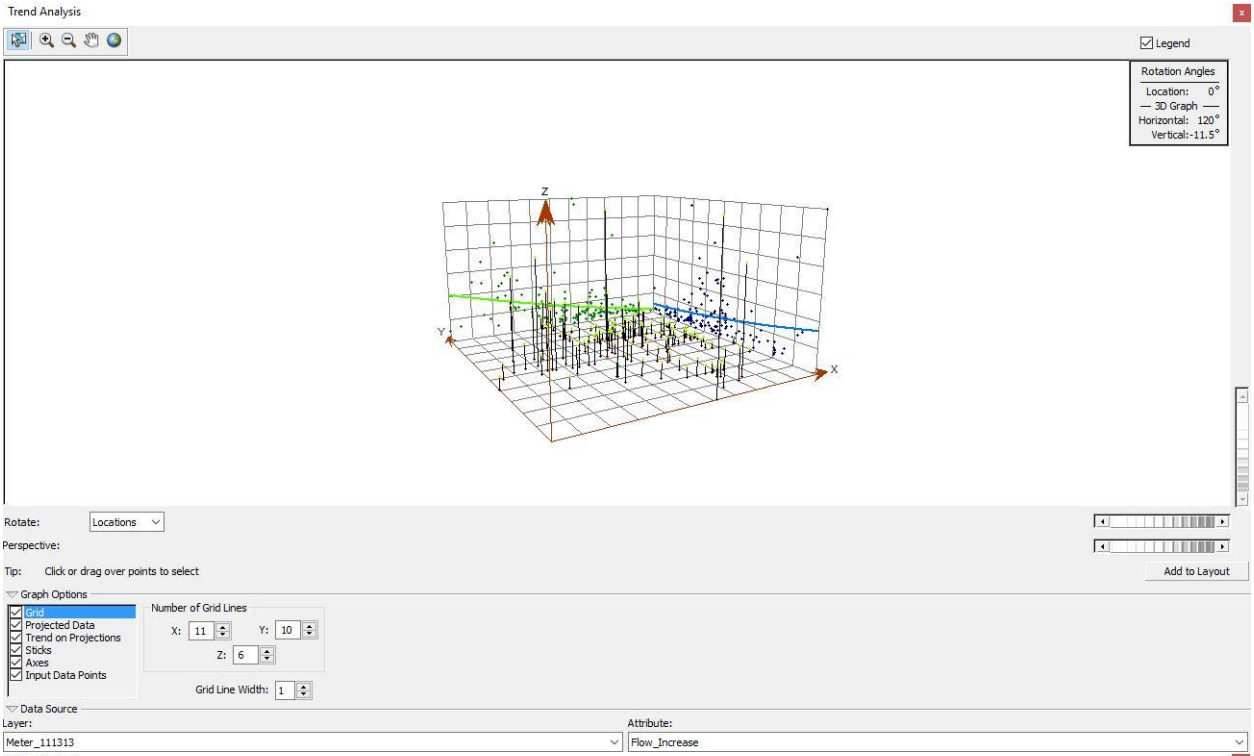
Trend Analysis
Legend
Rotation Angles
Location: 0°
3D Graph
Horizontal: 120°
Vertical:-11.5°
Z
Y
X
Rotate:
Locations
Perspective:
Tip: Click or drag over points to select
Add to Layout
Graph Options
Grid
Projected Data
Trend on Projections
Sticks
Axes
Input Data Points
Number of Grid Lines
X: 11
Y: 10
Z: 6
Grid Line Width: 1
Data Source
Layer:
Meter_111313
Attribute:
Flow_Increase

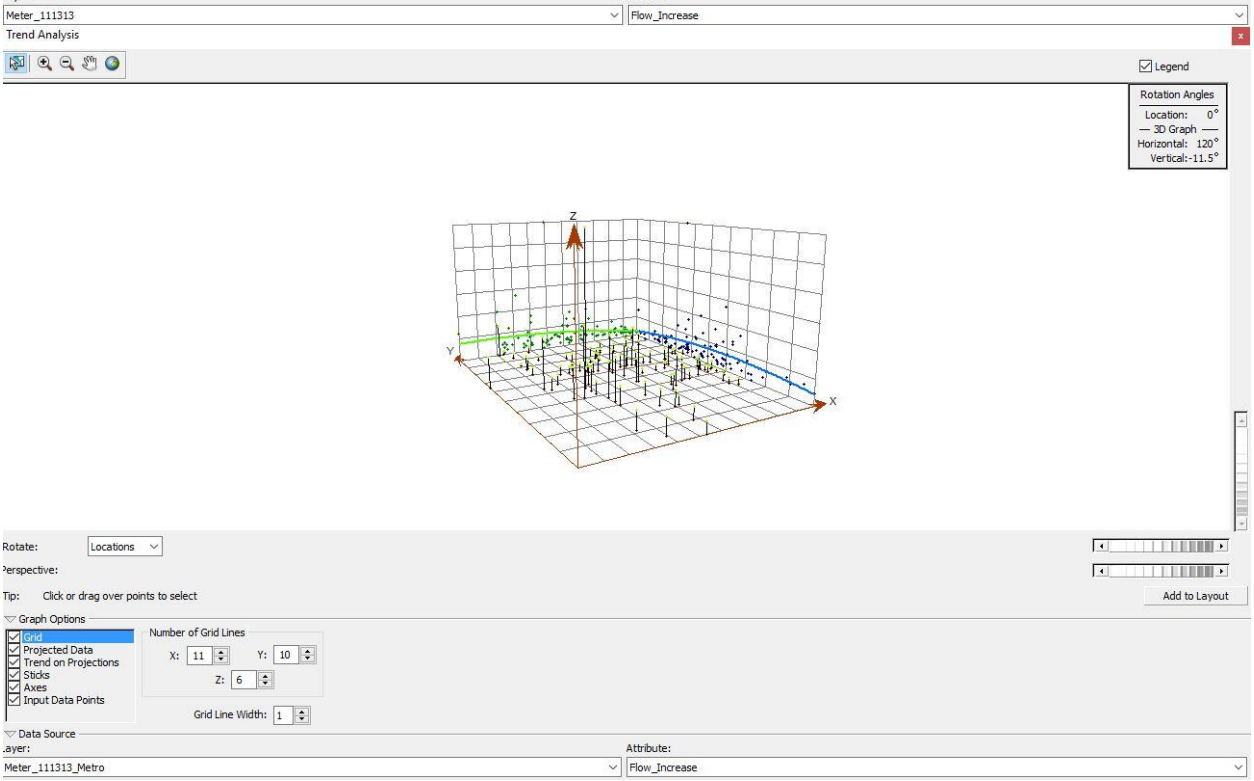
Trend Analysis
Legend
Rotation Angles
Location: 0°
3D Graph
Horizontal: 120°
Vertical:-11.5°
Z
Y
X
Rotate:
Locations
Perspective:
Tip: Click or drag over points to select
Add to Layout
Graph Options
Grid
Projected Data
Trend on Projections
Sticks
Axes
Input Data Points
Number of Grid Lines
X: 11
Y: 10
Z: 6
Grid Line Width: 1
Data Source
Layer:
Meter_111313_Metro
Attribute:
Flow_Increase

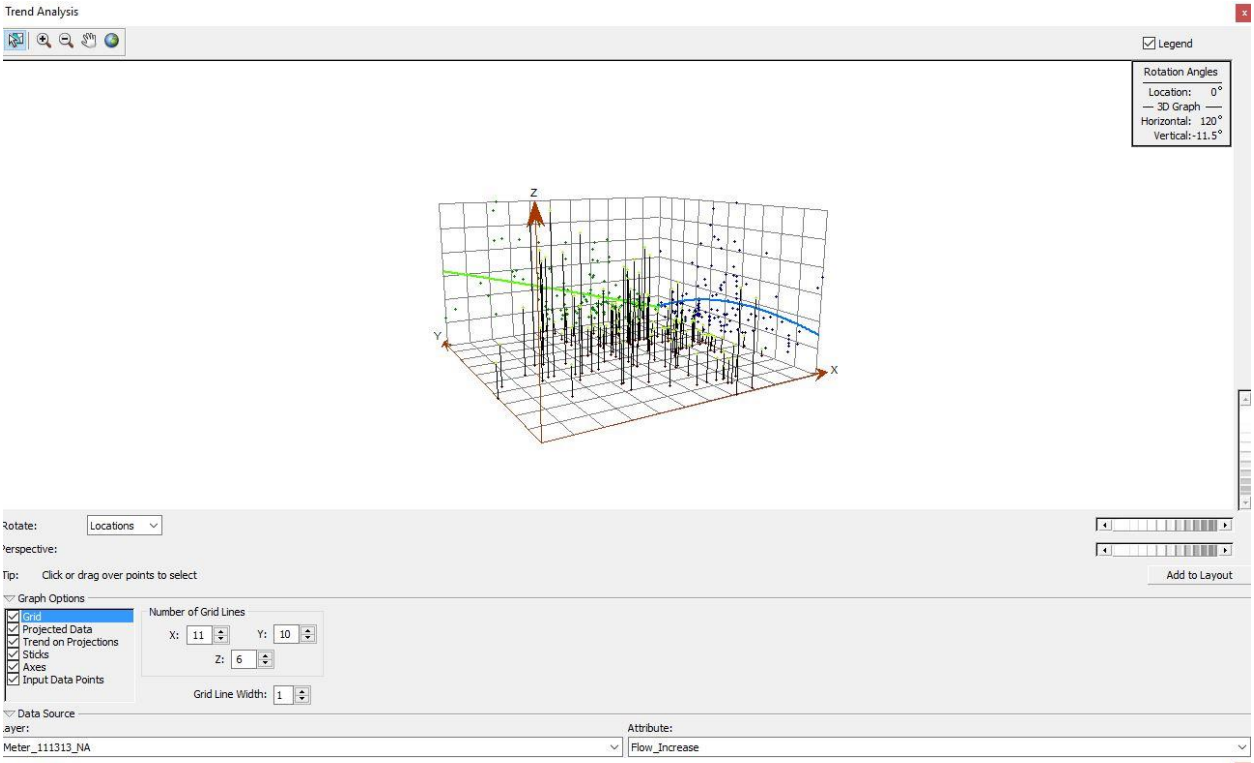
Trend Analysis
Legend
Rotation Angles
Location: 0°
3D Graph
Horizontal: 120°
Vertical: -11.5°
Z
Y
X
Rotate:
Locations
Perspective:
Tip: Click or drag over points to select
Add to Layout
Graph Options
Grid
Projected Data
Trend on Projections
Sticks
Axes
Input Data Points
Number of Grid Lines
X: 11
Y: 10
Z: 6
Grid Line Width: 1
Data Source
Layer:
Meter_111313_NA
Attribute:
Flow_Increase

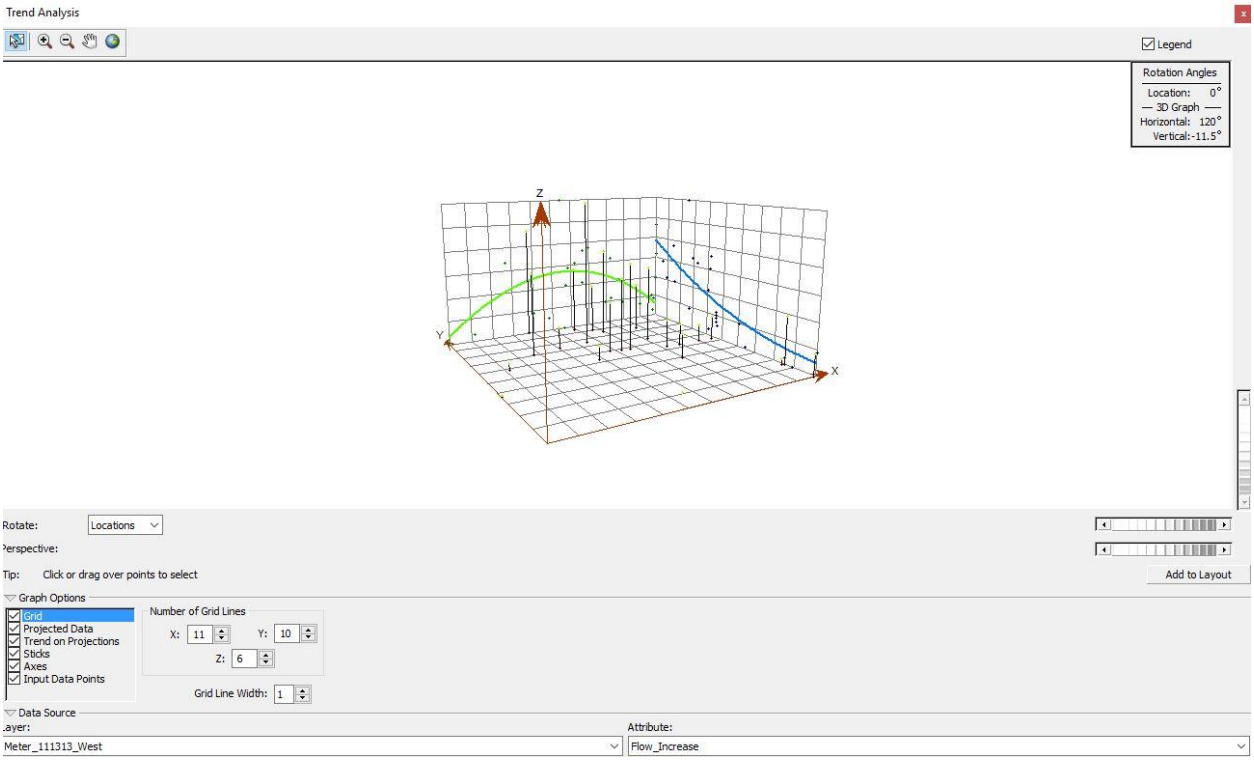
Trend Analysis
Legend
Rotation Angles
Location: 0°
3D Graph
Horizontal: 120°
Vertical: -11.5°
Z
Y
X
Rotate:
Locations
Perspective:
Tip: Click or drag over points to select
Add to Layout
Graph Options
Grid
Projected Data
Trend on Projections
Sticks
Axes
Input Data Points
Number of Grid Lines
X: 11
Y: 10
Z: 6
Grid Line Width: 1
Data Source
Layer:
Meter_111313_West
Attribute:
Flow_Increase

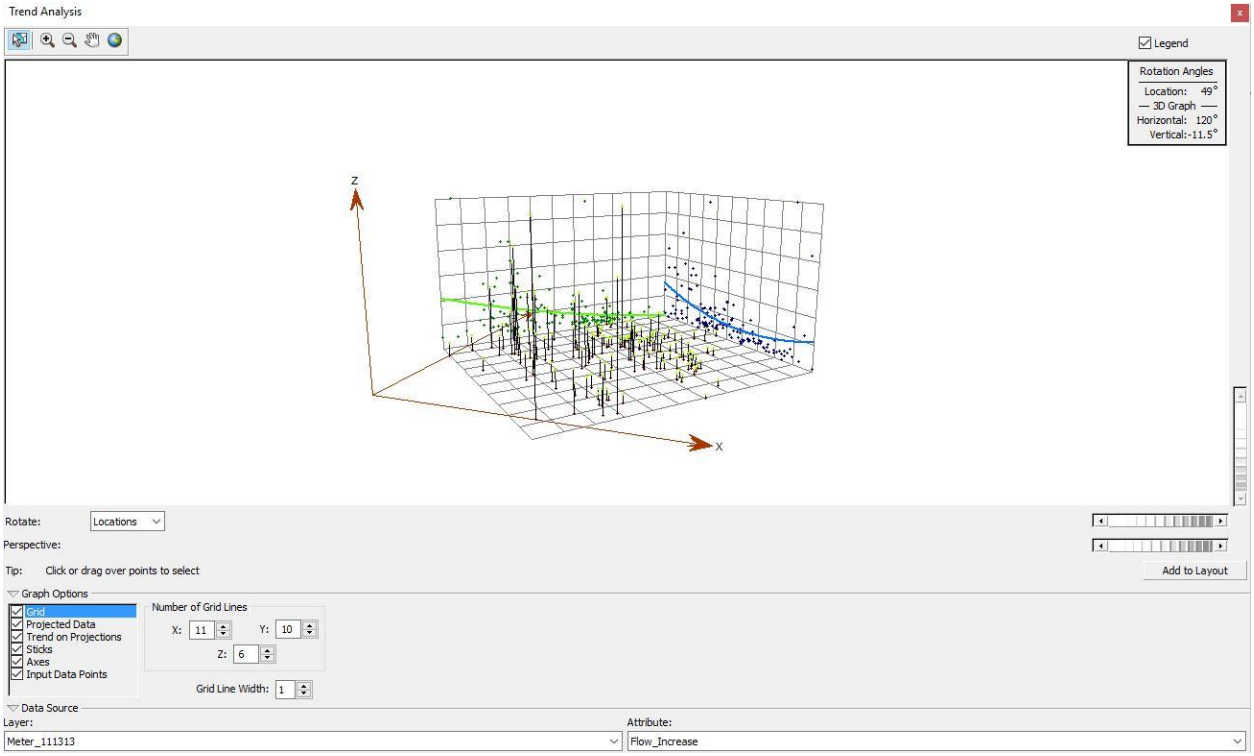
Trend Analysis
Legend
Rotation Angles
Location: 49°
3D Graph
Horizontal: 120°
Vertical:-11.5°
Z
X
Rotate:
Locations
Perspective:
Tip: Click or drag over points to select
Add to Layout
Graph Options
Grid
Projected Data
Trend on Projections
Sticks
Axes
Input Data Points
Number of Grid Lines
X: 11
Y: 10
Z: 6
Grid Line Width: 1
Data Source
Layer:
Meter_111313
Attribute:
Flow_Increase

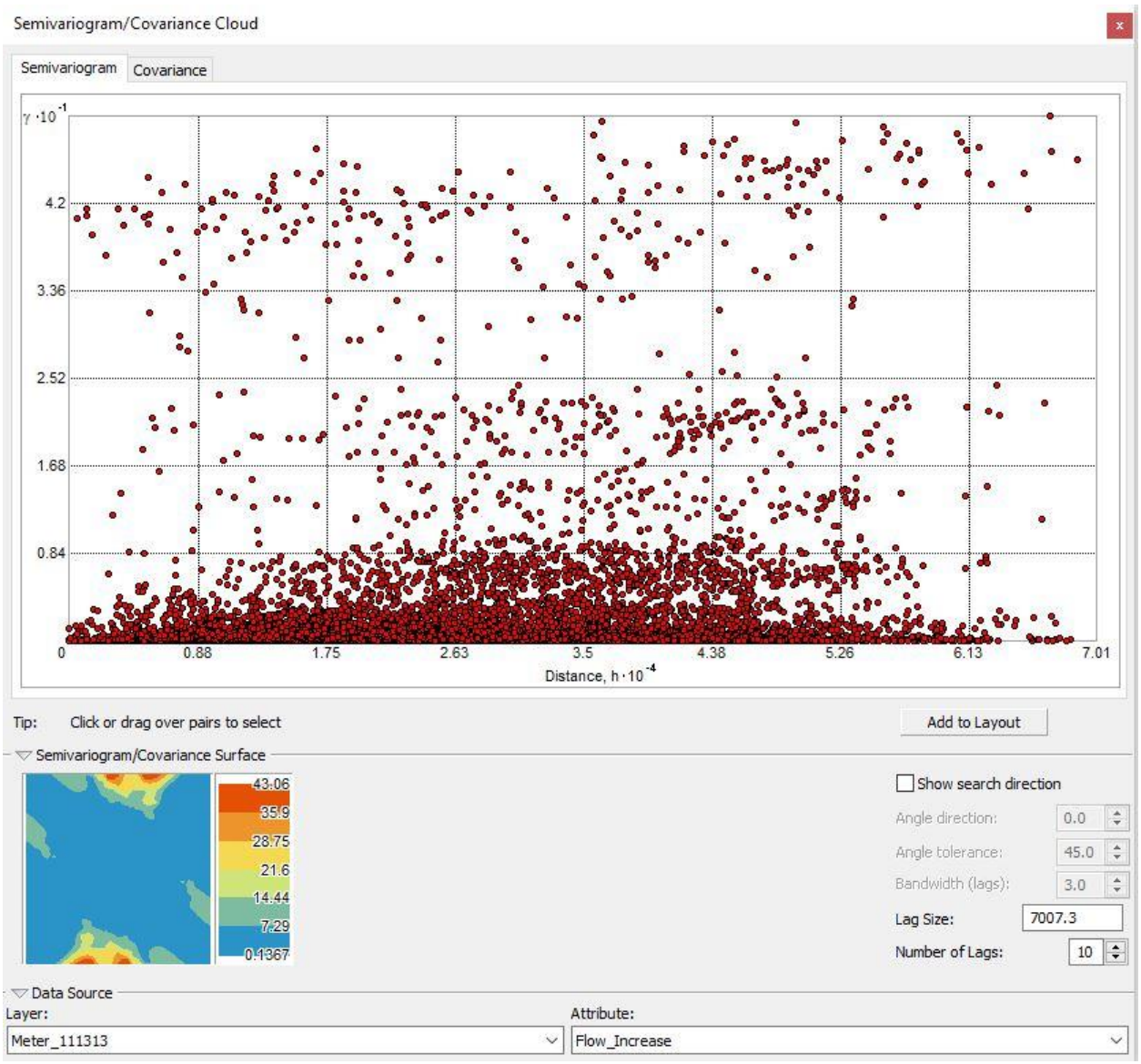
Semivariogram/Covariance Cloud
Semivariogram
Covariance
γ ·10^-1
4.2
3.36
2.52
1.68
0.84
0
0.88
1.75
2.63
3.5
4.38
5.26
6.13
7.01
Distance, h ·10^-4
Tip: Click or drag over pairs to select
Add to Layout
Semivariogram/Covariance Surface
43.06
35.9
28.75
21.6
14.44
7.29
0.1367
Show search direction
Angle direction: 0.0
Angle tolerance: 45.0
Bandwidth (lags): 3.0
Lag Size: 7007.3
Number of Lags: 10
Data Source
Layer: Meter_111313
Attribute: Flow_Increase

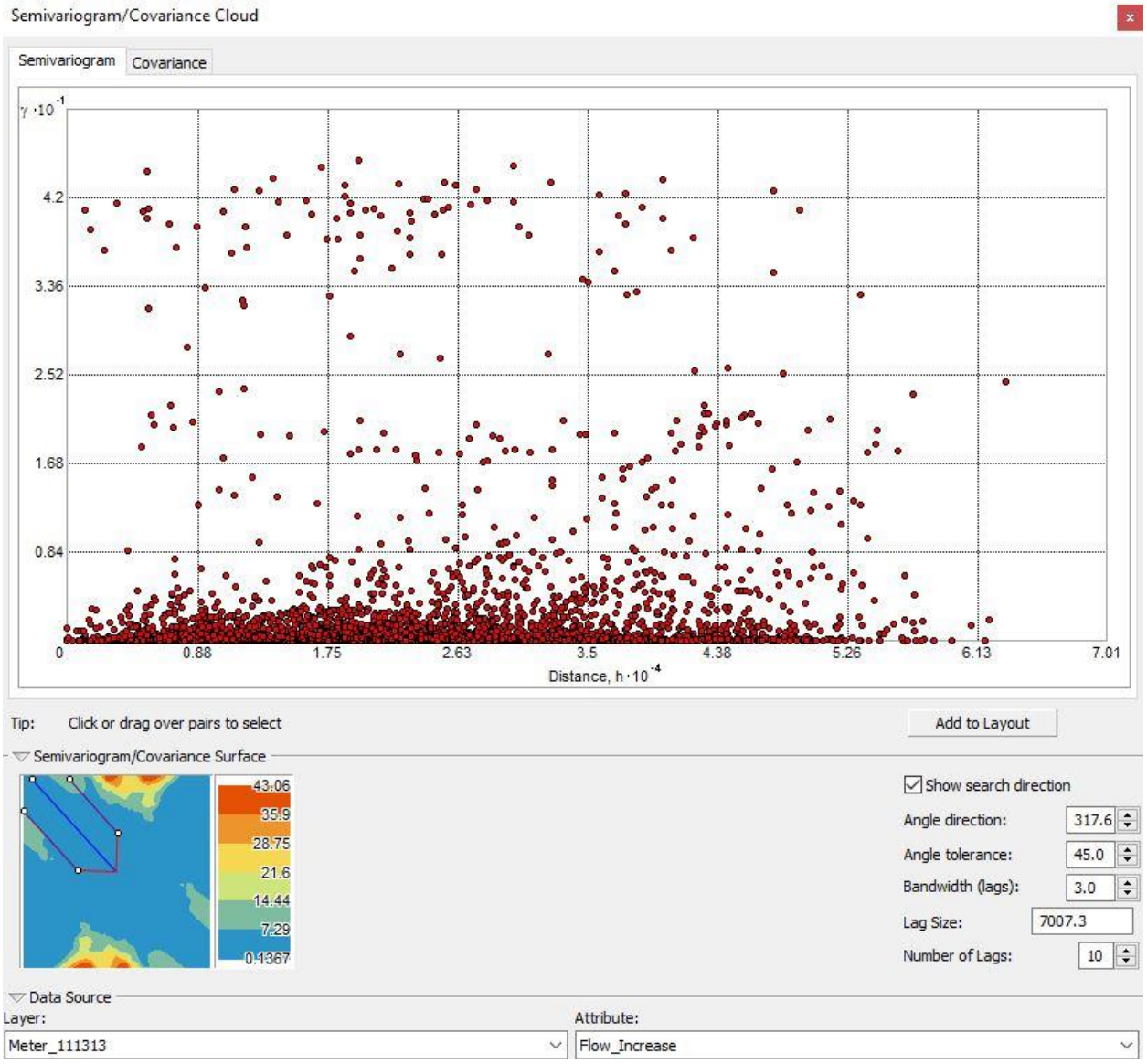
Semivariogram/Covariance Cloud
Semivariogram
Covariance
γ ·10^-1
4.2
3.36
2.52
1.68
0.84
0
0.88
1.75
2.63
3.5
4.38
5.26
6.13
7.01
Distance, h ·10^-4
Tip: Click or drag over pairs to select
Add to Layout
Semivariogram/Covariance Surface
43.06
35.9
28.75
21.6
14.44
7.29
0.1367
Show search direction
Angle direction: 317.6
Angle tolerance: 45.0
Bandwidth (lags): 3.0
Lag Size: 7007.3
Number of Lags: 10
Data Source
Layer:
Meter_111313
Attribute:
Flow_Increase

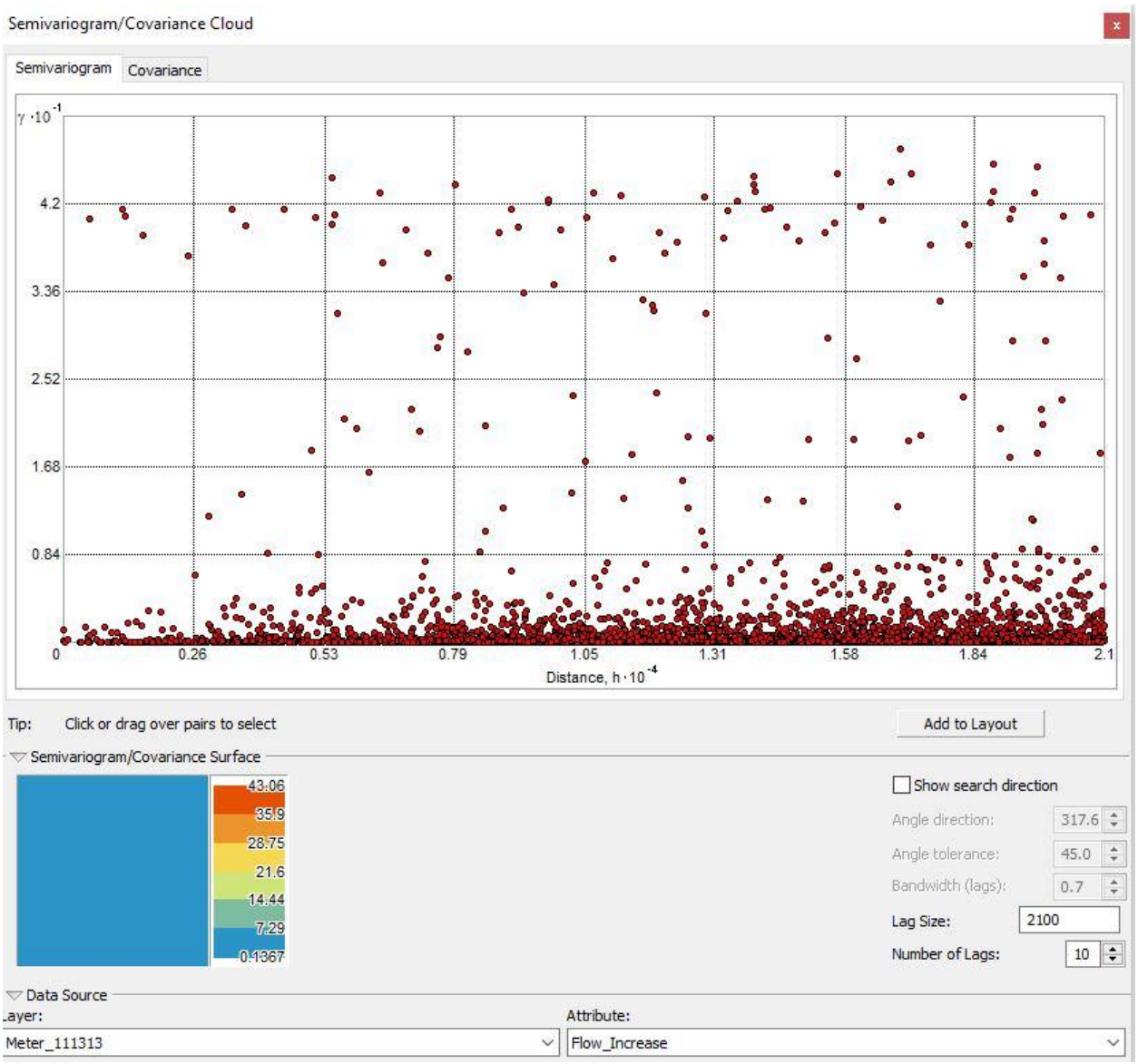
Semivariogram/Covariance Cloud
Semivariogram
Covariance
γ ·10 -1
4.2
3.36
2.52
1.68
0.84
0
0.26
0.53
0.79
1.05
1.31
1.58
1.84
2.1
Distance, h ·10 -4
Tip: Click or drag over pairs to select
Add to Layout
Semivariogram/Covariance Surface
43.06
35.9
28.75
21.6
14.44
7.29
0.1367
Show search direction
Angle direction: 317.6
Angle tolerance: 45.0
Bandwidth (lags): 0.7
Lag Size: 2100
Number of Lags: 10
Data Source
Layer:
Meter_111313
Attribute:
Flow_Increase

Appendix B. Cross Validation Comparisons

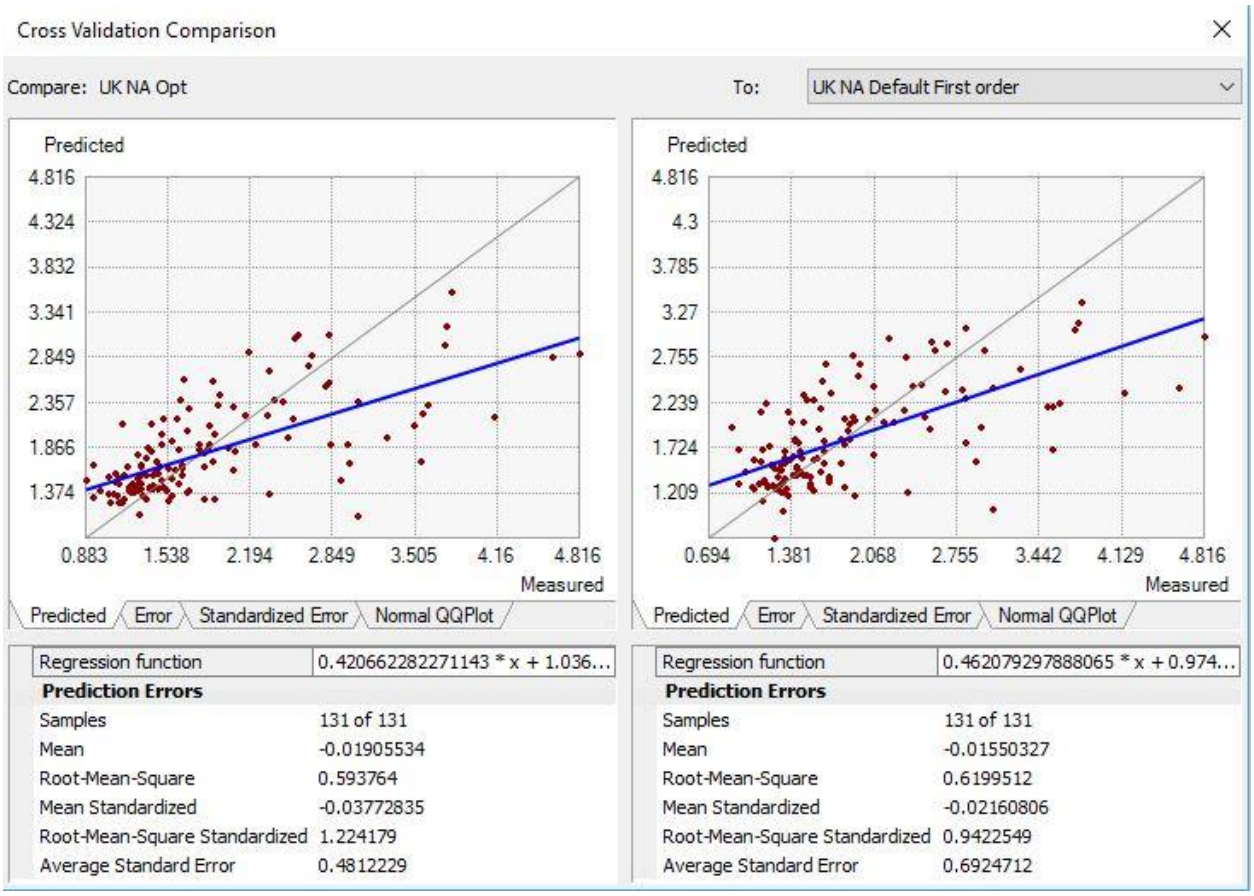

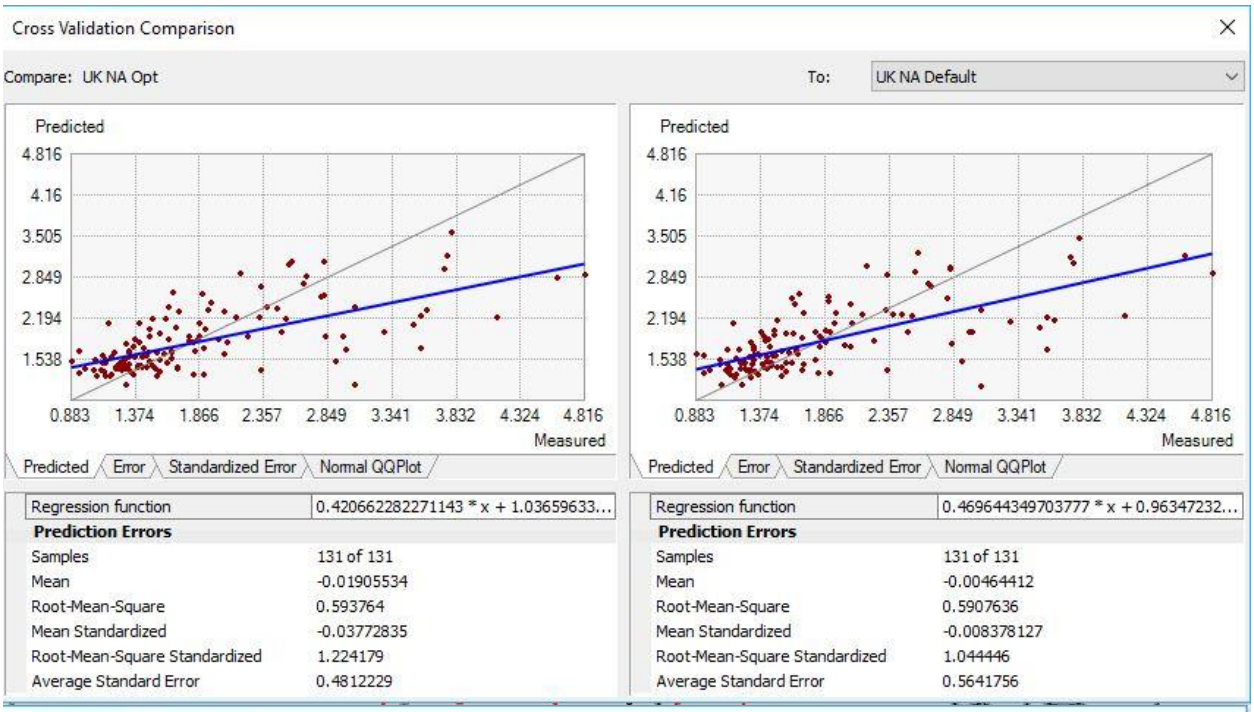
Cross Validation Comparison
Compare: UK NA Opt
To: UK NA Default
Predicted
4.816
4.16
3.505
2.849
2.194
1.538
0.883 1.374 1.866 2.357 2.849 3.341 3.832 4.324 4.816
Measured
Predicted Error Standardized Error Normal QQPlot
Regression function 0.420662282271143 * x + 1.03659633...
Prediction Errors
Samples 131 of 131
Mean -0.01905534
Root-Mean-Square 0.593764
Mean Standardized -0.03772835
Root-Mean-Square Standardized 1.224179
Average Standard Error 0.4812229
Regression function 0.469644349703777 * x + 0.96347232...
Prediction Errors
Samples 131 of 131
Mean -0.00464412
Root-Mean-Square 0.5907636
Mean Standardized -0.008378127
Root-Mean-Square Standardized 1.044446
Average Standard Error 0.5641756

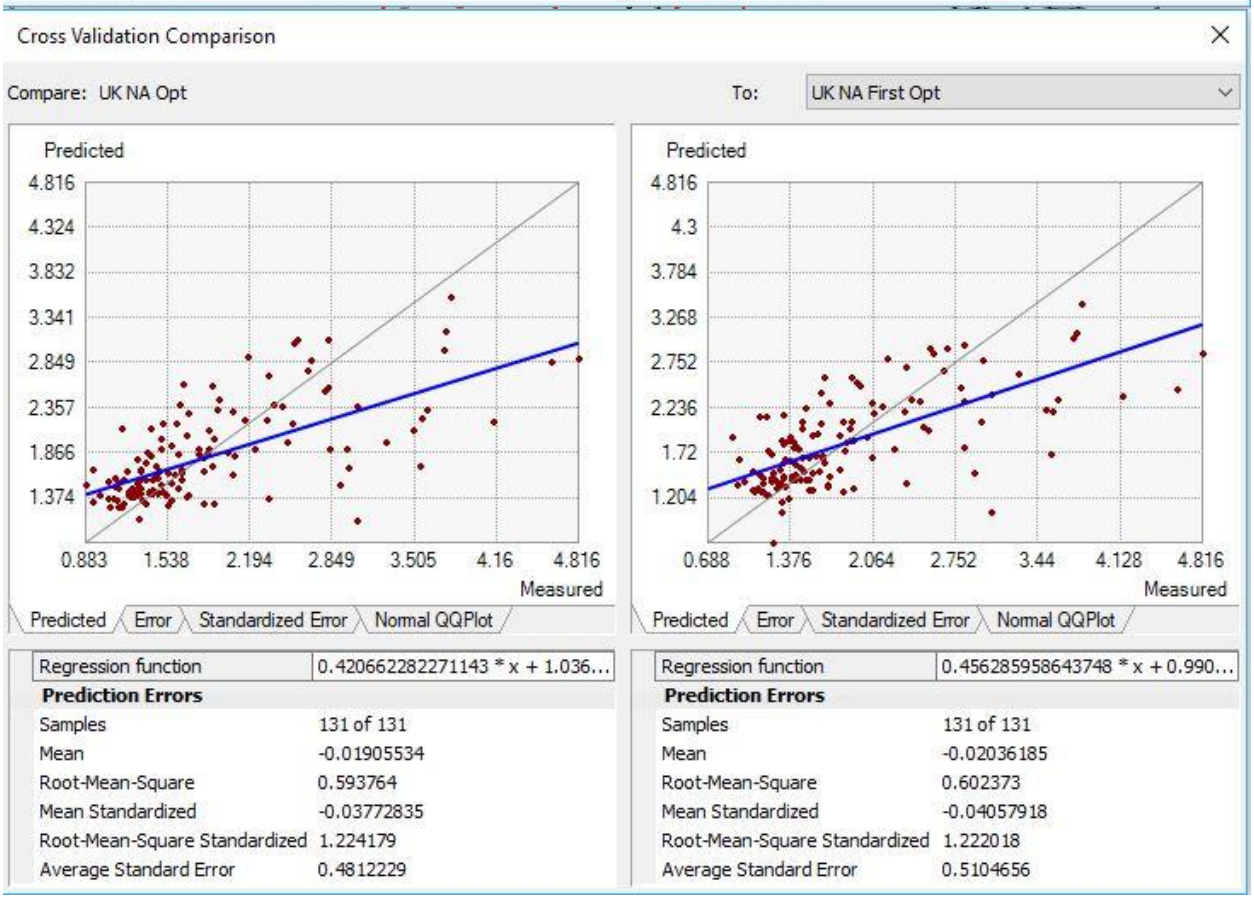
Cross Validation Comparison
Compare: UK NA Opt
To: UK NA First Opt
Predicted
4.816
4.324
3.832
3.341
2.849
2.357
1.866
1.374
0.883 1.538 2.194 2.849 3.505 4.16 4.816
Measured
Predicted Error Standardized Error Normal QQPlot
Regression function 0.420662282271143 * x + 1.036...
Prediction Errors
Samples 131 of 131
Mean -0.01905534
Root-Mean-Square 0.593764
Mean Standardized -0.03772835
Root-Mean-Square Standardized 1.224179
Average Standard Error 0.4812229
Predicted
4.816
4.3
3.784
3.268
2.752
2.236
1.72
1.204
0.688 1.376 2.064 2.752 3.44 4.128 4.816
Measured
Predicted Error Standardized Error Normal QQPlot
Regression function 0.456285958643748 * x + 0.990...
Prediction Errors
Samples 131 of 131
Mean -0.02036185
Root-Mean-Square 0.602373
Mean Standardized -0.04057918
Root-Mean-Square Standardized 1.222018
Average Standard Error 0.5104656

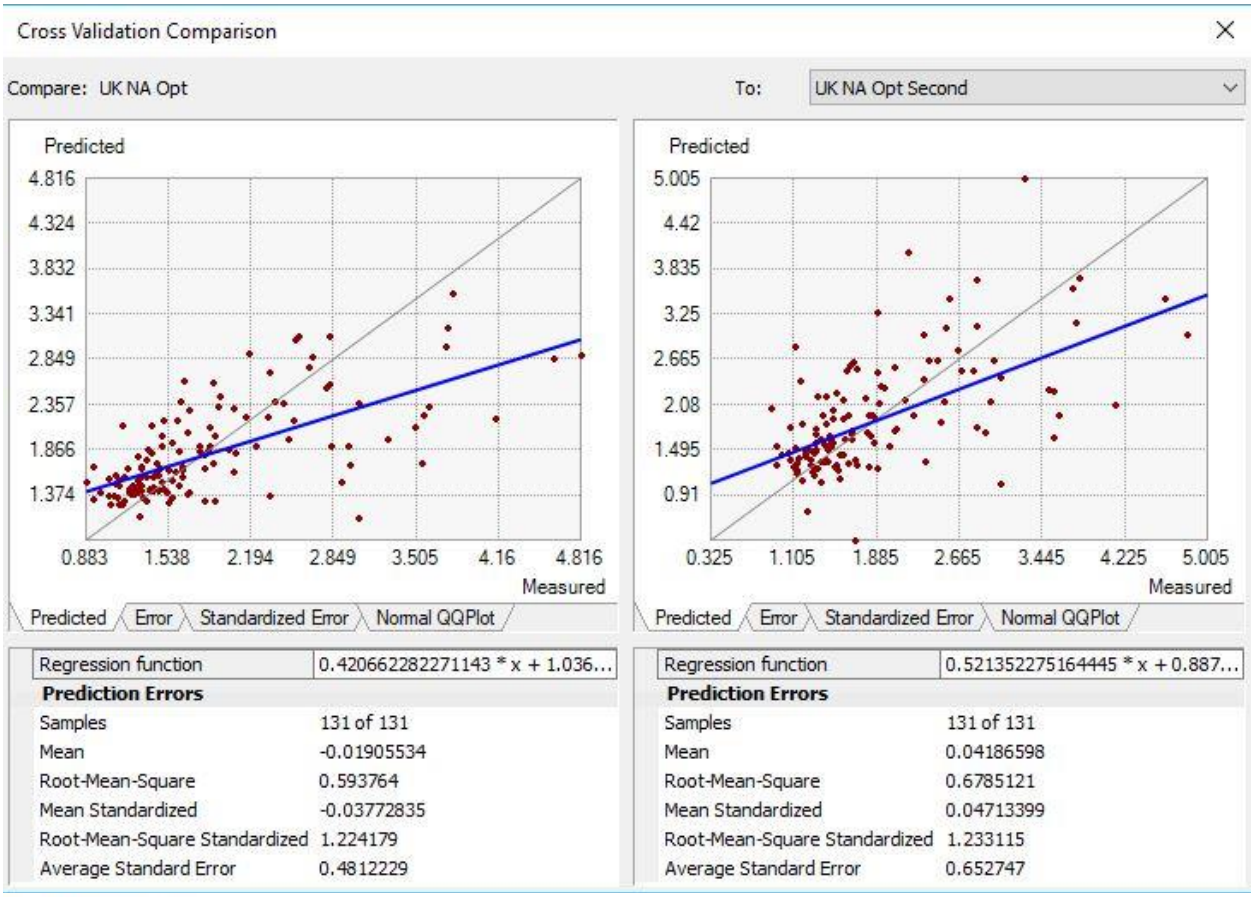
Cross Validation Comparison
Compare: UK NA Opt
To: UK NA Opt Second
Predicted
4.816
4.324
3.832
3.341
2.849
2.357
1.866
1.374
0.883 1.538 2.194 2.849 3.505 4.16 4.816
Measured
Predicted Error Standardized Error Normal QQPlot
Regression function 0.420662282271143 * x + 1.036...
Prediction Errors
Samples 131 of 131
Mean -0.01905534
Root-Mean-Square 0.593764
Mean Standardized -0.03772835
Root-Mean-Square Standardized 1.224179
Average Standard Error 0.4812229
Predicted
5.005
4.42
3.835
3.25
2.665
2.08
1.495
0.91
0.325 1.105 1.885 2.665 3.445 4.225 5.005
Measured
Predicted Error Standardized Error Normal QQPlot
Regression function 0.521352275164445 * x + 0.887...
Prediction Errors
Samples 131 of 131
Mean 0.04186598
Root-Mean-Square 0.6785121
Mean Standardized 0.04713399
Root-Mean-Square Standardized 1.233115
Average Standard Error 0.652747

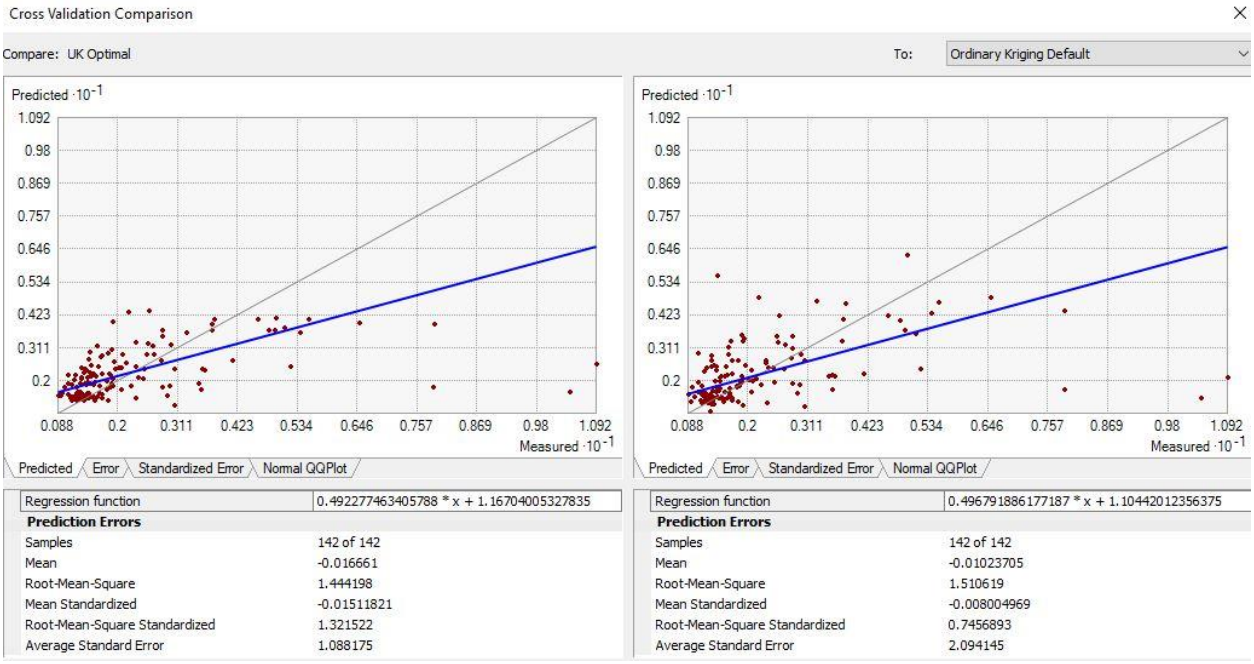
Cross Validation Comparison
Compare: UK Optimal
To: Ordinary Kriging Default
Predicted ·10-1
1.092
0.98
0.869
0.757
0.646
0.534
0.423
0.311
0.2
0.088 0.2 0.311 0.423 0.534 0.646 0.757 0.869 0.98 1.092
Measured ·10-1
Predicted Error Standardized Error Normal QQPlot
Regression function 0.492277463405788 * x + 1.16704005327835
Prediction Errors
Samples 142 of 142
Mean -0.016661
Root-Mean-Square 1.444198
Mean Standardized -0.01511821
Root-Mean-Square Standardized 1.321522
Average Standard Error 1.088175
Predicted ·10-1
1.092
0.98
0.869
0.757
0.646
0.534
0.423
0.311
0.2
0.088 0.2 0.311 0.423 0.534 0.646 0.757 0.869 0.98 1.092
Measured ·10-1
Predicted Error Standardized Error Normal QQPlot
Regression function 0.496791886177187 * x + 1.10442012356375
Prediction Errors
Samples 142 of 142
Mean -0.01023705
Root-Mean-Square 1.510619
Mean Standardized -0.008004969
Root-Mean-Square Standardized 0.7456893
Average Standard Error 2.094145

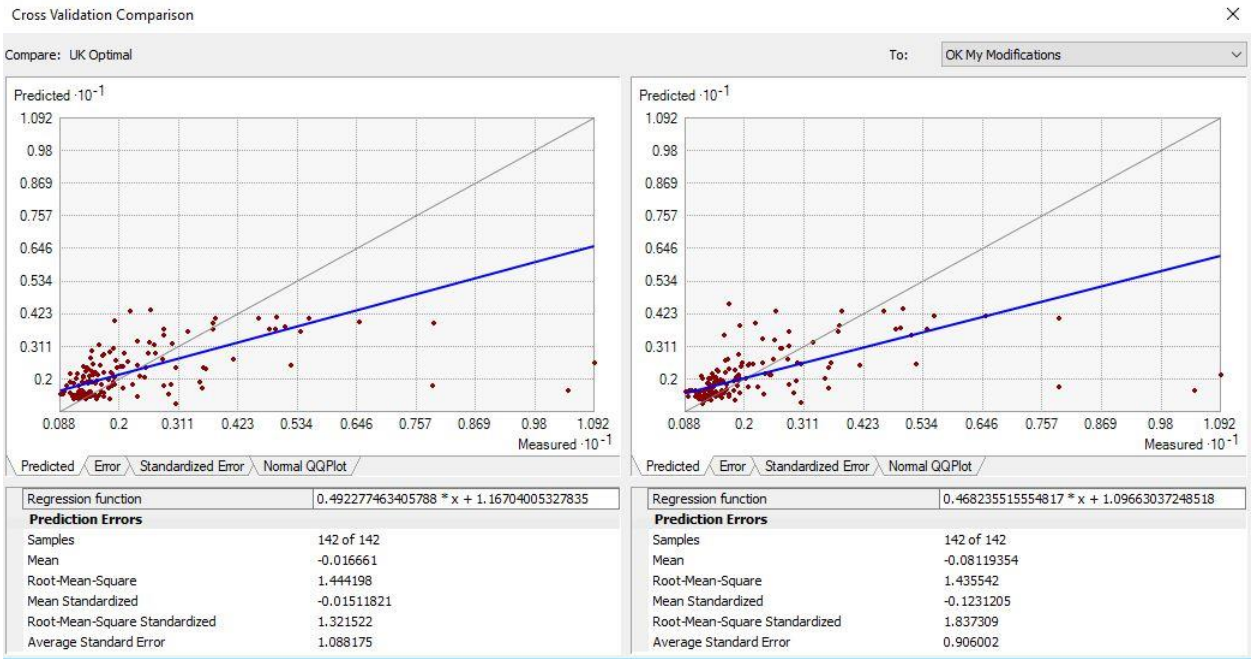
Cross Validation Comparison
Compare: UK Optimal
To: OK My Modifications
Predicted ·10-1
1.092
0.98
0.869
0.757
0.646
0.534
0.423
0.311
0.2
0.088 0.2 0.311 0.423 0.534 0.646 0.757 0.869 0.98 1.092
Measured ·10-1
Predicted Error Standardized Error Normal QQPlot
Regression function 0.492277463405788 * x + 1.16704005327835
Prediction Errors
Samples 142 of 142
Mean -0.016661
Root-Mean-Square 1.444198
Mean Standardized -0.01511821
Root-Mean-Square Standardized 1.321522
Average Standard Error 1.088175
Regression function 0.468235515554817 * x + 1.09663037248518
Prediction Errors
Samples 142 of 142
Mean -0.08119354
Root-Mean-Square 1.435542
Mean Standardized -0.1231205
Root-Mean-Square Standardized 1.837309
Average Standard Error 0.906002

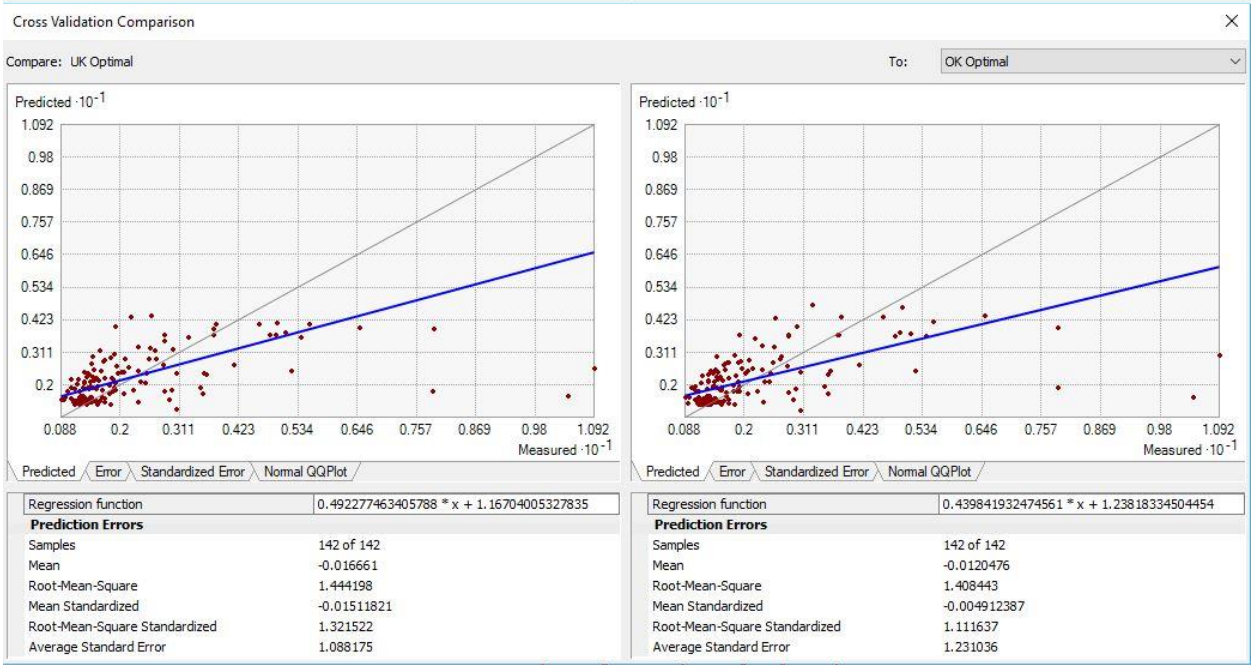
Cross Validation Comparison
Compare: UK Optimal
To: OK Optimal
Predicted ·10-1
1.092
0.98
0.869
0.757
0.646
0.534
0.423
0.311
0.2
0.088 0.2 0.311 0.423 0.534 0.646 0.757 0.869 0.98 1.092
Measured ·10-1
Predicted Error Standardized Error Normal QQPlot
Regression function 0.492277463405788 * x + 1.16704005327835
Prediction Errors
Samples 142 of 142
Mean -0.016661
Root-Mean-Square 1.444198
Mean Standardized -0.01511821
Root-Mean-Square Standardized 1.321522
Average Standard Error 1.088175
Regression function 0.439841932474561 * x + 1.23818334504454
Prediction Errors
Samples 142 of 142
Mean -0.0120476
Root-Mean-Square 1.408443
Mean Standardized -0.004912387
Root-Mean-Square Standardized 1.111637
Average Standard Error 1.231036

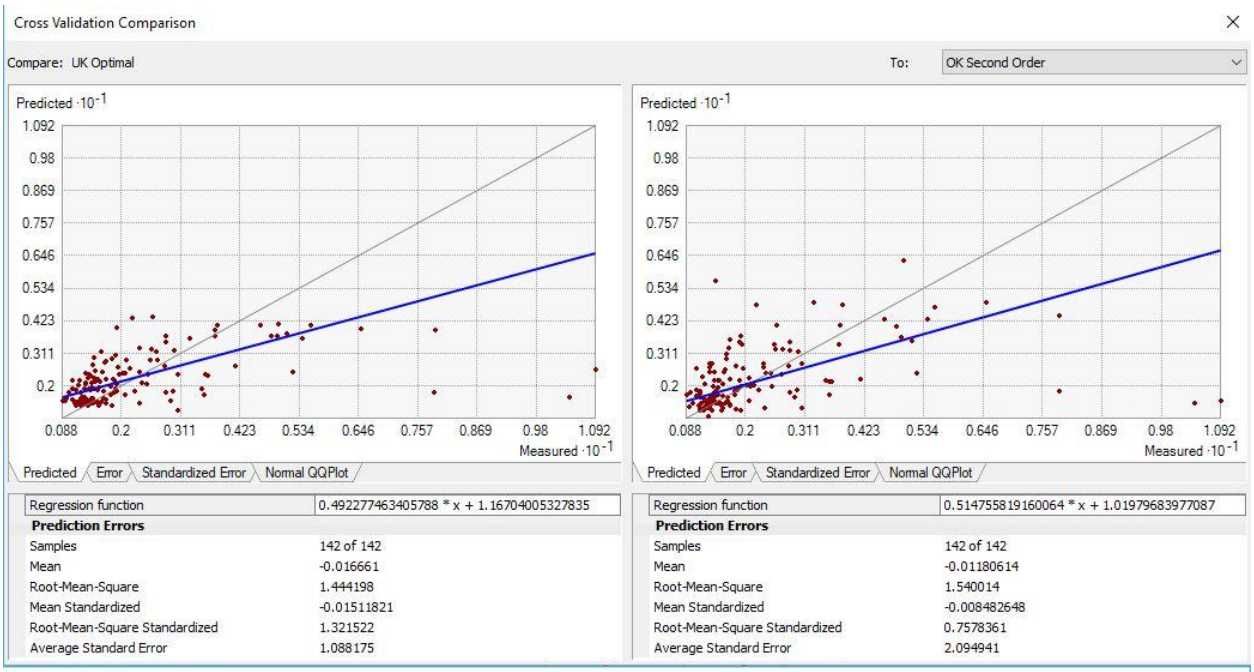
Cross Validation Comparison
Compare: UK Optimal
To: OK Second Order
Predicted ·10-1
1.092
0.98
0.869
0.757
0.646
0.534
0.423
0.311
0.2
0.088 0.2 0.311 0.423 0.534 0.646 0.757 0.869 0.98 1.092
Measured ·10-1
Predicted Error Standardized Error Normal QQPlot
Regression function 0.492277463405788 * x + 1.16704005327835
Prediction Errors
Samples 142 of 142
Mean -0.016661
Root-Mean-Square 1.444198
Mean Standardized -0.01511821
Root-Mean-Square Standardized 1.321522
Average Standard Error 1.088175
Regression function 0.514755819160064 * x + 1.01979683977087
Prediction Errors
Samples 142 of 142
Mean -0.01180614
Root-Mean-Square 1.540014
Mean Standardized -0.008482648
Root-Mean-Square Standardized 0.7578361
Average Standard Error 2.094941

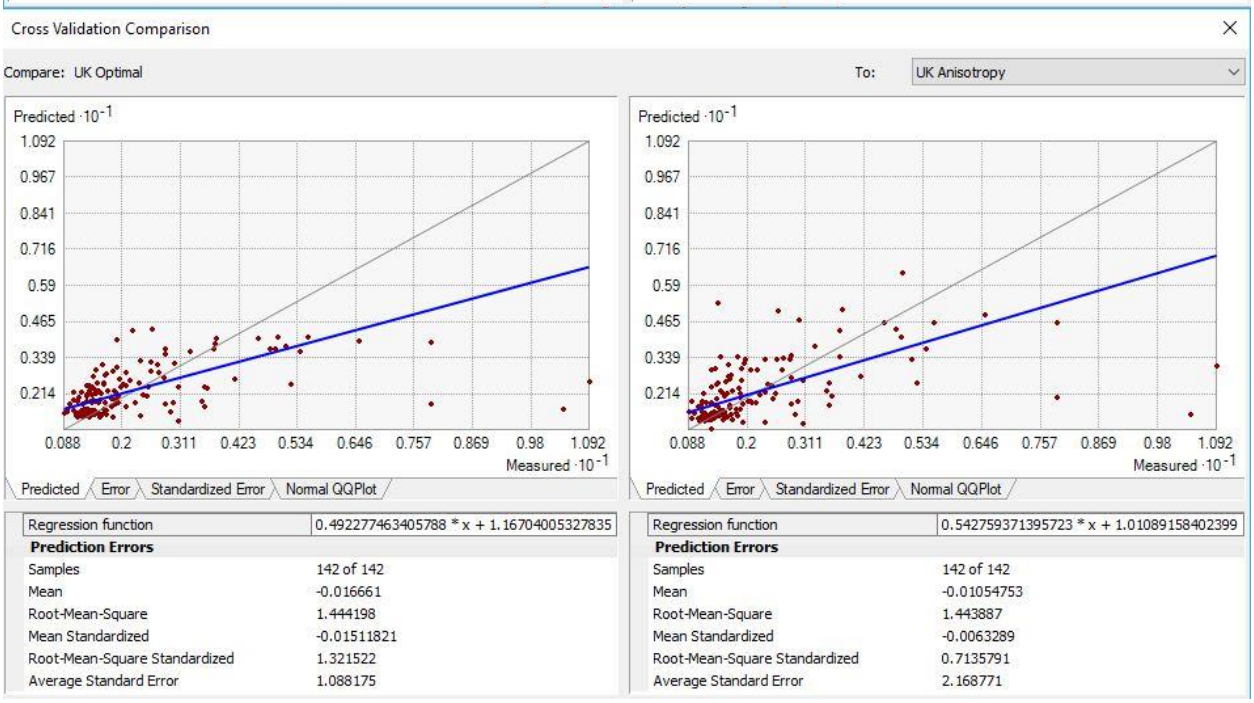
Cross Validation Comparison
Compare: UK Optimal
To: UK Anisotropy
Predicted ·10-1
1.092
0.967
0.841
0.716
0.59
0.465
0.339
0.214
0.088 0.2 0.311 0.423 0.534 0.646 0.757 0.869 0.98 1.092
Measured ·10-1
Predicted Error Standardized Error Normal QQPlot
Regression function 0.492277463405788 * x + 1.16704005327835
Prediction Errors
Samples 142 of 142
Mean -0.016661
Root-Mean-Square 1.444198
Mean Standardized -0.01511821
Root-Mean-Square Standardized 1.321522
Average Standard Error 1.088175
Regression function 0.542759371395723 * x + 1.01089158402399
Prediction Errors
Samples 142 of 142
Mean -0.01054753
Root-Mean-Square 1.443887
Mean Standardized -0.0063289
Root-Mean-Square Standardized 0.7135791
Average Standard Error 2.168771

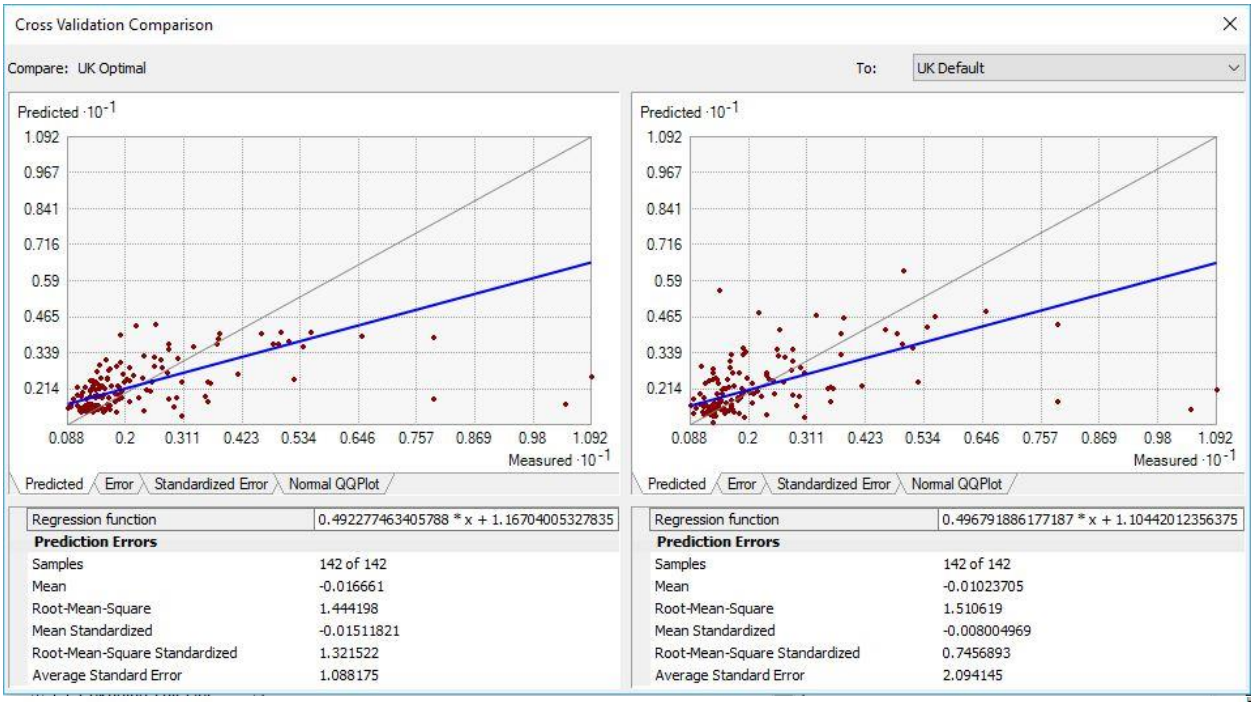
Cross Validation Comparison
Compare: UK Optimal
To: UK Default
Predicted ·10-1
1.092
0.967
0.841
0.716
0.59
0.465
0.339
0.214
0.088 0.2 0.311 0.423 0.534 0.646 0.757 0.869 0.98 1.092
Measured ·10-1
Predicted Error Standardized Error Normal QQPlot
Regression function 0.492277463405788 * x + 1.16704005327835
Prediction Errors
Samples 142 of 142
Mean -0.016661
Root-Mean-Square 1.444198
Mean Standardized -0.01511821
Root-Mean-Square Standardized 1.321522
Average Standard Error 1.088175
Predicted ·10-1
1.092
0.967
0.841
0.716
0.59
0.465
0.339
0.214
0.088 0.2 0.311 0.423 0.534 0.646 0.757 0.869 0.98 1.092
Measured ·10-1
Predicted Error Standardized Error Normal QQPlot
Regression function 0.496791886177187 * x + 1.10442012356375
Prediction Errors
Samples 142 of 142
Mean -0.01023705
Root-Mean-Square 1.510619
Mean Standardized -0.008004969
Root-Mean-Square Standardized 0.7456893
Average Standard Error 2.094145

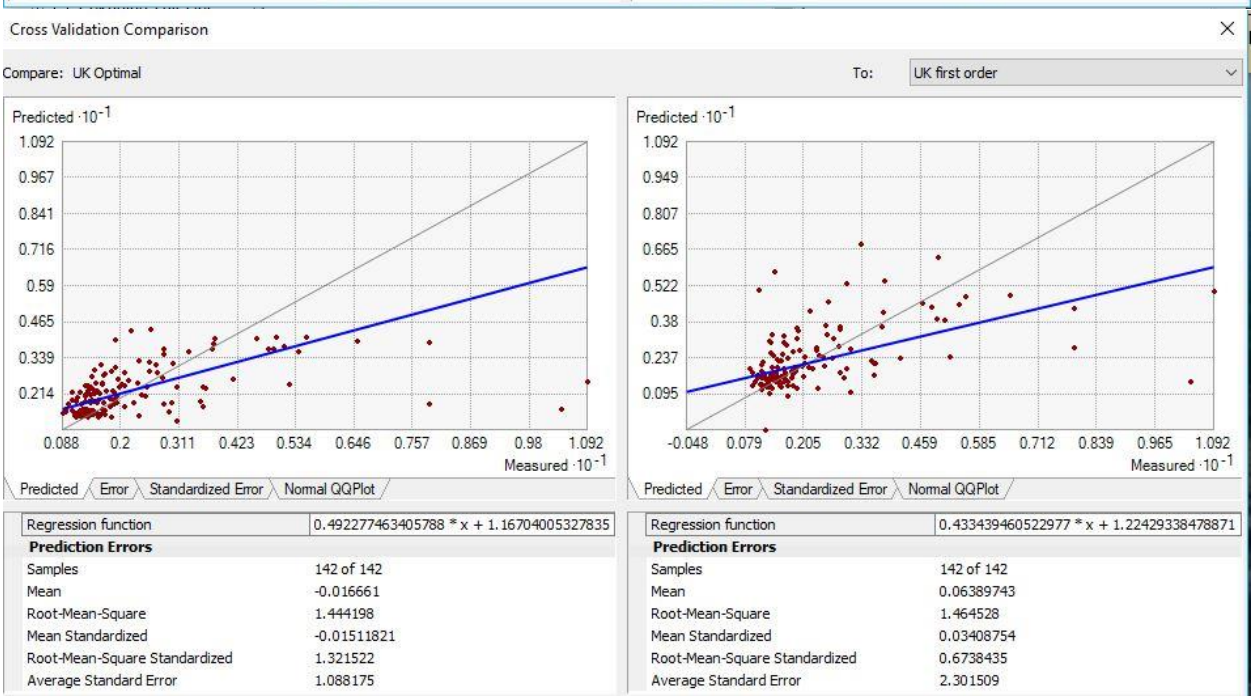
Cross Validation Comparison
Compare: UK Optimal
To: UK first order
Predicted ·10-1
1.092
0.967
0.841
0.716
0.59
0.465
0.339
0.214
0.088 0.2 0.311 0.423 0.534 0.646 0.757 0.869 0.98 1.092
Measured ·10-1
Predicted Error Standardized Error Normal QQPlot
Regression function 0.492277463405788 * x + 1.16704005327835
Prediction Errors
Samples 142 of 142
Mean -0.016661
Root-Mean-Square 1.444198
Mean Standardized -0.01511821
Root-Mean-Square Standardized 1.321522
Average Standard Error 1.088175
Predicted ·10-1
1.092
0.949
0.807
0.665
0.522
0.38
0.237
0.095
-0.048 0.079 0.205 0.332 0.459 0.585 0.712 0.839 0.965 1.092
Measured ·10-1
Predicted Error Standardized Error Normal QQPlot
Regression function 0.433439460522977 * x + 1.22429338478871
Prediction Errors
Samples 142 of 142
Mean 0.06389743
Root-Mean-Square 1.464528
Mean Standardized 0.03408754
Root-Mean-Square Standardized 0.6738435
Average Standard Error 2.301509

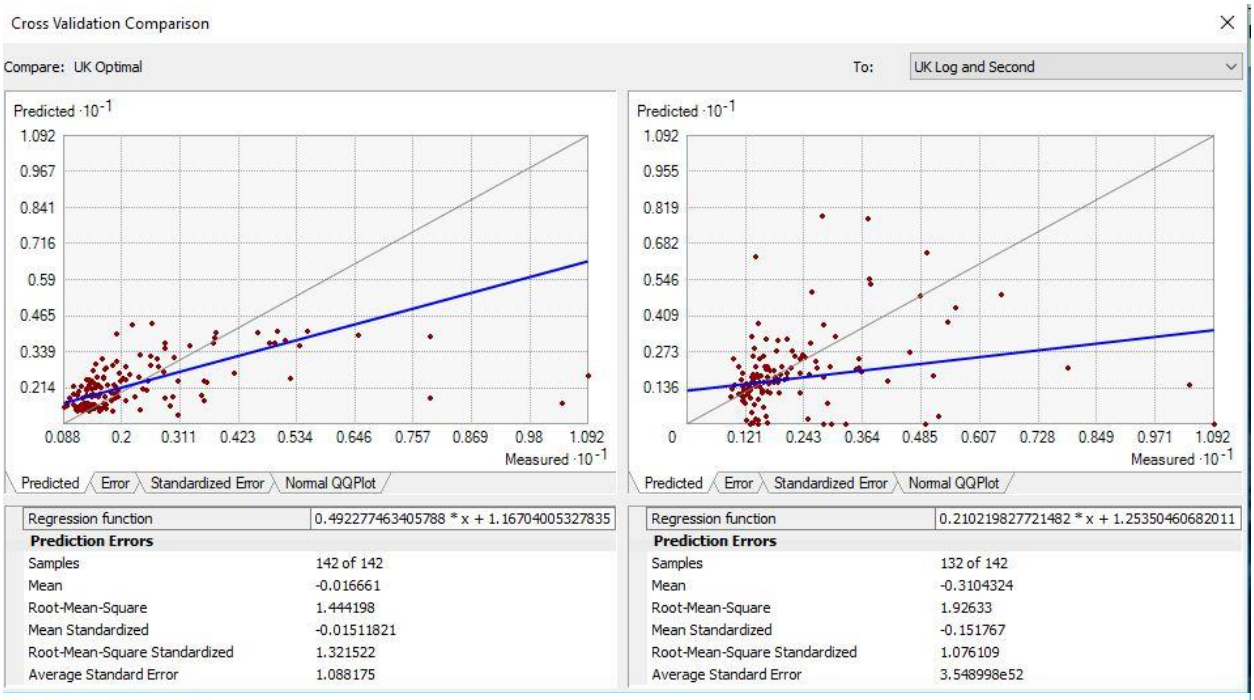
Cross Validation Comparison
Compare: UK Optimal
To: UK Log and Second
Predicted ·10-1
1.092
0.967
0.841
0.716
0.59
0.465
0.339
0.214
0.088 0.2 0.311 0.423 0.534 0.646 0.757 0.869 0.98 1.092
Measured ·10-1
Predicted Error Standardized Error Normal QQPlot
Regression function 0.492277463405788 * x + 1.16704005327835
Prediction Errors
Samples 142 of 142
Mean -0.016661
Root-Mean-Square 1.444198
Mean Standardized -0.01511821
Root-Mean-Square Standardized 1.321522
Average Standard Error 1.088175
Predicted ·10-1
1.092
0.955
0.819
0.682
0.546
0.409
0.273
0.136
0
0.121 0.243 0.364 0.485 0.607 0.728 0.849 0.971 1.092
Measured ·10-1
Predicted Error Standardized Error Normal QQPlot
Regression function 0.210219827721482 * x + 1.25350460682011
Prediction Errors
Samples 132 of 142
Mean -0.3104324
Root-Mean-Square 1.92633
Mean Standardized -0.151767
Root-Mean-Square Standardized 1.076109
Average Standard Error 3.548998e52

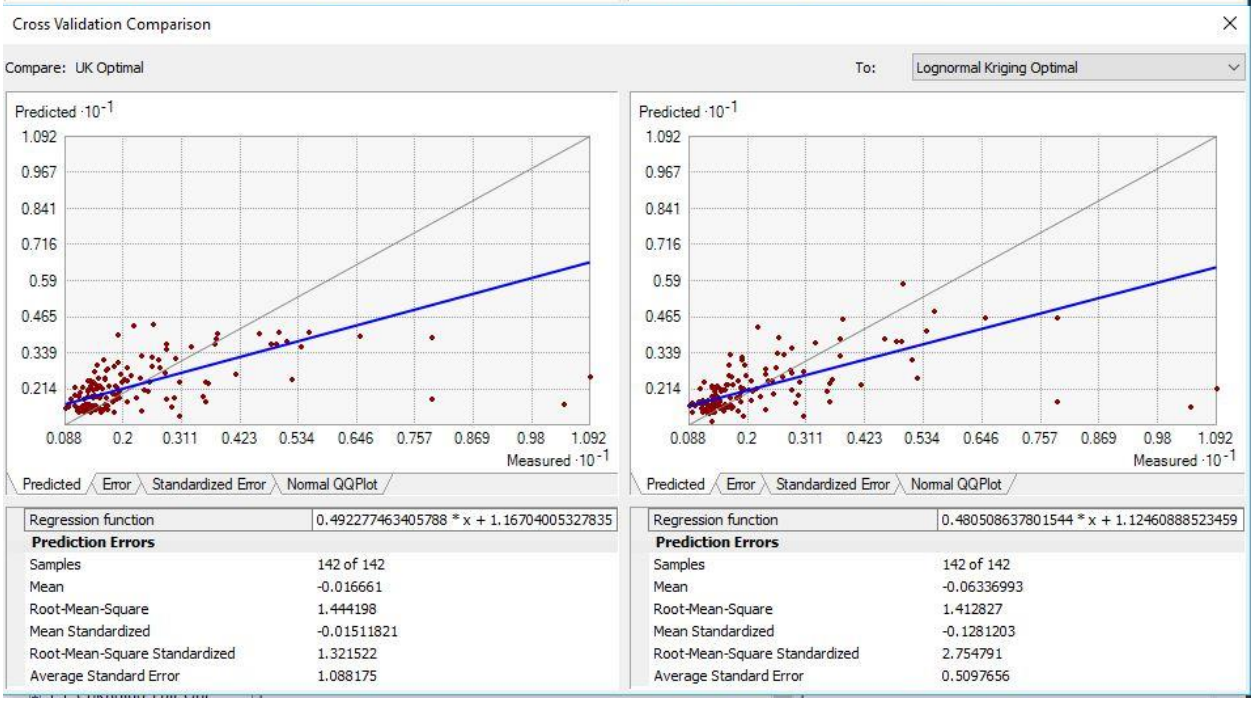
Cross Validation Comparison
Compare: UK Optimal
To: Lognormal Kriging Optimal
Predicted ·10-1
1.092
0.967
0.841
0.716
0.59
0.465
0.339
0.214
0.088 0.2 0.311 0.423 0.534 0.646 0.757 0.869 0.98 1.092
Measured ·10-1
Predicted Error Standardized Error Normal QQPlot
Regression function 0.492277463405788 * x + 1.16704005327835
Prediction Errors
Samples 142 of 142
Mean -0.016661
Root-Mean-Square 1.444198
Mean Standardized -0.01511821
Root-Mean-Square Standardized 1.321522
Average Standard Error 1.088175
Predicted ·10-1
1.092
0.967
0.841
0.716
0.59
0.465
0.339
0.214
0.088 0.2 0.311 0.423 0.534 0.646 0.757 0.869 0.98 1.092
Measured ·10-1
Predicted Error Standardized Error Normal QQPlot
Regression function 0.480508637801544 * x + 1.12460888523459
Prediction Errors
Samples 142 of 142
Mean -0.06336993
Root-Mean-Square 1.412827
Mean Standardized -0.1281203
Root-Mean-Square Standardized 2.754791
Average Standard Error 0.5097656

Cross Validation Comparison

Compare: UK Optimal

To: Lognormal Kriging

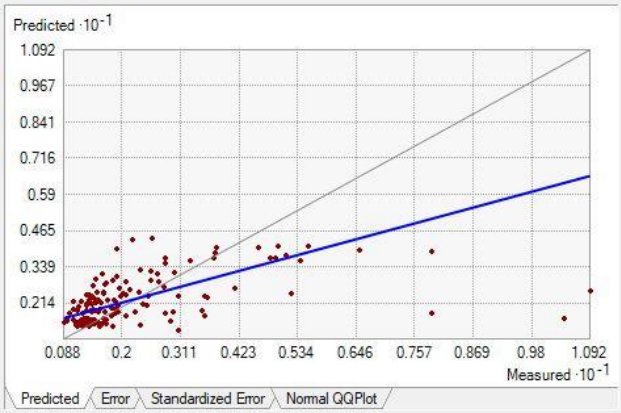

Regression function	0.492277463405788 * x + 1.16704005327835
Prediction Errors	
Samples	142 of 142
Mean	-0.016661
Root-Mean-Square	1.444198
Mean Standardized	-0.01511821
Root-Mean-Square Standardized	1.321522
Average Standard Error	1.088175

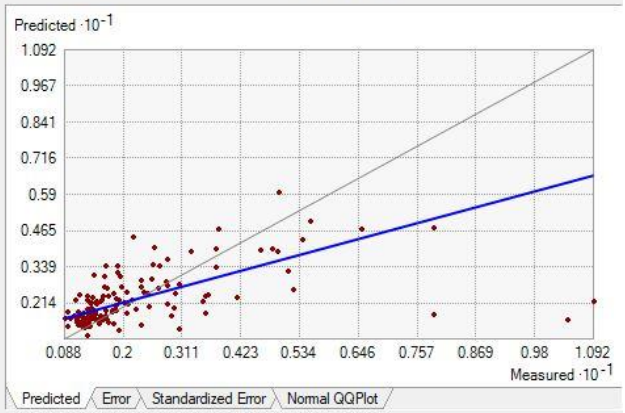

Regression function	0.494073102310607 * x + 1.16331448843477
Prediction Errors	
Samples	142 of 142
Mean	0.004765856
Root-Mean-Square	1.420043
Mean Standardized	0.001232584
Root-Mean-Square Standardized	2.293237
Average Standard Error	0.621968

Cross Validation Comparison

Compare: UK West Opt

To: UK West Opt Second

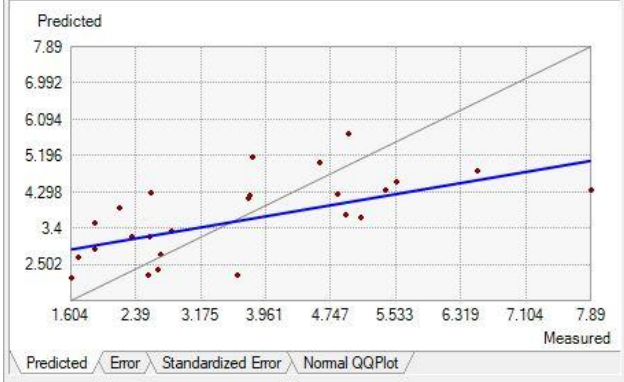

Regression function	0.349158305802727 * x + 2.3091007237...
Prediction Errors	
Samples	25 of 25
Mean	0.0446604
Root-Mean-Square	1.242165
Mean Standardized	0.02803502
Root-Mean-Square Standardized	0.9482626
Average Standard Error	1.310145

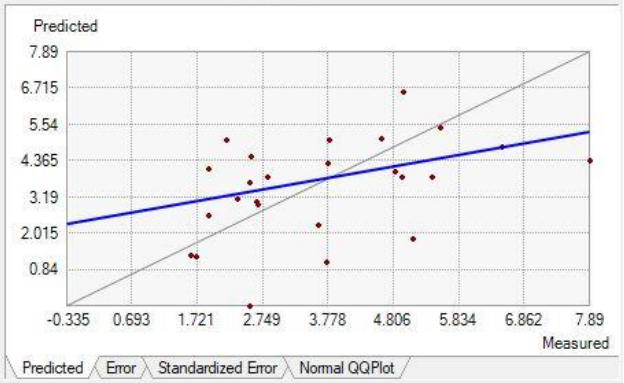

Regression function	0.362420360502972 * x + 2.43325096311...
Prediction Errors	
Samples	25 of 25
Mean	-0.1689692
Root-Mean-Square	1.703614
Mean Standardized	-0.02567354
Root-Mean-Square Standardized	1.197667
Average Standard Error	2.401363

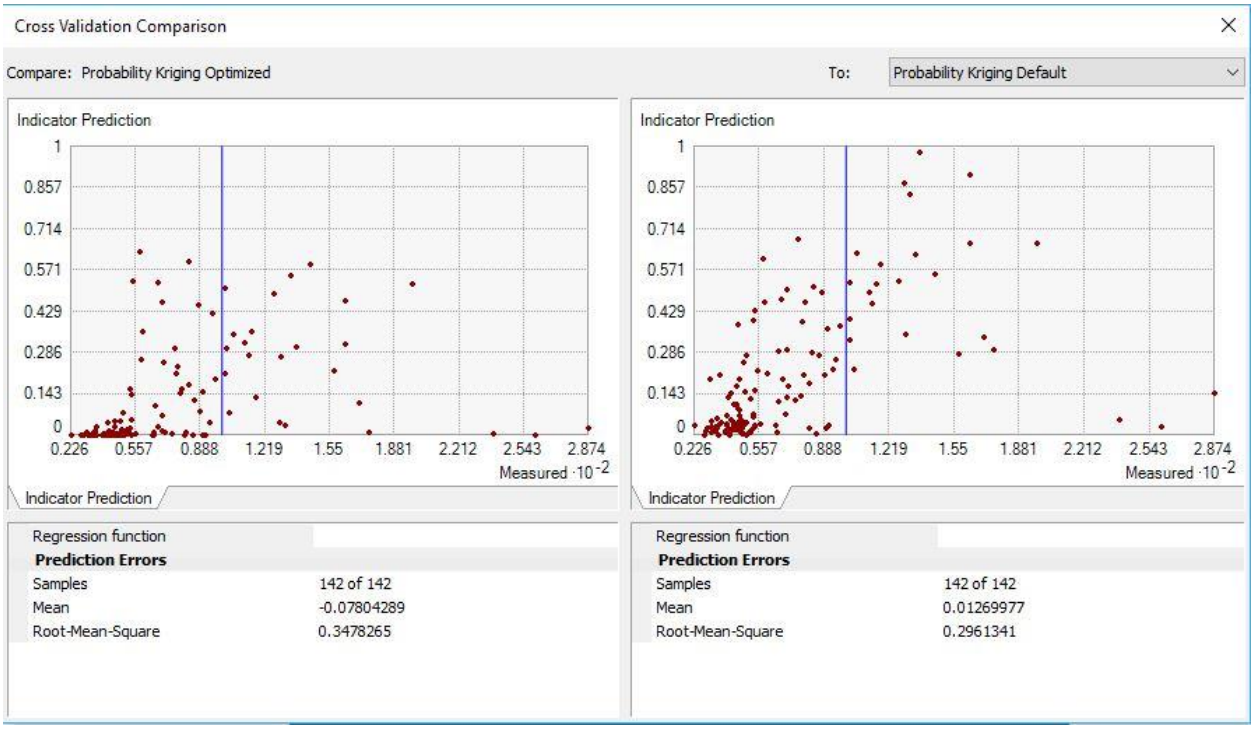
Cross Validation Comparison
Compare: Probability Kriging Optimized
To: Probability Kriging Default
Indicator Prediction
1
0.857
0.714
0.571
0.429
0.286
0.143
0
0.226 0.557 0.888 1.219 1.55 1.881 2.212 2.543 2.874
Measured ·10-2
Indicator Prediction
Regression function
Prediction Errors
Samples 142 of 142
Mean -0.07804289
Root-Mean-Square 0.3478265
Indicator Prediction
1
0.857
0.714
0.571
0.429
0.286
0.143
0
0.226 0.557 0.888 1.219 1.55 1.881 2.212 2.543 2.874
Measured ·10-2
Indicator Prediction
Regression function
Prediction Errors
Samples 142 of 142
Mean 0.01269977
Root-Mean-Square 0.2961341

Appendix C. 2016 Flow Increase Prediction Products

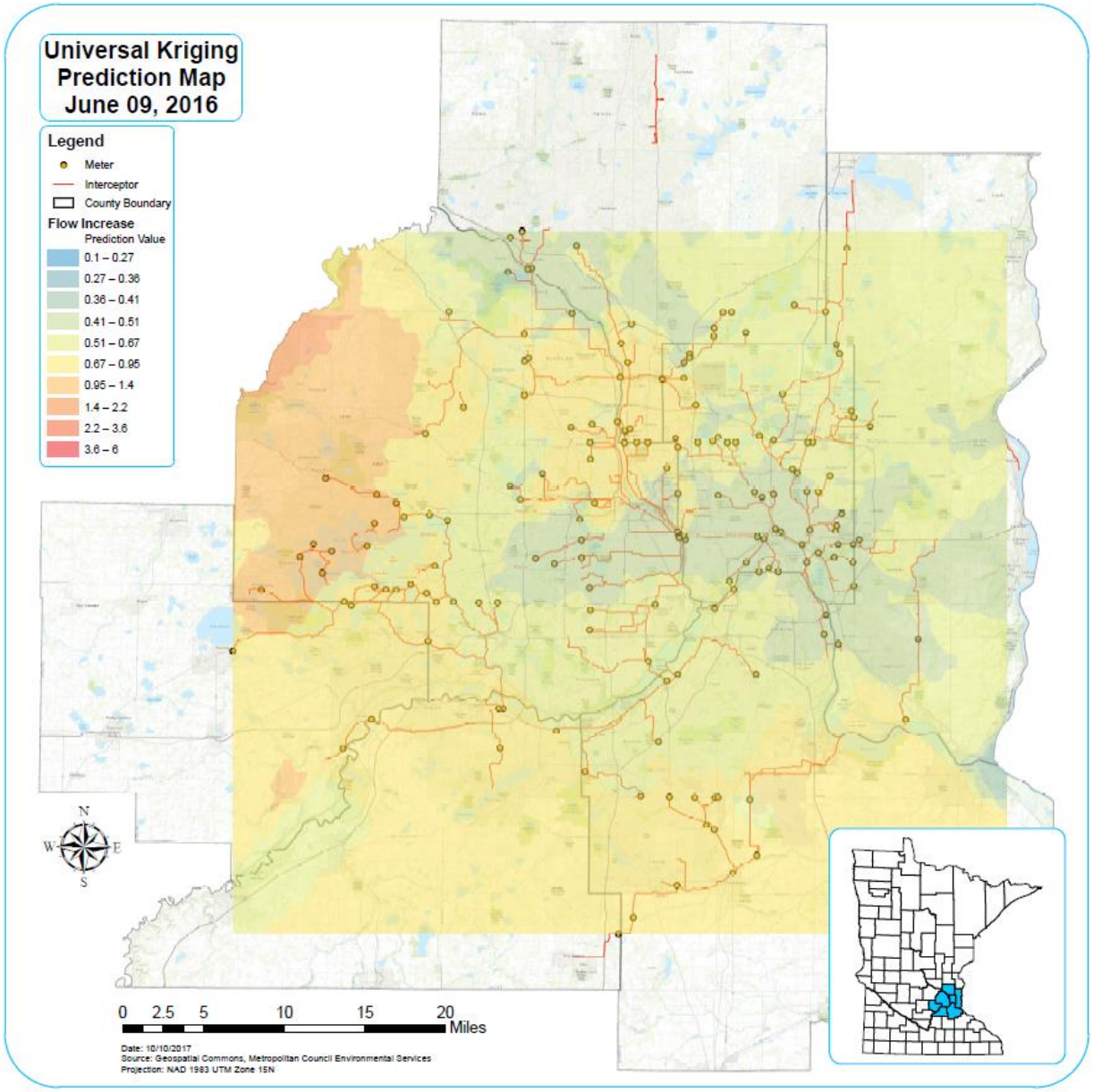
Universal Kriging
Prediction Map
June 09, 2016
Legend
Meter
Interceptor
County Boundary
Flow Increase
Prediction Value
0.1 – 0.27
0.27 – 0.36
0.36 – 0.41
0.41 – 0.51
0.51 – 0.67
0.67 – 0.95
0.95 – 1.4
1.4 – 2.2
2.2 – 3.6
3.6 – 6
N
W
E
S
0 2.5 5 10 15 20
Miles
Date: 10/10/2017
Source: Geospatial Commons, Metropolitan Council Environmental Services
Projection: NAD 1983 UTM Zone 15N

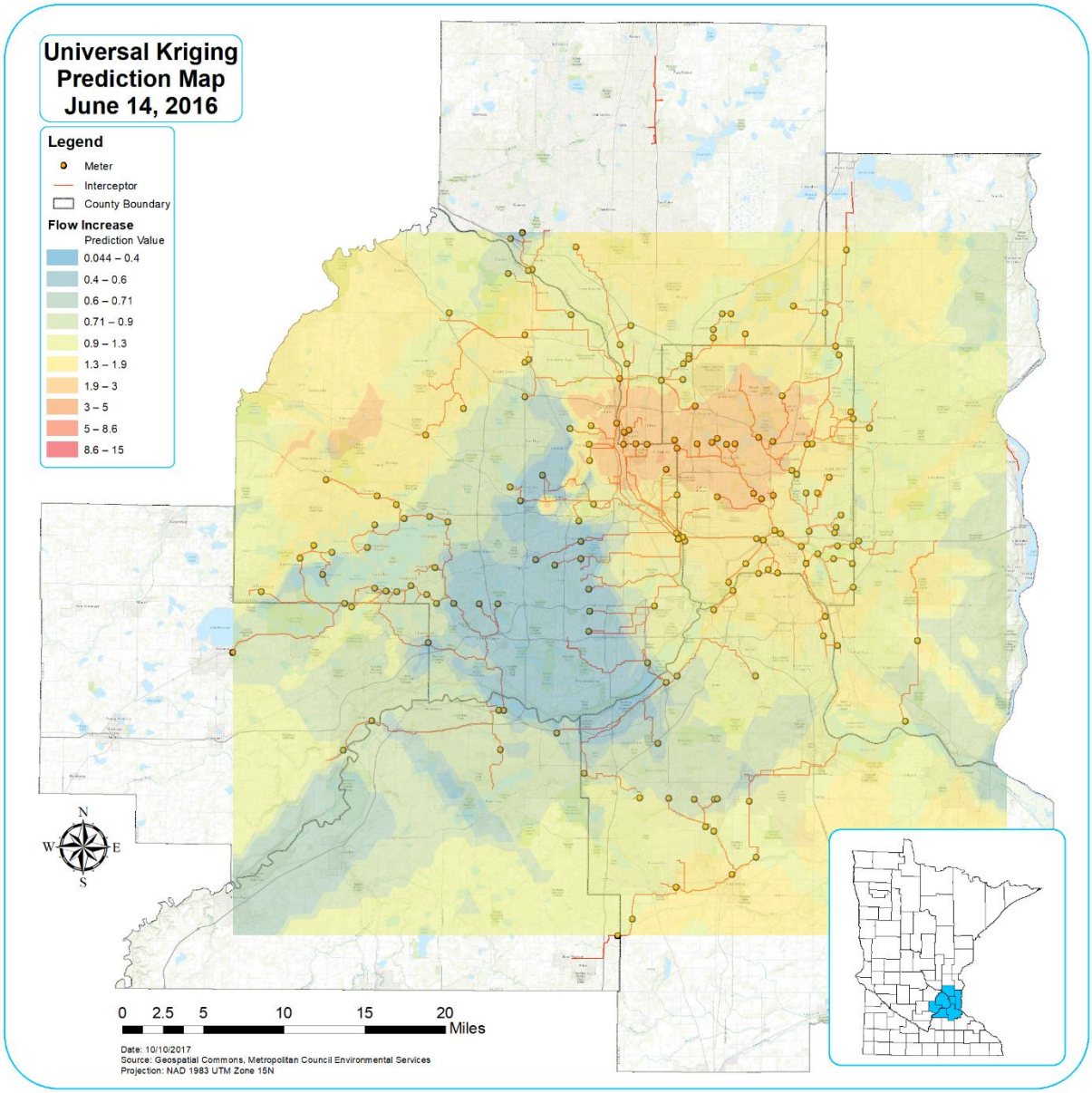
Universal Kriging
Prediction Map
June 14, 2016
Legend
Meter
Interceptor
County Boundary
Flow Increase
Prediction Value
0.044 – 0.4
0.4 – 0.6
0.6 – 0.71
0.71 – 0.9
0.9 – 1.3
1.3 – 1.9
1.9 – 3
3 – 5
5 – 8.6
8.6 – 15
N
W
E
S
0 2.5 5 10 15 20
Miles
Date: 10/10/2017
Source: Geospatial Commons, Metropolitan Council Environmental Services
Projection: NAD 1983 UTM Zone 15N

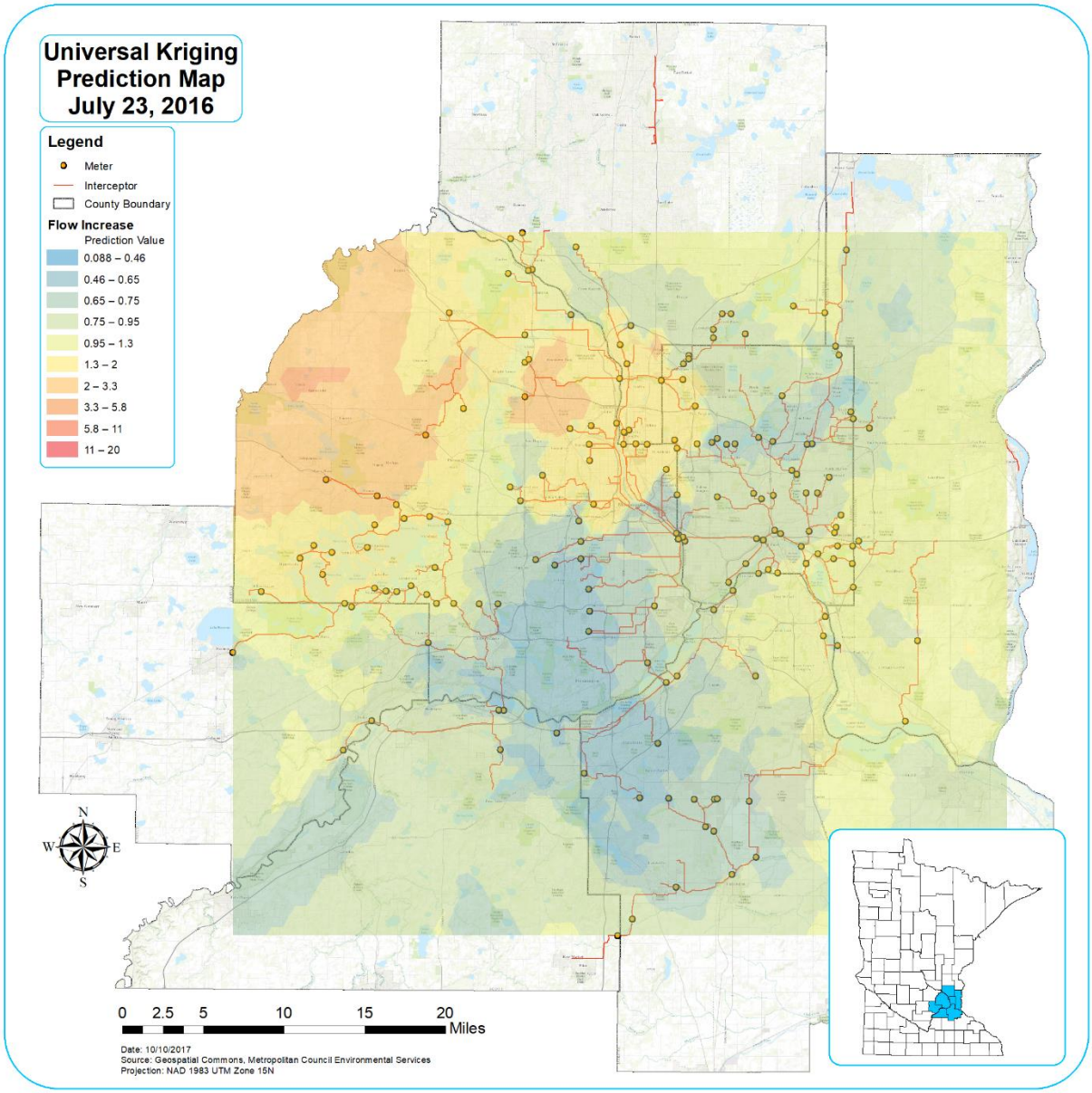
Universal Kriging
Prediction Map
July 23, 2016
Legend
Meter
Interceptor
County Boundary
Flow Increase
Prediction Value
0.088 – 0.46
0.46 – 0.65
0.65 – 0.75
0.75 – 0.95
0.95 – 1.3
1.3 – 2
2 – 3.3
3.3 – 5.8
5.8 – 11
11 – 20
N
W
E
S
0 2.5 5 10 15 20
Miles
Date: 10/10/2017
Source: Geospatial Commons, Metropolitan Council Environmental Services
Projection: NAD 1983 UTM Zone 15N

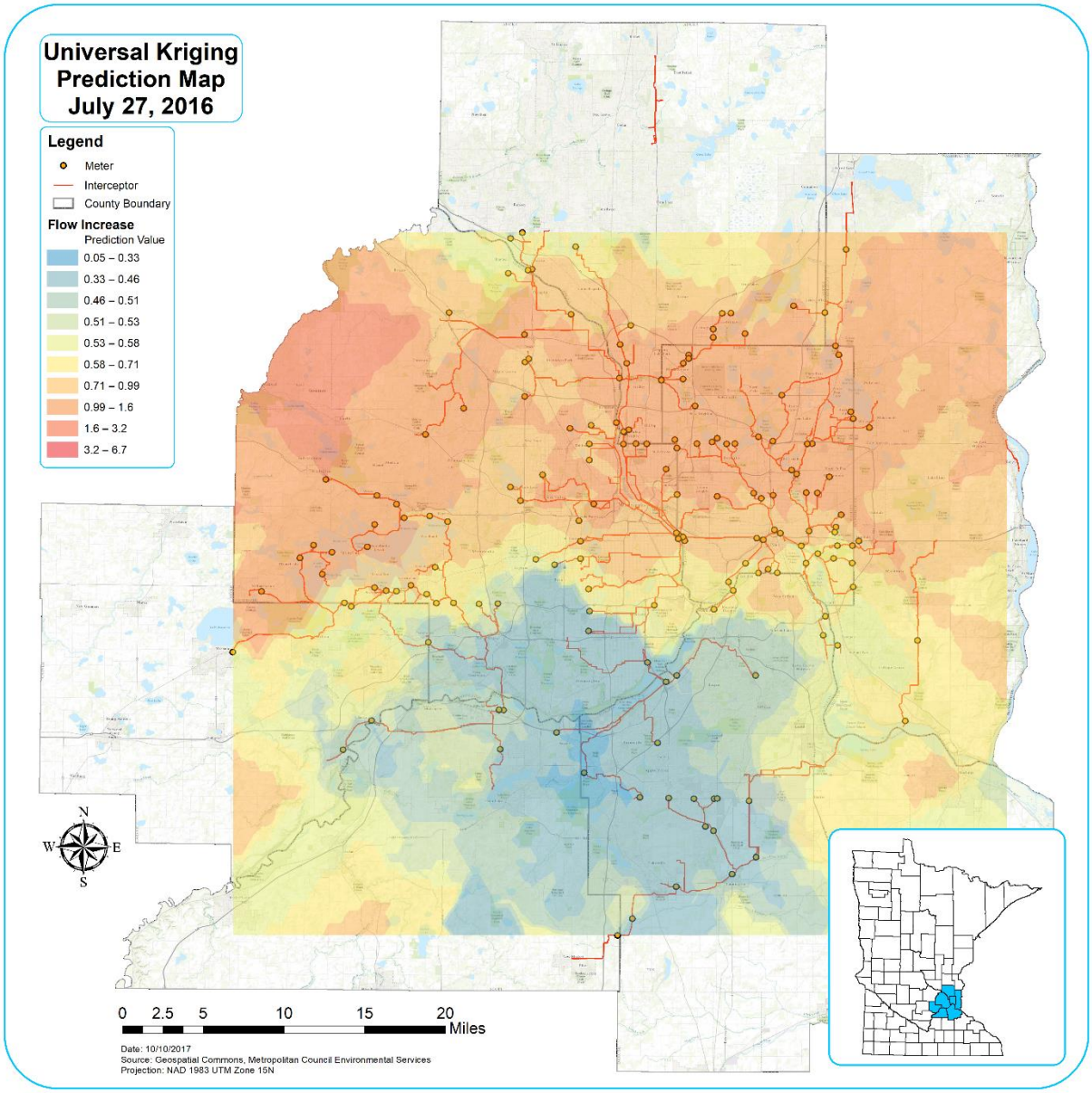
Universal Kriging
Prediction Map
July 27, 2016
Legend
Meter
Interceptor
County Boundary
Flow Increase
Prediction Value
0.05 – 0.33
0.33 – 0.46
0.46 – 0.51
0.51 – 0.53
0.53 – 0.58
0.58 – 0.71
0.71 – 0.99
0.99 – 1.6
1.6 – 3.2
3.2 – 6.7
N
W
E
S
0 2.5 5 10 15 20
Miles
Date: 10/10/2017
Source: Geospatial Commons, Metropolitan Council Environmental Services
Projection: NAD 1983 UTM Zone 15N

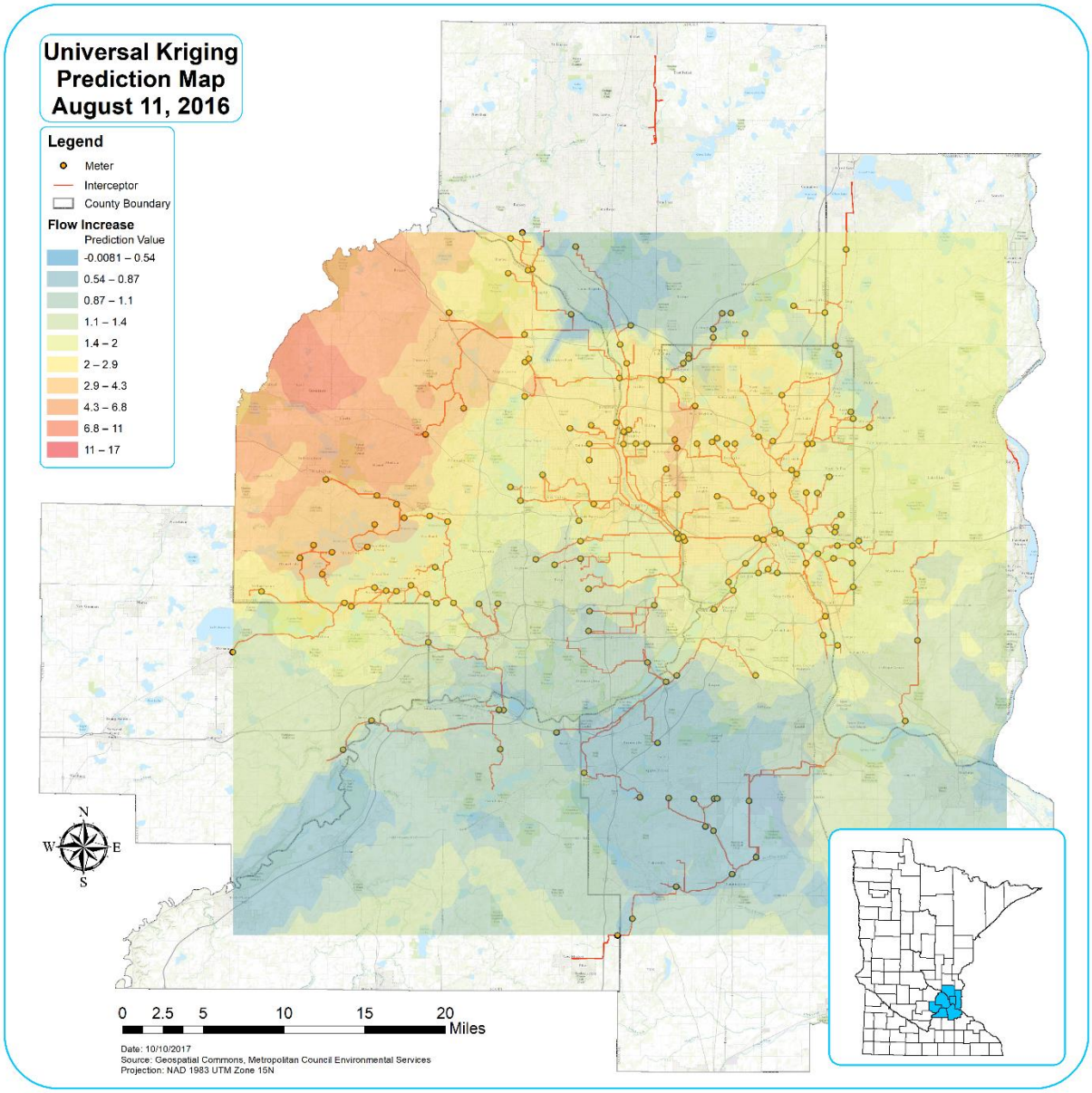
Universal Kriging
Prediction Map
August 11, 2016
Legend
Meter
Interceptor
County Boundary
Flow Increase
Prediction Value
-0.0081 – 0.54
0.54 – 0.87
0.87 – 1.1
1.1 – 1.4
1.4 – 2
2 – 2.9
2.9 – 4.3
4.3 – 6.8
6.8 – 11
11 – 17
N
W
E
S
0 2.5 5 10 15 20
Miles
Date: 10/10/2017
Source: Geospatial Commons, Metropolitan Council Environmental Services
Projection: NAD 1983 UTM Zone 15N

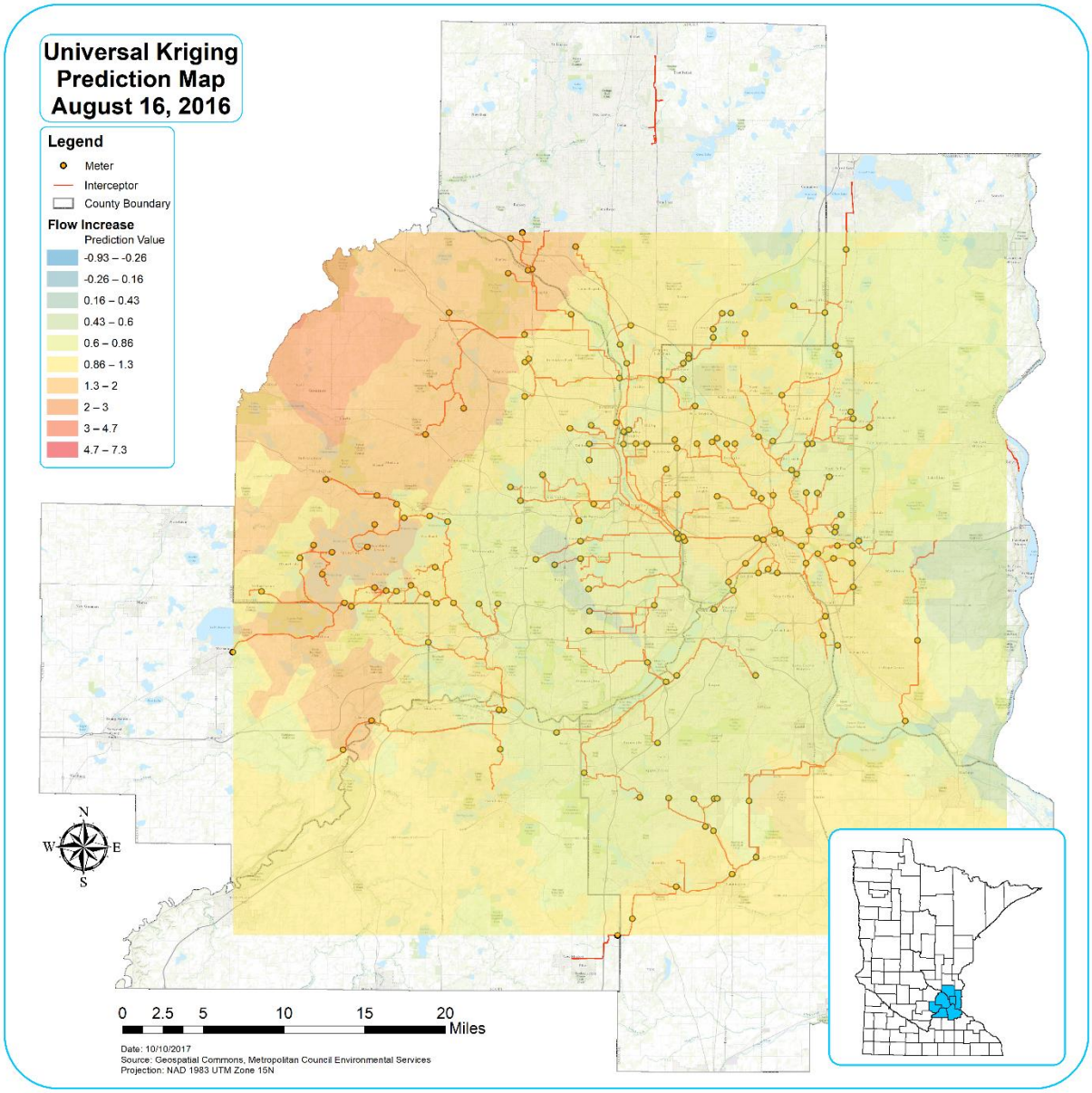
Universal Kriging Prediction Map August 16, 2016
Legend
Meter
Interceptor
County Boundary
Flow Increase
Prediction Value
-0.93 – -0.26
-0.26 – 0.16
0.16 – 0.43
0.43 – 0.6
0.6 – 0.86
0.86 – 1.3
1.3 – 2
2 – 3
3 – 4.7
4.7 – 7.3
N
W
E
S
0 2.5 5 10 15 20
Miles
Date: 10/10/2017
Source: Geospatial Commons, Metropolitan Council Environmental Services
Projection: NAD 1983 UTM Zone 15N

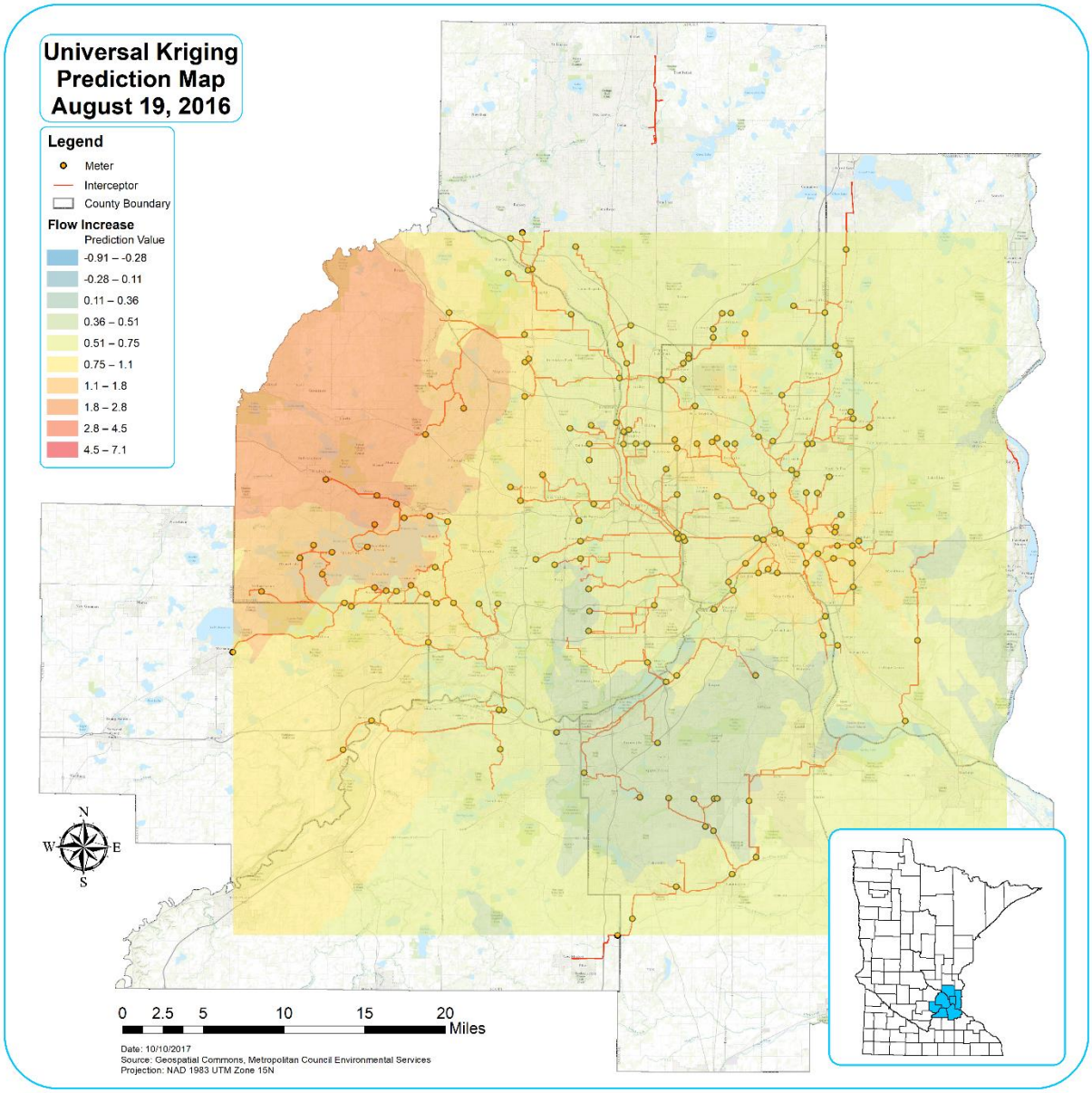
Universal Kriging
Prediction Map
August 19, 2016
Legend
Meter
Interceptor
County Boundary
Flow Increase
Prediction Value
-0.91 – -0.28
-0.28 – 0.11
0.11 – 0.36
0.36 – 0.51
0.51 – 0.75
0.75 – 1.1
1.1 – 1.8
1.8 – 2.8
2.8 – 4.5
4.5 – 7.1
N
W
E
S
0 2.5 5 10 15 20
Miles
Date: 10/10/2017
Source: Geospatial Commons, Metropolitan Council Environmental Services
Projection: NAD 1983 UTM Zone 15N

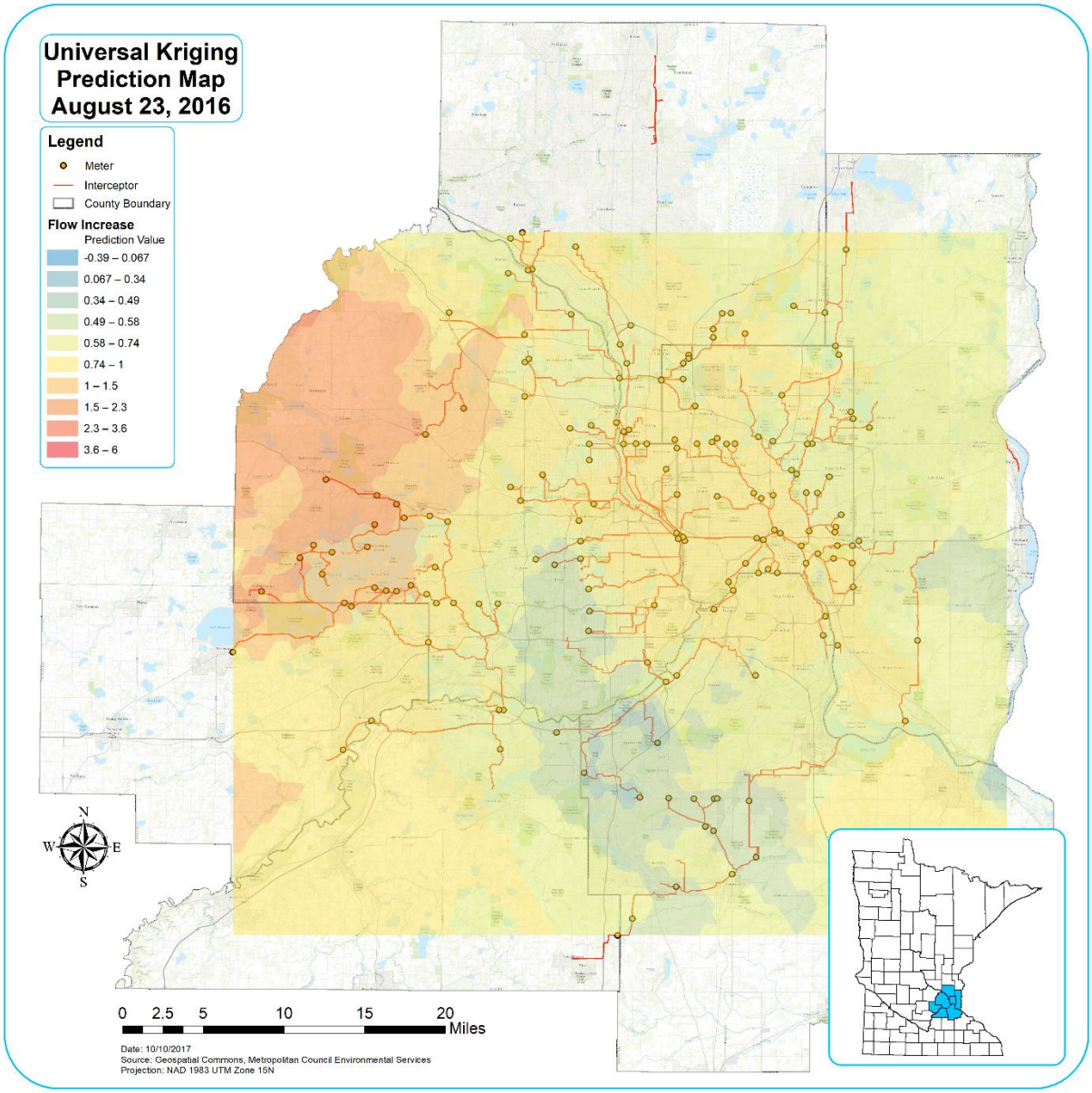
Universal Kriging
Prediction Map
August 23, 2016
Legend
Meter
Interceptor
County Boundary
Flow Increase
Prediction Value
-0.39 – 0.067
0.067 – 0.34
0.34 – 0.49
0.49 – 0.58
0.58 – 0.74
0.74 – 1
1 – 1.5
1.5 – 2.3
2.3 – 3.6
3.6 – 6
N
W
E
S
0 2.5 5 10 15 20
Miles
Date: 10/10/2017
Source: Geospatial Commons, Metropolitan Council Environmental Services
Projection: NAD 1983 UTM Zone 15N

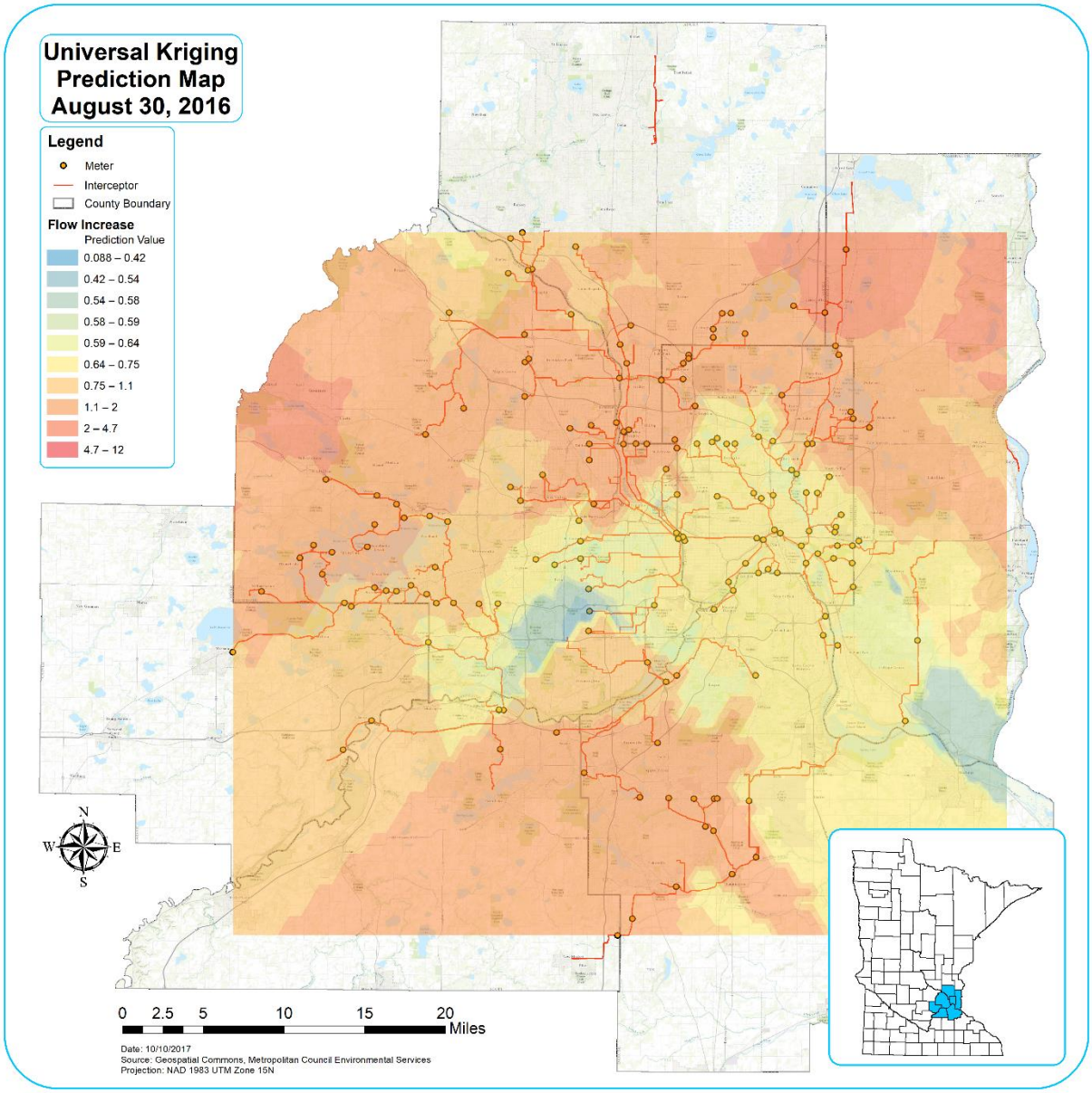
Universal Kriging
Prediction Map
August 30, 2016
Legend
Meter
Interceptor
County Boundary
Flow Increase
Prediction Value
0.088 – 0.42
0.42 – 0.54
0.54 – 0.58
0.58 – 0.59
0.59 – 0.64
0.64 – 0.75
0.75 – 1.1
1.1 – 2
2 – 4.7
4.7 – 12
N
W
E
S
0 2.5 5 10 15 20
Miles
Date: 10/10/2017
Source: Geospatial Commons, Metropolitan Council Environmental Services
Projection: NAD 1983 UTM Zone 15N

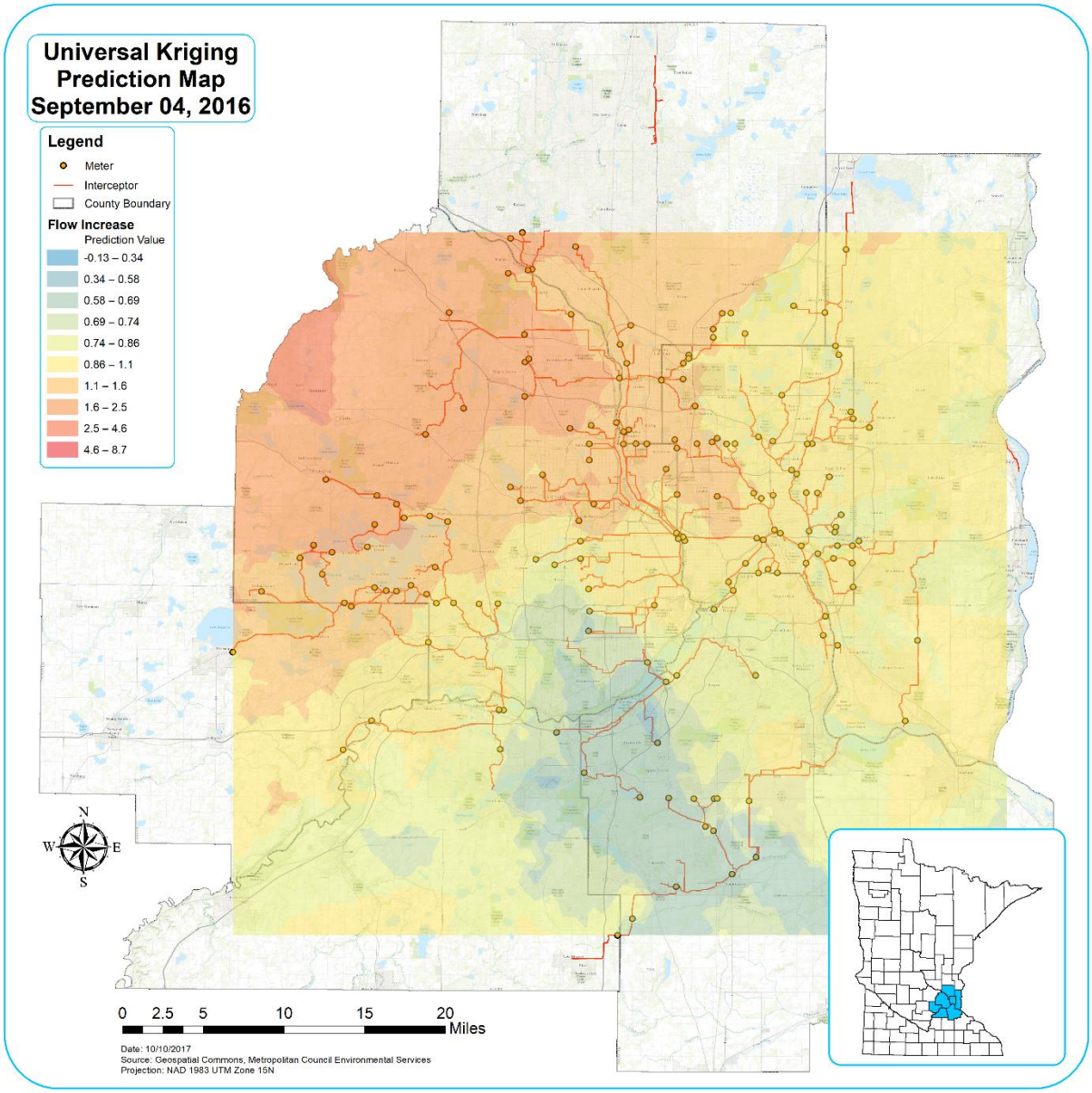
Universal Kriging
Prediction Map
September 04, 2016
Legend
Meter
Interceptor
County Boundary
Flow Increase
Prediction Value
-0.13 – 0.34
0.34 – 0.58
0.58 – 0.69
0.69 – 0.74
0.74 – 0.86
0.86 – 1.1
1.1 – 1.6
1.6 – 2.5
2.5 – 4.6
4.6 – 8.7
N
W
E
S
0 2.5 5 10 15 20
Miles
Date: 10/10/2017
Source: Geospatial Commons, Metropolitan Council Environmental Services
Projection: NAD 1983 UTM Zone 15N

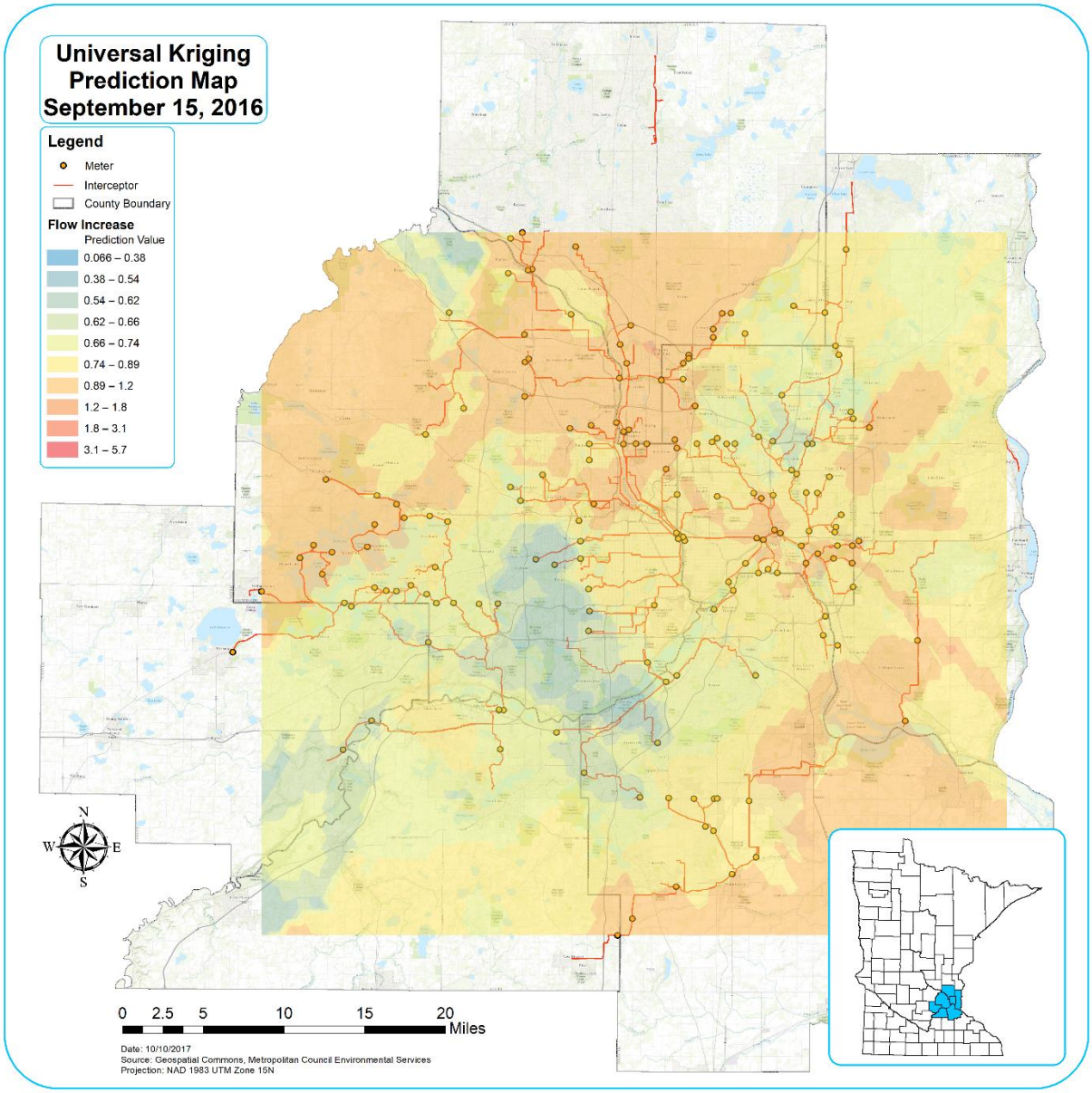
Universal Kriging Prediction Map September 15, 2016
Legend
Meter
Interceptor
County Boundary
Flow Increase
Prediction Value
0.066 – 0.38
0.38 – 0.54
0.54 – 0.62
0.62 – 0.66
0.66 – 0.74
0.74 – 0.89
0.89 – 1.2
1.2 – 1.8
1.8 – 3.1
3.1 – 5.7
N
W
E
S
0 2.5 5 10 15 20
Miles
Date: 10/10/2017
Source: Geospatial Commons, Metropolitan Council Environmental Services
Projection: NAD 1983 UTM Zone 15N

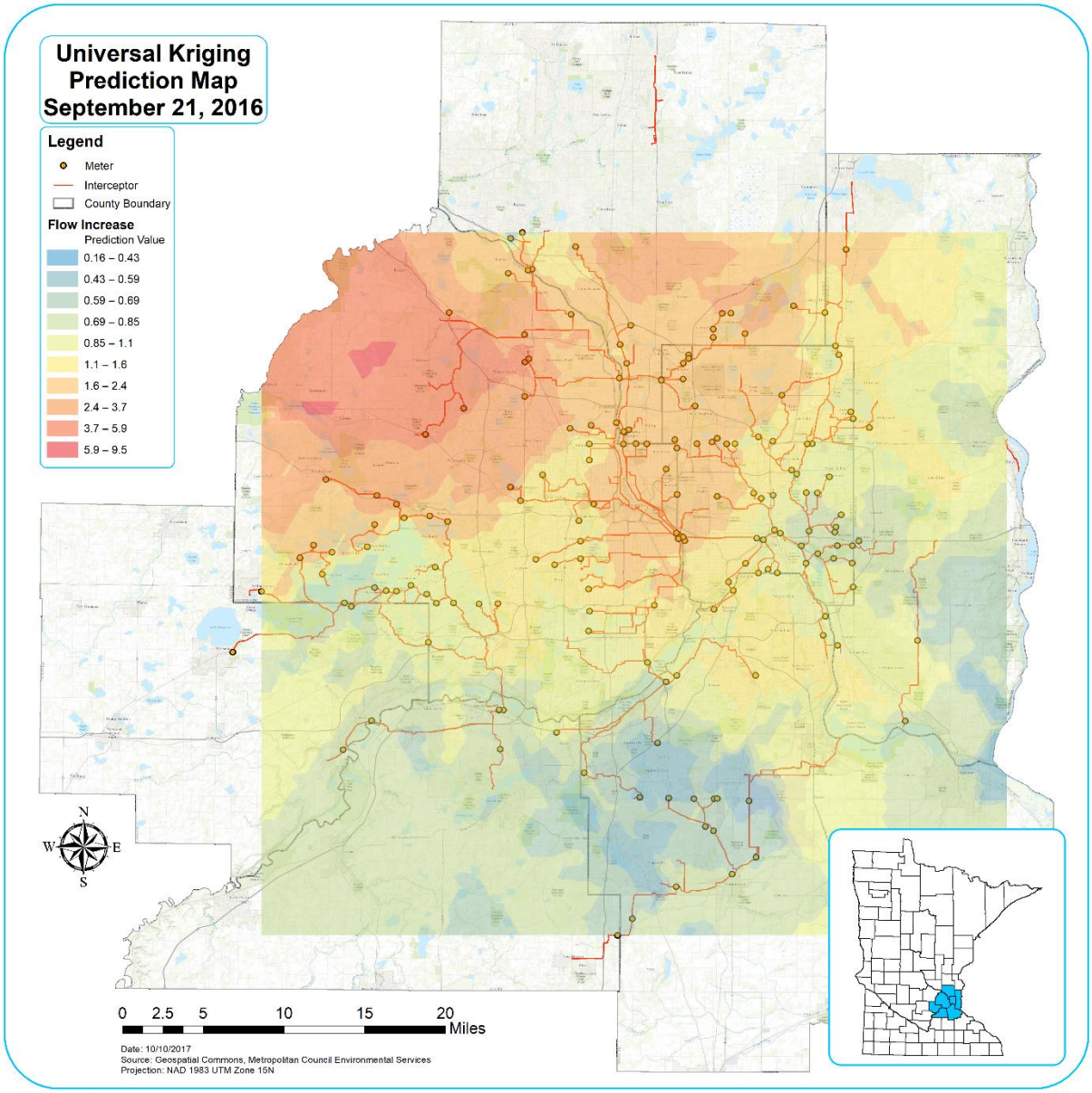
Universal Kriging
Prediction Map
September 21, 2016
Legend
Meter
Interceptor
County Boundary
Flow Increase
Prediction Value
0.16 – 0.43
0.43 – 0.59
0.59 – 0.69
0.69 – 0.85
0.85 – 1.1
1.1 – 1.6
1.6 – 2.4
2.4 – 3.7
3.7 – 5.9
5.9 – 9.5
N
W
E
S
0 2.5 5 10 15 20
Miles
Date: 10/10/2017
Source: Geospatial Commons, Metropolitan Council Environmental Services
Projection: NAD 1983 UTM Zone 15N

Appendix D. 2016 Rainfall Prediction Products

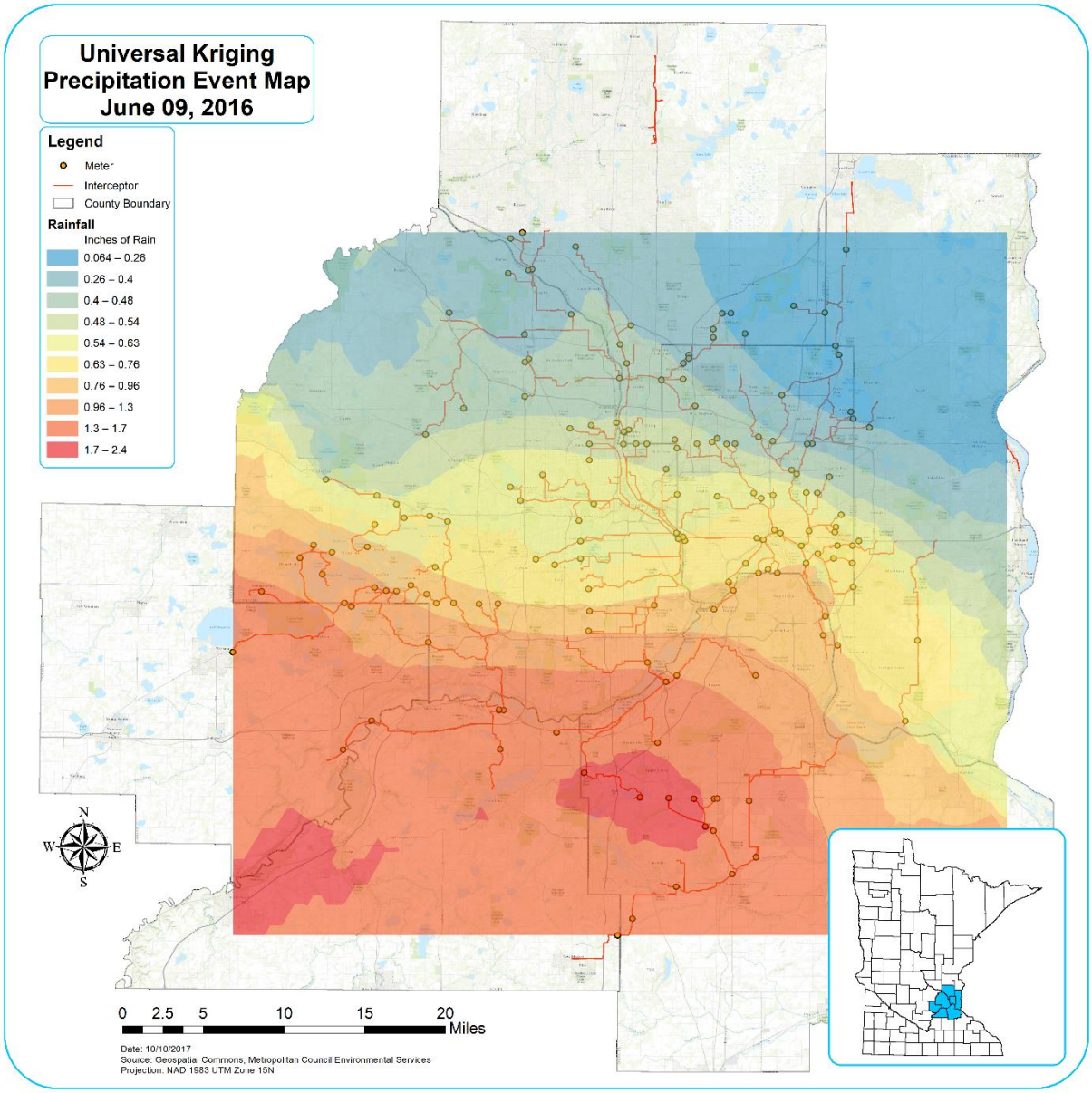
Universal Kriging
Precipitation Event Map
June 09, 2016
Legend
Meter
Interceptor
County Boundary
Rainfall
Inches of Rain
0.064 – 0.26
0.26 – 0.4
0.4 – 0.48
0.48 – 0.54
0.54 – 0.63
0.63 – 0.76
0.76 – 0.96
0.96 – 1.3
1.3 – 1.7
1.7 – 2.4
N
W
E
S
0 2.5 5 10 15 20
Miles
Date: 10/10/2017
Source: Geospatial Commons, Metropolitan Council Environmental Services
Projection: NAD 1983 UTM Zone 15N

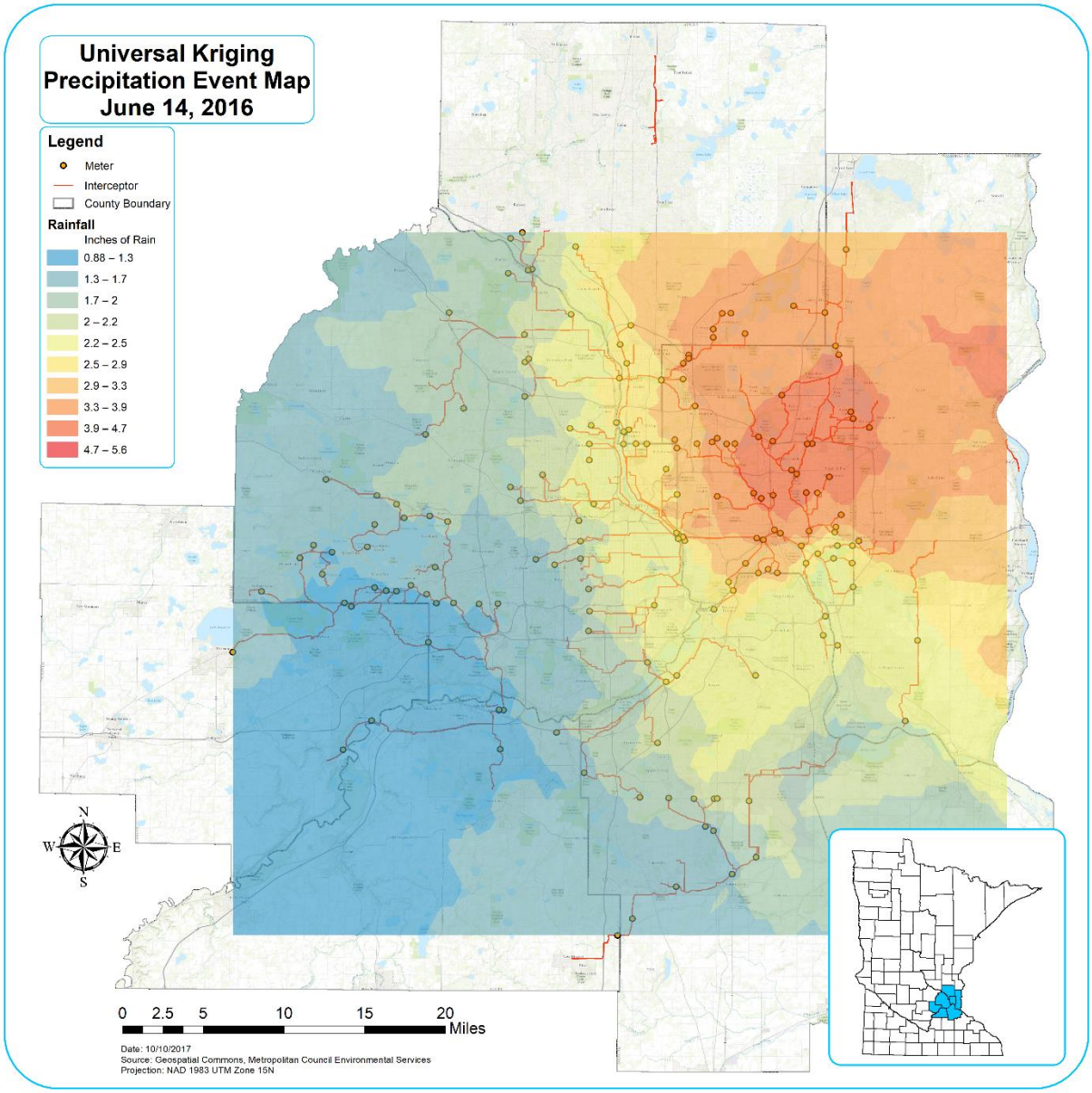
Universal Kriging
Precipitation Event Map
June 14, 2016
Legend
Meter
Interceptor
County Boundary
Rainfall
Inches of Rain
0.88 – 1.3
1.3 – 1.7
1.7 – 2
2 – 2.2
2.2 – 2.5
2.5 – 2.9
2.9 – 3.3
3.3 – 3.9
3.9 – 4.7
4.7 – 5.6
N
W
E
S
0 2.5 5 10 15 20
Miles
Date: 10/10/2017
Source: Geospatial Commons, Metropolitan Council Environmental Services
Projection: NAD 1983 UTM Zone 15N

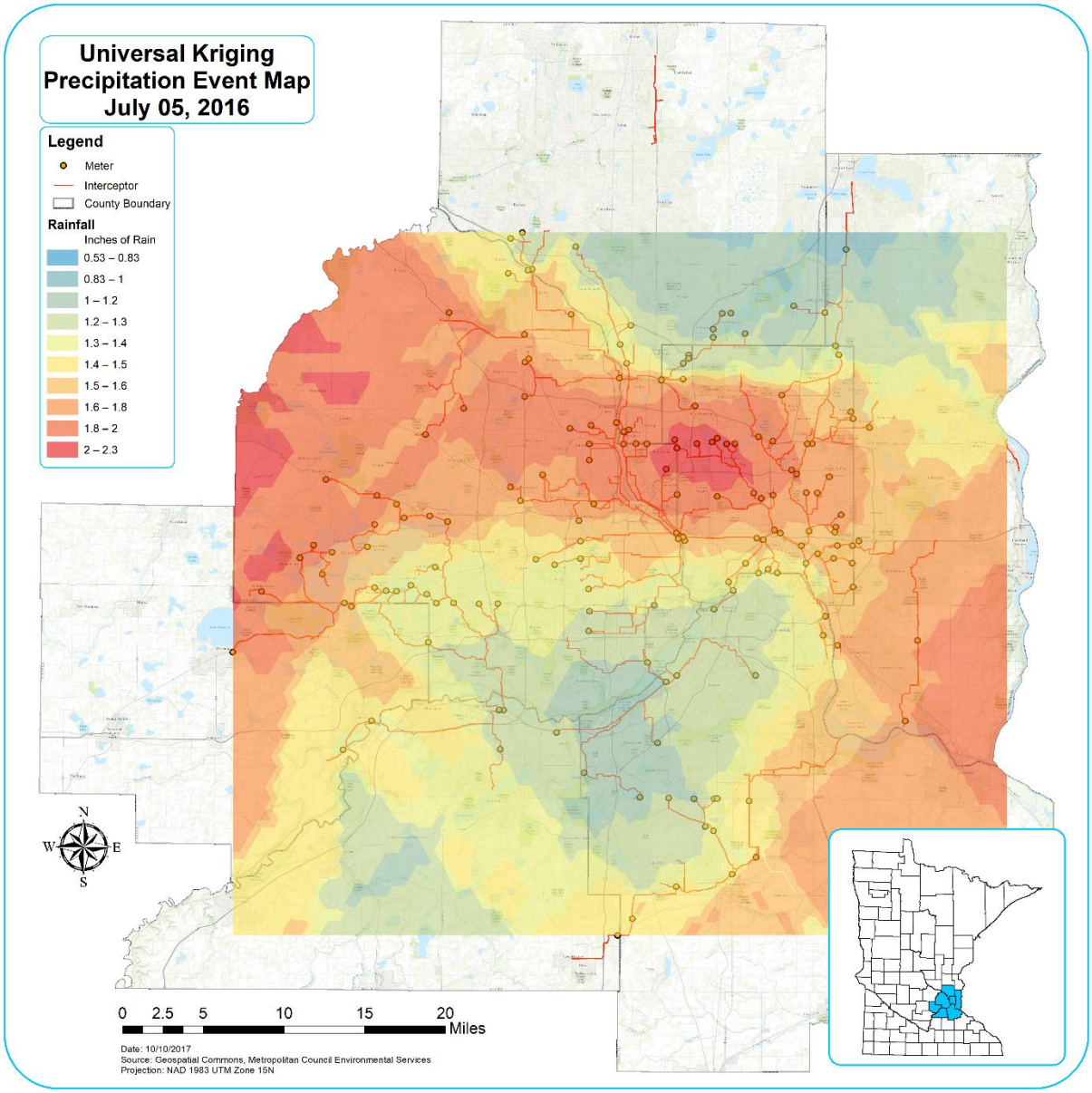
Universal Kriging
Precipitation Event Map
July 05, 2016
Legend
Meter
Interceptor
County Boundary
Rainfall
Inches of Rain
0.53 – 0.83
0.83 – 1
1 – 1.2
1.2 – 1.3
1.3 – 1.4
1.4 – 1.5
1.5 – 1.6
1.6 – 1.8
1.8 – 2
2 – 2.3
N
W
E
S
0 2.5 5 10 15 20
Miles
Date: 10/10/2017
Source: Geospatial Commons, Metropolitan Council Environmental Services
Projection: NAD 1983 UTM Zone 15N

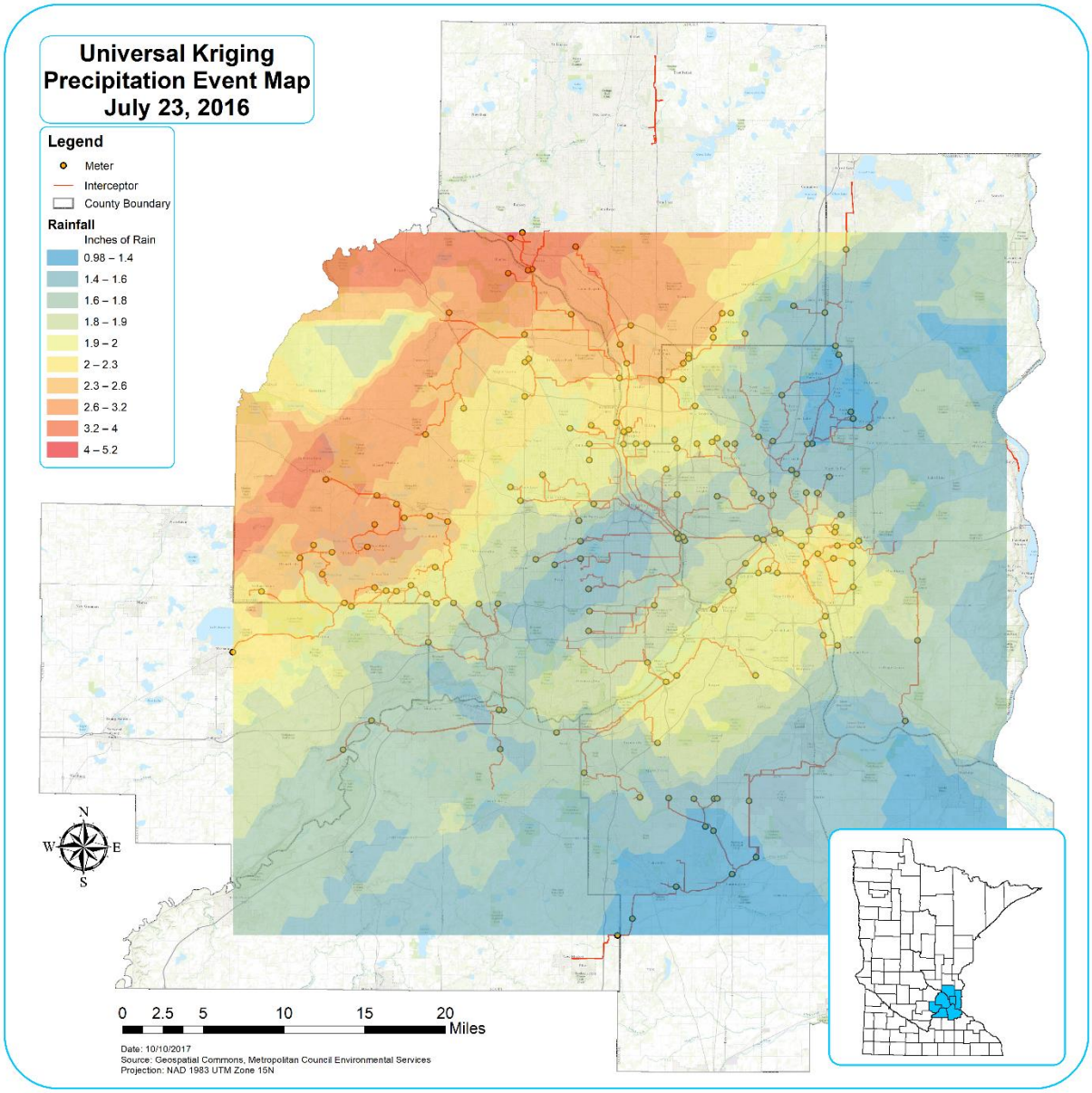
Universal Kriging
Precipitation Event Map
July 23, 2016
Legend
Meter
Interceptor
County Boundary
Rainfall
Inches of Rain
0.98 – 1.4
1.4 – 1.6
1.6 – 1.8
1.8 – 1.9
1.9 – 2
2 – 2.3
2.3 – 2.6
2.6 – 3.2
3.2 – 4
4 – 5.2
N
W
E
S
0 2.5 5 10 15 20
Miles
Date: 10/10/2017
Source: Geospatial Commons, Metropolitan Council Environmental Services
Projection: NAD 1983 UTM Zone 15N

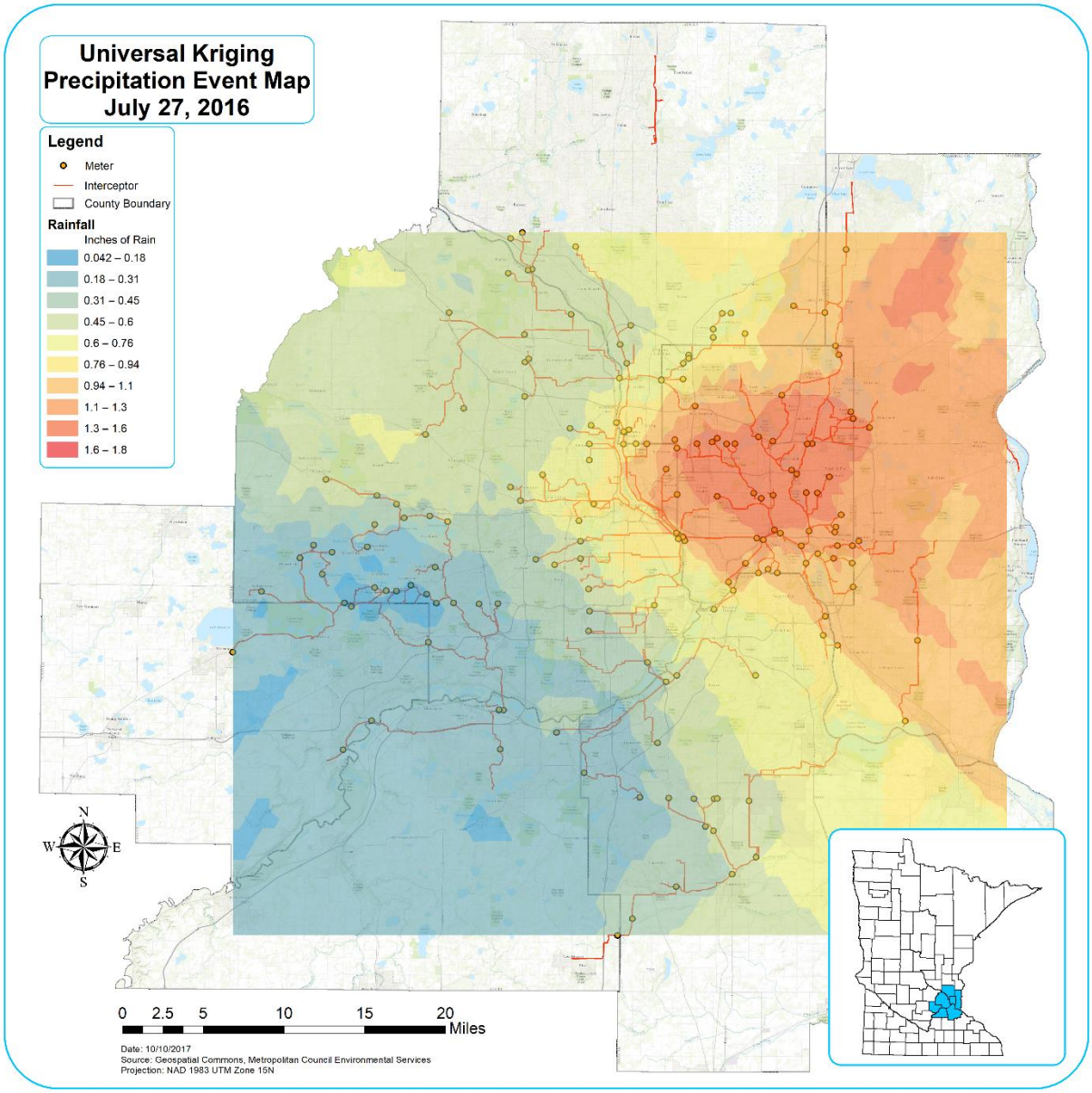
Universal Kriging
Precipitation Event Map
July 27, 2016
Legend
Meter
Interceptor
County Boundary
Rainfall
Inches of Rain
0.042 – 0.18
0.18 – 0.31
0.31 – 0.45
0.45 – 0.6
0.6 – 0.76
0.76 – 0.94
0.94 – 1.1
1.1 – 1.3
1.3 – 1.6
1.6 – 1.8
N
W
E
S
0 2.5 5 10 15 20
Miles
Date: 10/10/2017
Source: Geospatial Commons, Metropolitan Council Environmental Services
Projection: NAD 1983 UTM Zone 15N

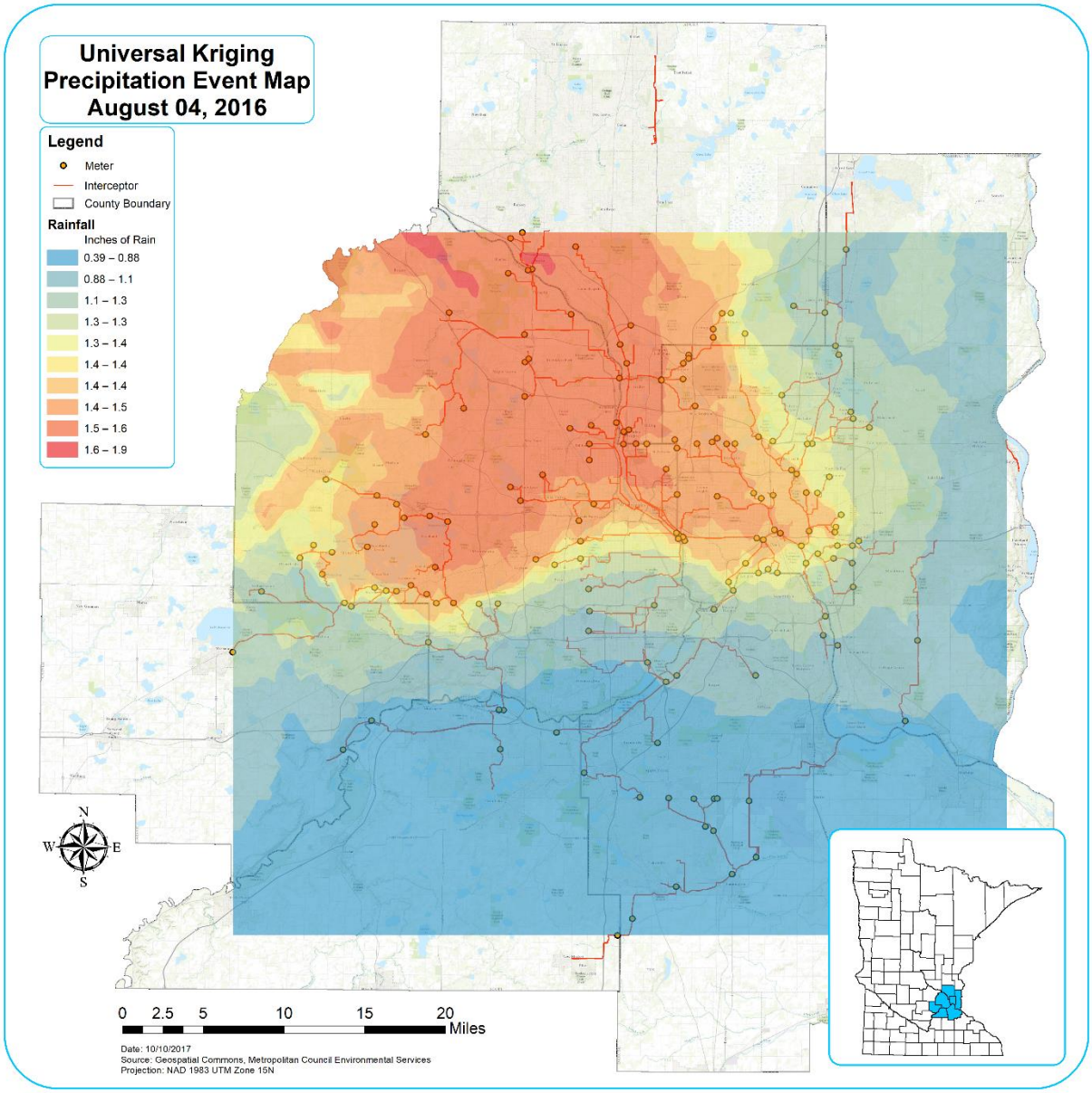
Universal Kriging
Precipitation Event Map
August 04, 2016
Legend
Meter
Interceptor
County Boundary
Rainfall
Inches of Rain
0.39 – 0.88
0.88 – 1.1
1.1 – 1.3
1.3 – 1.3
1.3 – 1.4
1.4 – 1.4
1.4 – 1.4
1.4 – 1.5
1.5 – 1.6
1.6 – 1.9
N
W
E
S
0 2.5 5 10 15 20
Miles
Date: 10/10/2017
Source: Geospatial Commons, Metropolitan Council Environmental Services
Projection: NAD 1983 UTM Zone 15N

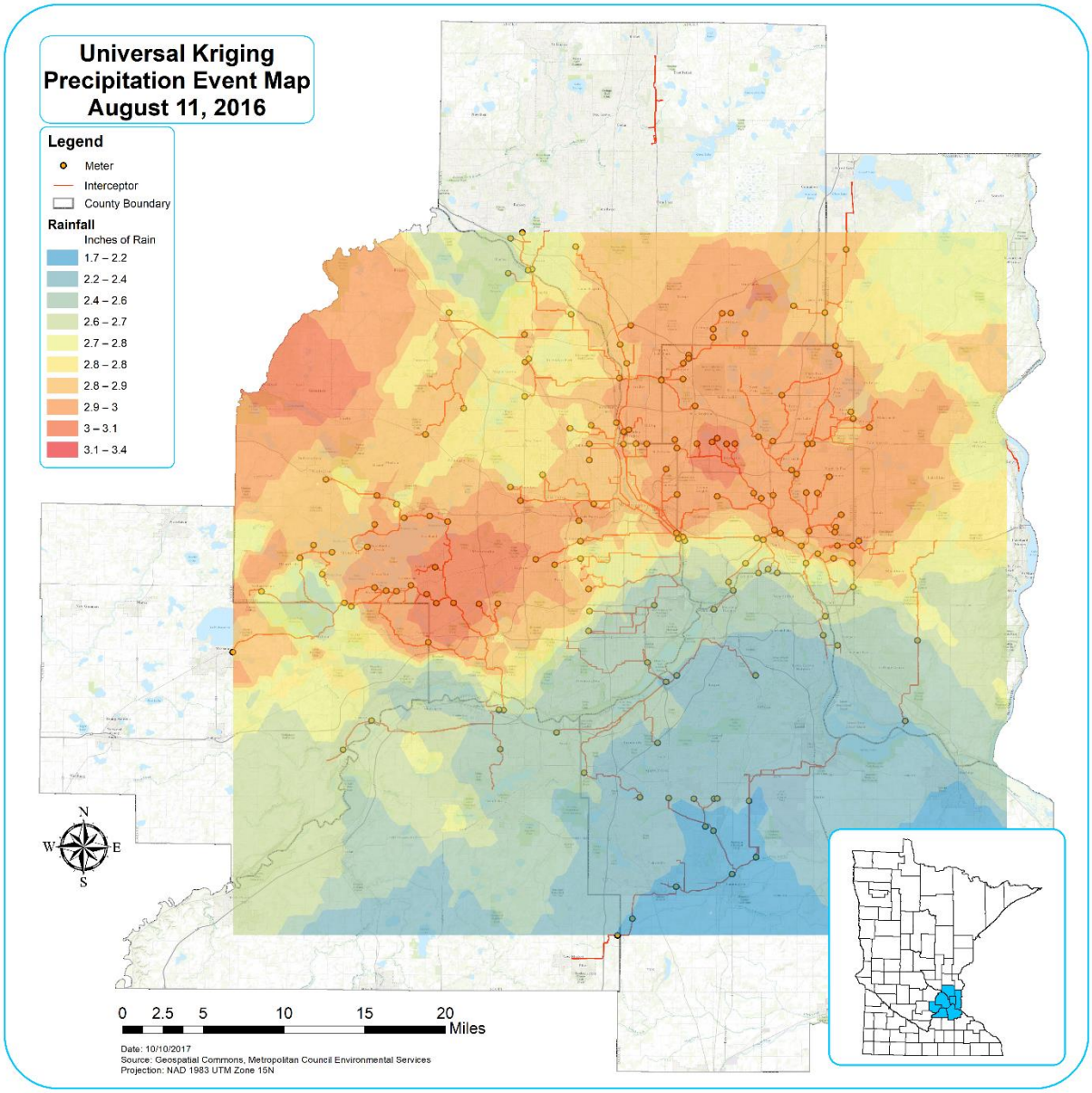
Universal Kriging
Precipitation Event Map
August 11, 2016
Legend
Meter
Interceptor
County Boundary
Rainfall
Inches of Rain
1.7 – 2.2
2.2 – 2.4
2.4 – 2.6
2.6 – 2.7
2.7 – 2.8
2.8 – 2.8
2.8 – 2.9
2.9 – 3
3 – 3.1
3.1 – 3.4
N
W
E
S
0 2.5 5 10 15 20
Miles
Date: 10/10/2017
Source: Geospatial Commons, Metropolitan Council Environmental Services
Projection: NAD 1983 UTM Zone 15N

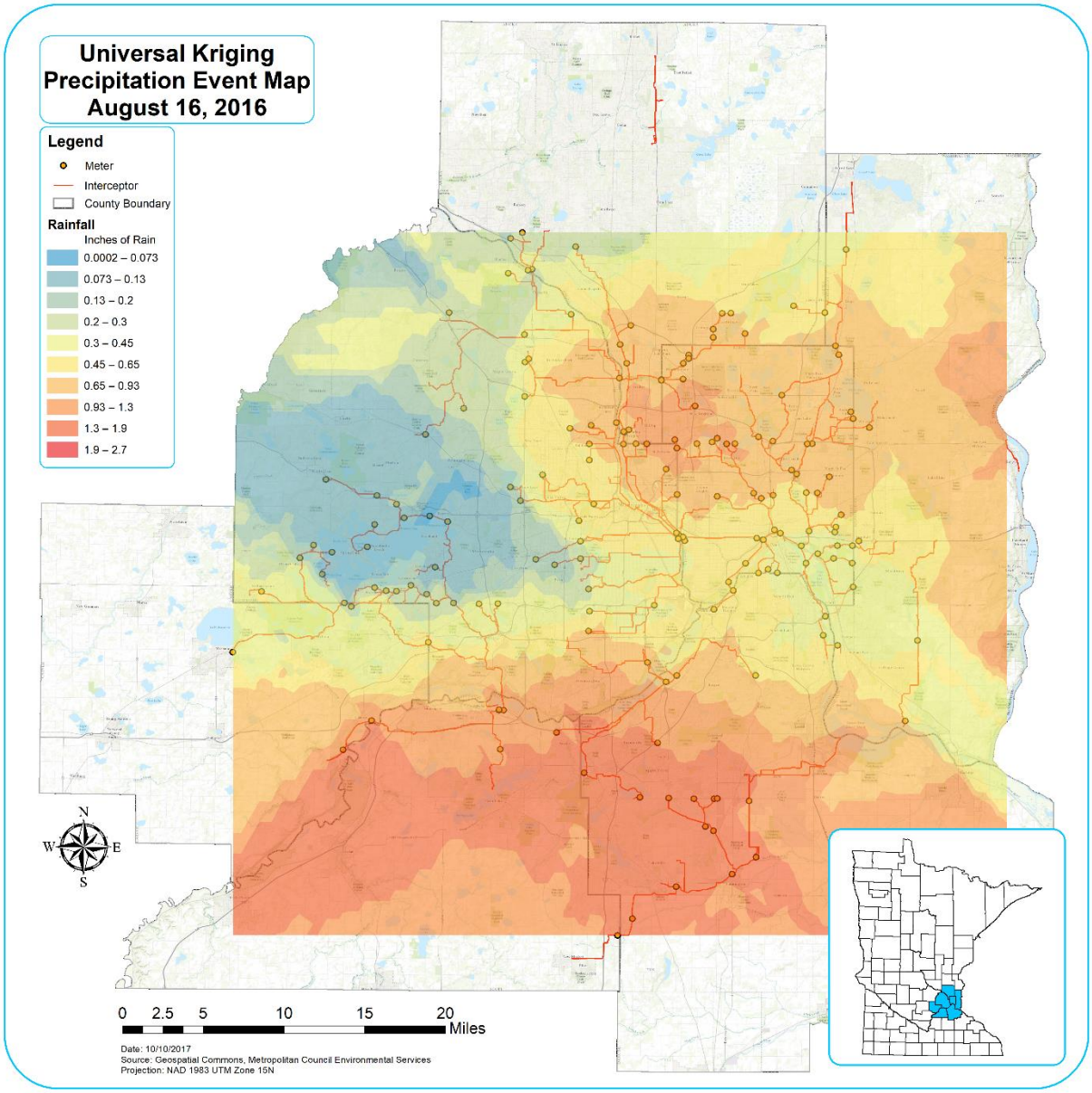
Universal Kriging
Precipitation Event Map
August 16, 2016
Legend
Meter
Interceptor
County Boundary
Rainfall
Inches of Rain
0.0002 – 0.073
0.073 – 0.13
0.13 – 0.2
0.2 – 0.3
0.3 – 0.45
0.45 – 0.65
0.65 – 0.93
0.93 – 1.3
1.3 – 1.9
1.9 – 2.7
N
W
E
S
0 2.5 5 10 15 20
Miles
Date: 10/10/2017
Source: Geospatial Commons, Metropolitan Council Environmental Services
Projection: NAD 1983 UTM Zone 15N

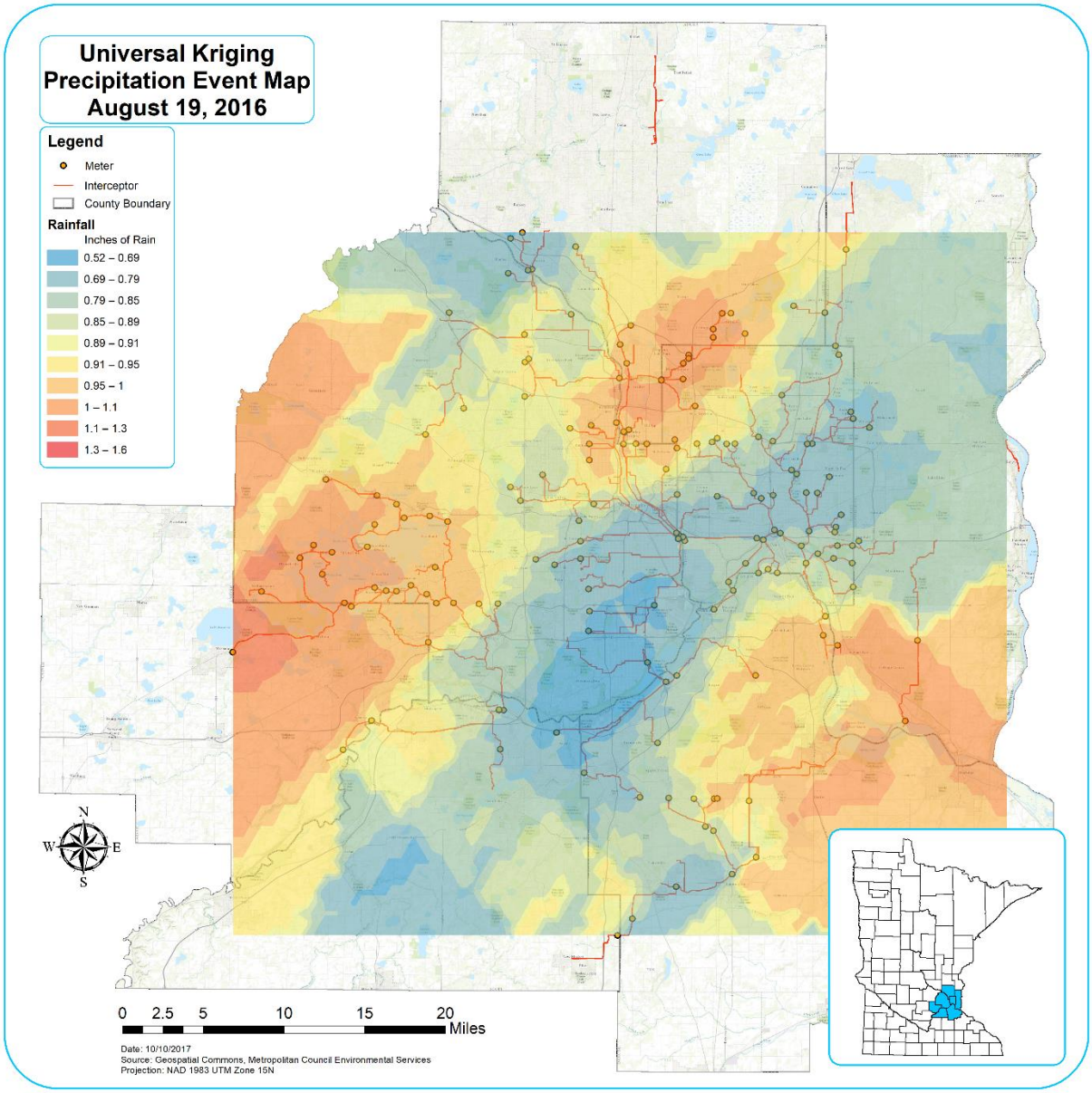
Universal Kriging
Precipitation Event Map
August 19, 2016
Legend
Meter
Interceptor
County Boundary
Rainfall
Inches of Rain
0.52 – 0.69
0.69 – 0.79
0.79 – 0.85
0.85 – 0.89
0.89 – 0.91
0.91 – 0.95
0.95 – 1
1 – 1.1
1.1 – 1.3
1.3 – 1.6
N
W
E
S
0 2.5 5 10 15 20
Miles
Date: 10/10/2017
Source: Geospatial Commons, Metropolitan Council Environmental Services
Projection: NAD 1983 UTM Zone 15N

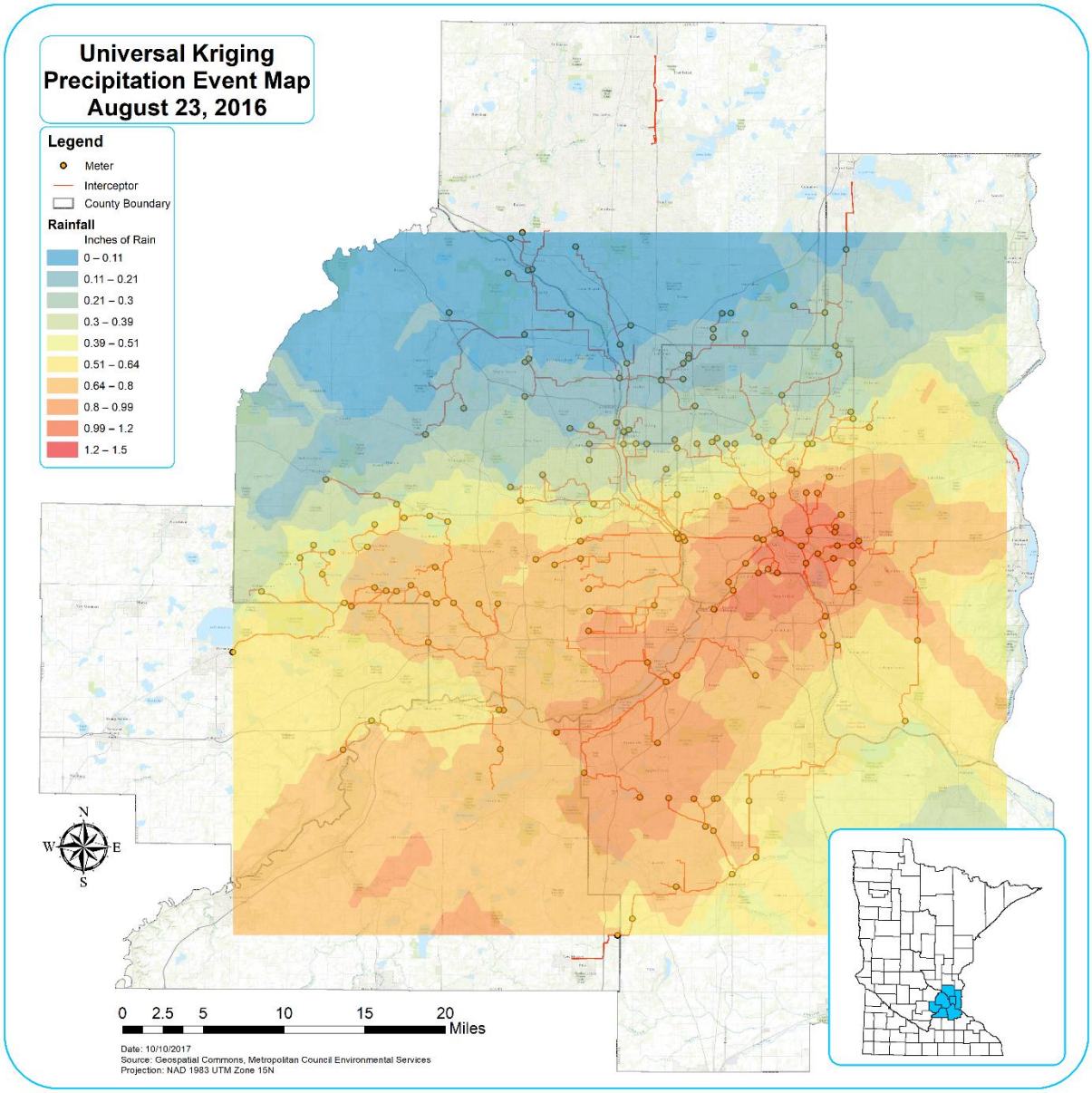
Universal Kriging
Precipitation Event Map
August 23, 2016
Legend
Meter
Interceptor
County Boundary
Rainfall
Inches of Rain
0 – 0.11
0.11 – 0.21
0.21 – 0.3
0.3 – 0.39
0.39 – 0.51
0.51 – 0.64
0.64 – 0.8
0.8 – 0.99
0.99 – 1.2
1.2 – 1.5
N
W
E
S
0 2.5 5 10 15 20
Miles
Date: 10/10/2017
Source: Geospatial Commons, Metropolitan Council Environmental Services
Projection: NAD 1983 UTM Zone 15N

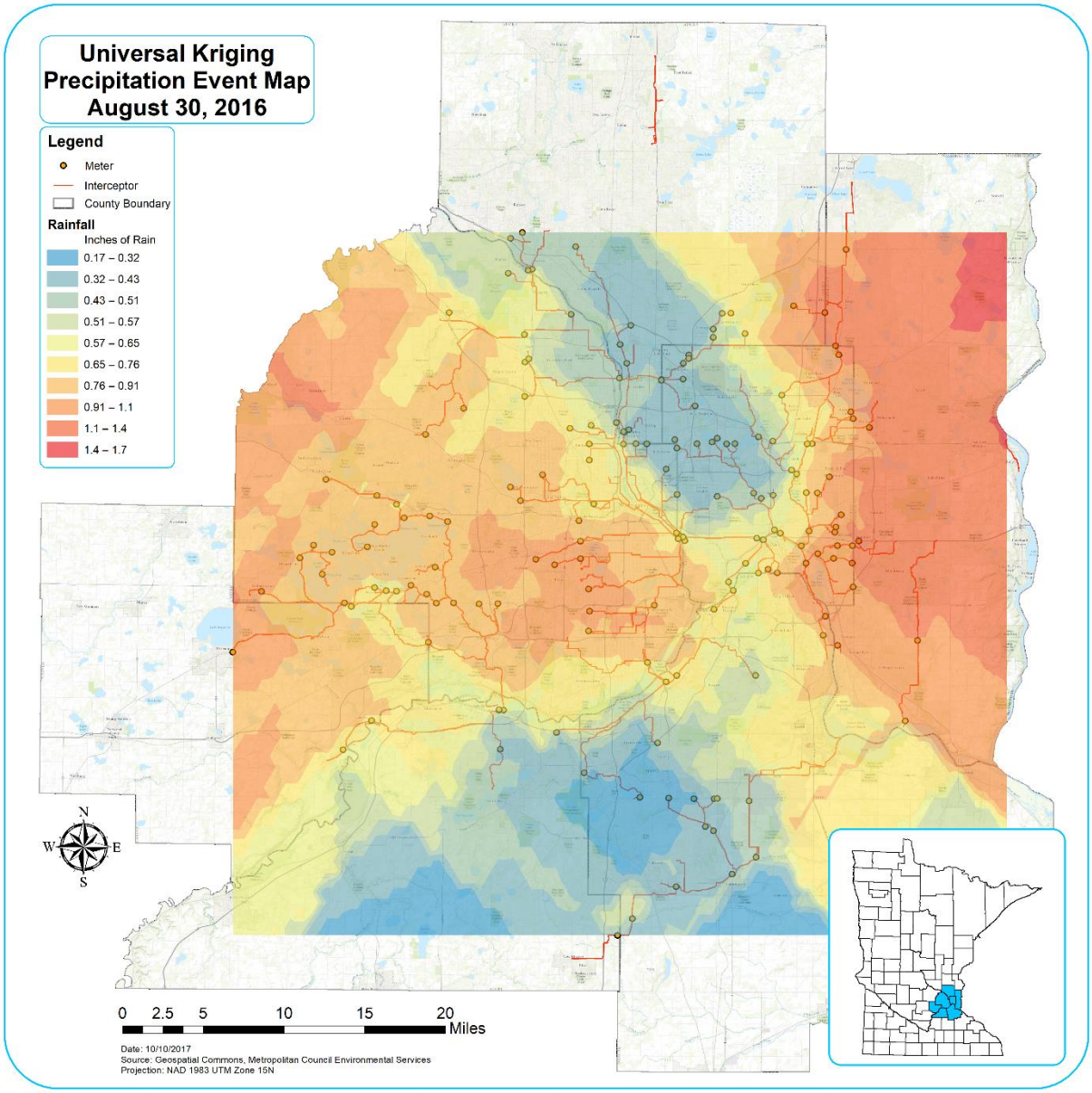
Universal Kriging
Precipitation Event Map
August 30, 2016
Legend
Meter
Interceptor
County Boundary
Rainfall
Inches of Rain
0.17 – 0.32
0.32 – 0.43
0.43 – 0.51
0.51 – 0.57
0.57 – 0.65
0.65 – 0.76
0.76 – 0.91
0.91 – 1.1
1.1 – 1.4
1.4 – 1.7
N
W
E
S
0 2.5 5 10 15 20
Miles
Date: 10/10/2017
Source: Geospatial Commons, Metropolitan Council Environmental Services
Projection: NAD 1983 UTM Zone 15N

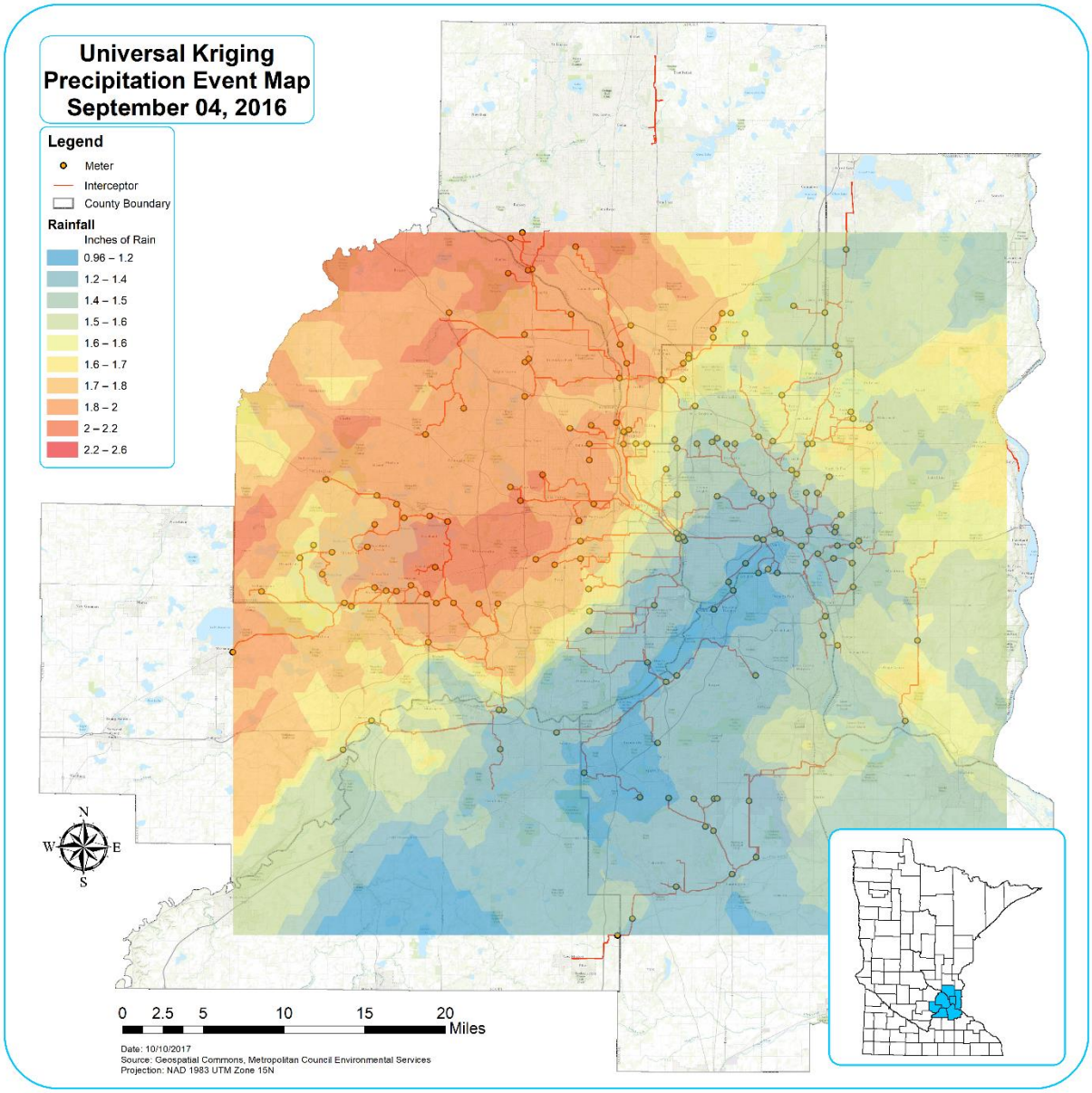
Universal Kriging
Precipitation Event Map
September 04, 2016
Legend
Meter
Interceptor
County Boundary
Rainfall
Inches of Rain
0.96 – 1.2
1.2 – 1.4
1.4 – 1.5
1.5 – 1.6
1.6 – 1.6
1.6 – 1.7
1.7 – 1.8
1.8 – 2
2 – 2.2
2.2 – 2.6
N
W
E
S
0 2.5 5 10 15 20
Miles
Date: 10/10/2017
Source: Geospatial Commons, Metropolitan Council Environmental Services
Projection: NAD 1983 UTM Zone 15N

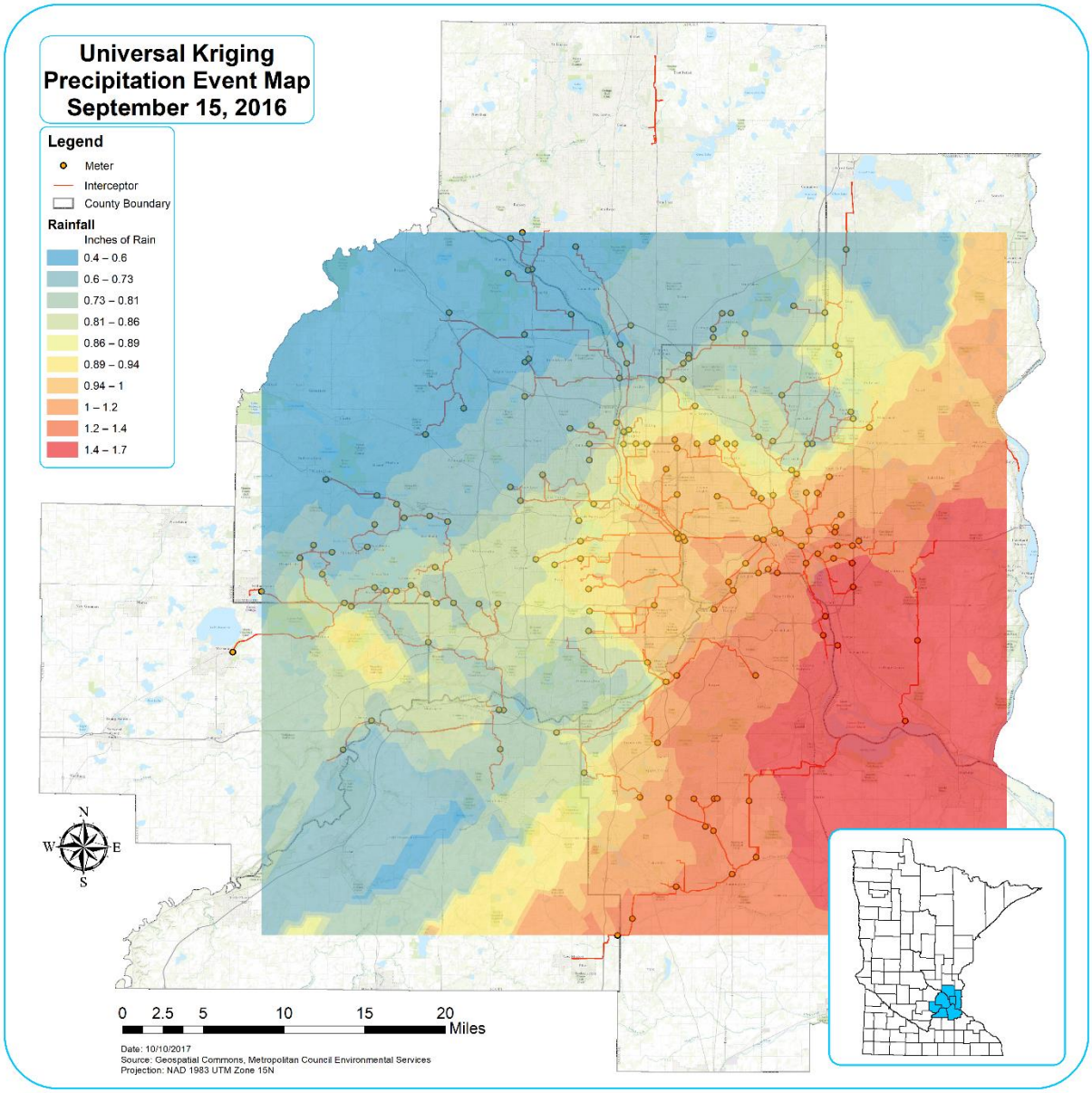
Universal Kriging
Precipitation Event Map
September 15, 2016
Legend
Meter
Interceptor
County Boundary
Rainfall
Inches of Rain
0.4 – 0.6
0.6 – 0.73
0.73 – 0.81
0.81 – 0.86
0.86 – 0.89
0.89 – 0.94
0.94 – 1
1 – 1.2
1.2 – 1.4
1.4 – 1.7
N
W
E
S
0 2.5 5 10 15 20
Miles
Date: 10/10/2017
Source: Geospatial Commons, Metropolitan Council Environmental Services
Projection: NAD 1983 UTM Zone 15N

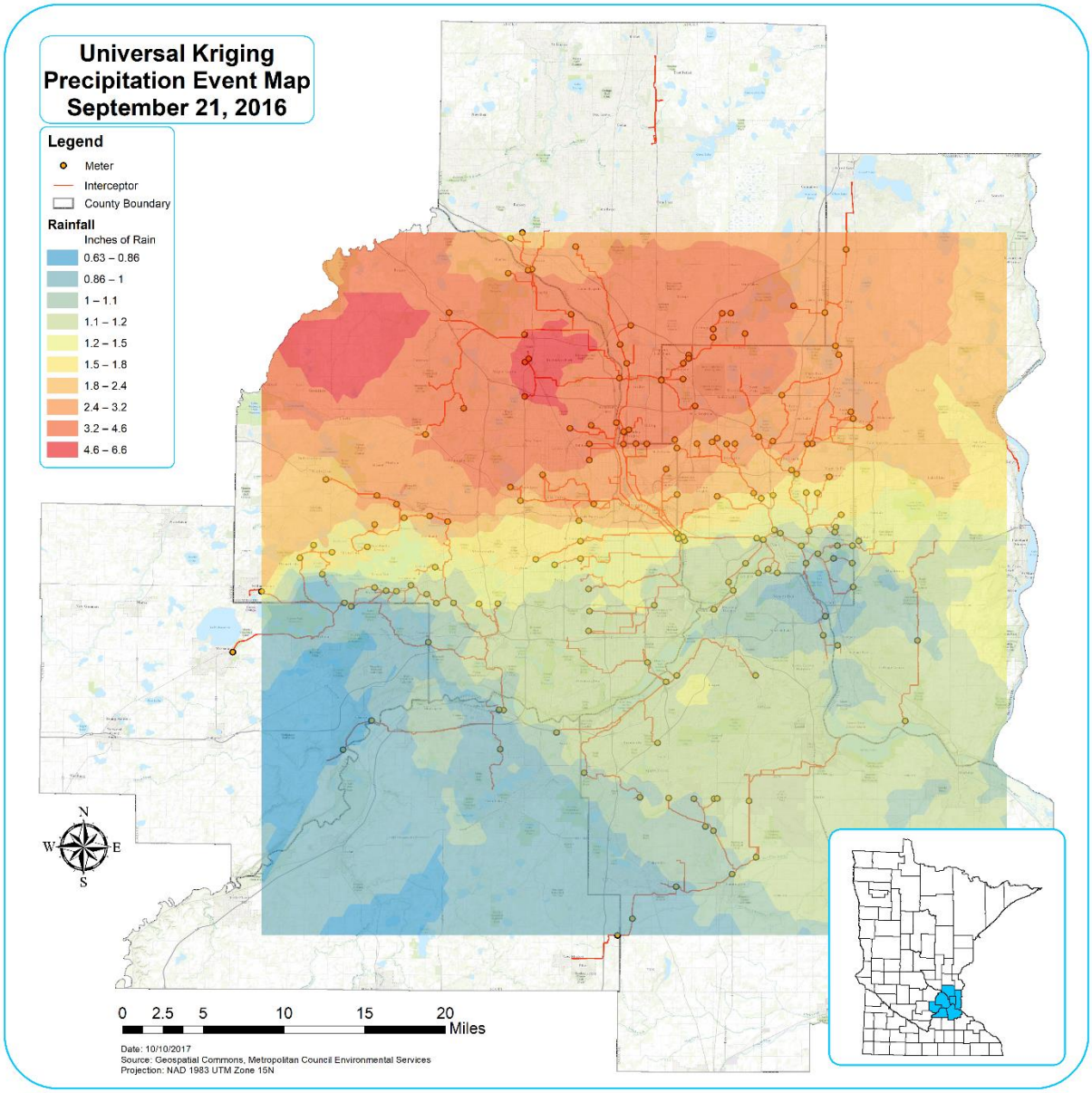
Universal Kriging
Precipitation Event Map
September 21, 2016
Legend
Meter
Interceptor
County Boundary
Rainfall
Inches of Rain
0.63 – 0.86
0.86 – 1
1 – 1.1
1.1 – 1.2
1.2 – 1.5
1.5 – 1.8
1.8 – 2.4
2.4 – 3.2
3.2 – 4.6
4.6 – 6.6
N
W
E
S
0 2.5 5 10 15 20
Miles
Date: 10/10/2017
Source: Geospatial Commons, Metropolitan Council Environmental Services
Projection: NAD 1983 UTM Zone 15N